Photoinduced Electron Transfer in Ruthenium-Bis(*p*-anisyl)amine Dyads Equipped with Boronmesityl or Tetramethoxybenzene Bridging Units

Inauguraldissertation

zur Erlangung der Würde eines Doktors der Philosophie

vorgelegt der

Philosophisch-Naturwissenschaftlichen Fakultät

der Universität Basel

von

Luisa G. Heinz (geb. Reuter)

aus Dresden, Deutschland

Basel 2016

Genehmigt von der Philosophisch-Naturwissenschaftlichen Fakultät auf Antrag von

Fakultätsverantwortlicher/Dissertationsleiter: Prof. Dr. Oliver S. Wenger
Korreferentin: Prof. Dr. Catherine E. Housecroft

Basel, den 09.12.2014

<div align="right">

Prof. Dr. Jörg Schibler

Dekan

</div>

Die vorliegende Arbeit wurde in der Zeit von März 2011 bis November 2014 am Institut für Anorganische Chemie der Universität Göttingen sowie Universität Basel unter der Leitung von Herrn Prof. Dr. O. Wenger angefertigt.

Zwei Dinge sind zu unserer Arbeit nötig:
Unermüdliche Ausdauer und die Bereitschaft
etwas, in das man viel Zeit und Arbeit gesteckt hat,
wieder wegzuwerfen.

Albert Einstein

Ich habe gelernt,

dass der Weg des Fortschritts weder *kurz* noch *unbeschwerlich* ist.

Marie Curie

Für meine Eltern

und

Michael

Contents

List of Abbreviations, Acronyms and Symbols

A	acceptor
alkyne	triple bond
amine	bis(*p*-anisyl)amine
AQ	anthraquinone
b	bridge
B-H-A	Buchwald-Hartwig amination
bpy	2,2'-bipyridine
BQ	benzoquinone
BuLi	butyllithium
BV	benzylviologen
calc.	calculated
CV	cyclic voltammetry
Cyt	cytochrom
D	donor
d	doublet
δ	chemical shift
$-\Delta G$	driving force
dba	dibenzylideneacetone
dmb	dimethoxybenzene
dmbq	dimethoxy benzoquinone
DMSO	dimethylsulfoxide
e.g.	exempli gratia
EA	elemental analysis
EA	ethyl acetate
EDTA	ethylenediaminetetraacetic acid
eq	equivalent(s)
ESI-MS	electrospray ionization-mass spectroscopy
EtOH	ethanol
fl	9,9'-dihexylfluorene
h	hour(s)
His_{190}	histidine190
Hz	hertz (s^{-1})
ISC	intersystem crossing
J	coupling constant
k_{ET}	electron transfer rate
λ	reorganization energy

|	
LC	ligand centered
M	molarity (mol/L^{-1})
m	multiplet
MC	metal centered
Me	methyl
MEBYNOL	2-methyl-3-butyn-2-ol
mebynol	2-methyl-3-butyn-2-ol attached to a molecule
MeOH	methanol
mes	mesityl
min	minute(s)
MLCT	metal-to-ligand charge transfer
MV	methylviologen
NDI	1,4,5,8-naphthalenetetracarboxylic diimide
OEC	oxygen evolving complex
OLED	organic light-emitting diode
OV	octylviologen
P	pentane
PCET	proton coupled electron transfer
PET	photoinduced elelctron transfer
Ph	phenyl
phe	pheophytine
ppm	parts per million
PQ	plastoquinone
PS	photosystem
Q	quencher
q	quartet
quant.	quantitative
R$_f$	retention factor
r.t.	room temperature
s	singlet
t	triplet
τ	lifetime
TBAF	tetrabutylammonium fluoride
TCNB	tetracyanobenzene
TCNE	tetracyanoethylene
TCNQ	tetracyanoquinone
tmb	1,2,4,5-tetramethoxybenzene
TMS	trimethyl silan
TMS	trimethylsilyl
TMSCl	trimethylsilyl chloride
Tyr$_z$	tyrosine
xy	xylol

Abstract

Investigation of natural processes is one of the main topics for scientists. Designing molecular systems that mimic natural processes has become important to understand the reaction pathways. Multiple artificial systems were synthesized to study intramolecular electron transfer which is triggered by photoexcitation. These molecules are usually comprised of an electron acceptor moiety, a photosensitizer, and/or an electron donor moiety. The donor and acceptor moiety are linked by a bridge. The molecular dyads investigated in this thesis consist of a tris(bipyridine)ruthenium(II) part which acts as the photosensitizer and electron acceptor. This part is linked by different bridging units to the electron donor bis(*p*-anisyl)amine. Two different bridging units are presented in this thesis.
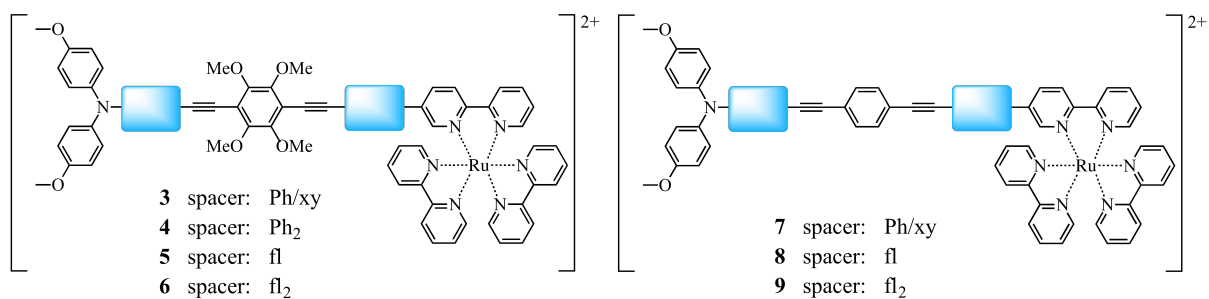
Chapter 1   starts with a general introduction to photosynthesis and photoinduced electron transfer. In the third part of this chapter the reasons for choosing tris(bipyridine)ruthenium(II) as photosensitizer are discussed.

Chapter 2   focuses on donor-bridge-acceptor systems with an electron-poor benzene as bridging unit. A dimesitylboron substituent is attached to the central benzene ring of the bridge. The resulting three-coordinate organoboron compound is known as sensor for small anions like CN^- or F^-. The ability to be bound by anions might have an influence on the charge transfer rate which we wanted to investigate. We assumed that upon fluoride attachment the energy barrier of the bridge increases. Therefore, the photoinduced electron transfer might come to a stop or there might be a change from a hopping to a tunneling mechanism. The figure below shows the two synthesized donor-bridge-acceptor systems. To increase the probability for charge transfer the bridge of dyad **2** was shortened and the photosensitizer was modified to increase its electron-withdrawing character.
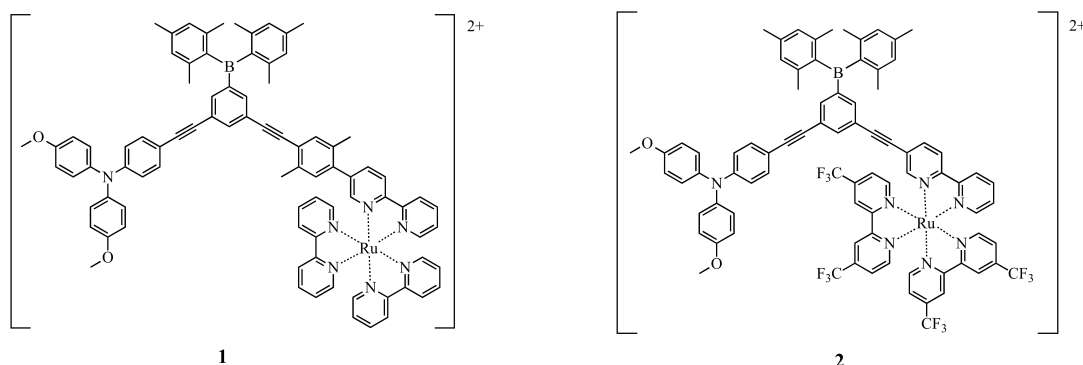
Chapter 3   focuses on dyads with an electron rich benzene molecule in the bridge. Therefore, 1,2,4,5-tetramethoxybenzene is placed in the middle of the bridging unit. 1,2,4,5-tetramethoxybenzene is has a low oxidation potential. Our goal was to investigate the charge transfer rates and the charge transfer mechanism in these dyads. Due to the low oxidation potential of 1,2,4,5-tetramethoxybenzene it might

act as a hopping station whereas in unsubstituted benzene bridging units the charge transfer through the whole bridge usually occurs *via* a tunneling mechanism. Hence, we synthesized four molecules with different spacers and three different donor-acceptor distances (figure below, left side). Similar dyads with an unsubstituted benzene instead of tetramethoxybenzene served as reference molecules as shown in the figure below on the right side.

3 spacer: Ph/xy
4 spacer: Ph$_2$
5 spacer: fl
6 spacer: fl$_2$

7 spacer: Ph/xy
8 spacer: fl
9 spacer: fl$_2$

1 Introduction

The population of the world grows constantly. Until 2100 there will be over 10 billion people on the planet (see figure 1.1)[1]. The increasing population will not only lead to space problems. It will also have an effect on the consumption of energy. The required energy which comes from fossil fuels like coal, natural gas, or oil will increase the amount of CO_2 emitted into the atmosphere. CO_2 is known as the primary cause of global warming. In the future we have to face two major problems. First, how to cover the energy consumption without additional pollution of the environment and second, how to reduce the huge amount of CO_2 to prevent the planet from global warming?
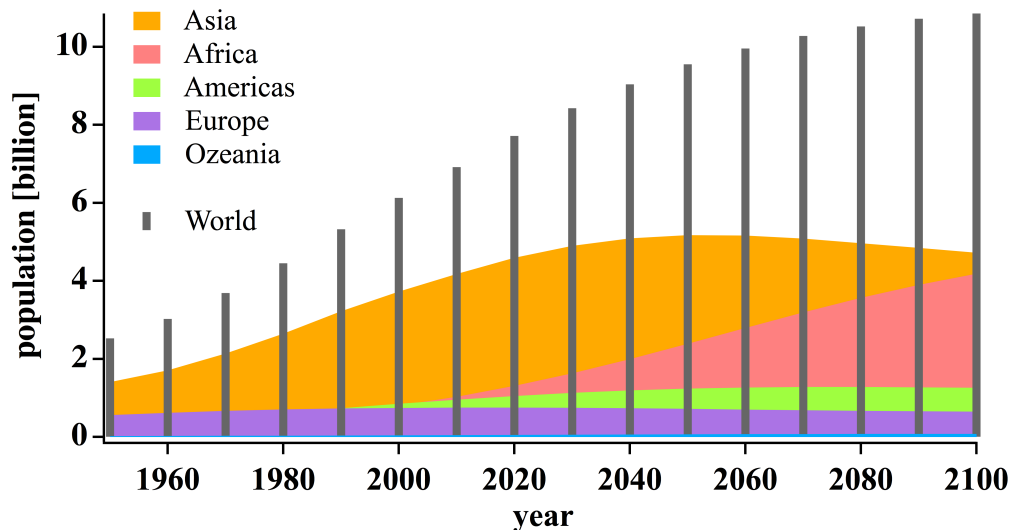
Figure 1.1 Population of all continents and the world.

Alternative energy sources are e.g. wind, water, and sun light. All those sources are convenient, free, and do not lead to CO_2 emitted into the atmosphere. Would it not be more efficient to combine the two major problems in one project? The nature is the perfect template for a solution. Green plants produce their energy *via* photosynthesis and therefore they consume CO_2.

1.1 Photosynthesis

Natural photosynthesis does not only consist of one reaction. It incorporates a series of those. The most important photochemical process is the water splitting to generate hydrogen in the form of NADPH[2] and oxygen. This process stores the required energy. The released hydrogen is stored by carbohydrate (in the Calvin cycle) (see scheme 1.1).
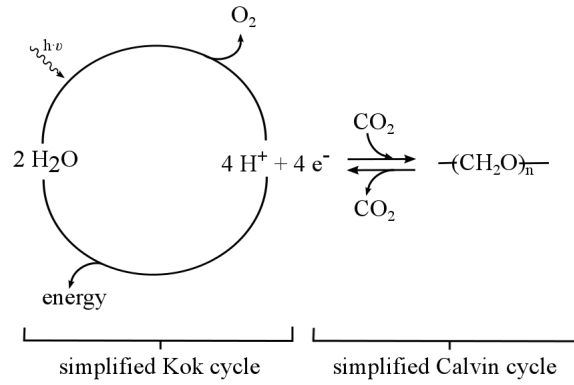
Scheme 1.1   Energy storage (Kok cylce) and hydrogen storage (Calvin cycle).

Water splitting in photosynthesis is performed by the OEC (oxygen evolving complex) in the so called Kok cycle. This complex is loc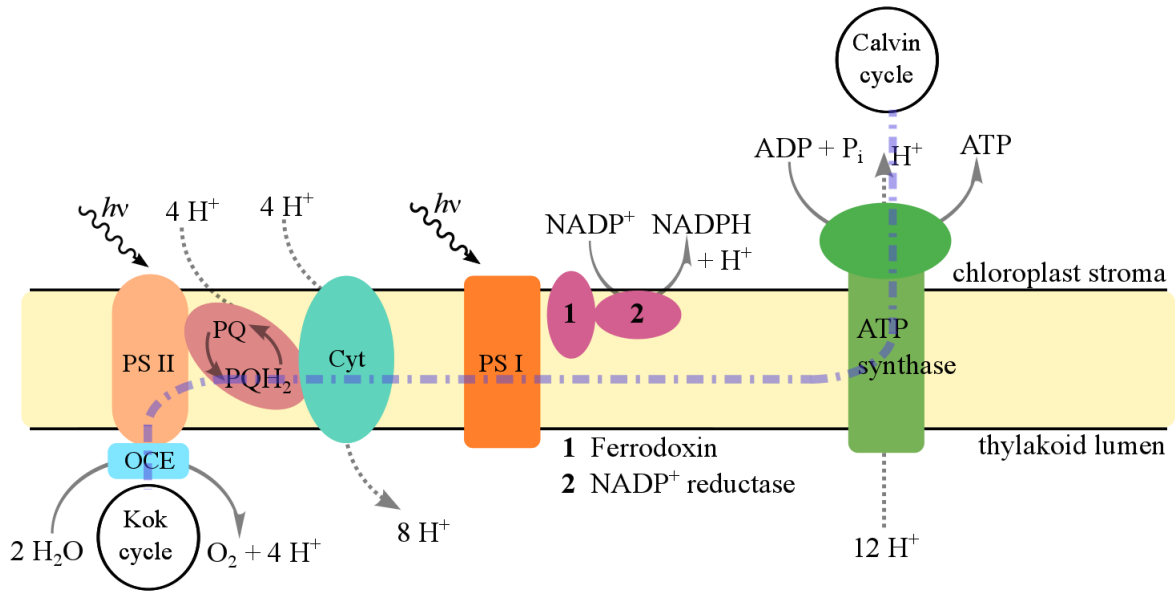ated in the photosystem II (PS II). Scheme 1.2 shows a simplified picture of the light-driven part of photosynthesis in a thylakoid membrane.

Scheme 1.2   Simplified scheme of the light-driven part of photosynthesis in thylakoid membranes of chloroplasts in plants and algae. Electron transport is marked by the dash-dotted purple line.

First, water is split in the OEC. This process generates four protons. Another eight protons are generated by the cytochrome (Cyt) and the plastoquinone unit where plastoqiunone (PQ) is transferred into plastohydroquinone (PQH_2). Those twelve protons are needed to fuel ATP synthase unit. ATP and NADPH + H^+ which is generated by $NADP^+$ reductase are necessary to store hydrogen as carbohydrate compounds in the Calvin cycle. Those previous mentioned processes lead as well to an electron transport (marked by the dash-dotted purple line) from the Kok cycle to the Calvin cycle. During the Kok cycle four electrons are liberated (see small cycle on the left in scheme 1.3). Each electron reacts with a Tyr_z-PQH radical pair.
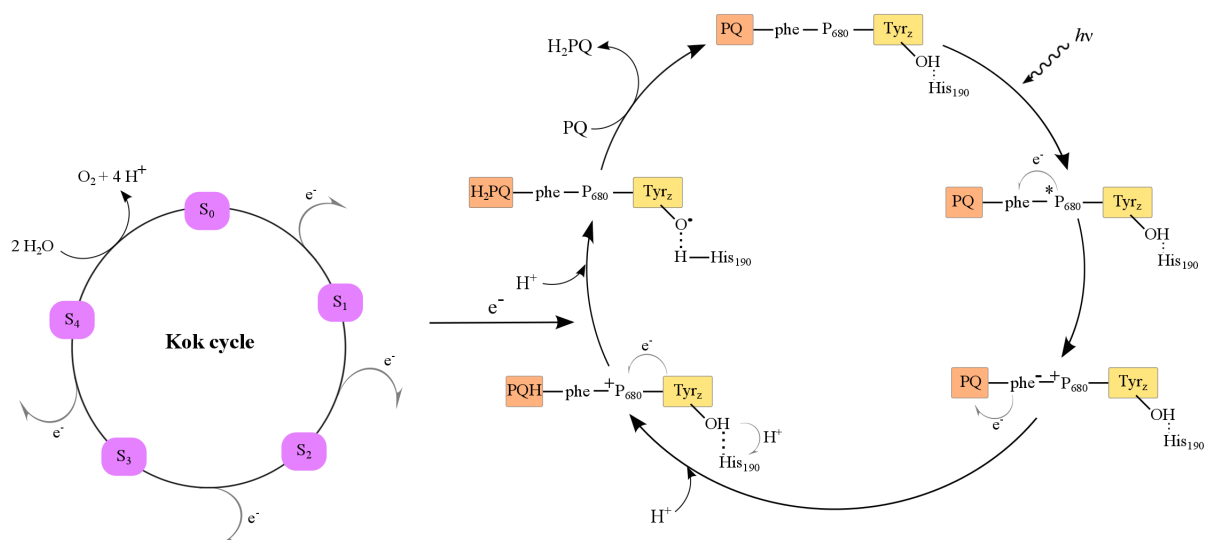
Scheme 1.3   Kok cycle and proton coupled electron transfer (PCET) in PS II. S_0, S_1, S_2, S_3, S_4 are interme-
diates of the Mn_4-Ca cluster and represent the oxidation states of the manganese centers.

To generate the Tyr_z-PQH radical pair multiple steps are needed as shown in scheme 1.3 on the right
side. Under the term plastoquinone (PQ) two quinones (PQ_A and PQ_B) are combined to simplify the
illustration. PQ_A is tightly bound whereas PQ_B is mobile.

First, the chlorophyll species (P_{680}) which is located in PS II absorbs a photon. The resulting excited state
of P_{680} (marked by *) is oxidized by pheophytine (phe) *via* electron transfer. A charge separated state is
generated (phe$^-$-$^+P_{680}$). To increase the distance between the electron and the hole, the electron is trans-
ferred to the tightly bound PQ_A and subsequently to PQ_B. With a proton from the stroma PQ_B forms a
semiquinone (PQH). This prevents the recombination and increases the lifetime of this charge-separated
state. The $^+P_{680}$ oxidizes the bound tyrosine (Tyr_z) over a distance of 10 Å. Meanwhile histidine190
(His_{190}) abstracts a proton from Tyr_z and the above mentioned Tyr_z-PQH radical pair is built. Following,
the semiquinone takes an electron from the Kok cycle as well as another proton from the stroma side of
the thylakoid membrane and a hydroquinone (H_2PQ) is generated. A mobile plastoquinone replaces in
the final step the hydroquinone and the neutral molecule can enter the cycle again.

To mimic photoinduced water splitting several fundamental and challenging steps with complicated
chemical transformations are needed. In 2011, D. Nocera invented in the artificial leaf[3]. The leaf
consisted of a silicon wafer which was coated on each side with a different catalyst. One for water ox-
idation and the other one for reducing protons into hydrogen gas. The energy was provided by sunlight
to drive the reaction, creating a simple system for solar fuel.

Not only in photosynthesis electron transfer reactions are present. They also take place in oxygen bind-
ing, respiration, and detoxification[4].

A challenging part in this field of studies is to investigate donor-acceptor systems where the charge re-
combination is prevented by increasing length of the system.

As described before many complex reactions take place and also electrons are released. Our ambition is
to transport those electrons over long distances.

1.2 Photoinduced electron transfer (PET)

Photoinduced electron transfer, short PET, occurs between an electron donor (D) and an electron acceptor (A) which are linked by a bridging unit. If such a donor-bridge-acceptor system is excited by light, **[D-bridge-A]*** is formed. Following, an intramolecular electron transfer from the donor moiety to the acceptor unit takes place and a charge-separated state is formed (see scheme 1.4). These steps lead to a quenching of the fluorescence[5].
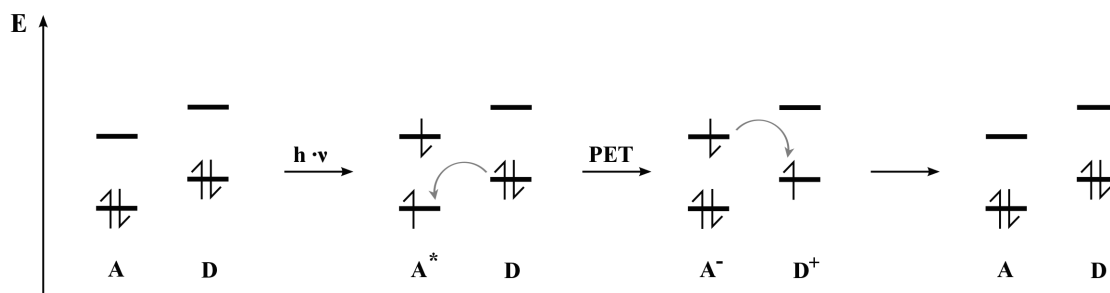
Scheme 1.4 Photoinduced eletron transfer (PET).

Jablonski diagrams are often used to describe the process that occurs between absorption and emission of light[6]. A typical diagram is shown in scheme 1.5.

With absorption of light an electronic transition occurs. The molecule is transferred from the ground state (S_0) to the first excited state (S_1). Each electronic energy level is coupled to numerous vibrational levels (dashed lines). Usually a fluorophore is excited to some higher vibrational level and relaxes rapidly to the lowest level of S_1. This process occurs within 10^{-12} s or less and is called internal conversion. Within this transition the electron in the excited orbital is paired by opposite spin compared to the second electron in the ground-state orbital. Fluorescence, the return to the ground state is spin allowed and therefore a fast process (10^8 s^{-1}). A typical lifetime for fluorescence is near 10 ns. The deactivation back to the ground state can also happen in a non-radiative way *via* formation of heat. It is also possible that molecules in the S_1 state undergo a spin conversion to T_1 (first triplet state), so called intersystem crossing (ISC). Emission from T_1 is called phosphorescence. Phosphorescence is shifted to lower energy (longer wavelength) compared to fluorescence. The electron in the excited orbital has the same spin orientation as the electron in the ground state. The transition to the ground state is slow (10^3 - 10^0 s^{-1}) because it is a spin-forbidden process. Phosphorescence lifetimes are usually in a milliseconds to even seconds time range.
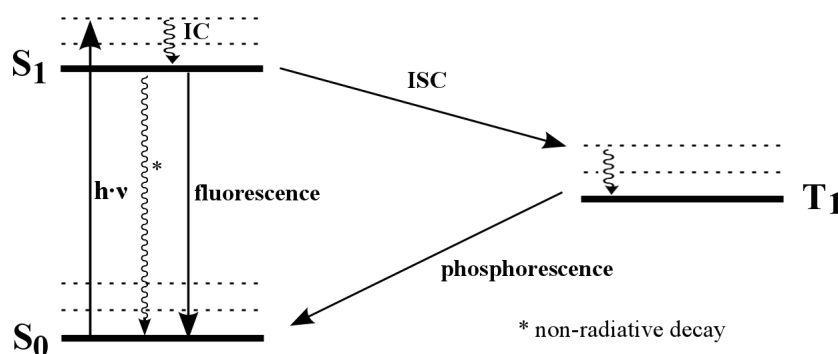
Scheme 1.5 Simplified Jablonski diagram for fluorescence and phosphorescence.

If the lifetime of the excited state is long enough, interactions among molecules and deactivation processes such as energy or electron transfer can occur.

In 1956, R. A. Marcus developed a theory to explain the rates of electron transfer reactions – the rate at which an electron can be transferred from one chemical species (donor) to another (acceptor)[7,8]. He was awarded with the Nobel Prize in chemistry in 1992. He investigated the parameters that control electron transfer reactions. Electron transfer reaction can take place in the inner sphere or outer sphere of a complex. Marcus focused on the outer sphere reaction. In outer sphere reactions the chemical bonds are neither broken nor ones formed. An example for an outer-sphere reaction is the self-exchange reaction. An electron transfer can only take place at the connection point of both parabolas. This crossing point represents the activation energy.
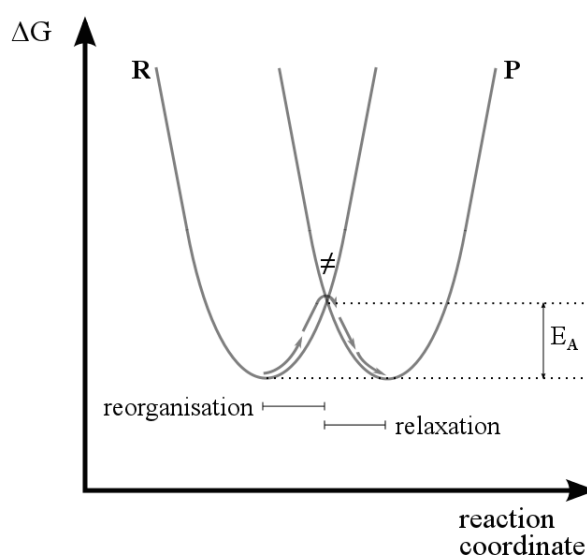
Figure 1.2 Energy scheme for a self-exchanged reaction (ΔG°=0).

The reaction system is first on the reactant side (R) in its equilibrium until its thermal energy is high enough to reach the transition state ($\neq$). At this point the electron transfer can occur. After the transfer, the reaction system relaxes into the equilibrium of the product state (P). The rate constant (k) depends on the activation energy (E_A) (equation 1.1).

$$k = A \cdot e^{-\frac{E_A}{R \cdot T}} \tag{1.1}$$

With an activation energy:

$$E_A = \frac{\lambda}{4} \cdot [1 + \frac{\Delta G}{\lambda}]^2 \tag{1.2}$$

Important parameters are the driving force (-ΔG) and the reorganization energy (λ). The electron transfer rate (k_{ET}) can be expressed by a combination of equations 1.1 and 1.2.

$$k_{ET} = A \cdot e^{-\frac{(\Delta G + \lambda)^2}{4 \cdot \lambda R \cdot T}} \tag{1.3}$$

The aforementioned equation has the form of a Gaussian function. There are three cases for electron

transfer rates: $\Delta G = -\lambda$, $\Delta G < -\lambda$, $\Delta G > -\lambda$. Equation 1.2 lead to the conclusion that with a very exergonic driving force a decrease of k_{ET} can be observed.
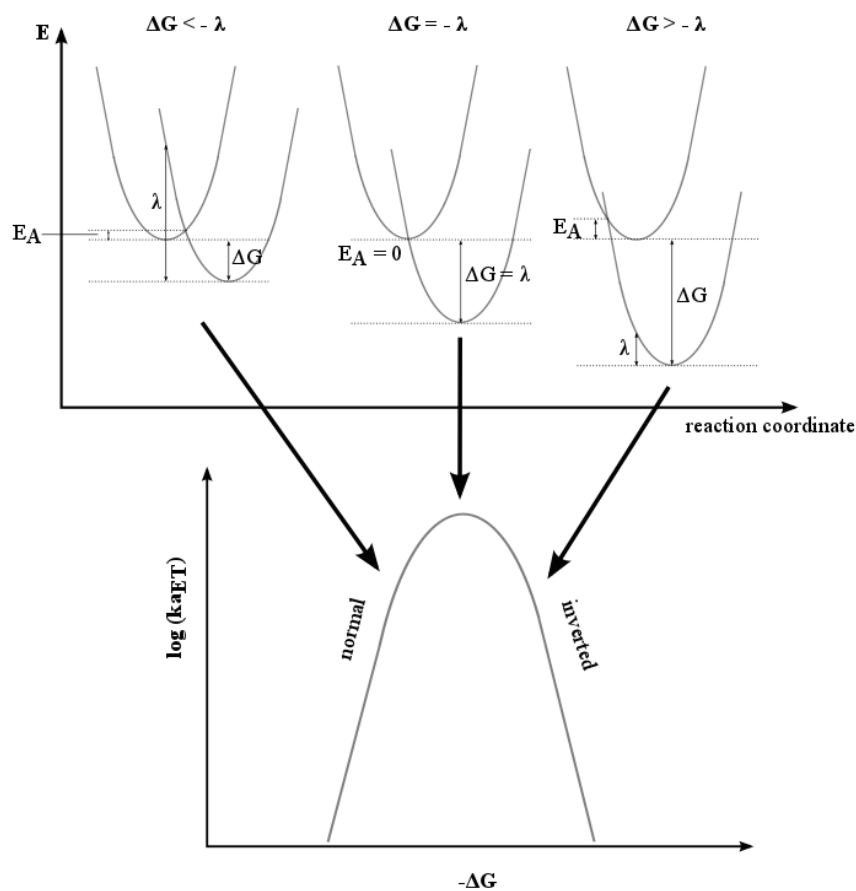
Figure 1.3 Three free energy regimes after Marcus (top) and the corresponding dependence of the electron transfer rates k_{ET} on ΔG (bottom). R and P represent the reactant and product state, respectively.

By increasing the free energy of the reaction (driving force (-ΔG)), the activation energy (E_A) decreases. This leads to an increase of the electron transfer rate (normal regime). If $\Delta G > -\lambda$, decreasing ΔG further leads to an increase of E_A and consequently to a decrease of the electron transfer rate (inverted regime). In simple words: With less energy difference between the parabolas the reaction process becomes faster and vice versa. PET processes for charge separation usually are in the Marcus normal region, whereas charge recombination often takes place in the inverted region.

1.3 Tris(bipyridine)ruthenium(II) complex

In 1959, Paris and Brandt detected the light emission of $Ru(bpy)_3^{2+}$ [9]. Crosby and co-workers characterized the luminescence of the complex in 1965[10]. Within a few years scientists were aware that $Ru(bpy)_3^{2+}$ shows a unique combination of properties. It is chemically stable, shows excited state reactivity as well as a long excited state lifetime[11]. Since then numerous publications surfaced where the complex was investigated upon its use in energy[12] and electron transfer reactions[13].

The geometry of $Ru(bpy)_3^{2+}$ is nearly octahedral. In its ground state the five 3d-orbitals are split into two e_g and three t_{2g} orbitals as shown in figure 1.4.
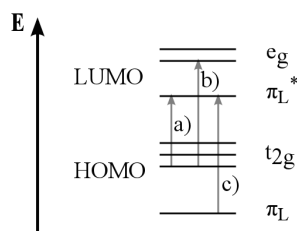
Figure 1.4 Molecule orbital diagram for a) MLCT, b) MC and c) LC.

The absorption spectrum in the visible region shows mainly three bands (figure 1.5). First an intense band at 290 nm due to $\pi - \pi^*$ transition which are ligand centered (LC). The band at 450 nm is caused by a metal-to-ligand charge transfer (MLCT).
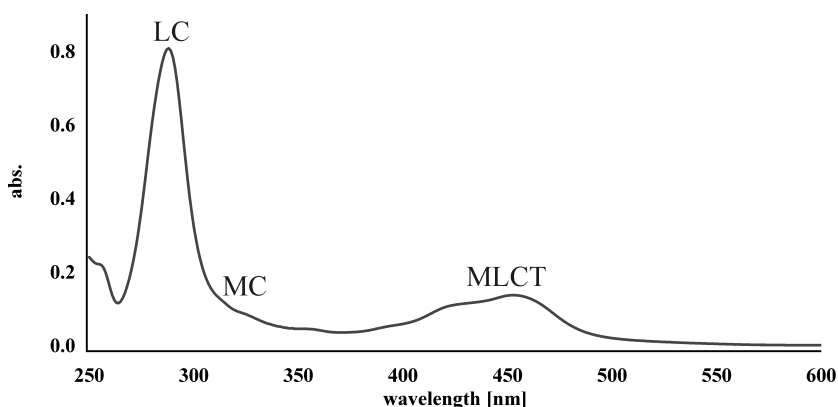
Figure 1.5 UV/Vis spectrum of $Ru(bpy)_3^{2+}$ in methylene chloride solution.

Excitation at 450 nm leads to an energy rich ^{1}MLCT state. *Via* spin reverse (300 fs, almost quantitative $\phi_{ISC} \approx 1$) a triplet MLCT (^{3}MLCT) excited state is generated. It has a lifetime (τ) of approximately 0.8 μs in deoxygenated acetonitrile. One electron of the long-lived excited state can be transferred in a bimolecular fashion *via* a quencher like viologen or quinone. Neat $Ru(bpy)_3(PF_6)_2$ has a yellow-orange luminescence (610 nm)[14] with a quantum yield of 9 % in deoxygenated acetonitrile[15].

As shown in scheme 1.6 oxidation of the metal center in $Ru(bpy)_3^{2+}$ occurs at positive potentials (E_{ox} = +1.26 V vs. SCE). An electron is removed from a metal-centered orbital (Ru^{3+}/Ru^{2+}). Three reduction waves which are ligand centered occur between -1.28 V and -1.70 V vs. SCE. The redox potentials of $Ru(bpy)_3^{2+}$ in its excited state are +0.84 V and -0.86 V[16].
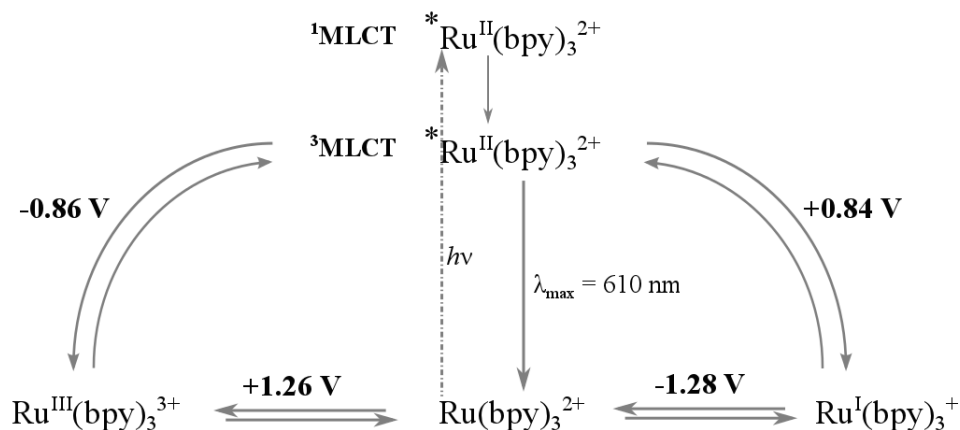
Scheme 1.6 Electrochemical and photophysical properties of $Ru(bpy)_3{}^{2+}$ in acetonitrile. All listed potentials are in Volts vs. SCE.

Summarizing the previous findings, excited $Ru(bpy)_3{}^{2+}$ (marked by *) can act as a good electron acceptor or electron donor[17].

The equations to estimate the redox potentials of the ^{3}MLCT excited state are collected below[11].

$$E(Ru^{3+}/{}^*Ru^{2+}) = E(Ru^{3+}/Ru^{2+}) - E_{00} \tag{1.4}$$

$$E({}^*Ru^{2+}/Ru^+) = E(Ru^{2+}/Ru^+) + E_{00} \tag{1.5}$$

Potentials for the ground state: oxidation $E(Ru^{3+}/Ru^{2+})$ and reduction $E(Ru^{2+}/Ru^+)$. $E_{00} = 2.12$ V[18] and is called excitation energy; it is the energy stored in the ^{3}MLCT excited state. By addition of electron-withdrawing or donating substituents on the bpy ligands, a change of the redox potentials in the ground state takes place. Therefore the excited state potentials change as well[12,13].

2 Photoinduced Electron Transfer in Ruthenium-Bis(p-anisyl)amine Dyads Equipped with a Boronmesityl Bridging Unit

2.1 Introduction

Three-coordinate organoboron compounds have been investigated intensively due to their applications in e.g. anion sensing[19,20,21], luminescence materials[22], nonlinear optics[23,24,25] as well as electron-transport materials and fluorescence emitters in OLEDs[26]. In many cases triarylboranes were used because of their strong luminescence in solution and in the solid state. As excellent acceptors for electrons by means of their empty p_π orbital they can be used in a wide area.
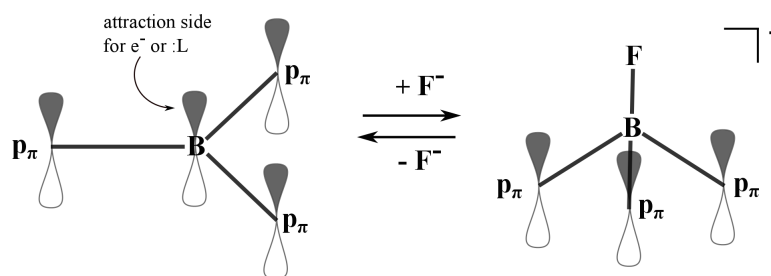

Figure 2.1 Anion sensing of three-coordinate organoboron compounds.

In figure 2.1 a three-coordinate organoboron compound is shown where the sp^2-hybridized boron atom posseses a vacant p_π orbital. Therefore, it can act as Lewis acid and form a complex with hard bases like hydoxy or fluoride anions. Upon anion binding the geometry changes from trigonal planar to tetrahedral. When an appropriate electron donor like triarylamine is present in a boron compound, an intense intramolecular charge-transfer transition takes place. Upon base addition, the initially vacant p_π is occupied with an electron from the base, and this leads to the disruption of the p_π-π^* conjugation. This results in a quenching of the charge-transfer fluorescence[27].

The aryl groups attached to the boron atom play a major role in stabilizing the electron poor character of the boron. If bulky aryl groups like mesityl are used, the chance of a nucleophilic attack by relatively bulky molecules such as water or oxygen minimizes. Therefore, many inert organoboron compounds could be obtained. Only small nucleophiles can pass the bulky aryl groups. Hence those compounds are highly sensitive to small anions like cyanide[28] or fluoride[29]. The bulky aryl groups also prevent intermolecular stacking and interaction in the solid state. This is important for the intense solid-state emission of these compounds[30,31].

As mentioned before, boron-doped π-systems are relevant for a broad range of applications. Two cases

for the design of boron-containing π-conjugated polymers have to be distinguished. One, where the boron atoms are introduced as lateral substituents, in the second case they are incorporated as integral parts of the polymer main chain[32,33]. The figure below shows two examples for both cases.
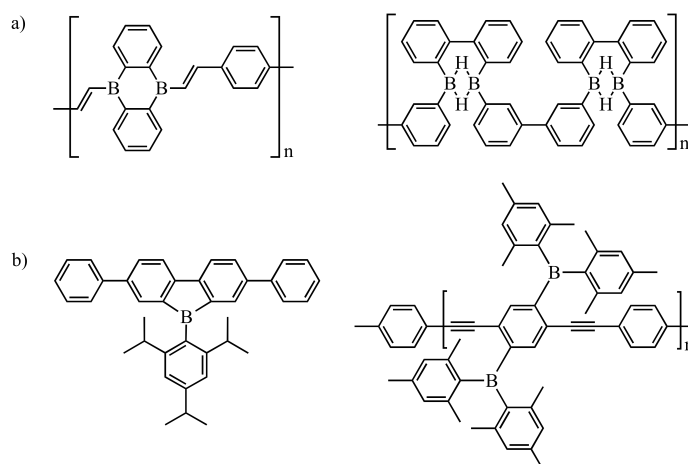
Figure 2.2 Examples for boron atoms as integral part[34,35] (a) and in lateral position[26,36] (b) in polymer chains.

Due to the huge variety of publications on this subject only the most relevant ones will be cited here. The photophysical properties of organoboron compounds can be tuned by combination with other electronic systems in one molecule. Wang and co-workers investigated several triarylboron-triarylamine compounds as shown in figure 2.3.
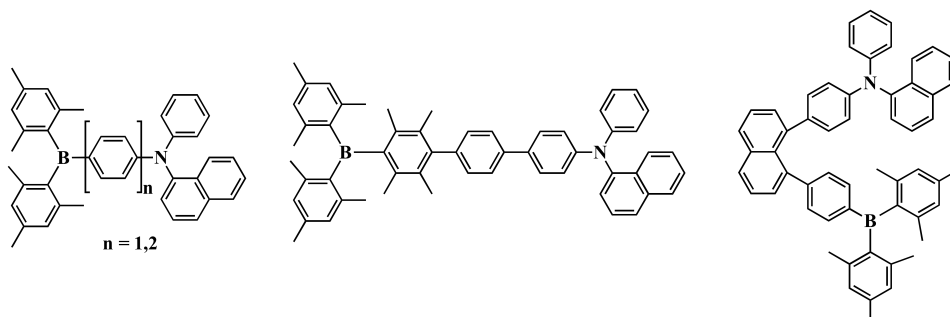
Figure 2.3 Examples for boron-amine compounds investigated by Wang[37].

Their goal was to develop new stable donor-acceptor triarylboranes which can be used as efficient blue emitters in OLEDs. Kaim and co-workers found that certain three-coordinated boron centers in their one-electron-reduced forms are isoelectronic to carbocations[38].

Transition metal complexes with tunable spectroscopic and redox properties are attractive to scientists. Gabbaï[39], Yam[40], Wang[22,41], and other scientists investigated boron-metal complexes. They used different metals like copper, rhenium, platinum, ruthenium or lanthanides (examples see figure 2.4). Wang found that coordination to metals can enhance the electron-accepting ability of the resulting complexes.
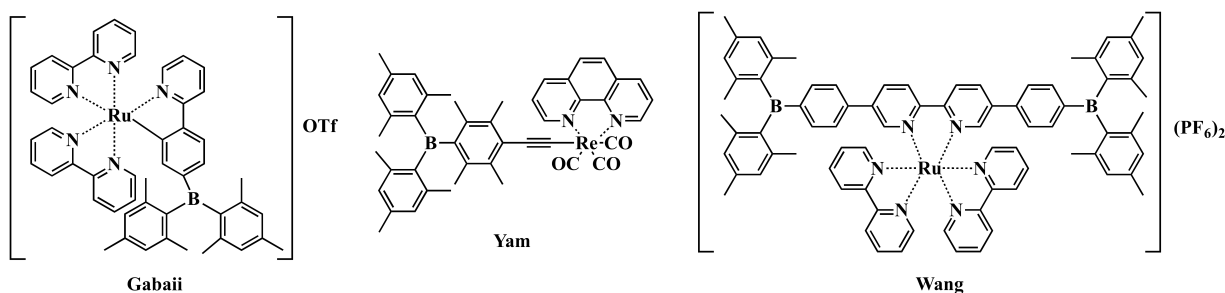
Figure 2.4 Examples for metal complexes with three-coordnated boron substituents[39,40,41].

Our goal is to combine both concepts and create amine-boron-ruthenium dyads in which the amine acts as an electron donor and ruthenium as an electron acceptor. With these molecules we want to investigate how photoinduced electron transfer from a triarylamine to an excited Ru(II) complex is affected by F^- binding to a bridge containing mesitylboron. Ruthenium as metal center was chosen due to its favorable photophysical and electrochemical properties (see Chapter 1).

Long-range electron transfer processes have been investigated for several decades[42]. Long-range electron transfer may occur *via* a hopping or a tunneling mechanism. The electron hopping mechanism requires matching energy levels of the donor and the bridge. In this case the electron transfer from the donor to the acceptor moiety may reduce the bridge first before the electron is transferred to the acceptor. The distance dependence in this scenario is shallow. If the reduction of the bridge is thermodynamically unfavorable, a tunneling mechanism remains possible. In the past couple of years, scientists found direct evidence for the importance of the tunneling energy-gap that might be interpreted as the barrier height in donor(D)-bridge(b)-acceptor(A) systems. Semiclassical theory of electron transfer is useful to understand the reaction rates in this case (see equation 2.1).

$$k_{ET} = \sqrt{\frac{4\pi^3}{\hbar^2 \lambda k_B T}} \cdot H_{DA}^2 \cdot e^{-\frac{(\Delta G^\circ + \lambda)^2}{4\lambda k_B T}} \tag{2.1}$$

$\hbar$	Planck's constant
λ	reorganization energy
k_B	Boltzmann's constant
T	temperature
H_{DA}^2	electronic coupling between donor and acceptor and their products
$-\Delta G^\circ$	driving force

The electron transfer rate depends on three parameters: driving force, electronic coupling between the reactants (D, A) and their products (D^+, A^-) as well as the reorganization energy for the whole system. In 1961, McConnell developed a relationship for superexchange-assisted electron transfer[43] (equation 2.2).

$$H_{DA} = \frac{h_{Db}}{\Delta\varepsilon} \cdot \left(\frac{h_{bb}}{\Delta\varepsilon}\right)^{n-1} \cdot h_{bA} \tag{2.2}$$

|	
$\Delta\varepsilon$	tunneling energy gap
h_{Db}	coupling between donor and first bridging unit
h_{bb}	coupling between two adjacent bridging units
h_{bA}	coupling between last bridging unit and acceptor

Superexchange theory describes the coupling between a donor and an acceptor[44,45]. In McConnell's mathematical model donor and acceptor are separated by a bridge containing n identical molecules. The electronic factor depends on three electronic couplings: (1) on the coupling between the electron donor and the first bridging unit (h_{Db}), (2) coupling between two adjacent bridging molecules (h_{bb}) and (3) the coupling between the last molecule of the bridge and the electron acceptor (h_{bA}) as shown in figure 2.5.
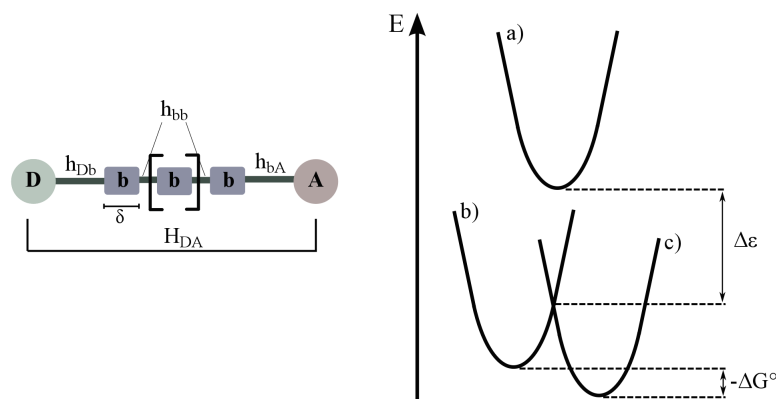
Figure 2.5 Illustration of the parameters in mathematical model from McConnell (equation 2.2). Energy levels: a) electron transfer (D^+-b^--A) or hole transfer (D-b^+-A^-), b) D-b-A, c) D^+-b-A^-.

The electronic coupling depends on the D-A distance as shown in equation 2.3[46].

$$H_{DA}^2 = H_{0DA}^2 \cdot e^{-\beta d} \tag{2.3}$$

The distance decay parameter β is a function of only three parameters as demonstrated in equation 2.4.

$$\beta = \frac{2}{\delta} ln(\frac{\Delta\varepsilon}{h_{bb}}) \tag{2.4}$$

δ length of one bridging unit

The previous equation 2.4 shows that the distance decay constant is a direct function of the tunneling energy gap (barrier height in D-b-A systems).

A hypothetical energy level scheme of a D-b-A system before and after fluoride addition is shown in scheme 2.1. Addition of fluoride to the boron atom leads to a rise of the LUMO from the bridge (contains the boron center). The bridge is now negatively charged. The reduction potential will be shifted to a highly negative potential. If a hopping mechanism is active before F^- binding, its barrier height is likely to increase significantly and might turn into a tunneling process. For tunneling processes the electron transfer distance dependence is steeper than for hopping processes. Hence the energy barrier height and width play a major role.
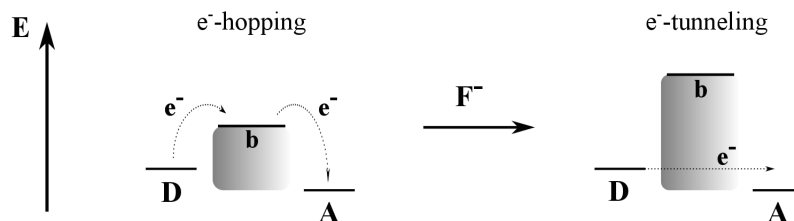
Scheme 2.1 Hypothetical energy scheme of a donor-bridge-acceptor system containing a boron site on the bridge. Before (left) and after (right) addition of fluoride .

2.2 Experimental

To investigate the aforementioned aspects two amine-boron-ruthenium dyads were synthesized. Dyad **1** is the longer molecule. It contains of a xylene unit between the triple bond and the ruthenium complex. The shorter molecule, further dyad **2**, contains two trifluormethyl substituents at two bpy ligands of the ruthenium complex.

Their molecular structures are shown in figure 2.6.
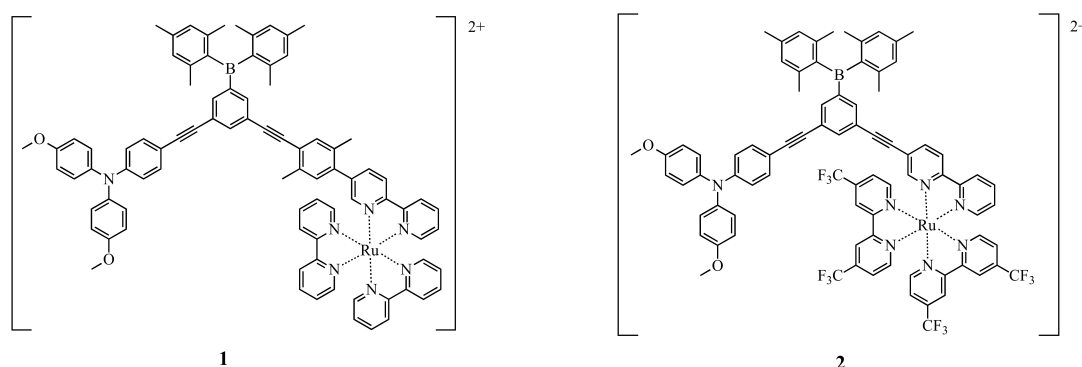
Figure 2.6 Long (**1**) and short (**2**) amine-boron-ruthenium dyad.

To synthesize these two dyads multiple steps are needed. In scheme 2.2 the shortened reaction pathway is shown. All amine compounds are marked with an **A**. All bipyridine molecules have a **B** and spacer molecules are named with **S**. Central molecules, ligands and complexes are numbered without a capital letter. For detailed reaction information see chapter 4 and 6.

To synthesize the boron-substituted central bridge (**12**) three reaction steps were needed (**a**). Starting with commercially available 1,3,5-tribromobenzene a Sonogashira-Hagihara reaction with MEBYNOL in dry triethylamine was applied to attach the alkyne moiety, then a lithiation with *n*-BuLi in dry diethylether is followed by a reaction with dimesitylfluoroborane to attach the boron part, and finally deprotection of the alkyne is achieved with NaH in dry toluene. To get the desired amine coupling compound **A-2**, two reaction steps are needed (**b**). The commercially available bis(*p*-anisyl)amine was reacted *via* a BHA with 1-bromobenzene in dry toluene. The next step is an iodination with [bis(trifluoroacetoxy)iodo]benzene in dry methylene chloride. The third coupling molecule is a bpy compound (**c**). First, the 5-bromo-2,2'-bipyridine further denoted as Br−bpy (**B-1**) was synthesized by a Negishi coupling of 2-pyridylzinc bromide with 5-bromo-2-iodopyridine in dry tetrahydrofuran. For bpy molecule **B-5**, Br−bpy (**B-1**) was coupled to B(OH)$_2$−xy−TMS (**S-2**) in tetrahydrofuran and water *via* a Suzuki coupling. Following the

replacement of the TMS protection group by iodine *via* ICl in dry methylene chloride and acetonitrile. For the synthesis of I–bpy (**B-3**) for dyad **2**, compound **B-1** was first treated with *n*-BuLi followed by addition of tributyltin chloride in diethylether. The resulting stannane was reacted with iodine in dry methylene chloride.
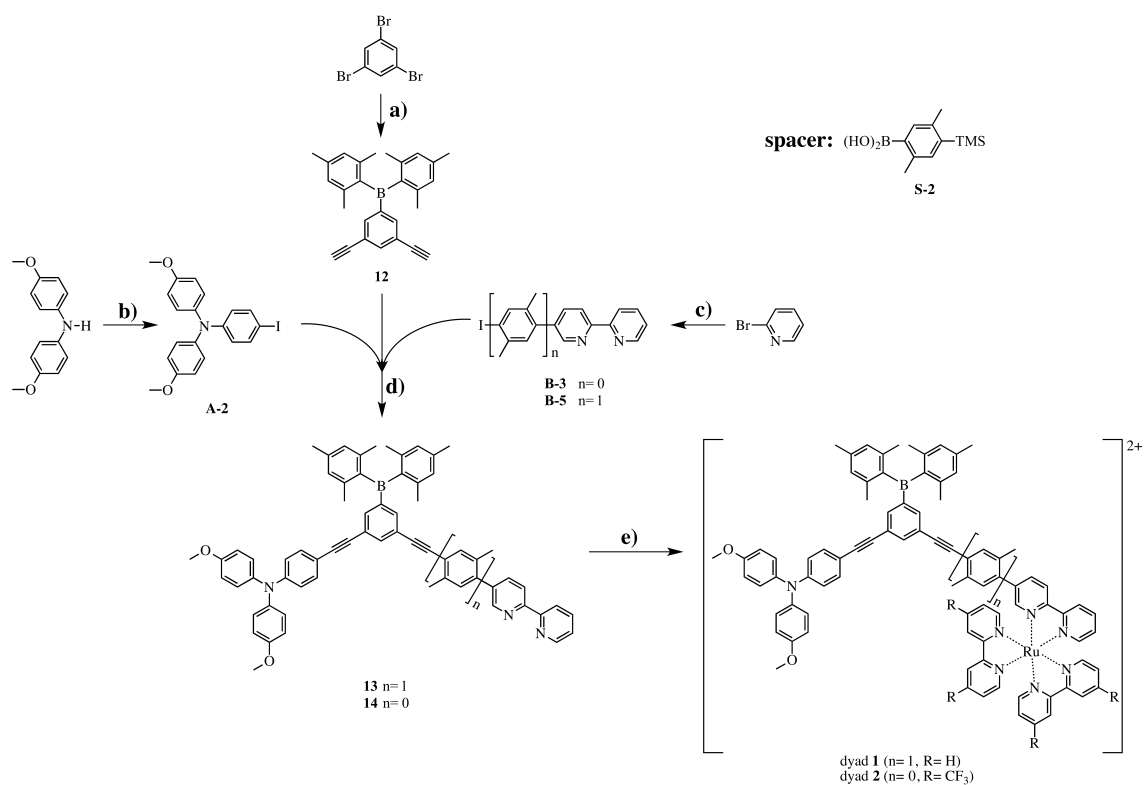

Scheme 2.2   Synthesis overview for dyads **1** and **2**.
a) 3-step synthesis: Sonogashira reaction with Pd(PPh$_3$)$_2$Cl$_2$, CuI, NEt$_3$ *n*-BuLi/FBmes$_2$, deprotection with NaH; **b)** 2-step synthesis: Buchwald-Hartwig amination (BHA) with NaO^{t}Bu, Pd(dba)$_2$, and (HP^{t}Bu)BF$_4$, iodination; **c)** 3-step synthesis: **n= 0**: Negishi coupling with Pd(PPh$_3$)$_4$, *n*-Buli/ClSn(*n*-Bu)$_3$, iodination; **n= 1**: Negishi coupling with Pd(PPh$_3$)$_4$, Suzuki reaction with B(OH)$_2$–xy–TMS (**S-2**) and Pd(PPh$_3$)$_4$, Na$_2$CO$_3$, iodination; **d)** one-pot Sonogashira reaction with Pd(PPh$_3$)$_2$Cl$_2$, CuI, NEt$_3$; **e)** complexation **n= 1** with Ru(bpy)$_2$Cl$_2$, **n= 0** with Ru(bpy(CF$_3$)$_2$)$_2$Cl$_2$ and AgNO$_3$.

The final ligands **13** and **14** were synthesized *via* a one-pot Sonogashira-Hagihara reaction in dry triethylamine (**d**). The last reaction step (**e**) to get the desired dyads **1** and **2** is a complexation with either Ru(bpy)$_2$Cl$_2$ or Ru(bpy(CF$_3$)$_2$)$_2$Cl$_2$ as precursor in dry methanol and chloroform. The complexation with the latter precursor has to be performed with silver nitrate to achieve good yields. Dyad **1** was synthesized *via* a twelve-step synthesis route. Dyad **2** was obtained in a ten-step synthesis.

The one-pot reaction to create the final ligands **13** and **14** also led to my reference molecule **R-1** which is shown in figure 2.7.
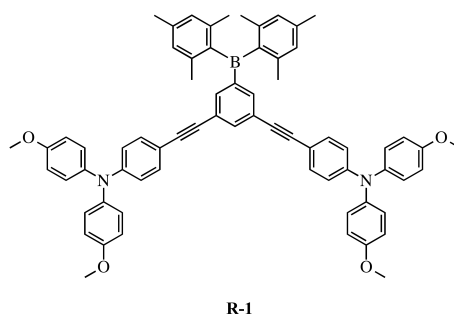
Figure 2.7 Reference molecule **R-1**.

The reference molecule **R-1** could also be synthesized *via* a Sonogashira-Hagihara coupling of the central molecule **12** with the amine compound **A-2**. The synthesis is described in the appendix.

2.3 Results

Dyad **2** is not only by 4 Å shorter than dyad **1** but it also differs in the ruthenium moiety. The distance between the amine and the ruthenium moiety in dyad **1** is approximately 22 Å whereas dyad **2** has a distance of approximately 18 Å. Those approximations were made on the basis of crystal structures of two related boron compounds (see appendix). The CF_3- groups in dyad **2** are electron withdrawing and therefore are expected to accelerate photoinduced electron transfer.

Due to some changes in the commercially available tetrabutylammonium fluoride solution (TBAF) upon standing, the reference molecule **R-1** was used to calibrate the actual F^- concentration of the commercial solution. The 1M TBAF solution in tetrahydrofuran was purchased from Sigma-Aldrich (in a Sure/Seal™ bottle).

2.3.1 Spectral absorption

First, the reference molecule **R-1** was treated with TBAF to confirm the concentration of the solution and to explore the behavior of triarylamine-triarylboron molecules as described in the literature[47]. Upon fluoride addition changes in the nitrogen-to-boron absorption band (N-B band, maximum at 356 nm) should occur as a result of the conjugation change in the molecules, as mentioned above. The UV/Vis spectra in methylene chloride of the reference molecule (figure 2.8) show that the characteristic N-B band is blue shifted to 351 nm by addition of fluoride and becomes more intense. One equivalent of fluoride is expected to bind to **R-1** which is consistent with the spectra. After one equivalent no further changes occur. The initially yellow solution turned colorless with one equivalent TBAF, the visible fluorescence was quenched.
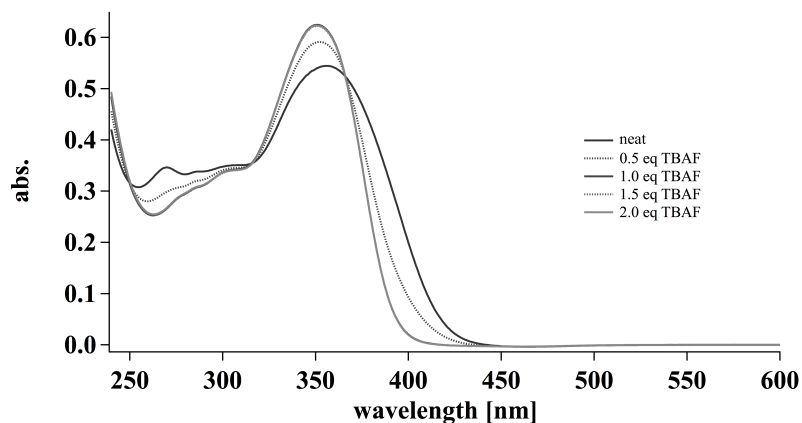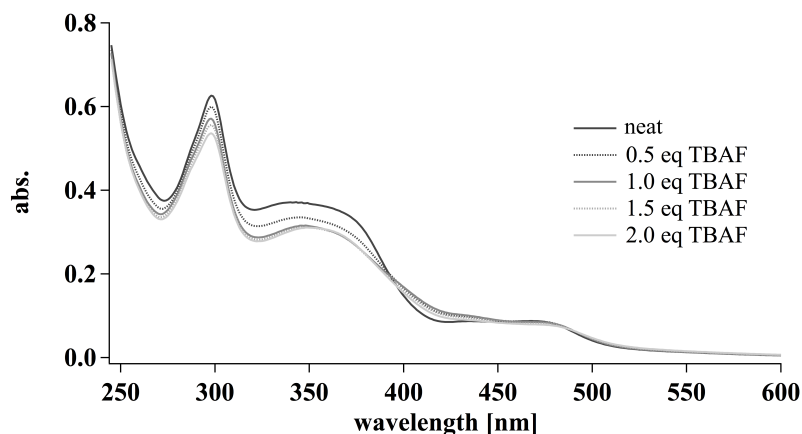
Figure 2.8   UV/Vis specta of **R-1** before and after TBAF addition (in CH_2Cl_2, c = 1 · 10^{-5} M, fluoride addition in 0.5 eq steps).

After the concentration of the TBAF solution was confirmed by **R-1**, the dyads were measured. Addition of fluoride to dyads **1** and **2** lead to a decrease in intensity of the N-B band around 370 nm. Even after one equivalent of TBAF has been added, the prominent bands around 290 nm (π-π^*), 460 nm (MLCT) and the N-B band changes (see figure 2.9 and 2.10).
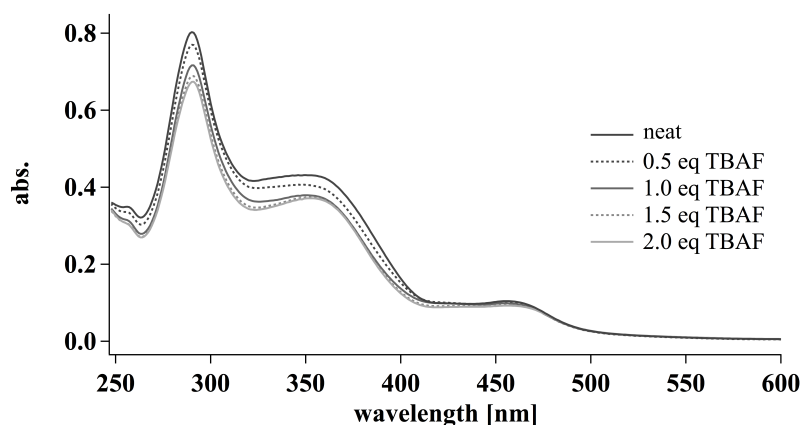
Figure 2.9   UV/Vis spectra of dyad **1** before and after TBAF addition (in CH_2Cl_2, c = 1 · 10^{-5} M, fluoride addition in 0.5 eq steps).


Figure 2.10   UV/Vis spectra of dyad **2** before and after TBAF addition (in CH_2Cl_2, c = 1 · 10^{-5} M, fluoride addition in 0.5 eq steps).

For determination of the fluoride binding constant (K_s) of the 1:1 adduct for dyads **1** and **2** equation 2.5 was used [48].

$$A = A_0 + \frac{A_{lim} - A_0}{2 \cdot c_0} \cdot \sqrt{c_0 + c_F + \frac{1}{K_s} - (c_0 + c_F + \frac{1}{K_s})^2 - 4 \cdot c_0 \cdot c_F} \qquad (2.5)$$

A   absorbance at the selected wavelength (370 or 375 nm) in the presence of fluoride (titrant)

A_0 absorbance of the sample at the selected wavelength (370 or 375 nm) in the absence of any fluoride

A_{lim} limiting absorbance value, obtained once the solution contains a large excess of fluoride

c_0 concentration of the dyad

c_F concentration of added fluoride (see x axes in figure 2.11)

The binding constant of fluoride anions to dyad **1** as well as **2** were determined under the same conditions in methylene chloride (see figure 2.11). The solid lines in figure 2.11 are the results of least-squares fits to the experimental data in methylene chloride with equation 2.5. The fluoride binding constant for dyad **1** is $K_s = 3.3 \pm 1.2 \cdot 10^6$ M^{-1} whereas fluoride binds to the shorter dyad **2** with $K_s = 3.1 \pm 0.2 \cdot 10^5$ M^{-1}. These binding constants are similar to published constants for mesitylboron molecules in apolar solutions [47].
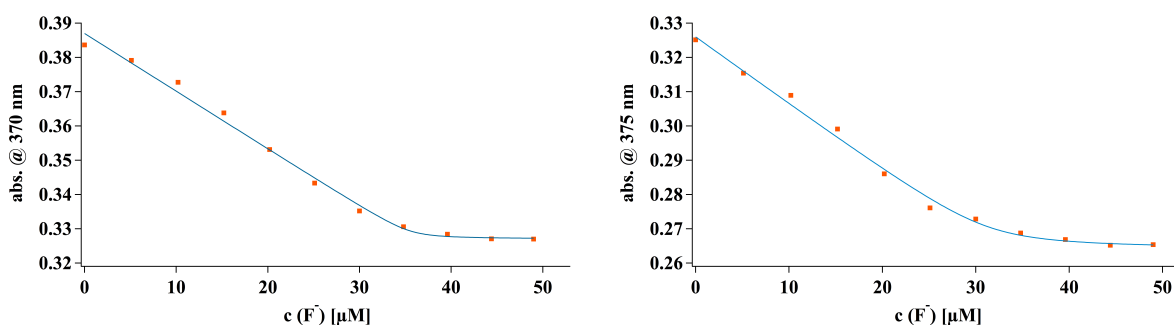
Figure 2.11   Binding constant determination of dyad **1** at 370 nm (left) and **2** at 375 nm (right figure) in the course of TBAF addition to $1 \cdot 10^{-5}$ M solutions in methylene chloride. The solid lines are least-squares fits to the experimental data with equation 2.5.

The reason why methylene chloride was used as solvent is that F$^-$ has a high binding affinity for mesitylboron under these conditions The binding constant for fluoride to both boron dyads in different solvents are summarized in table 2.1.

Table 2.1   Fluoride binding constant for dyads **1** and **2** in methylene chloride, acetonitrile, and dimethylformamide.

dyad	K_s [M^{-1}] (CH$_2$Cl$_2$)	K_s [M^{-1}] (CH$_3$CN)	K_s [M^{-1}] (DMF)
1	$3.3 \pm 1.2 \cdot 10^6$ [a]	$3.2 \pm 1.9 \cdot 10^4$ [c]	$3.2 \pm 1.2 \cdot 10^4$ [d]
2	$3.1 \pm 0.2 \cdot 10^5$ [b]	$1.3 \pm 0.5 \cdot 10^4$ [d]	$4.8 \pm 3.3 \cdot 10^4$ [e]

Absorbance detected at: [a] at 370 nm, [b] at 375 nm, [c] at 345 nm, [d] at 350 nm, [e] at 360 nm.

Another reason for chosing methylene chloride as a solvent are the small absorption changes in the UV/Vis spectra after one equivalent of fluoride. In acetonitrile or dimethylforamide further significant absorption changes after one equivalent were observable (UV/Vis spectra, see appendix).

In the data from figure 2.12 Ru(bpy)$_3$(PF$_6$)$_2$ in methylene chloride was treated with TBAF. The π-π^* band at 290 nm changed constantly. In the MLCT band the absorbance decreased as well. The reason

for this might be an interaction between the negatively charged fluoride anion and the double positively charged metal center. This could explain why there are still changes in the spectrum for dyads **1** and **2** after one equivalent fluoride whereas in the reference molecule those changes do not occur.
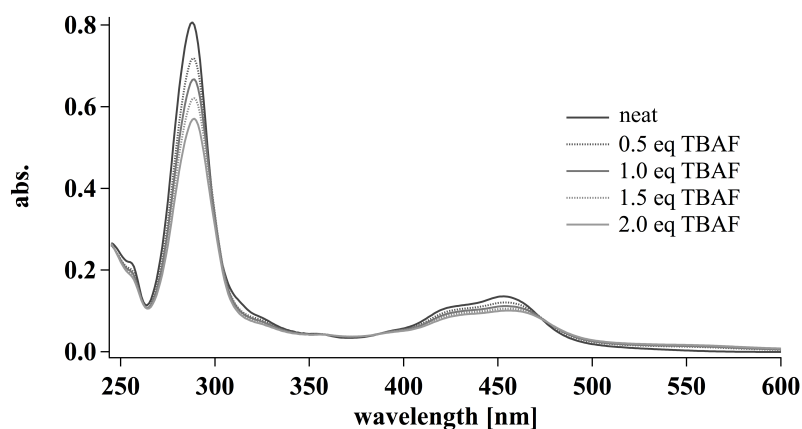
Figure 2.12   UV/Vis spectra of $Ru(bpy)_3(PF_6)_2$ before and after TBAF addition (in CH_2Cl_2, c = $1 \cdot 10^{-5}$ M, fluoride addition in 0.5 eq steps).

Direct comparison between the long dyad (**1**) and $Ru(bpy)_3(PF_6)_2$ shows an almost identical absorbance decrease at 290 nm (figure 2.13). Upon addition of the first fluorides both curves are not identical due to the overlap of the π-π^* band with the N-B band.
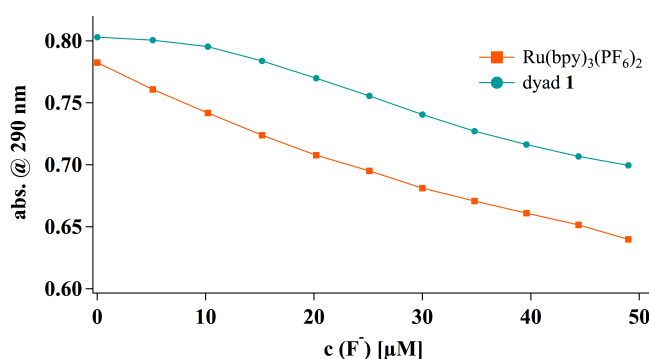
Figure 2.13   Absorbance change at 290 nm of dyad **1** (blue) and $Ru(bpy)_3(PF_6)_2$ (orange) in the course of TBAF addition to $1 \cdot 10^{-5}$ M solutions in methylene chloride.

2.3.2 Steady-state luminescence spectroscopy

Luminescence quenching can be observed when efficient PET takes place. In figure 2.14 the normalized luminescence spectra of $Ru(bpy)_3(PF_6)_2$ and dyad **1** (blue traces) compared to $Ru(bpy(CF_3)_2)_3(PF_6)_2$ and dyad **2** (green traces) are shown. Dyad **1** and $Ru(bpy)_3(PF_6)_2$ have their maxima at around 600 nm whereas the attachment of two CF_3-groups in 4,4'-position at the bpy result in a red shift by approximately 30 nm. Figure 2.14 also shows that the luminescence intensity of the reference complex $Ru(bpy(CF_3)_2)_3(PF_6)_2$ is weaker compared to $Ru(bpy)_3(PF_6)_2$. Therefore dyad **2** can not be compared to $Ru(bpy)_3(PF_6)_2$. The luminescence for both dyads (**1** and **2**) is quenched by approximately 90 %.
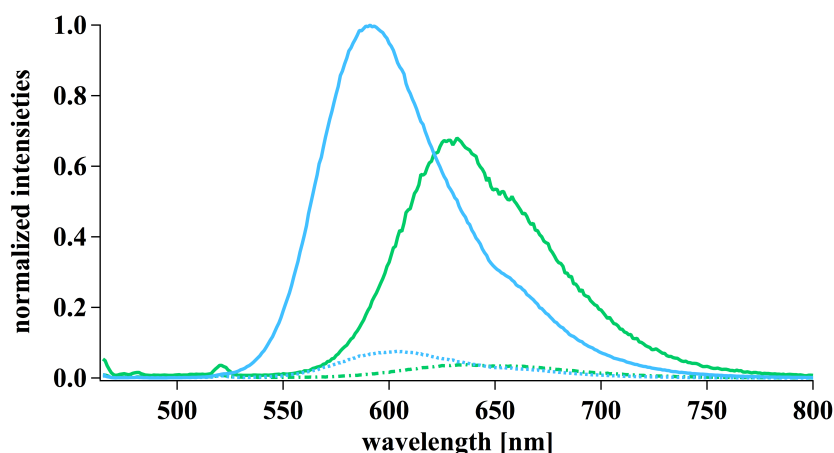
Figure 2.14 Normalized steady-state luminescence for dyad **1** (dashed blue line) and $Ru(bpy)_3(PF_6)_2$ (solid blue trace) compared to dyad **2** (dash-dotted green line) and $Ru(bpy(CF_3)_2)_3(PF_6)_2$ (solid green trace) (c = $1 \cdot 10^{-5}$ M in CH_2Cl_2, excitation: 450 nm).

The emission of dyad **1** is quenched efficiently. This quenching could be an indication of a strong intra-molecular PET. Also the luminescence of dyad **2** is quenched. The shoulders at around 650 nm are caused by the instrument and not by the compounds.

These results suggest that in my dyads **1** and **2** PET takes place.

2.3.3 Electrochemistry

Cyclic voltammograms were recorded in deoxygenated acetonitrile ($Ru(bpy)_3(PF_6)_2$, dyad **1**, dyad **2**, and compound **12**) or dry methylene chloride (for reference molecule **R-1**, see appendix) at room temperature. Measurement conditions are summarized on page 75.
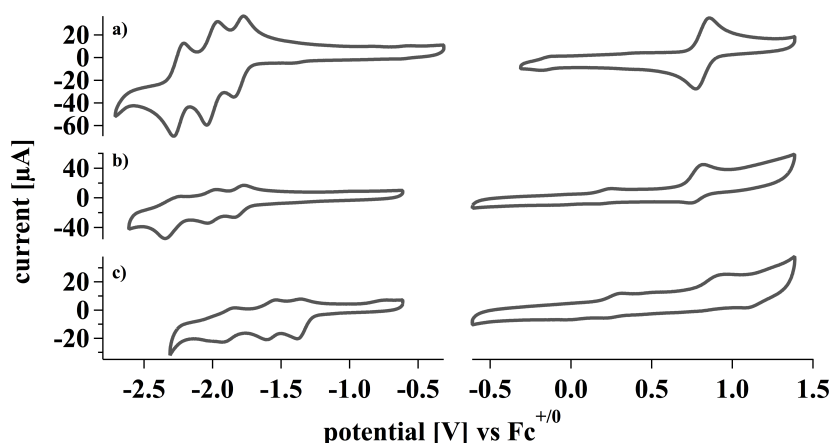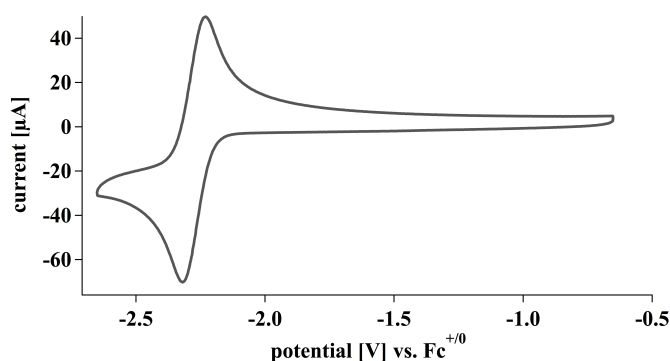

Figure 2.15 CV of $Ru(bpy)_3(PF_6)_2$ (a), dyad **1** (b), and dyad **2** (c). Mesurements were performed in CH_3CN with $Fc^{+/0}$ as internal reference.

In figure 2.15 the reversible oxidative waves of the ruthenium couple $Ru^{III/II}$, expected around 0.9 V vs. $Fc^{+/0}$ [49] and triarylamine (amine$^{+/0}$), expected around 0.3 V vs. $Fc^{+/0}$ [50] are visible. In addition, one observes the reduction waves of unsubstituted bpy which should occur between -1.68 and -2.15 V vs. $Fc^{+/0}$. In complexes with CF_3- groups attached to the bpy ligand the potentials shift to more positive values. The first reduction of 4,4'-trifluoromethyl-2,2'-bpy in a ruthenium complex should occur at -0.45

vs. Fc$^{+/0}$[49]. Unfortunately, the oxidation of ruthenium in dyad **2**, which is expected between 1.25 V and 1.37 V vs. Fc$^{+/0}$[49], was not observable. The second wave in the oxidation part of dyad **2** is the irreversible second oxidation of the amine which is also well known from the literature. In table 2.2 all potentials are summarized.

The reduction of the boron center which should be observable at around -2.6 V vs. Fc$^{+/0}$[51] was not detectable. Due to the lack of the boron related wave, an attempt to measure the respective reduction in the alkyne$-$Bmes$_2$$-$alkyne (**12**) reference compound was made.

Figure 2.16 CV of compound **12** in CH$_3$CN.

In figure 2.16 the additional CV of alkyne$-$Bmes$_2$$-$alkyne in deoxygenated acetonitrile is shown. This voltammogram shows that the reversible boron wave at -2.3 V vs. Fc$^{+/0}$ is in the range of the bpy reduction. It is possible that it overlaps with the reduction wave in dyads **1** and **2**. This might explain why in the dyads it was not possible to detect.

Upon addition of one equivalent of fluoride, the oxidative waves for the amine and ruthenium part turned into a broad and undefined wave (see appendix). Even the reductive waves became poorly defined. The goal was to see a shift of the boron reduction wave as described in scheme 2.1. Unfortunately, this shift was not observable. For Ru(bpy)$_3$(PF$_6$)$_2$ no real changes in the reductive waves were detectable and this is shown in figure 2.17. The new waves at 0.2 V and 0.7 V might be caused by impurities associated with the *t*-butyl solution.
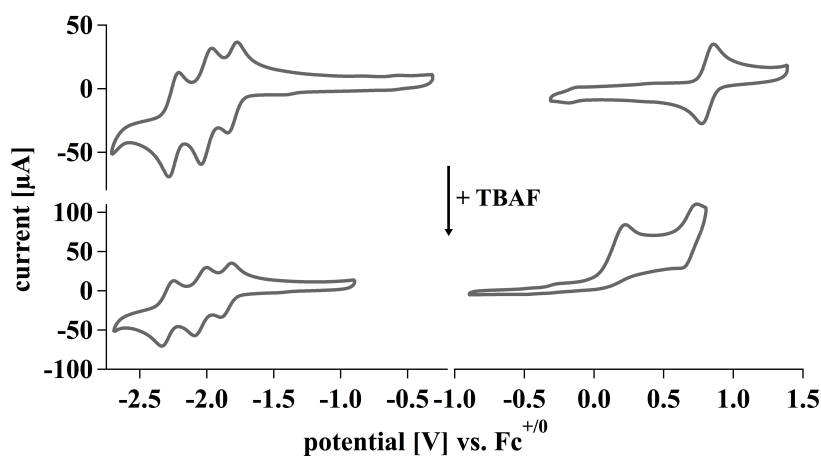
Figure 2.17 CV of Ru(bpy)$_3$(PF$_6$)$_2$ without and with 1 eq TBAF in acetonitrile.

In table 2.2 all electrochemical potentials in Volts vs. Fc$^{+/0}$ for the aforementioned compounds measured

in deoxygenated acetonitrile or methylene chloride are summarized.

Table 2.2 Electrochemical potentials in Volts vs. $Fc^{+/0}$ for boron compounds **1**, **2**, **12**, **R-1**, and $Ru(bpy)_3(PF_6)_2$ without TBAF.

Compound	$E(amine^{+/0})$ [V]	$E(Bmes_2^{0/-})$ [V]	$E(Ru^{3+/2+})$ [V]	$E(bpy^{0/-})$ [V]
$Ru(bpy)_3(PF_6)_2{}^a$	-	-	0.8	-1.8
compound **R-1**^{b}	0.1	-	0.8	-
compound **12**^{a}	-	-2.3	-	-
dyad **1**^{a}	0.2	-	0.8	-1.8
dyad **2**^{a}	0.2	-	*	-1.3

* could not be determined, ^{a} measured in deoxygenated acetonitrile, ^{b} measured in deoxygenated methylene chloride

With those measured potentials an estimation of the driving force (ΔG_{ET}) for PET in both boron dyads is possible. The driving force for PET can be calculated according to equation 2.6.

$$\Delta G_{ET} = e \cdot (E_{ox} - E_{red}) - E_{00} - \frac{e^2}{4\pi\varepsilon_0\varepsilon_s R_{DA}} \qquad (2.6)$$

e	elemental charge ($1.6022 \cdot 10^{-19}$ C)
E_{ox}	oxidation potential for triarylamine
E_{red}	reduction potential for ruthenium complex (ligand-based)
E_{00}	energy of the photoactive ^{3}MLCT state (2.12 eV for $Ru(bpy)_3{}^{2+}$)
ε_0	vacuum permittivity ($8.854 \cdot 10^{-12}$ $\frac{C}{V \cdot m}$)
ε_s	dielectric constant of the solvent (CH_2Cl_2: 8.93, CH_3CN: 35.94)
R_{DA}	donor-acceptor distance (center to center)

Because of the high binding affinity of F^- in CH_2Cl_2, methylene chloride is the favorable solvent. The calculation of ΔG_{ET} based on equation 2.6 by using the redox potentials shown in tables 2.2 and 7.1 (see chapter 7) yields a driving force of -0,19 eV for dyad **1** and -0,70 eV for dyad **2** (see table 2.3). When changing the dielectric constant of methylene chloride to that of acetonitrile, PET between the ruthenium and the amine moiety remains exergonic.

Table 2.3 Driving force estimation of dyads **1** and **2** in two different solvents according to equation 2.6.

| Dyad	R_{DA} [Å]	ΔG_{ET} (CH_3CN) [eV]	ΔG_{ET} (CH_2Cl_2) [eV]
1	22	-0.14	-0.19
2	18	-0.64	-0.70

These results are in agreement with the observations made in the luminescence spectroscopy. Both boron dyads are able to perform PET. The upcoming scheme (2.3) shows the possible photoinduced electron transfer pathways for dyad **1**.
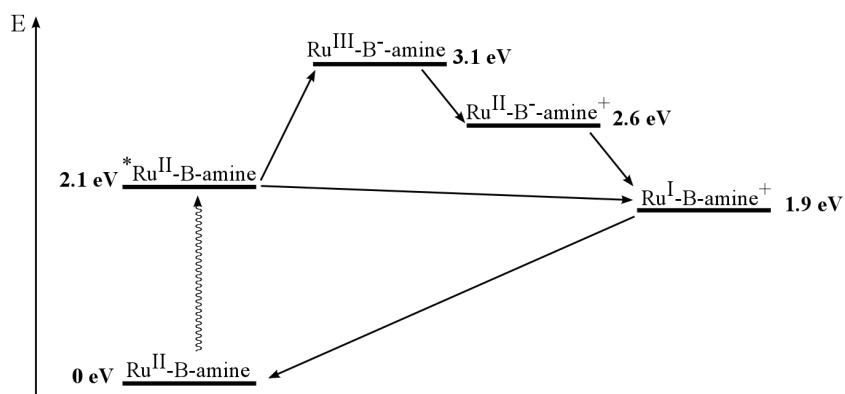
Scheme 2.3 Energy diagram for PET in dyad **1**. B stands for the boron part.

First, the ground state Ru^{II}-B-amine is excited by light and forms $^*Ru^{II}$-B-amine. In principle, this intermediate can undergo two different pathways. In one hypothetical pathway the ruthenium complex is oxidized while the boron substituted bridge is reduced and Ru^{III}-B^--amine is formed. In the subsequent step, Ru^{III}-B^--amine will then transfer an electron from the amine to the ruthenium moiety which results in Ru^{II}-B^--amine$^+$. This path requires 1.0 eV to form Ru^{III}-B^--amine. This is not possible at room temperature (thermal energy: 0.02 eV). In the second hypothetical pathway, an electron of the excited ruthenium species ($^*Ru^{II}$-B-amine) is transferred intramolecularly from the amine to the ruthenium complex. In this pathway, the excited ruthenium complex is quenched reductively. The resulting intermediate (Ru^I-B-amine$^+$) is exergonic by 0.2 eV and therefore more favorable. The final step is the relaxation to the initial oxidation states *via* thermal charge recombination.

In scheme 2.4 the analogous energy diagram for PET in dyad **2** is shown.
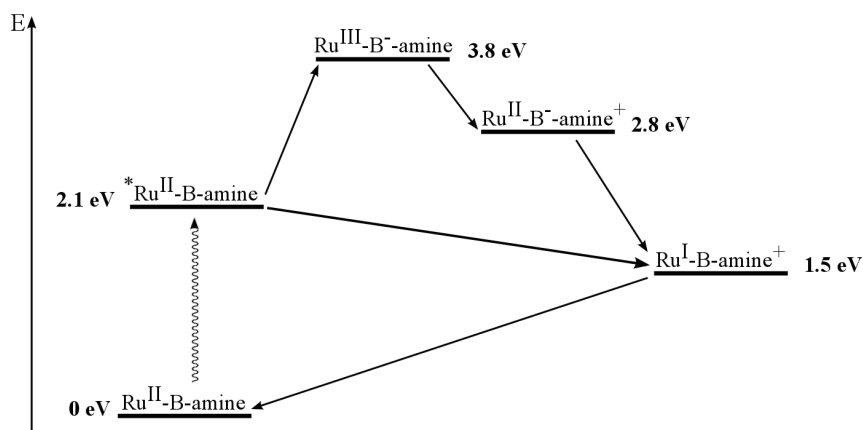
Scheme 2.4 Energy diagram for PET in dyad **2**. B stands for the boron part.

Like in dyad **1**, in dyad **2** the initial step is the formation of the excited state by light. The resulting species ($^*Ru^{II}$-B-amine) can undergo two possible pathways. One way is the oxidation of the ruthenium moiety and simultaneous reduction of the boron-substituted bridge (Ru^{III}-B^--amine). As mentioned before, the attached CF_3-groups cause a shift of the oxidation potential by 0.4 V to more positive values. Therefore the formation of Ru^{III}-B^--amine is more endergonic (0.7 eV) than for dyad **1**. Following, the electron can be transferred intramolecularly from the amine to the ruthenium part and Ru^{II}-B^--amine$^+$ is formed. The described hypothetical pathway requires in the initial step 1.7 eV and is highly endergonic.

This is the reason why this path is not energetically favorable. In the second hypothetical pathway, the excited species transfers one electron intramolecular from the amine to the ruthenium complex resulting Ru^I-B-amine$^+$. Like dyad **1**, this step is exergonic (0.6 eV). Finally, the formation of the initial ground states out of the Ru^I-B-amine$^+$ state is very exergonic.

For both boron dyads the formation of reduced ruthenium and oxidized amine is favored. This should be observable in transient absorption spectroscopy.

2.3.4 Transient absorption spectroscopy

To obtain definite proof that PET in our donor-bridge-acceptor systems does take place, transient absorption spectroscopy is a useful method. Transient absorption (TA) spectroscopy is a powerful method for studies of dynamic photochemical processes and monitors absorption changes induced by flash excitation. The changes are measured as a function of time or wavelength. *Via* transient absorption spectroscopy the detection of photoproducts which are formed after flash excitation by a laser pulse is possible. $Ru(bpy)_3^{2+}$ can be used as standard for direct comparison of results obtained in different laboratories or on different setups[52].

Photoexcitation of the neat dyads at 532 nm, based on the electrochemical data mentioned above, should lead to the formation of Ru^+ and amine$^+$. Amine oxidation and bpy reduction spectra were measured separately to compare them with the obtained TA spectra. The reference spectra of the bpy reduction to observe the formation of Ru^I was obtained *via* spectroelectrochemistry in acetonitrile. A $1 \cdot 10^{-4}$ M solution of the dyad was used. 0.1 M $(Bu_4N)PF_6$ solution was used as the electrolyte. A potential of -1.8 (dyad **1**) and -1.5 V (dyad **2**) vs. $Fc^{+/0}$ respectively, was applied to measure the optical spectrum after the first bipyridine reduction. The amine oxidation reference spectra were measured by spectroelectrochemistry as well. A potential of 0.2 V vs. $Fc^{+/0}$ was applied to measure the first amine oxidation.

The common features associated with the ^{3}MLCT excited state of $Ru(bpy)_3^{2+}$ are absorption maxima around 375 and 545 nm caused by the bpy radical anion, and a ground state bleach around 450 nm[53].
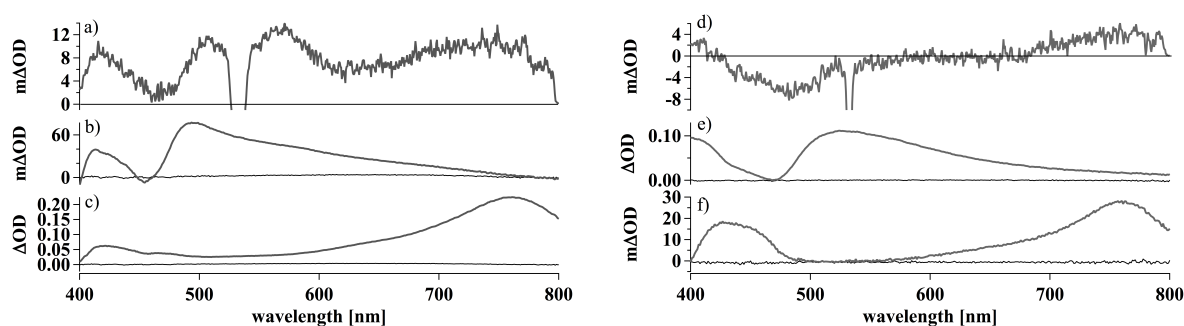

Figure 2.18 Transient absorption spectra of dyads **1** (left) and **2** (right) compared to data obtained from spectroelectrochemistry. Transient absorption spectra were measured in methylene chloride. Amine oxidation and bpy reduction were measured *via* spectroelectrochemistry in acetonitrile with $(Bu_4N)PF_6$ as electrolyte. Dyad **1** (left): a) transient absorption spectra, b) bpy reduction, and c) amine oxidation. Dyad **2** (right): d) transient absorption spectra, e) bpy reduction, and f) amine oxidation.

Both transient absorption spectra (a and d in figure 2.18) were measured in a time range of 40 ns. The transient absorption spectra were measured in aerated methylene chloride solution with a concentration of $1 \cdot 10^{-4}$ M of both boron dyads. The TA spectrum of dyad **1** shows positive signals around 400,

550 and 750 nm. In the TA spectrum of dyad **2** a bleach around 480 nm and a positive signal around 750 nm are observable. The bpy reduction of dyad **1** is indicated by signals around 415 and 495 nm (see spectra b) in figure 2.18). The signals for reduced bpy for dyad **2** occur around 400 nm and 520 nm (see spectra e) in figure 2.18). The oxidized triarylamine has a prominent signal at 750 nm and a weaker signal around 400 nm as shown in spectra c) and f) (figure 2.18) which is in agreement with the literature[54]. The sharp signal at 532 nm in both transient absorption spectra is caused by the laser pulse. Comparison of the spectrocelectrochemistry data with the TA spectra supports the hypothesis that the photoinduced formation of Ru^+ and $amine^+$ take place. This is in agreement with the energy diagram (figure 2.3) where the formation of Ru^I-B-$amine^+$ is favorable.

In figure 2.19 kinetic absorption decays at 415 nm, 560 nm and 750 nm for dyad **1** (left figure) as well as the decays on the right of dyad **2** (480 nm, 750 nm) are shown. This indicates that all selected signals of each dyad belong to the same charge separated state.
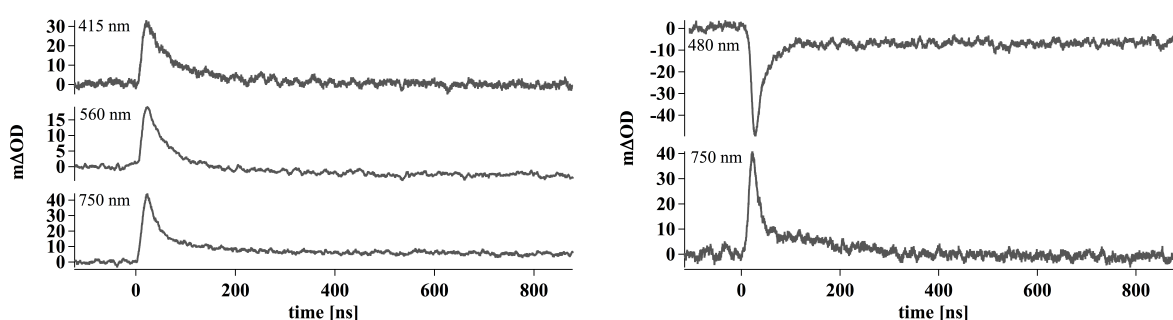
Figure 2.19   Kinetic absorption decays for dyads **1** (left) and **2** (right).

The formation of the charge separated state for dyads **1** and **2** is complete within the 10 ns laser pulse whereas the recovery occurs in a biexponential fashion.

At 415 nm in dyad **1** (figure 2.19) the lifetime of the short lived species is 38 ns whereas the long lived species lives 170 ns. The lifetime of the long lived part is close to $Ru(bpy)_3(PF_6)_2$ (τ =164 nm). This indicates that excited ruthenium(II) decays either in a nonradive or radiative way instead of electron transfer. The short decay might belong to the PET reaction. The decay at 560 nm shows a short lived part (28 ns) and a longer lived part (240 nm). The long lived part suggests that ^{3}MLCT decay of a luminescence $Ru(bpy)_3(PF_6)_2$ impurity is detected. The short lived part might be evidence for a PET reaction.

In dyad **2** the decay of the transient absorption signal at 480 nm has a short lived part with a lifetime of 9 ns which is within the duration of the laser pulse. The long lived part does not decay completely in this time window. Therefore an estimation of the lifetime is not possible. At 480 nm the ^{3}MLCT absorption of the ruthenium complex is present. This means that the temporal evolution of this transient absorption signal comprises two species. At 750 nm $amine^+$ decays within the laser pulse whereas the long lived part consists of a lifetime of 177 ns.

As mentioned before the short lived species might be evidence for PET whereas the long lived part shows a nonradiative or radiative like the free $Ru(bpy)_3(PF_6)_2$ complex. In a $1 \cdot 10^{-4}$ M solution bimolecular quenching processes are more likely than in more diluted solutions.

In table 2.5 all lifetimes at the aforementioned wavelengths are summarized.

Table 2.4 Lifetimes of dyads **1** and **2** at different wavelength.

| Dyad	Wavelength [nm]	Recovery lifetime τ_1 [ns]	Recovery lifetime τ_2 [ns]
1	415	35	170
	560	28	240
	750	17	170
2	480	9	-
	750	9	177

As described on page 13 the barrier height for ET in both dyads should increase upon fluoride addition. This can cause two possible scenarios. Either the PET is blocked completely so no amine$^+$ is generated. Therefore the amine$^+$ signal at 750 nm is not present anymore. The second scenario is a slight variation of the barrier height resulting a slower formation of amine$^+$. Upon addition of fluoride *via* TBAF solution we hoped to see changes in the amine$^+$ signal around 750 nm. In figure 2.20 the TA spectra before and after addition of one and two equivalents of TBAF are shown.
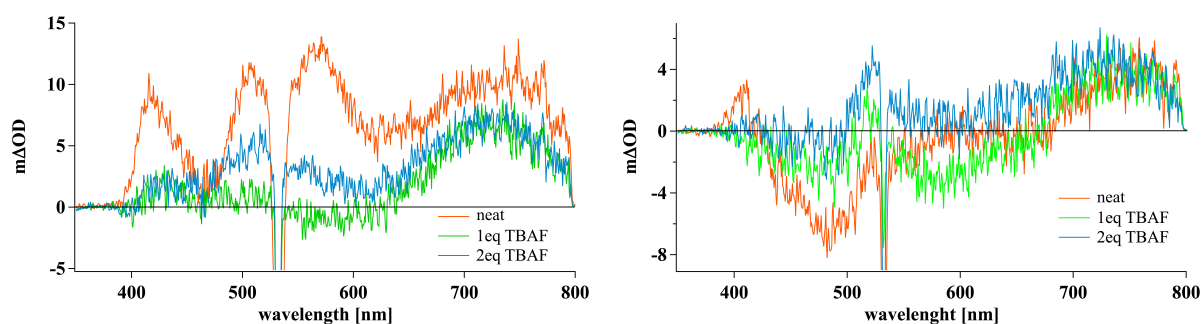
Figure 2.20 Transient absoprption spectra for dyads (**1**) (left) and (**2**) (right) in CH_2Cl_2.

The transient absorption spectra of dyad **1** shows no changes in the shape of the amine band whereas in dyad **2** the maximum of the amine band shifts from 750 nm to 700 nm. These observations rule out the scenario of a completely blocked PET. Fluoride addition to dyad **2** lead to a less negative signal around 500 nm. This signal might be caused by the ^{3}MLCT absorption of the ruthenium complex. Fluoride addition to dyad **1** resulted in a color change of the solution (see figure 2.21). Dyad **2** showed the same color change.
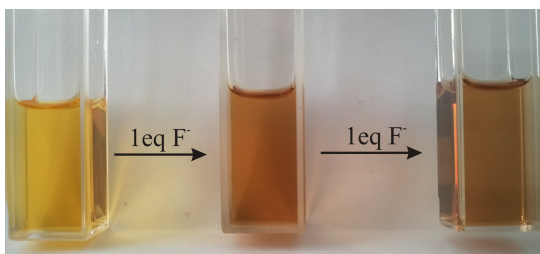
Figure 2.21 Picture of the color change before and after addition of 1 and 2 eq TBAF to dyad **1**.

The kinetic absorption spectra at 750 nm for both dyads showed a biexponential decay (see figure 2.19). In dyad **1** the intensity of the signals decreases upon TBAF addition but the shape does not change. The intensity of the short lived species in dyad **2** decreased by addition of fluoride whereas the formation of the amine$^+$ still takes place within the duration of the laser pulse as shown in figure 2.22.
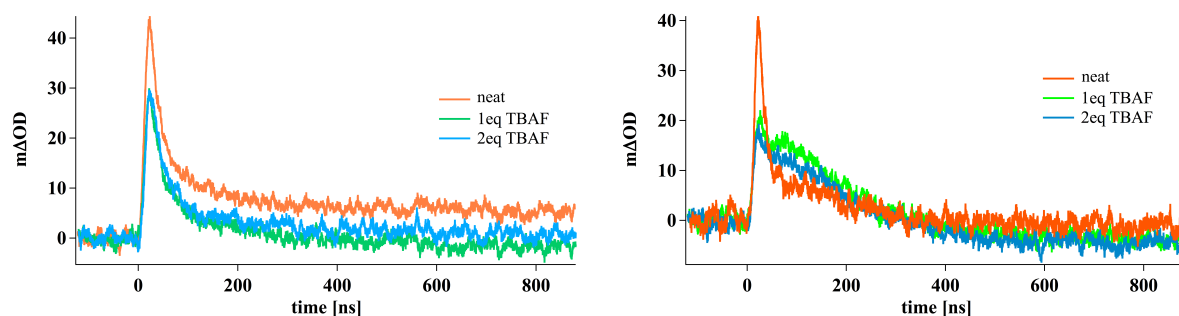
**Figure 2.22**   Kinetic absorption at 750 nm of dyads **1** (left) and **2** (right) upon fluoride addition.

We assumed that the short lived species showed the desired formation of Ru^{I}-B-amine^{+} which could be confirmed in the TA spectra that were measured in a 40 ns window (see figure 2.18). Upon fluoride addition, the intensity of this short lived species decreases and the long lived part becomes more prominent. Also the shape of the long lived part changes upon addition of TBAF. This might be evidence that the amine^{+} recombination becomes slower.

Table 2.5   Recovery lifetimes τ of dyads **1** and **2** at 750 nm before and after 1 and 2 eq TBAF.

Dyad	0eq TBAF		1eq TBAF		2eq TBAF	
	τ_1 [ns]	τ_2 [ns]	τ_1 [ns]	τ_2 [ns]	τ_1 [ns]	τ_2 [ns]
1	17	170	24	261	27	244
2	9	177	12	170	-	212

2.3.5 Flash-quench experiments

As mentioned before, $Ru(bpy)_3^{3+}$ is a better electron acceptor than $Ru(bpy)_3^{2+}$. $Ru(bpy)_3^{3+}$ had to be generated photochemically to trigger intramolecular charge transfer. This can be done by a so called flash-quench technique, as illustrated in scheme 2.5. With this method investigations of long-range charge transfer in proteins were carried out[55]. I hoped to get more insight into intramolecular electron transfer in dyads **1** and **2** with this method.
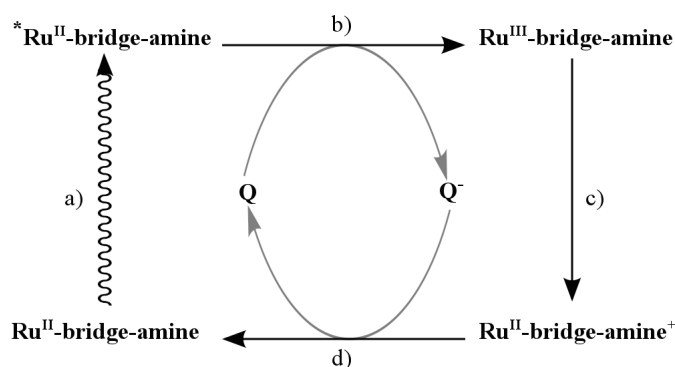

Scheme 2.5   Illustration of the flash-quench technique. a) Photoexcitation, b) "quenching" step, c) intramolecular charge transfer, and d) recombination.

First, photoexcitation (a), so called "flash", of the ruthenium moiety takes place. The ^{3}MLCT excited state of $Ru(bpy)_3^{2+}$ is oxidatively quenched in a bimolecular way by a proper electron acceptor (Q) like methylviologen dication (MV^{2+}). Upon addition of Q in a high concentration (MV^{2+}: 50 up to 80 mM)

the "quenching" step (b) occurs within a time range of a nanosecond laser pulse. Assuming that the intramolecular charge transfer is slow, it might be possible to observe a maximal amount of Ru^{III} and the quencher, in its reduced form (Q^-), immediately after the laser pulse. Subsequent intramolecular charge transfer (c) leads to the reduction of Ru^{III} to Ru^{II} and oxidation of amine to amine$^+$. In the final step (d), the reduced quencher reacts with the oxidized dyad back to its initial ground state.

In my case the flash-quench method had to be carried out in methylene chloride due to the higher fluoride binding constants obtained from UV/Vis titrations (see page 15). Many molecules are known as suitable quenchers. As shown in figure 2.23 there are the viologens (methylviologen (MV), benzylviologen (BV), and octylviologen (OV)), tetracyano compounds (tetracyanoethylene (TCNE)), tetracyanobenzene (TCNB), tetracyanoquinone (TCNQ)), quinones (benzoquinone (BQ), anthraquinone (AQ), substituted AQ (AQ-R)), nitro compounds, and NDI.
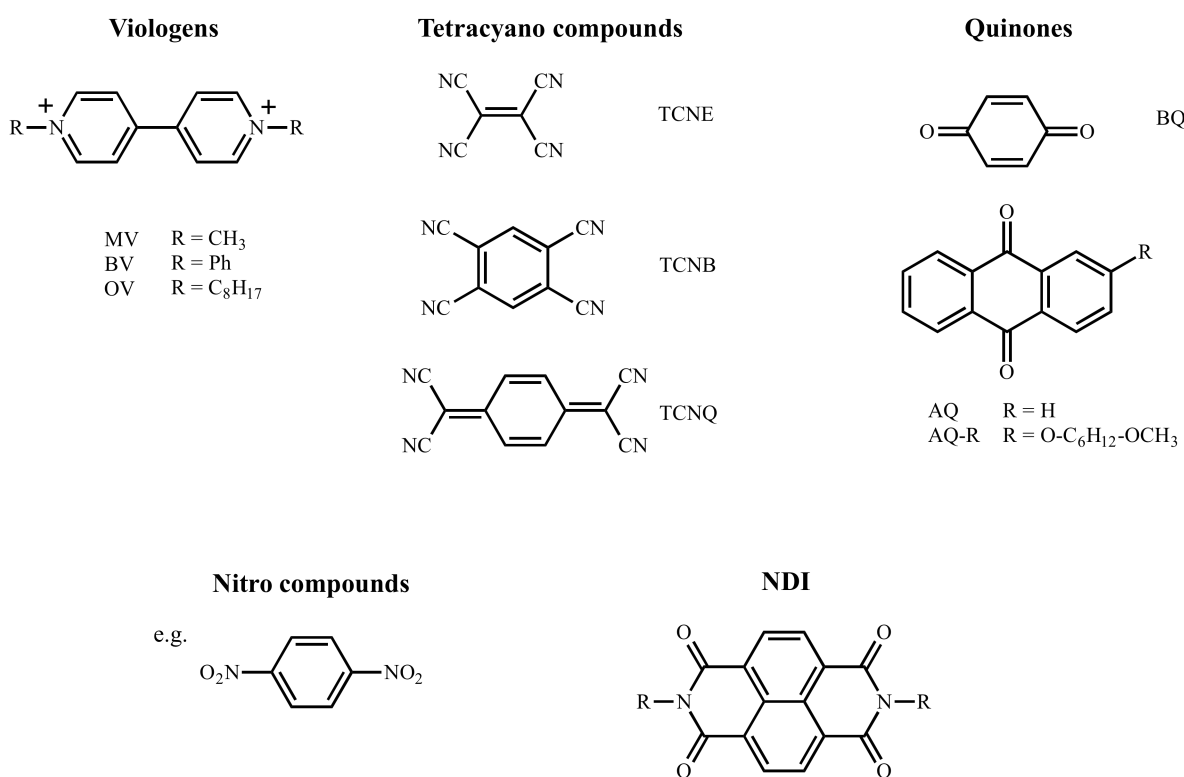
Figure 2.23   Possible electron acceptors for the flash-quench technique.

These quenchers work efficiently in different solvents. Unfortunately, not all of them are soluble in methylene chloride. In the flash-quench technique it is important that the electron acceptor does not react with the titrant (TBAF). Those reactions can result in a color change of the solution. In my case some quenchers already changed color even by addition of dyad **1**. The color change for TCNQ and TCNE might be caused by complexation of one of the cyanide groups of the quencher to ruthenium of dyad **1**[56]. Those quenchers were eliminated directly. With fluoride addition all solutions changed color. In table 2.6 all tried quenchers with their quenching abilities and color changes are summarized.

Table 2.6 Quencher for flash-quench technique and observed color changes upon fluoride addition.

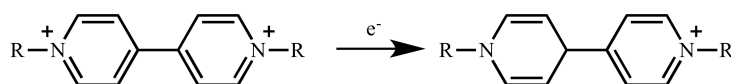| Quencher (Q)	Quenching ability in CH$_2$Cl$_2$	Quenching ability in CH$_3$CN	Color compound + Q	Color upon fluoride addition
MV(PF$_6$)$_2$	not soluble	good	yellow[b]	blue precipitate[b]
BV(PF$_6$)$_2$	not good soluble	-	yellow[a]	-
OV(PF$_6$)$_2$	not good soluble	-	yellow[a]	-
TCNE	-	good	orange-red[b]	greenish-brown[b]
TCNB	no quenching	good	yellow[b]	orange-red[b]
TCNQ	good	-	greenish[b]	greenish[b]
BQ	-	good	yellow[b]	dark brown[b]
AQ	not soluble	-	-	-
AQ-R	good	no quenching	yellow[a]	orange-brown[a]
CCl$_3$Br	-	no quenching	yellow[a]	-

[a] Tested with Ru(bpy)$_3$(PF$_6$), [b] Tested with dyad **1**, (-) not tested.

In the case of methylviologen a blue precipitate occurred. This precipitate is the mono cationic species of the viologen. In all viologens the initially yellow solution of Ru(bpy)$_3$(PF$_6$) or dyad **1** changed to blue or green upon addition of F$^-$. This behavior could also not be eliminated by changing the ion source. TBAF was exchanged by crown ether salts like K[18-crown-6]F or Rb[18-crown-6]F, tetrabutylammonium cyanide or tetramethylammonium fluoride.

All changes in color belong to one of the following three major phenomena (see figure 2.24):

1) Reduction: Viologens are reduced by amine impurities present in TBAF and led to the mono cationic species which is blue.

2) Nucleophilic aromatic substitution: The nitro groups are substituted by fluoride upon TBAF addition.

3) Ionic interactions: NDI, tetracyano compounds and quinones interact with an aryl with fluoride which lead to a color change to red.
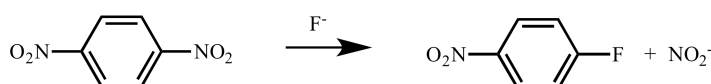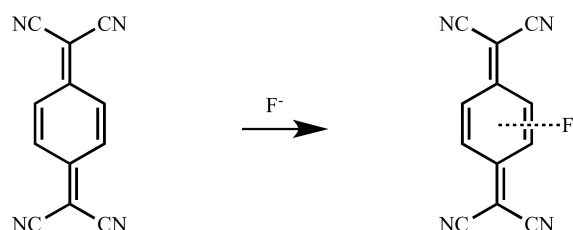

Figure 2.24 Three major phenomena by addition of fluoride anions to quenchers.

In the literature it is well known that TBAF can reduce MV^{2+} [57,58]. The nitrile compounds have been investigated upon fluoride addition as well. $TCNQ^{[59]}$ can participate in anion-π interactions with its benzene rings and fluoride anions like shown in figure 2.24 (phenomenon 3). Saha and co-workers investigated the fluoride ion sensing ability of NDI by an anion-π interaction (see phenomenon 3 in figure 2.24)[60]. In nitro compounds, one nitro group can be replaced by fluoride (see figure 2.24 phenomenon 2)[61,62,63].

2.4 Conclusions

We wanted to investigate photoinduced electron transfer in donor-bridge-acceptor systems where the bridge contains a boronmesityl unit. It was possible to synthesize two dyads. Dyad **1** is equipped with a triarylamine moiety as electron donor and tris(bipyridine)ruthenium(II) as electron acceptor. Dyad **2** is equipped with the same electron donor. To increase the driving-force for intramolecular electron transfer, two bpy molecules were modified. In 4,4'- position CF_3-groups were attached to create an electron poor bpy ligand.
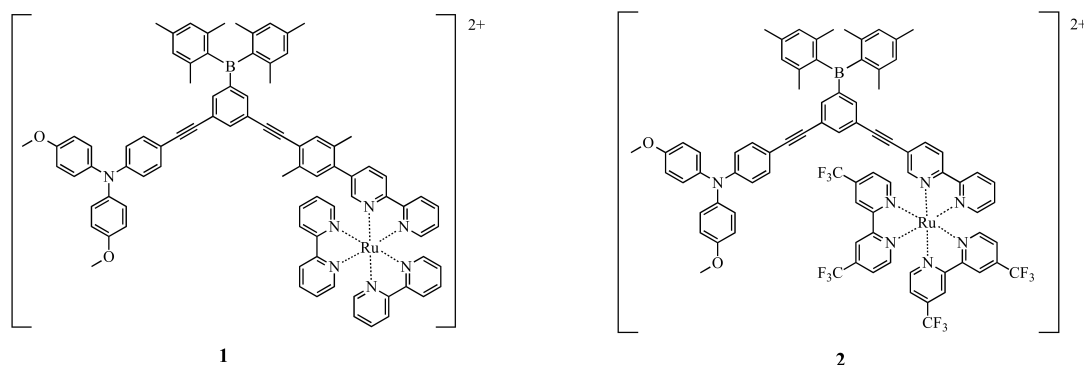
The synthesized dyads **1** and **2** showed the expected behavior in UV-Vis measurements upon fluoride addition. In methylene chloride the highest affinity for fluoride to bind to dyads **1** and **2** could be obtained compared to acetonitrile and dimethylformamide. Hence, further experiments (except CV, spectroelectrochemistry) were carried out in methylene chloride. The luminescence of both dyads compared to their free substituted or unsubstituted tris(bipyridine)ruthenium(II) complex showed that the proposed exergonic reaction pathway to form reduced ruthenium (Ru^I) and oxidized amine (amine$^+$) might take place. Additional investigations *via* transient absorption spectroscopy showed as well evidence for intramolecular PET in both boron dyads. The formation of the electron transfer photoproduct occurred within the laser pulse. To measure the formation lifetime a setup with a higher temporal resolution is needed. The second part of this project was to investigate the PET upon fluoride addition. The barrier height for electron transfer imposed by the bridge should increase upon addition of fluoride. The reduction of the boron atom which is located in the bridge was not observable *via* cyclic voltammetry. The reduction should occur at -2.3 V vs. $Fc^{+/0}$ and was probably masked by the bpy reduction. Transient absorption spectroscopy after addition of TBAF showed no significant changes in the important amine$^+$ band. Therefore, PET takes place even with fluoride attached to the boron atom. Dyad **2** showed a slower recombination of the charge separated state whereas dyad **1** showed no significant changes for the recombination process upon fluoride addition. I hoped that addition of electron acceptors like methylviologen might give me more insights into the intramolecular electron transfer. This experiment had to be carried

out in methylene chloride with TBAF. Unfortunately, either the quencher was not soluble or an undesired interaction with fluoride took place.

In summary, intramolecular PET takes place in both boron dyads as postulated in the energy level diagram (see page 22). Upon fluoride addition PET is not blocked, and clear evidence for a change of the electron transfer mechanism was not obtained.

3 Photoinduced Electron Transfer in Ruthenium-Bis(*p*-anisyl)amine Dyads Equipped with a Tetramethoxybenzene Bridging Unit as Possible Hopping Station

3.1 Introduction

The second project of this thesis focuses on dyads equipped with a ruthenium unit as photosensitizer and a triarylamine reaction partner. Those two moieties are connected *via* a bridge containing a tetramethoxybenzene (tmb) unit and different spacers as shown in figure 3.1.
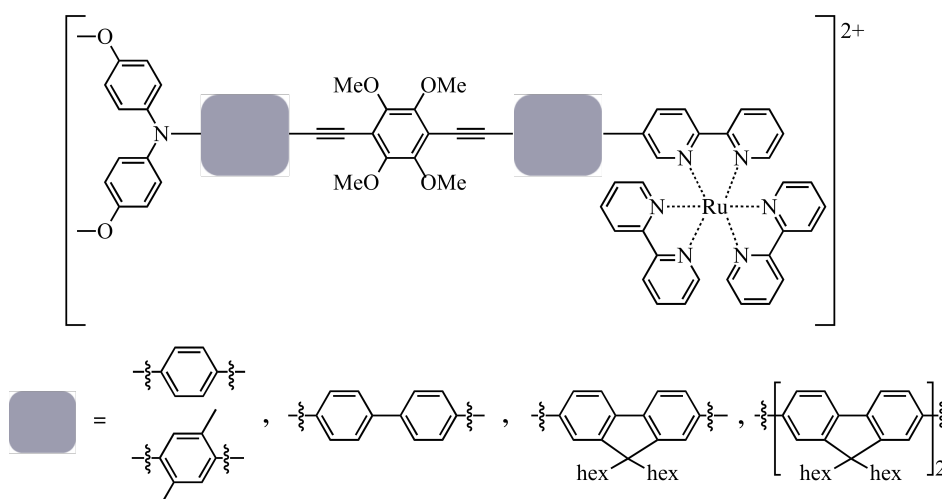
Figure 3.1 Generic molecular structure of the tetramethoxybenzene dyads. As spacer molecules phenyl and xylene (Ph/xy), biphenyl (Ph$_2$), 9,9'-dihexylfluorene (fl) or bis(9,9'-dihexylfluorene) (fl$_2$) were used.

In principle, long-range charge transfer in these D-b-A systems can proceed through hopping or tunneling mechanisms[64]. For an electron hopping mechanism, matching energy levels of the donor and the bridge are necessary. In electron hopping, the electron donor reduces the bridge, which in turn reduces the electron acceptor. In hole hopping, the electron acceptor oxidizes the bridge, which in turn oxidizes the electron donor. If reduction or oxidation of the bridge is thermodynamically unfavorable, a tunneling mechanism remains possible. Scientists found direct evidence for the tunneling energy-gap that might be interpreted as the barrier height in D-b-A systems. The bridging unit between the two moieties determines whether electron transfer rates have a strong or weak distance dependence. If the transferring electron can thermodynamically access the energy levels of the bridge (green square in scheme 3.1) a hopping mechanism takes place (green dotted arrow in scheme below). This long-range electron transfer

has a shallow distance dependence. In D-b-A systems with large donor-bridge energy gaps (red square, scheme below) the electron tunnels through the barrier which is illustrated by the red arrow in scheme 3.1. This process has a strong distance dependence. The electronic coupling H_{DA} in this case is expected to be a function of the tunneling barrier height (see equation 2.2 on page 11).
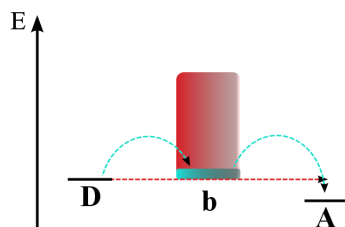
Scheme 3.1 Tunneling vs. hopping mechanisms.

When the bridge consists of molecules which can be easily oxidized or reduced, electron or hole hopping can become important. This can be observed in DNA[65], strongly π-conjugated molecular wires[66], as well as in proteins where the charge transfer pathway includes amino acids with redox-active side chains[67].

Upon irradiation with visible light, the photons are absorbed by the ruthenium moiety. The resulting ^{3}MLCT excited state (marked by *) can subsequently react towards a charge separated state[68]. Electron transfer (scheme 3.2 upper part) occurs when the charge exchange occurs between the lowest unoccupied molecular orbitals (LUMOs) of the bridge. This process is governed by the LUMO energy difference (d_{D_e}) of the electron donor (amine) and the bridging unit relative to the energy difference (d_{A_e}) between the electron acceptor (*Ru) and the bridge.
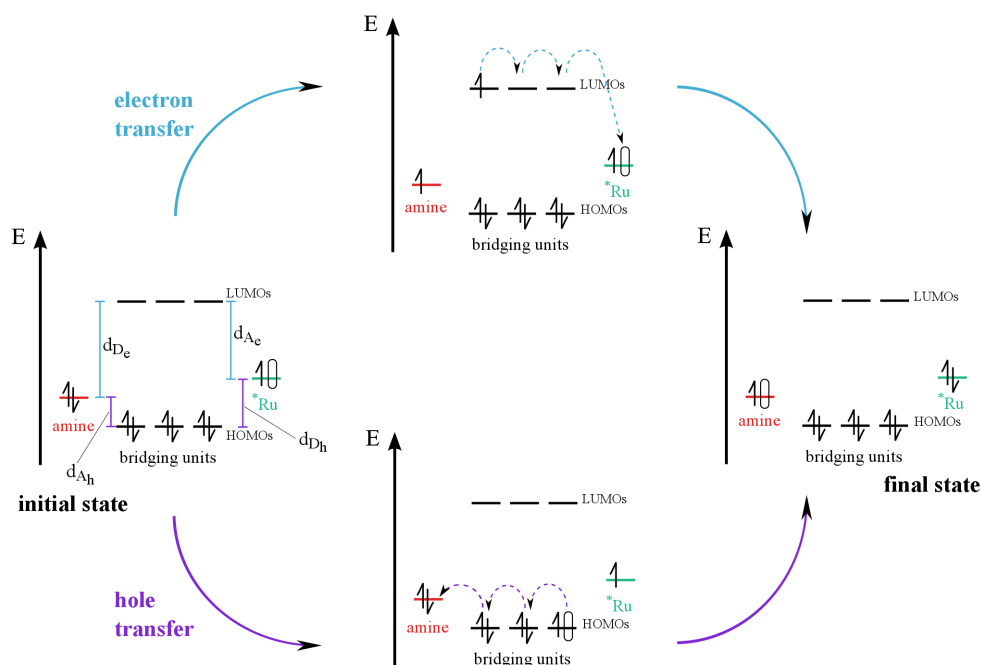

Scheme 3.2 Schematic electron Transfer vs. hole transfer in D-b-A dyads.

In hole transfer (see scheme 3.2 lower part) the charge separation involves the highest occupied molec-

ular orbitals (HOMOs) of the bridge[69,70]. This mechanism is governed by the energy difference (d_{D_h}) between the hole donor (*Ru) and the bridging unit (see scheme 3.2) versus the energy difference (d_{A_h}) between the hole acceptor (amine) and the bridge.

Friend and co-workers studied the kinetics of charge recombination for hole and electron transfer pathways. They observed in their systems that the kinetics for both mechanisms are very similar, suggesting that the generation of charge transfer states does not depend on the pathway[71].

Wenger and co-workers reported that phototriggered hole transfer occured in tmb dyads shown in figure 3.2[72,73].
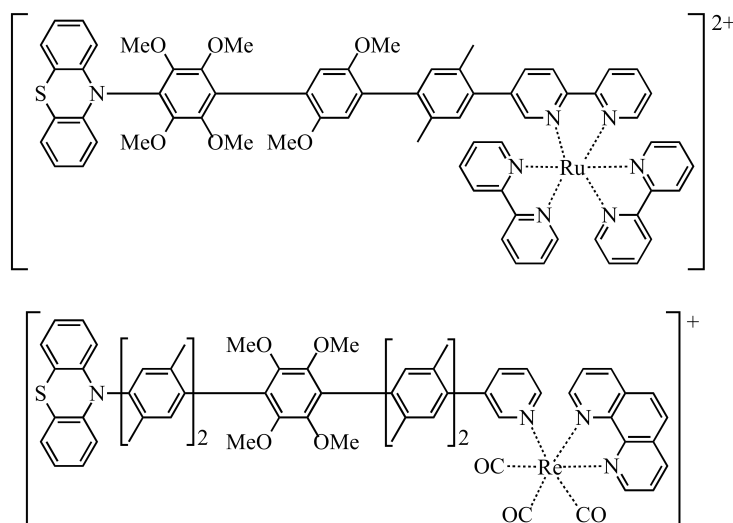
Figure 3.2   Investigated molecules upon hole transfer.

1,2,4,5- Tetramethoxybenzene is a molecule with a low oxidation potential and therefore was not only used by Wenger and co-workers. It is a popular intermediate to synthesize natural products[74,75,76,77,78,79,80]. It was even found in the floral scent emitted by orchids[81]. 1,2,4,5- Tetramethoxybenzene was also used to investigate oxidation behaviors of different peroxidase compounds[82,83,84] or hydrogen transfer combined with electron transfer in quinones[85,86]. To study the dynamics in excited donor-acceptor dyads, tmb was used as electron donor[87]. Tmb was also applied as fluoresence quencher[88] and as potential active material for Li-ion batteries[89].

With the above mentioned tetramethoxybenzene dyads our goal was to investigate whether hole hopping across tmb units is possible in order to accelerate long-range charge transfer rates between distant donors and acceptors. Three additional dyads of the same donor-acceptor couple bridged by phenyl/xylene, 9,9'-dihexylfluorene or bis(9,9'-dihexylfluorene) with benzene instead of tetramethoxybenzene were used as reference molecules.

3.2 Experimental

To investigate the aforementioned aspects two sets of donor-acceptor dyads have been synthesized as shown in figure 3.3. One set consists of a tetramethoxybenzene unit in the bridge. The other set contains the analogue structure but with a benzene unit in the center.
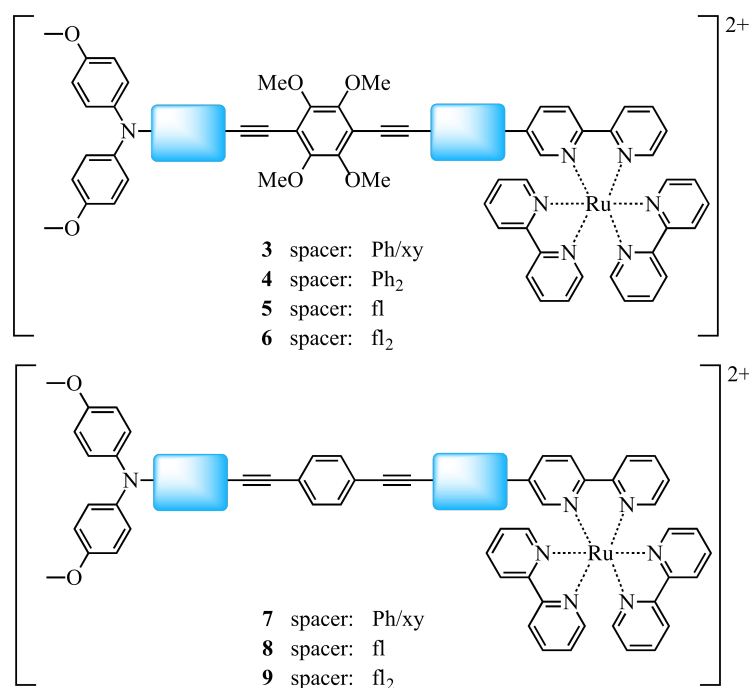
Figure 3.3 Donor-bridge-acceptor dyads containing tetramethoxybenzene and unsubstituted benzene units in the bridge. These compounds were synthesized in this thesis.

To synthesize these seven dyads multiple steps are needed. In scheme 3.3 the shortened reaction pathway for the tmb dyads **3**, **4**, **5** and **6** is shown. All amine compounds are marked with an **A**. All bipyridine molecules have a **B** and spacer molecules are named with **S**. Central molecules, ligands and complexes are numbered without a capital letter. For detailed reaction information see chapter 4 and 6.

First, the 2,5-dihydroxy-1,4-benzoquinone had to be synthesized *via* a six-step synthesis. Therefore, the commercially available 1,4-dihydroxybenzoquinone was reacted with boron trifluoride diethyl etherate in dry methanol to get 2,5-dimethoxy-1,4-benzoquinone. This molecule was then reacted with sodium borohydride in dry ethanol to synthesize 2,5-dimethoxy-1,4-dihydroxybenzene. A reaction in dry ethanol with dimethyl sulfate methylated the remaining hydroxy groups. The resulting 1,2,4,5- tetramethoxybenzene was treated with *n*-BuLi in dry diethyl ether followed by addition of iodine to get 1,4-diiodo-2,3,5,6-tetramethoxybenzene. Then a Sonogashira-Hagihara reaction with MEBYNOL in dry triethylamine was applied to attach the alkyne moiety. The final step is the deprotection with sodium hydride to get molecule **20**.

To synthesize the desired amine coupling compounds **A-2** to **A-9**, at least two reaction steps are needed (**b**). For compound **A-2** the commercially available bis(*p*-anisyl)amine was reacted *via* a BHA with 1-bromobenzene in dry toluene. The subsequent step was an iodination with [bis(trifluoroacetoxy)iodo]-benzene in dry methylene chloride. To get molecule **A-4** the BHA coupling was performed with Br−(Ph)$_2$−TMS (**S-3**) as halogen compound followed by the replacement of the TMS protection group by iodine with iodinie monochloride (ICl) in dry methylene chloride. For **A-6** the coupling was performed with Br−fl−TMS (**S-7**). Iodination with ICl lead to compound **A-6**. The first BHA coupling to get molecule **A-9** was performed with **S-7** followed by bromination with Br$_2$ in dry methylene chloride. For the second BHA reaction **S-7** was coupled again. The iodination with ICl lead to compound **A-9**. The third coupling molecule is a bpy compound (**c**). First, 5-bromo-2,2'-bipyridine (Br−bpy (**B-1**)) was synthesized *via* a Negishi coupling of 2-pyridylzinc bromide with 5-bromo-2-iodopyridine in dry

tetrahydrofuran. For the bpy molecules **B-5** to **B-11** Br−bpy (**B-1**) was attached to B(OH)$_2$−X−TMS (X = xylene (**S-2**), biphenyl (**S-4**) or 9,9'-dihexylfluorene (**S-8**)) in tetrahydrofuran and water by performing a Suzuki coupling. Followed the replacement of the TMS protection group by iodine *via* ICl in dry methylene chloride and acetonitrile. For the synthesis of **B-11**, I−fl−bpy (**B-9**) was first treated with **S-8** again, followed by iodination with ICl. The final ligands **21** to **24** were synthesized *via* a one-pot Sonogashira-Hagihara reaction in dry triethylamine (**d**). The final reaction step (**e**) to get the desired dyads **3** to **6** is a complexation with Ru(bpy)$_2$Cl$_2$ in dry methanol and chloroform. The complexation for compound **4** had to be performed with silver nitrate to get the desired dyad.
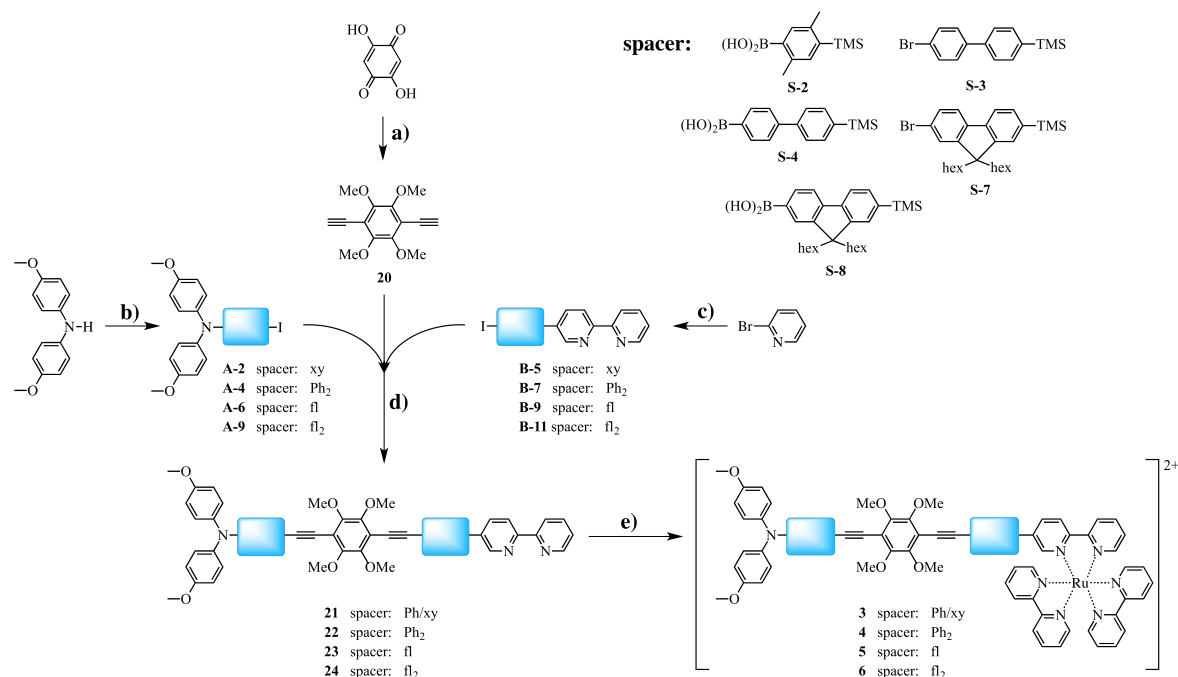
Scheme 3.3 Synthetic overview for tmb dyads **3** - **6**.
a) 6-step synthesis: methylation with BF$_3$ · OEt$_2$, reduction with NaBH$_4$, methylation with (CH$_3$)$_2$SO$_4$, iodination, Sonogashira reaction with Pd(PPh$_3$)$_2$Cl$_2$, CuI, NEt$_3$, deprotection with NaH; **b)** 2 to 4-step synthesis: Buchwald-Hartwig amination (BHA) with NaO^{t}Bu, Pd(dba)$_2$, and (HP^{t}Bu)BF$_4$, (iodination/bromination, BHA (same conditions), iodination; **c)** 3 to 5-step synthesis: Negishi coupling with Pd(PPh$_3$)$_4$, Suzuki reaction with B(OH)$_2$−X−TMS and Pd(PPh$_3$)$_4$, Na$_2$CO$_3$, iodination (Suzuki coupling (same conditions), iodination; **d)** one-pot Sonogashira reaction with Pd(PPh$_3$)$_2$Cl$_2$, CuI, NEt$_3$; **e)** complexation with Ru(bpy)$_2$Cl$_2$ (dyad **4** and **9** plus AgNO$_3$).

The reference molecules **7**, **8** and **9** comprise an unsubstituted benzene as center of the bridge. First, the central molecule was synthesized. In a two-step synthesis route the desired benzene unit could be obtained. At first, a double Sonogashira-Hagihara coupling in dry triethylamine to get the protected alkyne molecule was performed. Then, the deprotection of the alkyne unit *via* KOH in dry toluene was effected.

The subsequent step was a Sonogashira-Hagihara coupling in triethylamine with the amine and the bpy compound. The formation of an analouge of ligand **21** with an unsubstituted benzene instead of a tmb unit was not possible. Therefore, dyad **4** has no reference molecule. As counter anions hexafluorophosphate for dyad **3** and nitrate for D-b-A systems **4** to **9** were chosen.

3.3 Results

The synthesized tetramethoxybenzene dyads consist of bridges containing either a phenyl/xylene spacer (**3**), a biphenyl spacer (**4**), a 9,9'-dihexylfluorene (**5**) or a bis(9,9'-dihexylfluorene) (**6**). These spacers cause different torsion angles which might have an influence on the charge transfer. Further, in the tetramethoxybenzene dyads **3** to **6** the distance between the amine and the ruthenium moiety changes. Dyad **3** is the shortest in this series with a D-A distance of approximately 23.5 Å whereas dyads **4** and **5** have a 33.5 Å distance. Dyad **6** is the longest one with a D-A distance of 50.6 Å. These approximations were made on the basis of the crystal structure of ligand **21**. This crystal structure was obtained by slow evaporation from acetone.
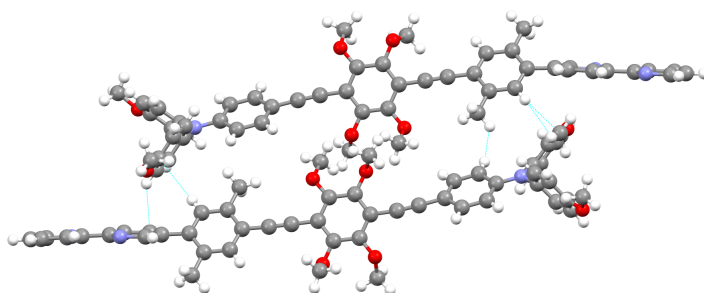
Figure 3.4 Crystallographic structure of ligand **21** in the asymmetric unit viewed along the crystallographic c-axes (red: oxygen, purple: nitrogen). Crystals could be obtained by slow evaporation from acetone.

The resulting X-ray structure of ligand **21** is shown in figure 3.4. This ligand crystallizes in the triclinic space group P-1. The two pyridine units of a given bpy ligand are oriented inversely to each other but in a coplanar fashion. The dihedral angle between the inner pyridine ring and the neighboring xylene measures 53.7°. The dihedral angle between the xylene and the tmb unit is 21.7° whereas the angle between the phenyl and the tmb measures 41.5°. The amine looks like a three-bladed propeller with a planar central N atom. The propeller shape is typical of triarylamines[90,91,92].
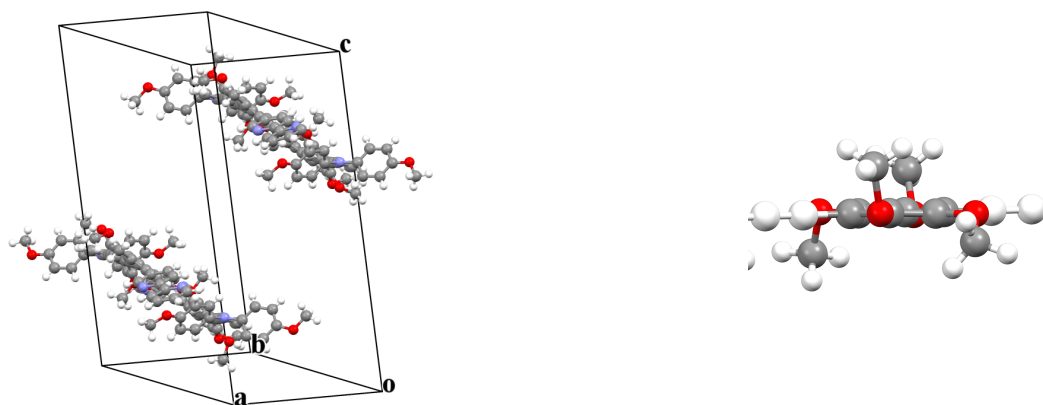

Figure 3.5 Packing structure (red: oxygen, purple: nitrogen) of ligand **21** (left) and magnified view of the tetramethoxybenzene unit (right).

Molecule **21** arranges in sheets along the crystallographic a- and b-axes (see figure 3.5, left side) and it is slightly bent. The O atom of the four methoxy substituents is in the phenyl ring plane of the tmb (right

image in figure 3.5). The methyl groups are placed outside of the plane. The CH_3-groups of the methoxy groups which are in para position of the ring are placed on one side of the plane whereas the other two are placed opposite.

Dyads **4** and **5** do not differ significantly in donor-acceptor distance. The reason why these dyads were synthesized is that there are different torsion angles between the two phenyl rings in biphenyl and in 9,9'-dihexylfluorene. In 2010, Wenger and co-workers explored those torsion angles in rhenium dyads[93]. In free biphenyl the equilibrium torsion angle between the two phenyl rings is approximately 44°[94]. When using biphenyl as spacer in a dyad the torsion angle changes from approximately 44° to 35°. The torsion angle of the two phenyl rings for free 9,9'-dihexylfluorene is approximately 1.3°[95]. By placing 9,9'-dihexylfluorene as a spacer in the bridging unit of a dyad the torsion angle increases (approximately 6°). These angles are important for the charge transfer rate. It was observed that electron transfer in the 9,9'-dihexylfluorene containing dyads was twice as fast compared to the biphenyl dyads (see figure below).
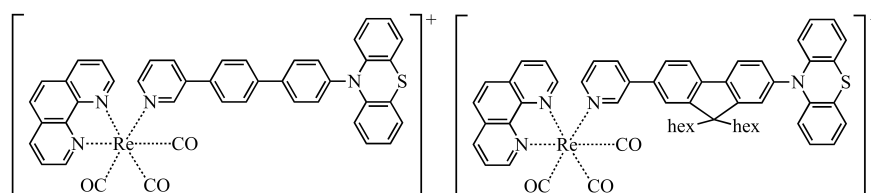
Figure 3.6   Previously investigated 9,9'-dihexylfluorene and biphenyl containing dyads.

3.3.1 Spectral absorption

In figure 3.7 the UV-Vis spectra for all dyads and $Ru(bpy)_3(PF_6)_2$ in acetonitrile are shown. One can observe that with increasing length of the bridge, the MLCT band at 450 nm (see spectrum of $Ru(bpy)_3(PF_6)_2$) is covered by an absorption band of the bridge. The band at 290 nm is caused by $\pi - \pi^*$ transition on the unsubstituted bpy ligands.
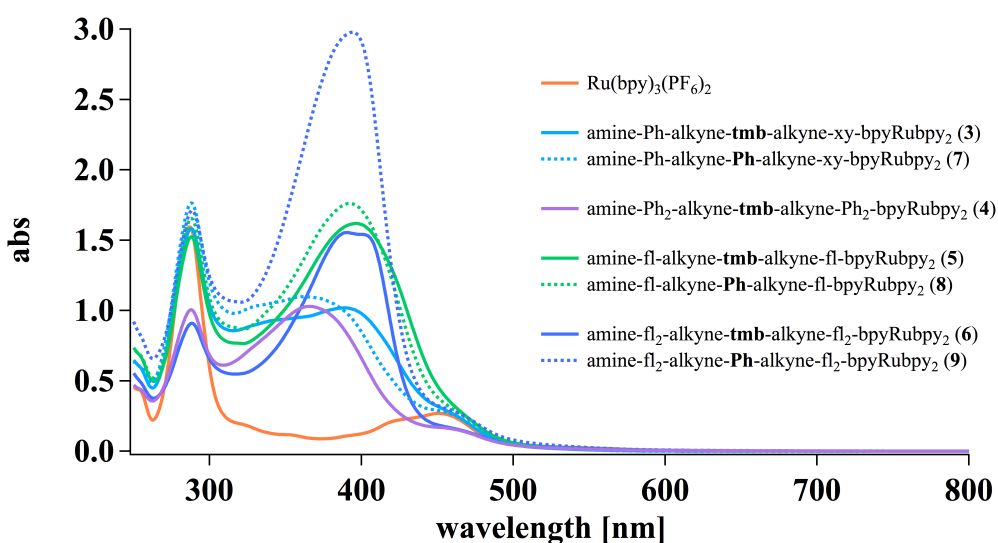
Figure 3.7   UV-Vis spectra of D-b-A systems **3** to **9** in CH_3CN, c = $2 \cdot 10^{-5}$ M.

In the following, I will focus on the bridge absorption bands where the biggest absorbance changes occur.

Comparison of dyad **3** with **7** reveals a shift in the bridge band. Dyad **3** has its maximum at 390 nm. In the absorption spectrum of reference molecule **7** this maximum is blue shifted by 26 nm. Dyad **4** has its maximum at 366 nm which in similar to dyad **7**. The absorption band has the same extinction as dyad **3**. For the D-b-A systems with 9,9'-dihexylfluorene as a spacer (**5** and **8**) the absorption band is quite similar. A blue shift by 5 nm for the unsubstituted benzene reference molecule (**8**) occurs. Dyad **6** shows two maxima (391 and 401 nm). Its reference molecule (**9**) has only one maximum which has a high extinction. The extinction is twice as high as for its tmb dyad.

3.3.2 Electrochemistry

Cyclic voltammetry (CV) with the tetramethoxybenzene dyads and their unsubstituted benzene reference molecules were carried out in deoxygenated acetonitrile solution at room temperature. Measurement conditions are summarized on page 75.

We expect to see the tmb$^{+/0}$ redox couple around 0.4 V vs. Fc$^{+/0}$[96]. By measuring neat tetramethoxy-benzene (**20**) the oxidation potential was found to be around 0.25 V vs. Fc$^{+/0}$ (shown in figure 3.8).
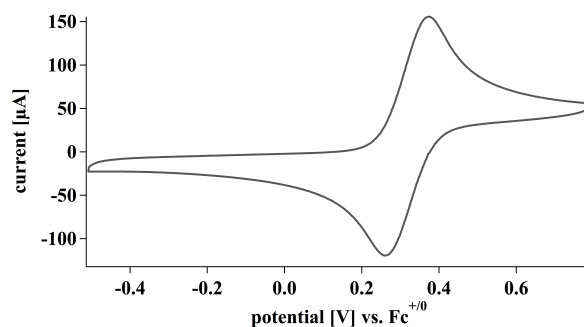
Figure 3.8   Cyclic voltammogram of tmb (**20**) in CH$_3$CN.

In figure 3.9 all voltammograms of the tetramethoxybenzene dyads are compared to their benzene analogues. The amine oxidation occurred in all cases around 0.15 V vs. Fc$^{+/0}$. The oxidation potential for the ruthenium(II) species to become Ru^{III} is around 0.80 V vs. Fc$^{+/0}$. The largest potential changes were observed in the bpy reduction part.

The bpy reduction waves for dyad **3** are shifted to more negative potentials (0.1 V) by introducing the benzene center. Cyclic voltammogram of reference molecule **8** shows in the bpy region an unusual behavior. The resolution of the reduction waves is good whereas the oxidation turned into an undefined wave. Only the first redox potential for the bpy part is detectable. Dyad **6** shows fine resolved reduction waves for the bpy part. The oxidation waves turned into a bulky undefinable wave as well. Comparison of all tmb dyads shows that the amine oxidation becomes easier with increasing spacer length. The ruthenium oxidation as well as the bpy reduction shows no clear trend upon increasing spacer length, as expected. The tmb oxidation could not be detected.

a) CV of dyad **3** and its reference molecule **7**.

b) CV of dyad **4**.

c) CV of dyad **5** and its reference molecule **8**.

d) CV of dyad **6** and its reference molecule **9**.
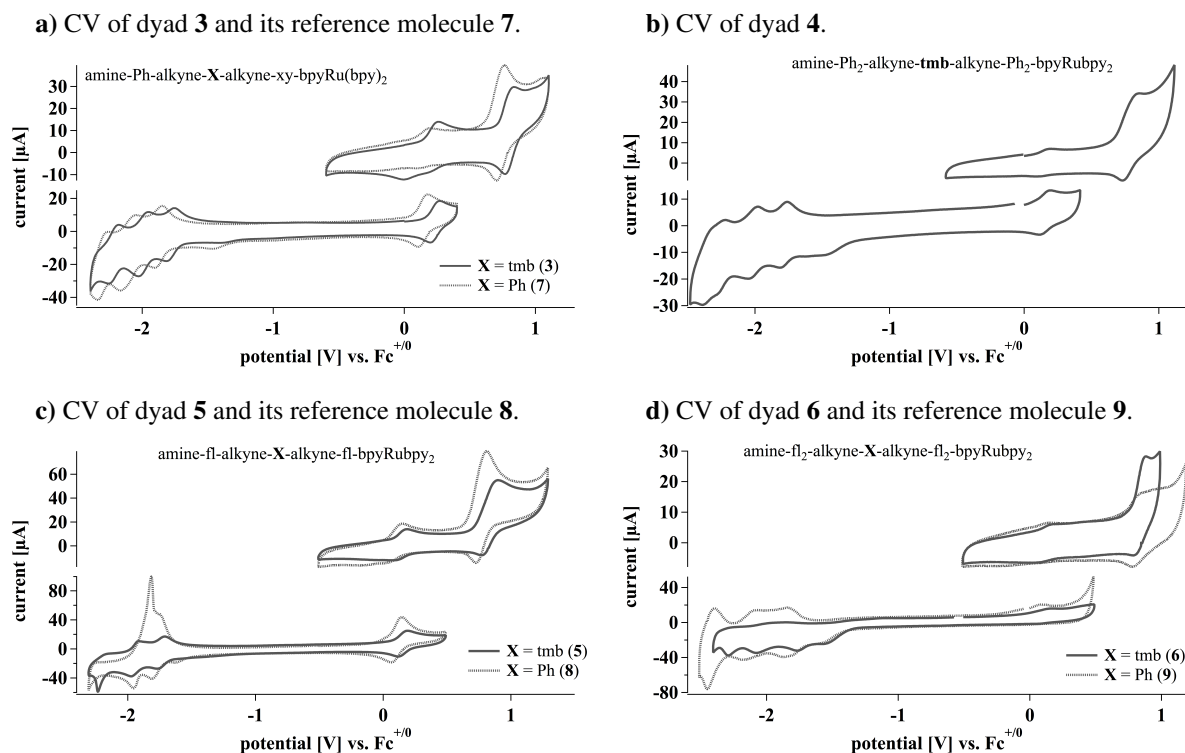
Figure 3.9   Cyclic voltammetry measurements carried out in deoxygenated CH_3CN. All electrochemical potentials were referred to $Fc^{+/0}$.

In table 3.1 all electrochemical potentials in Volts vs. $Fc^{+/0}$ for the aforementioned compounds measured in acetonitrile are summarized.

Table 3.1   Electrochemical potentials in Volts vs. $Fc^{+/0}$ for tmb dyads (**3** - **6**), their reference molecules (**7** to **9**) and $Ru(bpy)_3(PF_6)_2$ measured in deoxygenated acetonitrile.

D-b-A system/dyad	$E(amine^{+/0})$ [V]	$E(Ru^{3+/2+})$ [V]	$E(bpy^{0/-})$ [V]	ΔG_{ET} [eV]
$Ru(bpy)_3(PF_6)_2$	-	0.82	-1.81	
3	0.23	0.80	-1.77	-0.14 eV
4	0.16	0.79	-1.79	-0.13 eV
5	0.16	0.83	-1.74	-0.23 eV
6	0.11	0.84	-1.78*	-0.24 eV
7	0.14	0.74	-1.88	-0.12 eV
8	0.10	0.77	-1.78	-0.25 eV
9	0.09	0.81	-1.85	-0.19 eV

* $E_{1/2}$

Whether the electron transfer reaction is exergonic or endergonic can be determined by using equation 2.6 (see page 21) and the electrochemical potentials summarized in table 3.1. The driving force of dyads **3**, **4** and reference molecule **7** are exergonic (see table 3.1). The dyads with one fluorene spacer attached to the amine moiety as well as to the bpy unit (**5** and **8**) have a driving force which is more exergonic by approximately 0.1 eV than the D-b-A systems (dyads **3**, **4**, reference molecule **7**).

3.3.3 Steady-state luminescence spectroscopy

When efficient PET takes place, luminescence quenching can usually be observed. In figure 3.10 luminescence spectra for all D-b-A systems are shown. The dyads were excited at 450 nm. All intensities were corrected for differences in absorbance at 450 nm and normalized to the emission intensity of $Ru(bpy)_3(PF_6)_2$. The shoulders at around 660 nm are caused by the instrument and not by the dyads. Dyads **4** to **9** have their maxima at around 610 nm. Only dyad **3** has the same maximum as $Ru(bpy)_3(PF_6)_2$ (605 nm).
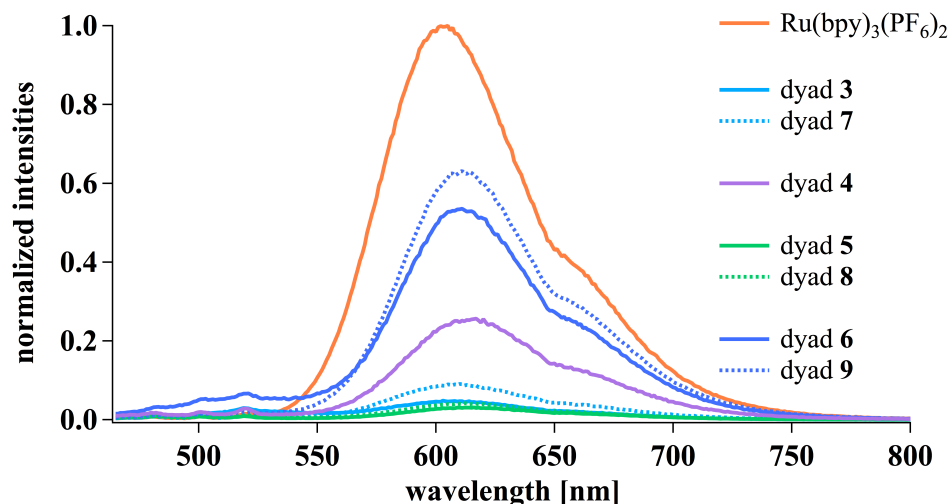
Figure 3.10   Normalized steady-state luminescence for D-b-A systems **3** to **9** and $Ru(bpy)_3(PF_6)_2$ (solid blue trace) (c = $2 \cdot 10^{-5}$ M in CH_3CN, excitation: 450 nm).

Based on the determined exergonic driving force in all tetramethoxybenzene dyads we expected a luminescence quenching. Figure 3.10 shows that quenching is indeed observed. The weakest luminescence quenching occurred in the longest dyads (**6** and **9**) with the bis(9,9'-dihexylfluorene) spacer. The emission in dyad **6** is quenched by 50% whereas the reference molecule **9** has an emission intensity of 63 % compared to $Ru(bpy)_3(PF_6)_2$. We expected that the biphenyl dyad (**4**) has an intermediate luminescence quenching ability. Its emission intensity is only 26 % compared to $Ru(bpy)_3(PF_6)_2$. The shorter D-A distance should lead to a faster charge transfer compared to dyads **6** and **9** but not as fast as in the shortest dyads **3** and **7**. The torsion angle between the two phenyl rings of the spacer should result in a slower charge transfer compared to dyads **5** and **8**. The most efficient luminescence quenching occurred in the tetramethoxybenzene dyads **3**, **5** and in reference molecules **7** and **8**. Their emission intensity is quenched by over 90 % compared to $Ru(bpy)_3(PF_6)_2$. I expected that the D-A distance in dyads **3** and **7**, which is 10 Å shorter compared to dyads **5** and **8**, is short enough to observe the strongest quenching in this series. Weaker electronic coupling between ruthenium and bis(p-anisyl)amine in dyad **3** and its reference molecule (**7**) compared to the fluorene dyads **5** and **8** caused by sterical reasons, might lead to less efficient excited rate quenching.

In figure 3.10 one can also observe that the luminescence of the tmb dyads is more quenched than in the case of their unsubstituted benzene analogues.

Luminescence decays

Figure 3.11 shows the luminescence decays of the tmb dyads, their reference molecules and of isolated ruthenium reference complex (Ru(bpy)$_3$(PF$_6$)$_2$). The measurements were carried out in an acetonitrile solution with a concentration of $2 \cdot 10^{-5}$ M. The dyads were excited at 532 nm and the emission was detected at 630 nm. These decays are the dynamic counterpart to the steady state luminescence data from figure 3.10.
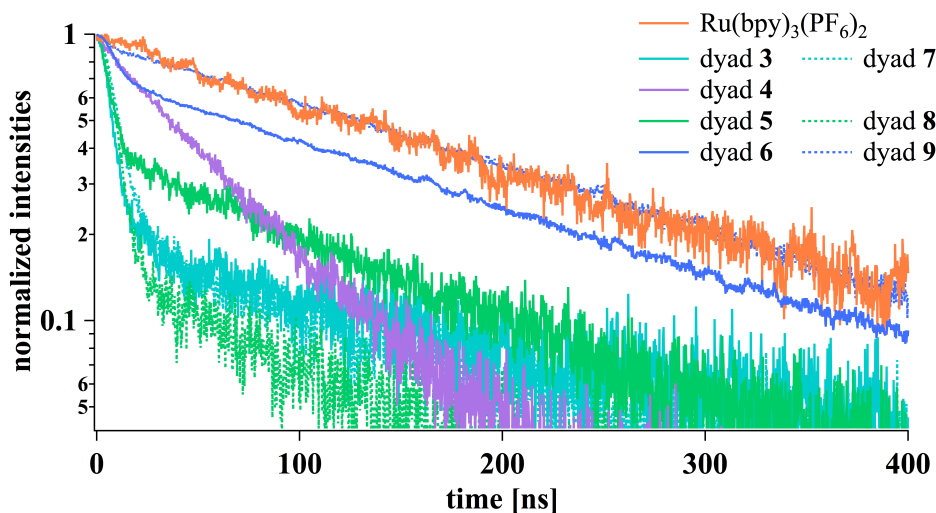

Figure 3.11   Normalized luminescence decay for dyads **3** to **9** and Ru(bpy)$_3$(PF$_6$)$_2$ (c = $2 \cdot 10^{-5}$ M in CH$_3$CN, excitation: 532 nm).

Fits to these single and bi-exponential decays gave the luminescence lifetimes of the dyads. The luminescence lifetime of the reference complex Ru(bpy)$_3$(PF$_6$)$_2$ is 164 ns. Reference molecule **9** has a luminescence lifetime of 217 ns and decays like Ru(bpy)$_3$(PF$_6$)$_2$. The bis(9,9'-dihexylfluorene) dyad **6** decays in 7 ns and 191 ns. The latter is similar to the lifetime of the isolated ruthenium complex. The dyad with the biphenyl spacer (**4**) exhibits a luminescence lifetimes of less than 7 ns and 55 ns. This may be evidence for PET. The other dyads **3**, **5** and their reference molecules **7**, **8** show a luminescence lifetime of less than 7 ns and around 160 ns. The latter decay is similar to the isolated ruthenium reference complex. Based on the luminescence quenching (see figure 3.10) and the obtained luminescence lifetimes, PET takes place in the phenyl/xylene dyad (**3**) and its reference molecule **7** as well as in the 9,9'-dihexylfluorene dyad **5** and its reference molecule **8**.

3.3.4 Transient absorption spectroscopy

Definite evidence for PET in these donor-bridge-acceptor dyads could be obtained by transient absorption (TA) spectroscopy. The spectra were recorded in a wavelength range from 300 to 800 nm. Excitation occurred with 10 ns excitation pulses. The data were acquired in a 200 ns time window, starting immediately after the laser pulse. Amine oxidation and bpy reduction spectra were measured separately to compare them with the obtained TA spectra. The reference spectra of the bpy reduction to observe the formation of Ru^I was obtained *via* spectroelectrochemistry in acetonitrile. A (Bu$_4$N)PF$_6$ solution in the same solvent was used as electrolyte. A potential of -1.8 V vs. Fc$^{+/0}$ was applied to measure the first bipyridine reduction. The amine oxidation reference spectra resulted from a titration of copper perchlo-

rate to a $2 \cdot 10^{-5}$ M solution of the dyad in acetonitrile. The sharp signal at 532 nm is caused by the laser pulse.
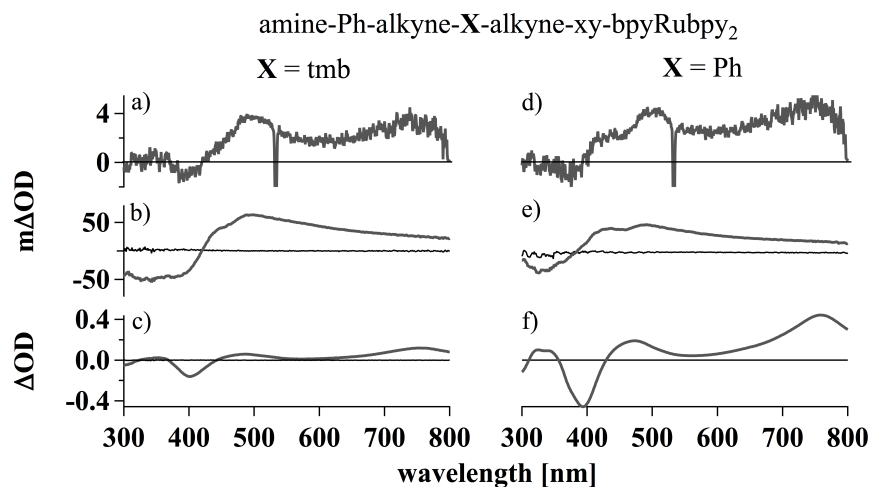
Figure 3.12 Transient absorption spectra of dyad **3** on the left side compared to its reference molecule **7** ($c = 2 \cdot 10^{-5}$ M). Transient absorption spectra (a and d) were measured in acetonitrile. Bpy reduction (b and e) were measured *via* spectroelectrochemistry in acetonitrile with $(Bu_4N)PF_6$ as electrolyte ($c = 1 \cdot 10^{-4}$ M). Amine oxidation (c and f) were obtained from $Cu(ClO_4)_2$ titration in acetonitrile ($c = 2 \cdot 10^{-5}$ M).

According to the driving force estimation PET should take place in the shortest dyads. In the resulting bpy reduction spectra (see figure 3.12) of dyad **3** (b) and its reference molecule **7** (e) one can see a bleach around 350 and a band around 500 nm indicating the reduction of the bipyridine. In the amine oxidation spectra (c and f) a band at 750 nm, a band around 500 nm and a bleach around 400 nm indicate the formation of amine$^+$. By comparison of the TA (a and d) spectra with the reference spectra (b,c as well as e and f) one can observe that in spectrum a) a band around 500 nm and at 750 nm is visible. This indicates that amine$^+$ and Ru^I are generated. In the TA of the reference molecule **7** these two bands are visible as well. The shoulder around 400 nm is caused by the bpy reduction. These results are evidence for with the proposed photoinduced charge transfer in the shortest dyads of this series.

PET should occur as well in the 9,9'-dihexylfluorene dyad **5** and it reference molecule **8** based on the exergonic electron transfer driving force and the steady-state luminescence results. To confirm that oxidized amine$^+$ and reduced ruthenium (Ru^I) are generated, reference measurements to determine the relevant absorption band were carried out in the same fashion as mentioned before. The TA spectra of dyad **5** shows a band around 700 nm. This band compared to the separately measured amine oxidation (spectra b) in figure 3.13 verifies that the amine$^+$ band is blue shifted by around 50 nm (compared to dyad **3**). The band around 500 nm in the TA spectra belongs to the Ru^I species. The TA spectra of reference molecule **8** shows the amine$^+$ band around 700 nm as well as the Ru^I band around 500 nm. These results are in line with the proposed PET.

amine-fl-alkyne-**X**-alkyne-fl-bpyRubpy$_2$
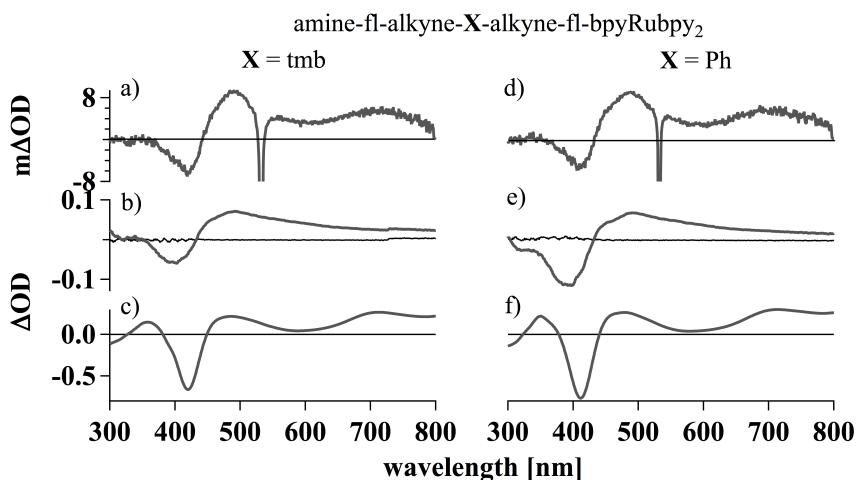
Figure 3.13 Transient absorption spectra of dyad **5** (left) compared to **8** (right) (c = 2 · 10^{-5} M in acetonitrile). Bpy reduction spectra (b and e) were measured *via* spectroelectrochemistry in acetonitrile with (Bu$_4$N)PF$_6$ as electrolyte (c = 1 · 10^{-4} M). Amine oxidation (c and f) were obtained from Cu(ClO$_4$)$_2$ titration in acetonitrile (c = 2 · 10^{-5} M).

In dyad **4** we expect to see PET based on the determined exergonic driving force for electron transfer and the luminescence experiments. In figure 3.14 the TA spectrum (a) is shown. The reference amine oxidation spectrum of dyad **4** was obtained from copper perchlorate titration in a 2 · 10^{-5} M solution in acetonitrile. The spectrum of Ru^{I} was obtained from spectroelectrochemistry using a 1 · 10^{-4} M solution in acetonitrile (electrolyte: (Bu$_4$N)PF$_6$).

amine-Ph$_2$-alkyne-**tmb**-alkyne-Ph$_2$-bpyRubpy$_2$
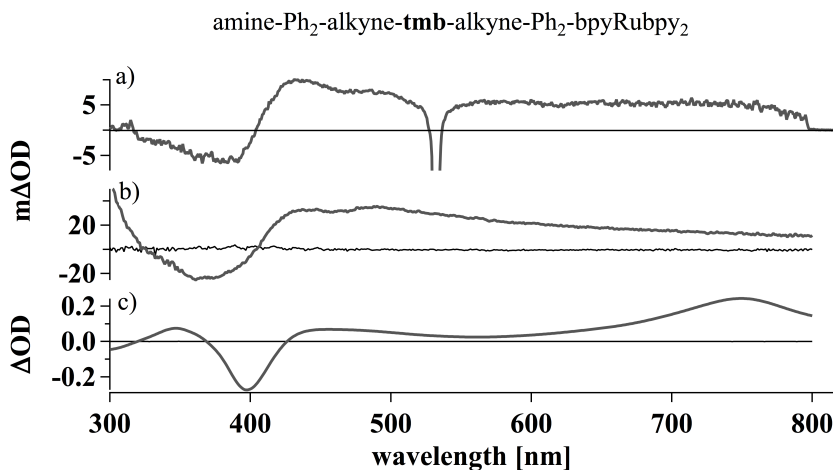
Figure 3.14 Transient absorption spectrum of dyad **4**. Transient absorption spectra (a) were measured in acetonitrile (c = 2 · 10^{-5} M). Bpy reduction (b) were measured *via* spectroelectrochemistry in acetonitrile with a 0.1 M (Bu$_4$N)PF$_6$ solution as electrolyte. Amine oxidation (c) were obtained from Cu(ClO$_4$)$_2$ titration in acetonitrile (c = 2 · 10^{-5} M).

If Ru^{I} is generated after photoexcitation, it should be observable in the TA spectrum. According to the separately measured bpy reduction (spectrum b) in figure above), a broad band around 450 nm and a bleach around 400 nm are expected. If amine^{+} is generated a band around 750 nm and a bleach around 400 nm should be observable as shown in spectrum c) in figure 3.14.

The TA spectrum of dyad **4** (spectrum a) in figure 3.14) shows no clear evidence for the amine^{+} formation. The band around 450 nm could be caused by the Ru^{I} formation. This might be evidence for a

competitive charge transfer pathway (see scheme 3.4). In the competitive mechanism it might be possible that an electron from the tmb unit reduced the excited ruthenium(II) takes place. In the subsequent step, no electron from the amine moiety is transferred to the tmb. Instead, a charge recombination between tmb^+ and Ru^I would be the final step.

$$e^-$$

$$^*Ru^{II} \underline{\quad\quad} tmb \underline{\quad\quad} amine$$

$$\downarrow$$

$$Ru^I \underline{\quad\quad} tmb^+ \underline{\quad\quad} amine$$

$$\downarrow \text{charge recombination}$$

$$Ru^{II} \underline{\quad\quad} tmb \underline{\quad\quad} amine$$
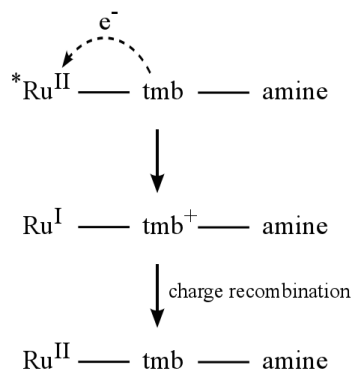
Scheme 3.4   Possible competitive charge transfer pathway.

A formation of tmb^+ might be visible in UV/Vis experiments around 290 nm[84]. The rather high optical density of the sample in the TA experiment between 200 and 310 nm made the observation of the tmb^+ band possible.

Based on the transient absorption data and the absence of the oxidized amine band, it seems not clear that the PET from the ^{3}MLCT excited state of ruthenium ($^*Ru^{2+}$) to the bis(p-anisyl)amine moiety is present.

For the largest D-A distance dyads (**6** and **9**) in this series we expect to observe PET based on the estimated electron transfer driving force. Based on the luminescence data, PET might not take place and it is known that by increasing the D-A distance the electron transfer becomes less likely. To confirm that the TA spectra show the bands which indicate the formation of $amine^+$ and Ru^I additional measurements were carried out. The bpy reduction (indication for Ru^I formation) was obtained from spectroelectrochemistry. In a $1 \cdot 10^{-4}$ M solution of dyad **6** in acetonitrile with a 0.1 M $(Bu_4N)PF_6$ solution as electrolyte a potential of -1.7 V vs. $Fc^{+/0}$ was applied. The oxidation of the amine moiety in dyad **6** were carried out in a $2 \cdot 10^{-5}$ M solution in acetonitrile. Titration of copper perchlorate lead to the formation of $amine^+$. The exact same measurements were carried out for the reference molecule **9**.

amine-fl$_2$-alkyne-**X**-alkyne-fl$_2$-bpyRubpy$_2$
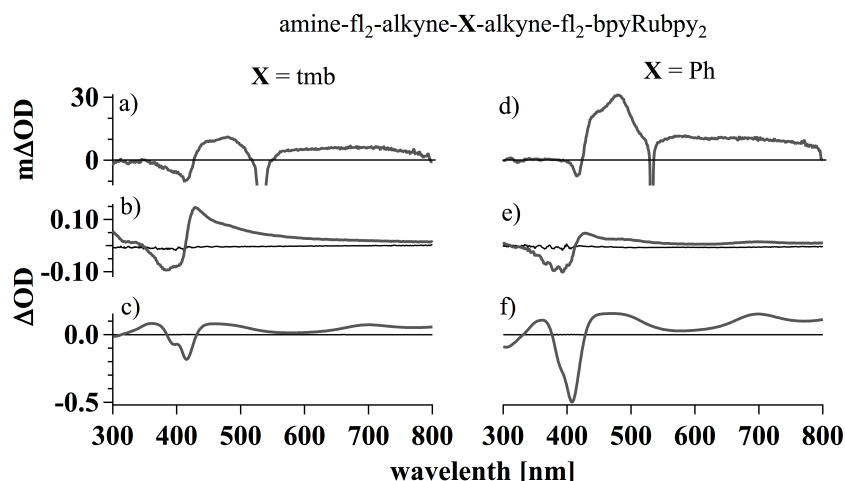
Figure 3.15 Transient absorption spectra of dyad **6** (left) compared to **9** (right). Transient absorption spectra (a and d) were measured in acetonitrile (c = 2 · 10^{-5} M). Bpy reduction (b and e) were measured *via* spectroelectrochemistry in acetonitrile with (Bu$_4$N)PF$_6$ as electrolyte. Amine oxidation (c and f) were obtained from Cu(ClO$_4$)$_2$ titration in acetonitrile.

In figure 3.15 the TA spectra of dyad **6** (left) and its reference molecule **9** are shown. According to the obtained spectra b) and e) should a band around 450 nm and a bleach around 400 nm indicate the formation of Ru^I . The formation of amine$^+$ should lead to a band around 700 nm, a band around 500 nm and a bleach around 400 nm. In both TA spectra (see figure 3.15) no clear evidence for the generation of amine$^+$ and Ru^I is visible. The rather high optical density of the samples in the TA experiments between 200 and 400 nm caused the absence of the bleach.

Now, that there is clear evidence for PET in dyads **3** and **5** as well as in their reference molecules (**7** and **8**) we focus on kinetic absorption experiments. With these experiments we should be able to proof our hypothesis that in tmb dyads the charge transfer process is faster compared to their unsubstituted benzene reference molecules. The rise of the absorption signal at selected wavelengths contains information about kinetics for the formation of the charge separated state. The decay shows the recombination of amine$^+$ with Ru^I. In figure 3.16 kinetic absorption (KA) monitored at 490 nm (Ru$^+$ formation/decay) and 750 nm (amine$^+$ formation/decay) for dyad **3** and for its reference molecule **7** (figure a) are shown. The transient absorption spectra on the right show dyad **5** and its reference molecule **8** (490 nm, 690 nm).

a) KA decays of dyad **3** (left) and its reference **7** (right).

b) KA decays of dyad **5** (left) and its reference **8** (right).

amine-Ph-alkyne-**X**-alkyne-xy-bpyRubpy$_2$

amine-fl-alkyne-**X**-alkyne-fl-bpyRubpy$_2$
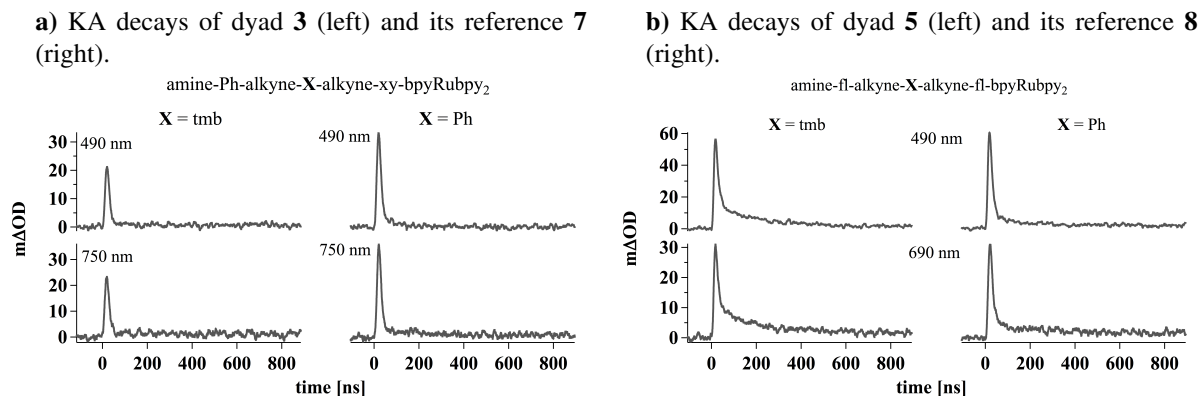
Figure 3.16 Kinetic absorption decays of dyad **3**, its reference molecule **7** (left) as well as dyad **5** and its reference molecule **8** (right). Measurements were carried out in acetonitrile (c = 2 · 10^{-5} M).

The shape of the KA decays at the two selected wavelengths in each D-b-A system are similar which indicates that the signals belong to the same charge separated state. The charge separated state is formed within the laser pulse for all four dyads in figure 3.16. The lifetimes at both wavelengths for the phenyl/xylene dyad **3** and its reference molecule **7** are approximately 11 ns. The charge separated state for the 9,9'-dihexylfluorene dyads (**5** and **8**) decays in a biexponential fashion. The decay times for dyad **5** and its reference molecule **8** are around 12 ns (fast decay part for both selected wavelengths). This decay time is similar to the shortest dyads in this series.

With these results, our hypothesis of faster electron transfer in the tmb dyads can not be supported. A higher temporal resolution setup would be needed to test our hypothesis with the synthesized molecules. Dyads **4**, **6** and reference molecule **9** did not show clear evidence for a PET mechanism from the amine to the ruthenium moiety. The reported KA measurement data (figure 3.17) show biexponential decays for the biphenyl dyad (**4**). The bis(9,9'-dihexylfluorene) dyads (**6** and **9**) decay in a single exponential fashion.

a) KA decays of dyad **4**.

b) KA decays of dyad **6** (left) and reference molecule **9** (right).
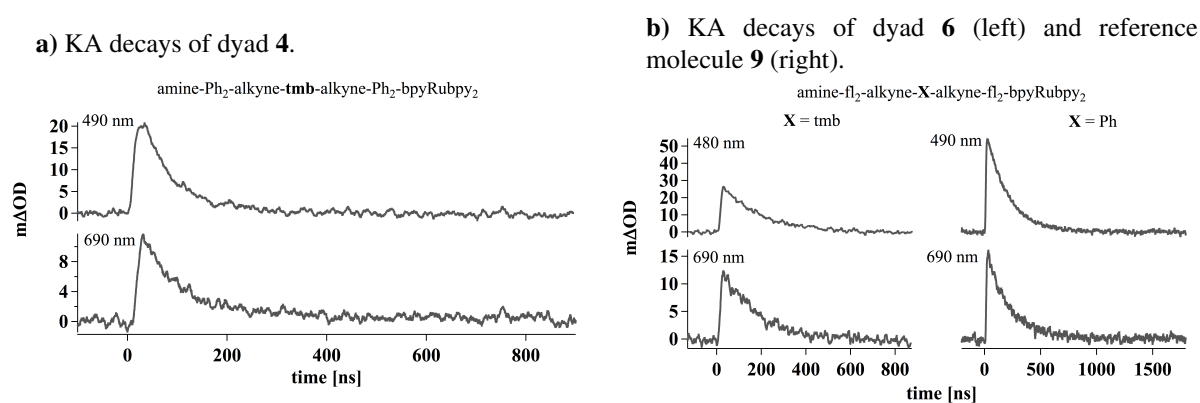
Figure 3.17 Kinetic absorption decays of dyad **4** (left) as well as dyad **6** and its reference molecule **9** (right). Measurements were carried out in a $2 \cdot 10^{-5}$ M solution in acetonitrile.

The shape of the KA decays at the two selected wavelengths are similar which indicates that the signals belong to the same photoproduct. The amine^{+} band in dyad **4** is expected around 750 nm based on the copper perchlorate titration in figure 3.14. Unfortunately, at 750 nm almost no signal was observed from the KA experiments. The TA spectrum shows a maximum at around 690 nm instead of 750 nm. Therefore this wavelength was used for lifetime measurements. The short lived species at both wavelengths decays within approximately 45 ns.

The longest lived photoproducts D-b-A systems of this series (**6** and **9**) decay in approximately 190 ns. This lifetime is close to that of neat Ru(bpy)$_3$(PF$_6$)$_2$ ($\tau \sim 170$ ns). This might be evidence that the excited state of these dyads decay through nonradiative and radiative processes like Ru(bpy)$_3$(PF$_6$)$_2$ and not through PET. Hence, our attention turned to flash-quench experiments. The photogenerated Ru^{III} species is a better electron acceptor compared to photoexcited Ru(bpy)$_3{}^{2+}$. Therefore, the electron transfer driving force should increase. The resulting intramolecular electron transfer will occur from the oxidized state instead of the excited state.

3.3.5 Flash-quench experiments

To explore whether charge transfer in dyad **4** as well as in the bis(9,9'-dihexylfluorene) dyad **6** and its reference molecule **9** occur, flash-quench experiments were carried out. Since the photoexcited $^*Ru^{II}$ complexes are not potent enough to perform charge transfer, the more oxidizing Ru^{III} had to be generated. The photogenerated Ru^{III} species is a better electron acceptor than photoexcited $Ru(bpy)_3{}^{2+}$. The scheme below summarizes the four important steps of the flash-quench procedure. For detailed information on flash-quench experiments see page 26.
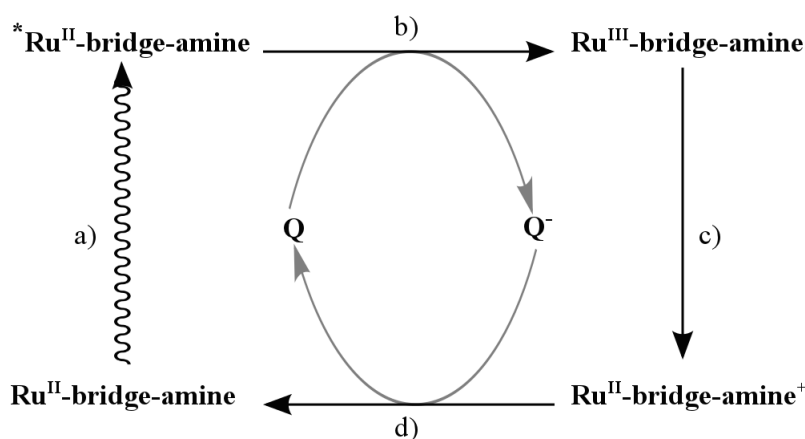
Scheme 3.5   Illustration of the flash-quench technique. a) Photoexcitation, b) "quenching" step, c) intramolecular charge transfer, and d) recombination.

Addition of 80 mM methylviologen hexafluorophosphate ($MV(PF_6)_2$) to the $2 \cdot 10^{-5}$ M dyad solution in acetonitrile followed by photoexcitation should lead to the formation of amine$^+$ and MV^+ or Ru^{3+} and MV^+. A signal around 400 and 600 nm will indicate the formation of the MV^+ species[58,97]. One should observe a negative signal at 450 nm due to the bleach of the MLCT absorption band of the metal center if Ru^{3+} is present.

In figure 3.18 the TA spectrum of the flash-quench experiment for dyad **4** is shown. The TA spectra were obtained under the same conditions as the TA spectra without quencher.

amine-Ph$_2$-alkyne-**tmb**-alkyne-Ph$_2$-bpyRu(bpy)$_2$
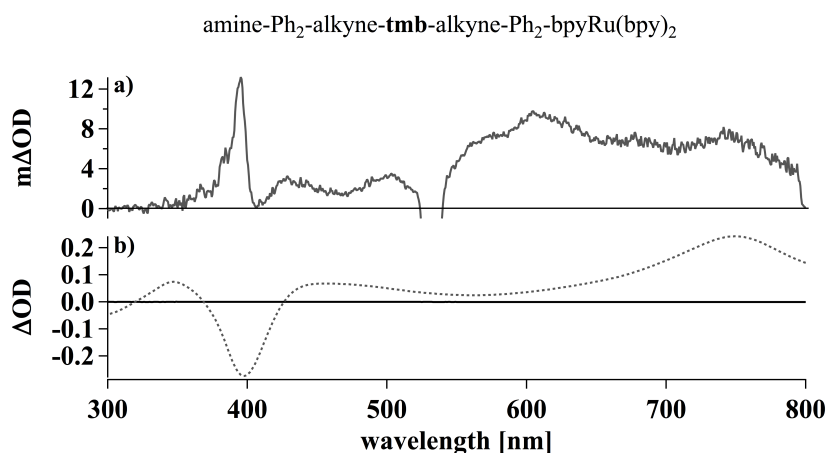
Figure 3.18   Transient absorption spectrum (a) of dyad **4** plus 80 mM $MV(PF_6)_2$. Measurements were carried out in a $2 \cdot 10^{-5}$ M solution in acetonitrile. Amine oxidation (b) were obtained from $Cu(ClO_4)_2$ titration in acetonitrile (c = $2 \cdot 10^{-5}$ M).

Addition of 80 mM $MV(PF_6)_2$ to the $2 \cdot 10^{-5}$ M solution of dyad **4** in acetonitrile did not lead to a color change. Comparison of the TA spectrum (see figure 3.18 spectrum a) with the amine oxidation reference spectrum (b) indicates the formation of amine$^+$ (band at 750 nm). The intense and structured signal around 400 nm and the less intense, broader band around 600 nm belong to MV^+. The formation of Ru^{3+} is not visible. As shown in scheme 3.5, Ru^{3+} will be generated during the flash-quench process. The signal is probably covered by the spectra of the amine and methylviologen mono cations. This suggests that photoinduced charge transfer takes place rapidly in dyad **4**. Immediately after the laser pulse Ru^{3+} has already disappeared and amine$^+$ has been formed.

Addition of 80 mM $MV(PF_6)_2$ to dyad **6** respective **9** lead to no color change either. Comparison of the TA spectrum (a in figure 3.19) with its amine oxidation reference spectrum (b) showed that amine$^+$ is formed after photoexcitation of the ruthenium complex. The band at 700 nm indicates the formation of amine$^+$.
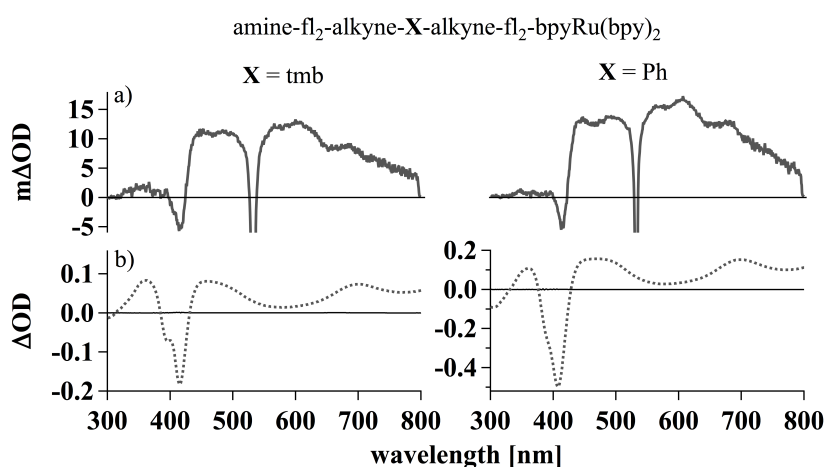
Figure 3.19   Transient absorption spectra (a) of dyad **6** and its reference molecule **9** (left) with 80 mM $MV(PF_6)_2$ in acetonitrile (c = $2 \cdot 10^{-5}$ M) obtained after pulsed excitation at 332 nm. Amine oxidation (b) were effected by addition of $Cu(ClO_4)_2$ to acetonitrile solution (c = $2 \cdot 10^{-5}$ M).

Unfortunately, in these experiments the formation of Ru^{3+} which is usually indicated by a bleach at 450 nm was not visible either.

Now, that there is evidence for photoinduced charge transfer in dyads **4**, **6** and reference molecule **9** we focus on kinetic absorption experiments. These experiments should support our hypothesis that in tmb dyads the charge transfer process is faster compared to their unsubstituted benzene reference molecules. Figure 3.20 shows the temporal evolution of some relevant transient absorption signals of these three D-b-A systems. In the dyads **4**, **6** and the reference molecule **9** the formation of the charge separated state is caused by the quencher (see b in scheme 3.5). The signal at 608 nm rises within the laser pulse and is caused by methylviologen (see appendix).

a) KA of dyad **4** with MV(PF$_6$)$_2$.

amine-Ph$_2$-alkyne-**tmb**-alkyne-Ph$_2$-bpyRubpy$_2$

b) KA of dyad **6** (left) and its reference molecule **9** (right) upon MV^{2+} addition.

amine-fl$_2$-alkyne-**X**-alkyne-fl$_2$-bpyRubpy$_2$
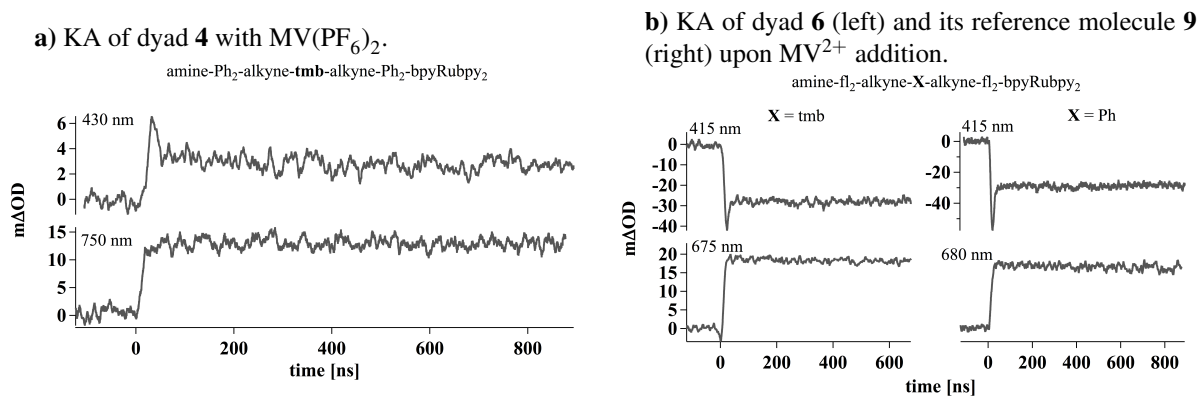
Figure 3.20   Kinetic absorption decays of dyad **4** (left) as well as dyad **6** and its reference molecule **9** (right). Measurements were carried out in a $2 \cdot 10^{-5}$ M solution in acetonitrile.

The formation of the charge separated state for dyad **4** as well as MV$^+$ is completed within the 10 ns laser pulse. A biexponential decay is observed at 430 nm for dyad **4**. This is related with the MLCT disappearance (around 450 nm in TA spectrum). The short lived signal in the upper left temporal evolution in figure 3.20 indicates that the ^{3}MLCT excited state of the ruthenium complex disappears within the 10 ns laser pulse. As shown in path c in scheme 3.5 the reduction of the ruthenium(III) to the ruthenium(II) should lead to the oxidation of the amine part. Amine$^+$ is formed in the same time range (> 10 ns). The recombination (step d in scheme 3.5) of Q$^-$ and amine$^+$ is significantly slower.

Dyad **6** and its reference molecule **9** show at 415 nm a negative signal with a short lived and long lived species (right picture in figure 3.20 upper temporal evolution). At this wavelength probably more than one species overlap therefore the temporal evolution of this transient absorption signal has a biexponential decay. Both D-b-A systems show the same lifetime of the short lived part which is less than 10 ns (within the instrumental limit). The short lived part might belong to Ru^{III}. In the subsequent step (scheme 3.5 step c) the charge is transferred to the amine moiety. In this scenario the resulting amine$^+$ formed within 10 ns. Recombination of Q$^-$ and amine$^+$ takes significantly longer.

We could show that charge transfer occurs in dyads **4**, **6** and reference molecule **9**. The transfer occurs within the 10 ns laser pulse. Hence, we could not proof our hypothesis that attachment of substituents can affect the rates for charge transfer in D-b-A systems. A higher temporal resolution setup might support this hypothesis.

3.4 Conclusions

It was possible to obtain in a multi-step synthesis four donor-bridge-acceptor (D-b-A) dyads equipped with a tetramethoxybenzene unit in the bridge (see picture below, left side). These dyads differ in donor-acceptor distance. The length of the donor-acceptor distance varies between 23 Å and 51 Å. Dyads **4** and **5** differ not significantly in length. There the torsion angle between the phenyl rings of the spacer might influence the charge transfer rate. For comparison of electron transfer properties and the influence of the electron rich tetramethoxybenzene, three reference molecules with an unsubstituted benzene molecule in the bridge instead of tetramethoxybenzene were prepared (see right picture below). The synthesis of the reference molecule to compare dyad **4** was not successful.
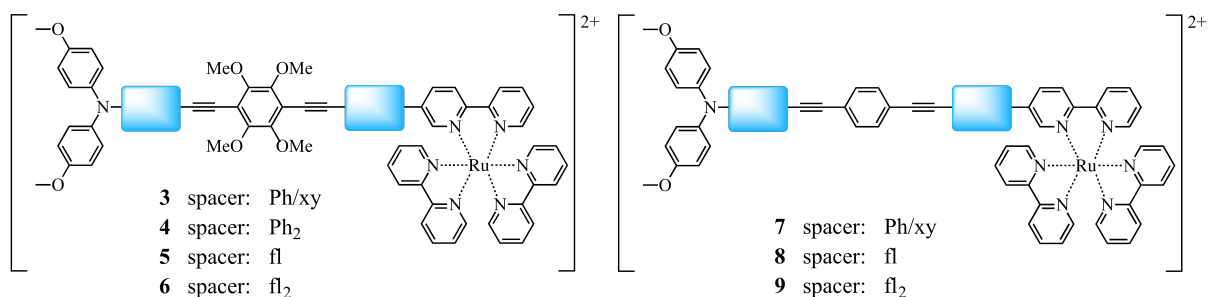
We proposed that in these four tetramethoxybenzene dyads the charge transfer is faster compared to similar dyads with an unsubstituted benzene in the bridge. Steady-state luminescence spectroscopy showed that in all tetramethoxybenzene dyads as well as in their reference molecules the luminescence is (partly) quenched. Luminescence decay measurements showed that in dyads **3** and **5** as well as in their reference molecules (**7** and **8**) photoinduced electron transfer (PET) might take place. In the longest dyad (**6**) and its reference molecule (**9**) PET is unlikely. To find direct evidence for PET, transient absorption spectroscopy was performed. Measurements confirmed that PET takes place in the D-b-A systems **3**, **5**, **7**, and **8**. Dyad **4** as well as **6** and its reference molecule **9** showed no clear evidence for a PET from the amine to the ruthenium moiety. Therefore, flash-quench experiments were carried out. In all three D-b-A systems (**4**, **6**, and **9**) PET was observed when methylviologen was used as quencher. Measurements of the temporal evolution of the relevant transient absorption signals showed that in all tetramethoxybenzene dyads (**3** - **6**) and their reference molecules (**7** - **9**) the formation as well as the recombination of the charge separated state is completed within the 10 ns laser pulse.

In summary, the hypothesis that in the tetramethoxybenzene dyads the charge transfer is faster compared to similar unsubstituted benzene molecules could not be supported nor excluded. Therefore, other facilities with a higher temporal resolution setup or longer donor-bridge-acceptor molecules are necessary to test our hypothesis of faster charge transfer across tmb bridging units.

4 Synthesis Part

4.1 Synthesis plan

As for every organic synthesis, a retrosynthetic approach is a good staring point to plan the synthesis of the desired molecule. The desired molecule can be split into smaller starting materials on paper. Then these smaller molecules need to be combined by chemical reactions. Retrosynthetic analysis gives also a first impression how many steps are necessary to produce the desired compound. In retrosynthetic analysis many possible ways can be drawn. Whether a way is more efficient than another can often not be seen at first glance.

The scheme below shows a general donor(**D**)-bridge(**b**)-acceptor(**A**) system split in a retrosynthetic way. The bridge consists of two spacer molecules (**s**) attached to a central molecule (**center**).
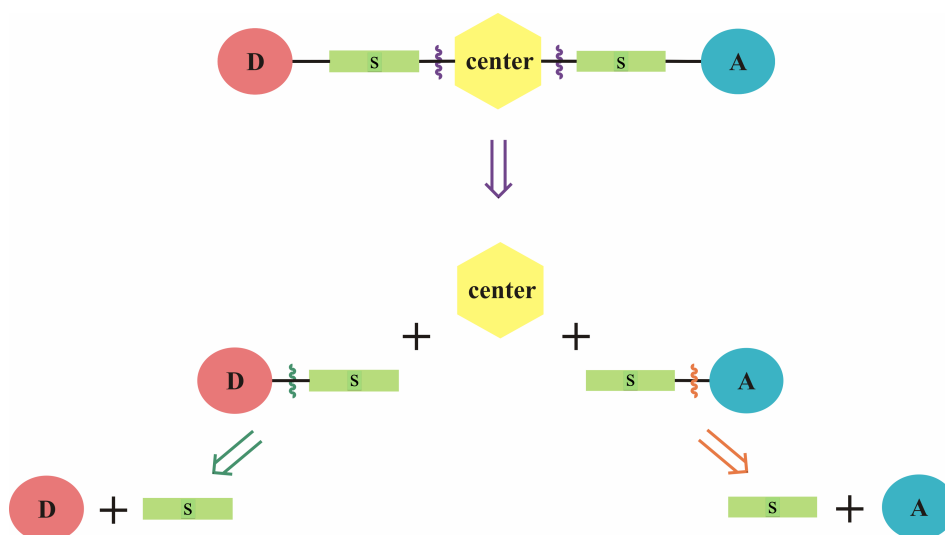
Scheme 4.1   Retrosynthetic analysis of a model D-b-A system.

As center (yellow hexagon in scheme above) unsubstituted and substituted benzene molecules were used. Dimesitylboron or methoxy substituents were attached to the benzene center. The spacer (green square in scheme 4.1) is either a phenyl/xylene, biphenyl, 9,9'-dihexylfluorene or bis(9,9'-dihexylfluorene) molecule. The electron donor (red cycle) used in this thesis is bis(*p*-anisyl)amine. As an electron acceptor (blue cycle) tris(bipyridine)ruthenium(II) was employed. Depending on the center the desired D-b-A systems can be linear or angled.

All desired D-b-A systems were synthesized in a linear synthesis strategy. In this chapter I will focus on the theory behind these reactions.
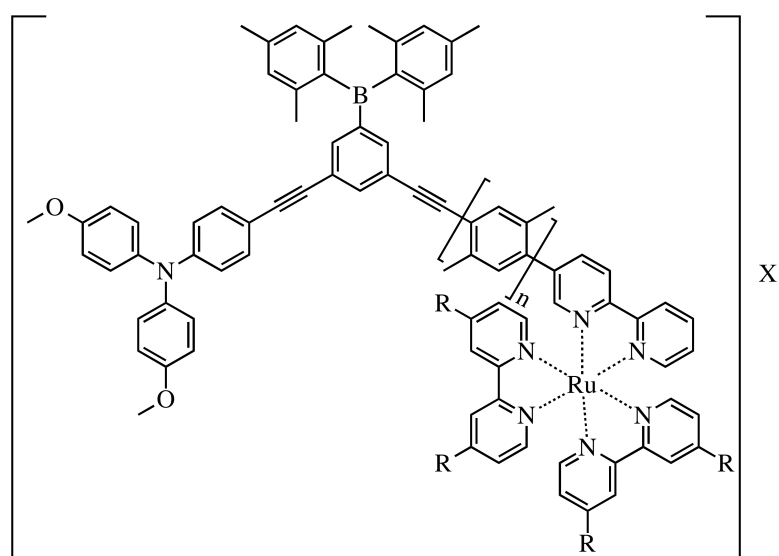
dyad **1** (n=1, R= H, X= (PF$_6$)$_2$)
dyad **2** (n=0, R= CF$_3$, X= (NO$_3$)$_2$)
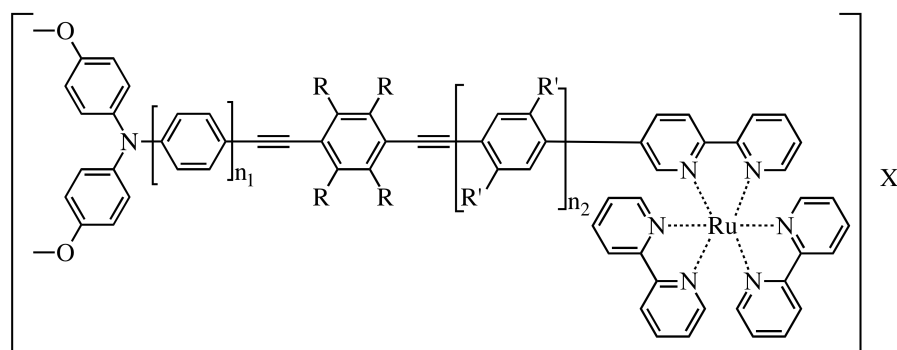
dyad **3** (n$_1$=1, n$_2$= 1, R= OCH$_3$, R'= CH$_3$, X= (PF$_6$)$_2$)
dyad **4** (n$_1$=2, n$_2$= 2, R= OCH$_3$, R'= H, X= (NO$_3$)$_2$)

dyad **7** (n$_1$=1, n$_2$= 1, R= H, R'= CH$_3$, X= (NO$_3$)$_2$)
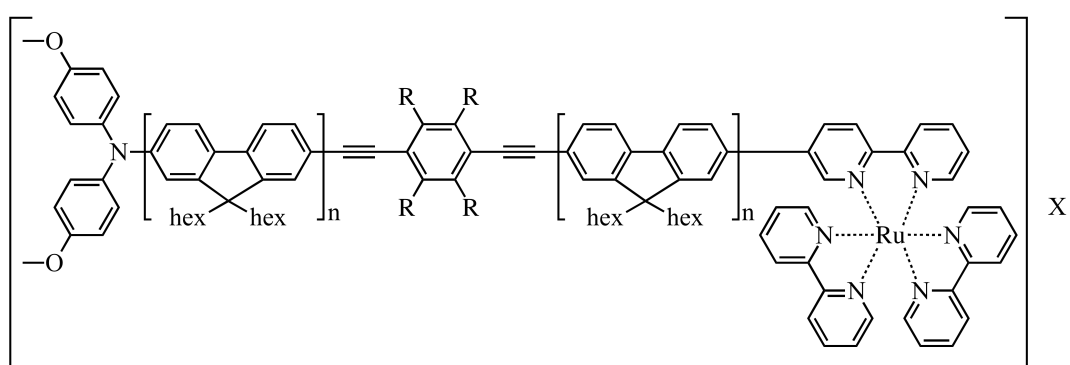
dyad **5** (n =1, R= OCH$_3$, X= (NO$_3$)$_2$)
dyad **6** (n =2, R= OCH$_3$, X= (NO$_3$)$_2$)

dyad **8** (n =1, R= H, X= (NO$_3$)$_2$)
dyad **9** (n =2, R= H, X= (NO$_3$)$_2$)

Figure 4.1 Dyads synthesized during this thesis.

4.2 Synthesis of precursor molecules

As shown in scheme 4.2, the retrosynthetic analysis will lead to amine and bipyridyl (bpy) precursors as well as to spacer molecules. To synthesize those molecules multiple steps are needed. But why did I choose this precursors? First, I started with the dimesitylboron dyads. To get to the desired molecules I had to do a retrosynthetic analysis. The upcoming scheme will show the result.
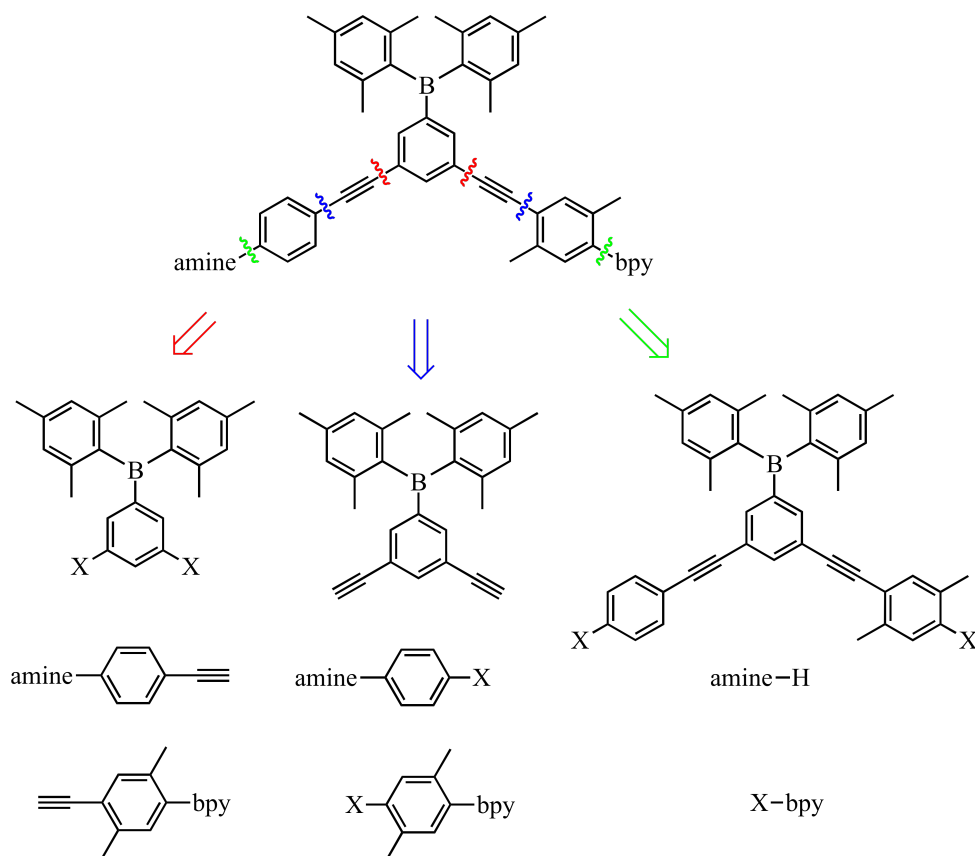
Scheme 4.2   Retrosynthetic analysis of dyad **1**.

Three possible ways are demonstrated. The red path led to some problems with the dimesitylboron compound. With 1,3,5-tribromobenzene as starting material it was not possible to get the monosubstituted dimesitylboron molecule in good yields. Separation of the mono- di-, trisubstituted dimesitylbroron benzenes by column chromatography was not possible. Protection with TMS groups at two sites gave the protected monosubstituted dimesitylboron molecule in good yield. The subsequent deprotection was unsuccessful. Therefore I tried the green way next. The synthesis of each single molecule was unproblematic. The bis(*p*-anisyl)amine (amine) is commercially available. Synthesis of 2,2'-bipyridine (bpy) is well studied and was used by the Wenger group before. Selectivity in the following N-C coupling (Buchwald-Hartwig reaction) or C-C coupling (Sonogashira-Hagihara reaction) was not possible. At the end I explored the blue path. The boronmesityl central molecule was synthesized in good yield. The final Sonogashira-Hagihara coupling with the bpy part and the amine species was also manageable. As a halogen source iodine was chosen to ensure good yields for the final Sonogashira-Hagihara coupling. For simplicity reasons all molecule names were shortened. Abbreviations used in this thesis:

amine   bis(*p*-anisyl)amine

bpy   2,2'-bipyridine

fl   9,9'-dihexylfluorene

fl_2 bis(9,9'-dihexylfluorene)

xy   xylene

Ph   phenyl

Ph_2 biphenyl

$Bmes_2$ dimesitylboron

tmb   1,2,4,5-tetramethxybenzene

4.2.1 Phenyl spacer

For the final donor-bridge-acceptor molecules, spacers are needed. Many molecules can be used as spacers. I chose different phenyl compounds due to their rigid structure. The figure below shows an overview of the three spacers used in this thesis.

R = H or CH_3; R' = hexyl (C_6H_{13})
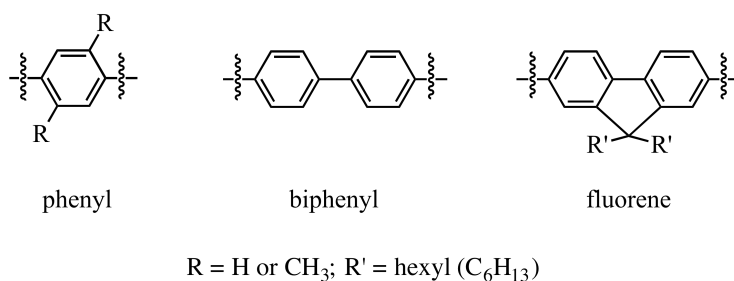
Figure 4.2   Phenyl spacers used in this thesis.

The lengths of the biphenyl and fluorene spacer are similar. With them, the idea was to control the twisting of the phenyl spacers. The equilibrium torsion angle between the phenyl rings in the biphenyl spacer measures approximately $44°$ [94] (unsubstituted). In unsubstituted fluorene molecules, the torsion angle measures $1.3°$ [95]. These angles are important for the electron transfer rate.

Xylene spacer

To synthesize $B(OH)_2-xy-TMS$ (**S-2**) a two step synthesis is necessary. First, the TMS group is introduced, followed by the boronic acid moiety.
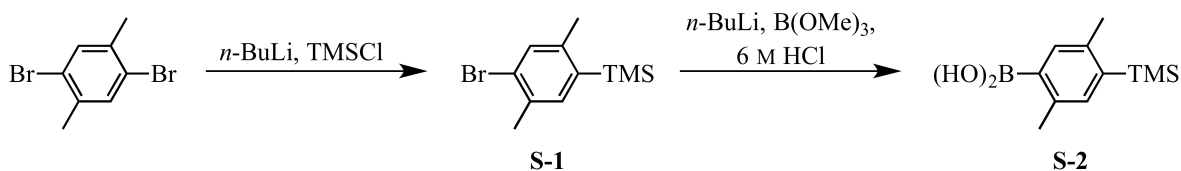
Scheme 4.3   Reaction pathway for xylene spacer.

Halogen-lithium exchange reactions are widely known but the mechanism is still not completely understood. In 1910, the first reaction of lithium and aryl halogen was published[98]. Wittig[99] and Gilman[100] pushed the research further with their discoveries how the reaction pathway might look like and what influence substituents have. There are three possible reaction ways:

1)   radical mechanism

2)   nucleophilic mechanism

3)   four-centered transition state model

For aryl halogen compounds the most likely way is the second. In 1951, Gilman published a possible nucleophilic mechanism[101] and in 1958 Wittig postulated the "ate-complex"[102].

Following the halogen-lithium exchange, a transmetalation[103] takes place, as drawn in scheme 4.4.
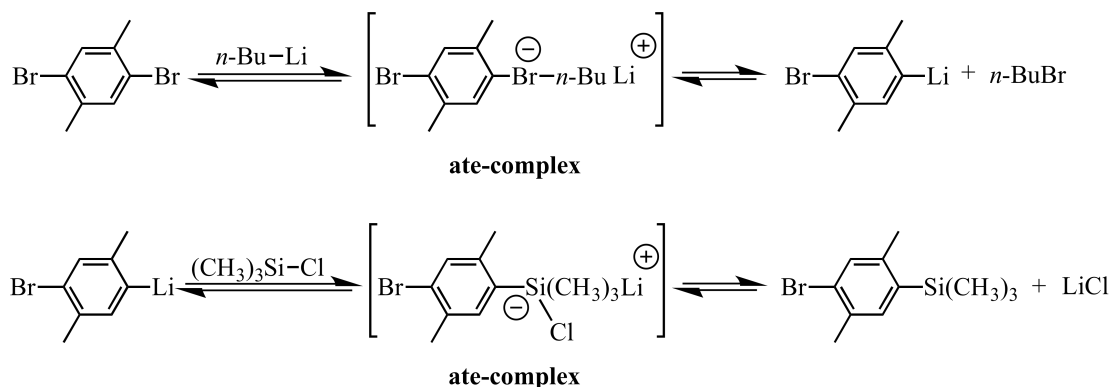
Scheme 4.4   Possible reaction pathway for halogen-lithium exchange and transmetalation.

Br−xy−TMS (**S-1**) was synthesized as a colorless oil in 98 % yield. This preparation was done before in our group[104] with 97 % yield.

The second part of this sequence of reactions can be done *via* two ways:

1)   Grignard reaction

2)   *n*-BuLi/ B(OMe)$_3$/ HCl

The Grignard reaction, starting with Br−xy−TMS (**S-1**), resulted in 65 % yield after recrystallization from diethyl ether. To minimize the failure rate of the Grignard reaction, I decided to synthesize compound **S-2** *via* an *n*-BuLi reaction. A halogen-lithium exchange is followed by the addition of trimethyl borate. To get the boronic acid, work up with 6 M hydrochloric acid is necessary.
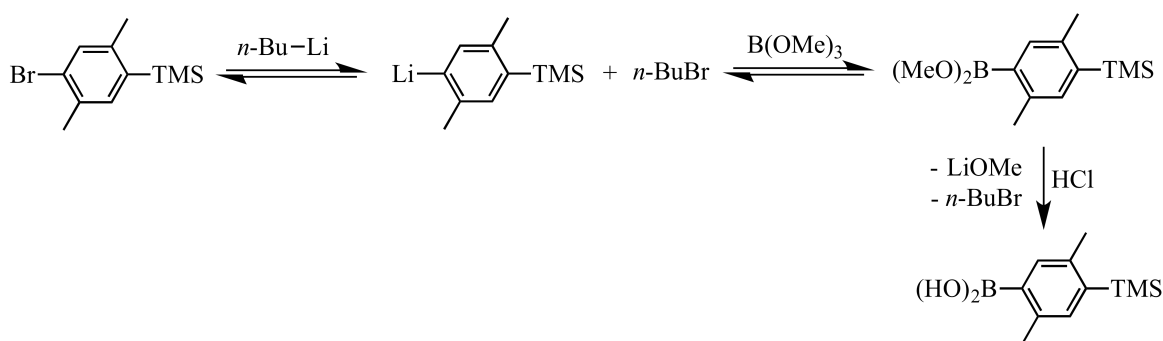
Scheme 4.5   Possible reaction path for B(OH)$_2$−xy−TMS synthesis using *n*-BuLi/ B(OMe)$_3$/ HCl.

B(OH)$_2$−xy−TMS (**S-2**) was recrystallized from a minimal amount hexane and gave 67 % yield of white crystals which is similar to yields described in the literature[105]. The second step of the reaction can be performed either *via* pathway 1) or 2), giving almost identical yields.

Biphenyl spacer

Starting from 4,4'-dibromobiphenyl or 4-bromo-4'-iodobiphenyl, compounds Br−(Ph)$_2$−TMS (**S-3**) and

B(OH)$_2$−(Ph)$_2$−TMS (**S-4**) can be synthesized (see scheme 4.6).
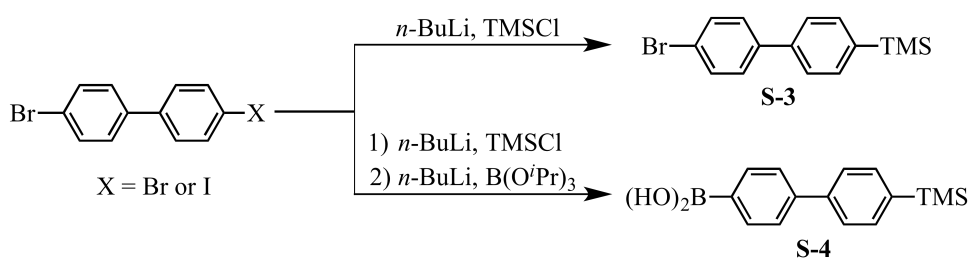
Scheme 4.6   Synthesis of the biphenyl spacer.

For Br−(Ph)$_2$−TMS (**S-3**), 4-iodo-4'-bromobiphenyl was used as starting material. After purification, white crystals were obtained in 89 % yield. A halogen-lithium exchange followed by a transmetalation step led to molecule **S-4**. In a one-pot reaction starting from 4,4'-dibromobiphenyl the TMS group was introduced first, followed by the boronic acid functionalization. The mechanism of the reaction is similar to scheme 4.4. The boronic acid was introduces using triisopropyl borate. When using this reagent a workup with 6 M hydrochloric acid is not needed. Addition of water is sufficient. This one-pot reaction is also known in the literature, giving yields between 59 and 72 %[106]. The desired compound **S-4** could be obtained as white product. Purification with a short column (maximum length 5 cm) first eluting with pentane, then with acetone lead to the pure product in 61 % yield.

Fluorene spacer

Fluorene is a cheap compound which can be used as spacer to enlarge molecules. To use this compound as a building block, three well-known reactions are necessary.
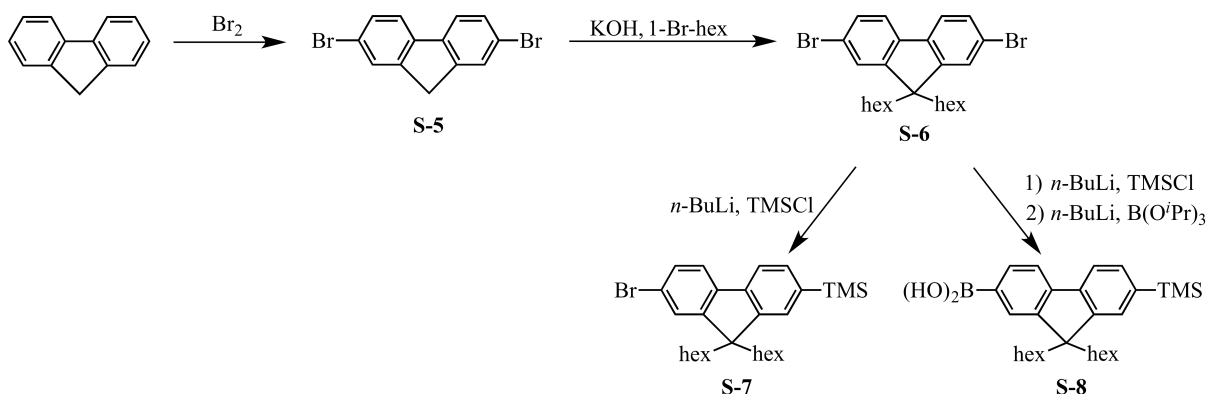
Scheme 4.7   Reaction scheme for the fluorene spacer.

Starting from commercially available fluorene first a bromination took place, according to the synthetic procedure from Hai and co-workers[107]. After recrystallization from ethanol, the desired product **S-5** was obtained in 84 % yield as white crystals. The possible mechanism for this reaction is shown in the scheme below. First, a homolytic splitting of the bromine bond by light leads to two bromine radicals. One cleaves the C-H bond homolytically and HBr is produced. The leftover bromine radical reacts with the carbon radical to form a C-Br bond. This step is repeated to synthesize Br−fluorene−Br (**S-5**).
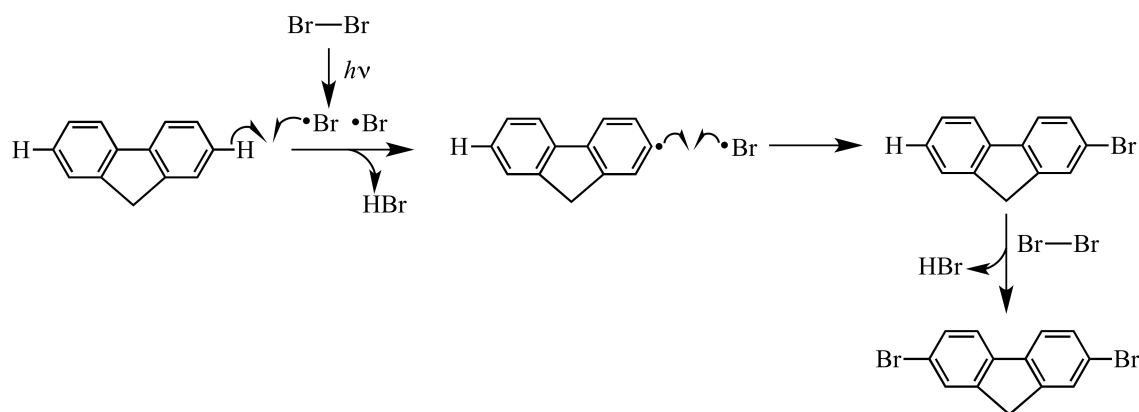
Scheme 4.8 Possible bromination mechanism.

To make fluorene molecules more soluble, the introduction of alkyl side chains is a useful option. In the reported case hexyl chains were chosen. The synthesis of Br−fl−Br (**S-6**) is known[108]. Following this procedure, Br−fl−Br (**S-5**) is treated with KOH and 1-bromohexane. The possible mechanism is drawn in scheme 4.9. The initial step includes the abstraction of a proton by KOH resulting in the formation of a carbanion and water as byproducts. This anion cleaves the hexyl group off 1-bromohexane. To synthesize molecule **S-6** these steps have to be carried out twice.
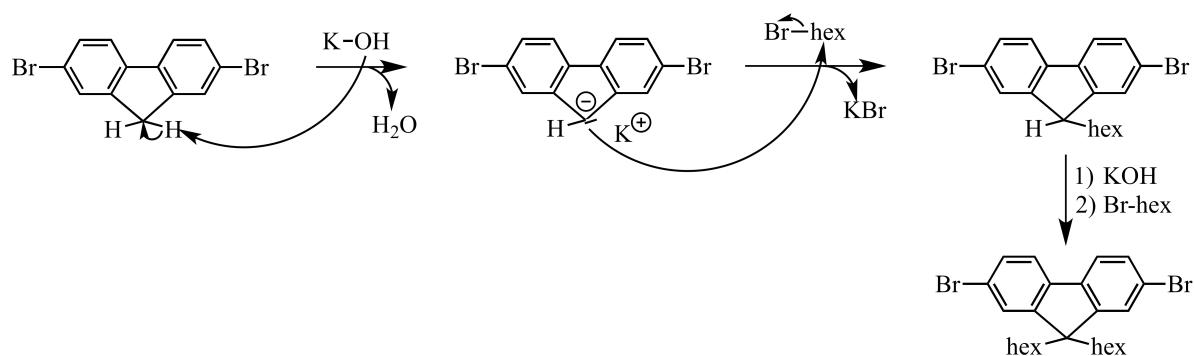
Scheme 4.9 Possible reaction pathway for compound **S-6**.

After purification by column chromatography, the product was obtained as white crystals in 99 % yield. The synthesis of Br−fl−TMS (**S-7**) was carried out with *n*-BuLi and trimethylsilyl chloride[109]. The mechanism is similar to scheme 4.4. For B(OH)$_2$−fl−TMS (**S-8**), a halogen-lithium exchange followed by a transmetalation takes place as shown in scheme 4.4. A one-pot reaction[110] was used to get B(OH)$_2$−fl−TMS. Purification *via* column chromatrography lead to 83 % yield of a colorless oil which crystallized over time.

4.2.2 Amine compounds

As shown in the scheme below, five different amine-spacer molecules used in this thesis starting from bis(*p*-anisyl)amine were synthesized (see figure 4.1). The length of the spacer between the amine moiety and the central molecules increases from phenyl to biphenyl, 9,9'-dihexylfluorene and finally bis(9,9'-dihexylfluorene).

n=1, X=I   **A-6**
n=1, X=Br   **A-7**
n=2, X=I   **A-9**
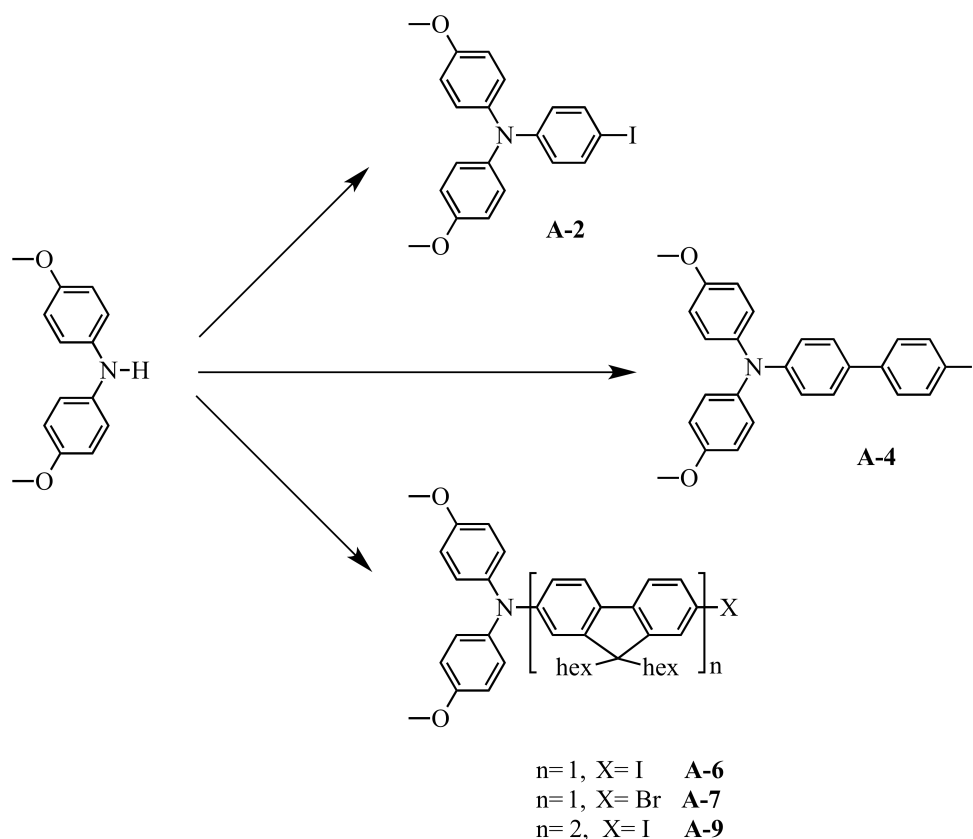
Scheme 4.10   Synthetic overview of the amine precursor synthesized in this thesis.

To get the desired amine compounds at least a two-step synthesis has to be done. First, an N-C coupling reaction followed by iodination is necessary. I used commercially available bis(*p*-anisyl)amine and either 1-bromobenzene, Br$-$(Ph)$_2$$-$TMS (**S-3**) or Br$-fl-$TMS (**S-7**) as halogen compounds.

To form an N-C atom connection, multiple ways were tested before[111,112,113,114,115]. Unfortunately, many of those ways include toxic chemicals or result in low yields. In 1994, Hartwig published an N-C coupling method including the presence of stannanes[116]. In 1995, Buchwald provided a well working way of reactions between amines and aryl halides without using tin[117]. This reaction is now known as Buchwald-Hartwig amination.

Via a palladium-catalyzed cross-coupling of aryl halides with amines a variety of molecules were synthesized. The mechanism is similar to a Sonogashira-Hagihara coupling and might follow the upcoming scheme.

Scheme 4.11 Buchwald-Hartwig amination (B-H-A) of bis(4-methoxyphenyl)amine with 1-bromobenzene.

Opening with oxidative addition of 1-bromobenzene a palladium(II) species is created. This intermediate reacts with the amine compound. In the following step sodium-*tert*-butanolate abstracts the bromine atom from the system. The final step is the reductive elimination of the desired product. The catalyst then undergoes further cycles.

This coupling reaction gave Ph−amine (**A-1**) as a light beige product after purification.

Ph−amine−I (**A-2**) was synthesized *via* iodination. In 1998, Fourrey and co-workers published a paper on mild and effective iodination[118]. They used [bis(trifluoroacetoxy)iodo]benzene in the presence of iodine. [Bis(trifluoroacetoxy)iodo]benzene is a hypervalent iodine compound and is known as strong oxidizing agent. Lambert and co-workers[119] used this procedure to synthesize the desired molecule **A-2**. Compound **A-1** was reacted with [bis(trifluoroacetoxy)iodo]benzene and iodine in methylene chloride. In their paper they stated that it is enough to react the amine **A-1** one time with the iodine-[bis(trifluoroacetoxy)iodo]benzene mixture. Unfortunately, in my case the reaction was not complete and separation of **A-1** and **A-2** is not possible. So I tried to react the amine **A-1** twice with the mixture and it worked. Also, it was not possible for me to reproduce the way of purification published by Lambert and co-workers. I had to do column chromatography with pure pentane first to remove the unreacted aryl compound of [bis(trifluoroacetoxy)iodo]benzene and finally isolate the desired iodinated compound with a 1:1 pentane/methylene chloride mixture as off-white crystals. When these crystals were stored in the dark over a longer period, the surface of the compound became slightly green. The color change is likely due to oxidized amine which is also observable when amine compounds are dissolved in chloroform.

For compounds **A-4**, **A-6** and **A-9** (yellow oils) first a Buchwald-Hartwig amination was performed followed by iodination *via* ICl. To synthesize compound **A-9** first I tried to perform the Miyaura-Suzuki coupling with the iodine compound **A-6**. Unfortunately this reaction gave not a trace of the desired

amine$-$fl$_2$$-$TMS (**A-8**). Therefore the brominated amine **A-7** was necessary. The bromination of compound **A-5** gave molecule **A-7** with 94 % yield. The coupling step with amine$-$fl$-$Br (**A-7**) and spacer **S-8** gave compound **A-8** in 50 % yield as a yellow oil.

In table 4.1 the yields of all synthesized iodinated amine compounds are summarized including yields for Buchwald-Hartwig amination as well as the iodination step.

Table 4.1   Yields for amine compounds.

Desired compound	B-H-A	Iodination
A-2	92 %	80 %
A-4	94 %	94 %
A-6	49 %	94 %
A-9	50 %	98 %

4.2.3 Bipyridine compounds

To build the desired 2,2'-bipyridine (bpy) compounds, 5-bromo-2,2'-bipyridine had to be synthesized.

a) 1) BuLi, ClSn(*n*-Bu)$_3$, 2) I$_2$
b) 1) **S-2**, 2) ICl
c) 1) **S-4**, 2) ICl
d) **B-9**   1) **S-8**, 2) ICl
   B-11   1) **S-8**, 2) ICl, 3) **S-8**, 4) ICl
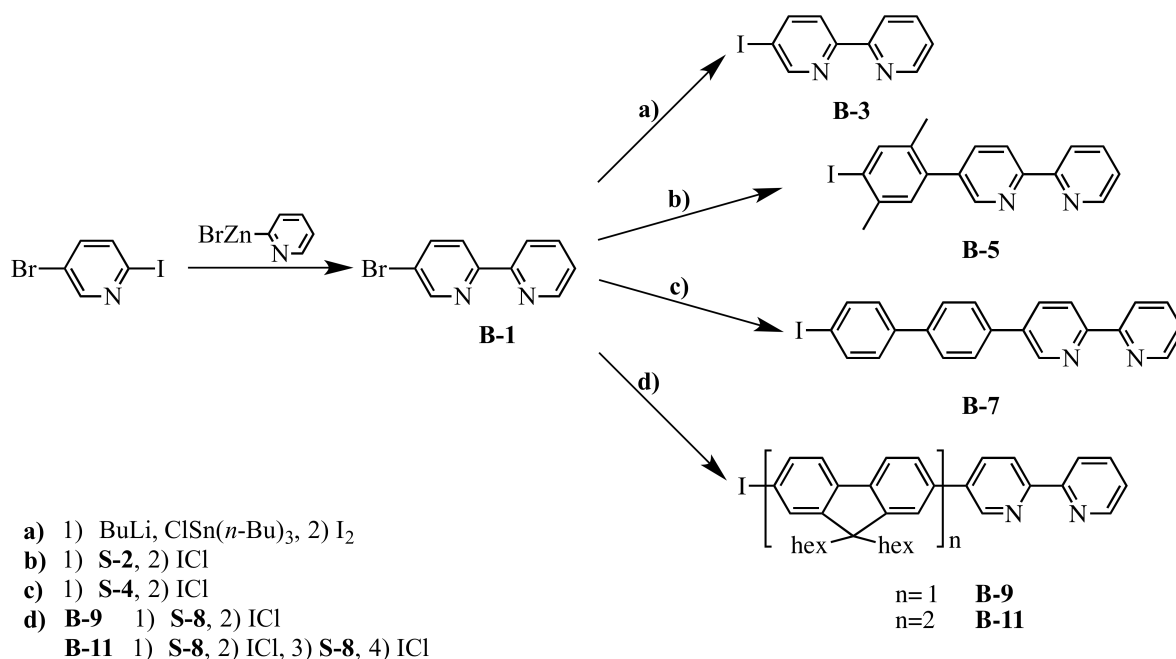
Scheme 4.12   Synthetic overview for bpy precursors.

One can see in the scheme above, at least two additional steps after the initial synthesis of 5-bromo-2,2'-bipyridine (Br$-$bpy) are needed to get compounds **B-3** to **B-11**.

To synthesize Br$-$bpy (**B-1**), a C-C coupling is needed. Three pathways are feasible:

a)   Stille coupling

b)   Miyaura-Suzuki coupling

c)   Negishi coupling

Stille coupling gave Br$-$bpy in 60% yield. Miyaura-Suzuki coupling gave no trace of compound **B-1**. The best results were achieved using a Negishi coupling.

Negishi coupling is done with a palladium or nickel[120] catalyst to couple a zinc compound with a

halogenated pyridine. Zinc is also an excellent agent for transmetalation which takes place in Negishi coupling[121]. The mechanism for this reaction could look like this:
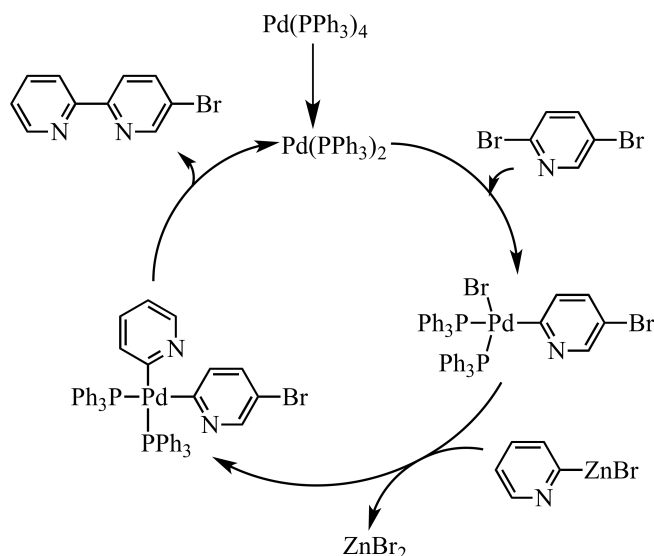
Scheme 4.13 Palladium-catalyzed Negishi coupling.

First, oxidative addition takes places when the 2,5-dibromopyridine interacts with the palladium species. This step is followed by the transmetalation between the zinc compound and the Pd-intermediate. Finally, reductive elimination of the desired compound occurs. Br−bpy (**B-1**) was synthesized in 96 % yield after column chromatography as off-white crystals.

To synthesize an aryl iodine compound, various ways are possible. Most common is the substitution of nitro groups *via* Sandmeyer reaction. To get the nitro substitution multiple steps are necessary. The more convenient way is to introduce a TMS protection group and react the intermediate with I_2[122,123] or ICl[124,125,126]. In the literature it is also known that pyridine-Sn bonds can be cleaved easier and faster than pyridine-H bonds by electrophiles like halogens[127]. Under mild conditions it is possible to exchange the stannyl group by iodine at room temperature.

Two ways to synthesize I−bpy (**B-3**) are described in the literature. One method is converting Br−bpy (**B-1**) directly into **B-3** with copper(I)iodide, sodium iodide and *trans*-N,N'-dimethyl-1,2-cyclohexane-diamine as solvent[128]. This reaction has to be refluxed for 70 hours and *trans*-N,N'-dimethyl-1,2-cyclohexanediamine is not a cheap compound. Therefore, I did not to choose this method even if the reported yield of 94 % is quite good. The second way to produce **B-3** is starting from 5-nitro-2,2'-bipyridine. First, the nitro functionality is replaced by an amine group followed by a Sandmeyer reaction. The overall yield of these two steps is 47 %[129]. To achieve better yields I tried to replace the bromine in br−bpy (**B-1**) directly by using *n*-BuLi followed by addition of iodine. Unfortunately, the desired compound was isolated only in 18 % yield. By using ICl instead of iodine, the yield raised up to 32 % which was still not satisfying. Therefore, I decided to replace a stannyl group by iodine. The synthesis of stannane−bpy (**B-2**) is well known in the literature[104]. To get to the desired molecule first a reaction with *n*-BuLi takes place followed by a transmetalation with tributyltin chloride (see scheme 4.4). The exchange of Li by Sn is usually quite fast[103]. As an intermediate in both reaction parts, an ate-complex is possibly formed. Stannane−bpy (**B-2**) is synthesized in 69 % yield as a light brown oil. 15 minutes reaction time with ICl were enough to synthesize compound **B-3** in 84 % yield.

As drawn in scheme 4.14 below the iodonium ion reacts in an electrophilic aromatic substitution with the stannyl−bpy. The iodide anion removes the stannyl leaving group and forms iodide tributyltin.
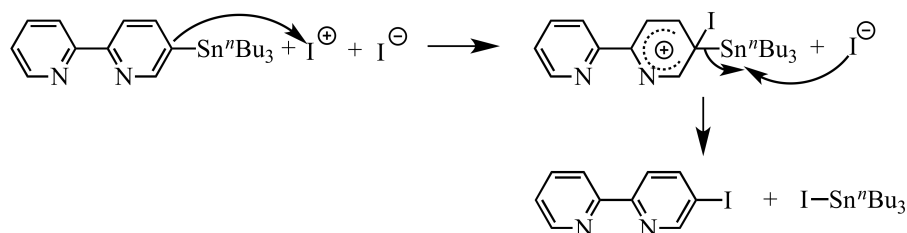
Scheme 4.14 Possible reaction mechanism for electrophilic substitution.

The synthesis of I−xy−bpy (**B-5**) first the attachement of the xylene spacer will be described, and in the second part the removal of the TMS protection group by iodine will be described.

The desired molecule TMS−xy−bpy (**B-4**) was synthesized *via* a Miyaura-Suzuki reaction.

First step is an oxidative addition. Compound **B-1** reacts with the catalyst and forms an intermediate which undergoes a transmetalation step and in the end with reductive elimination the desired compound **B-4** is set free.
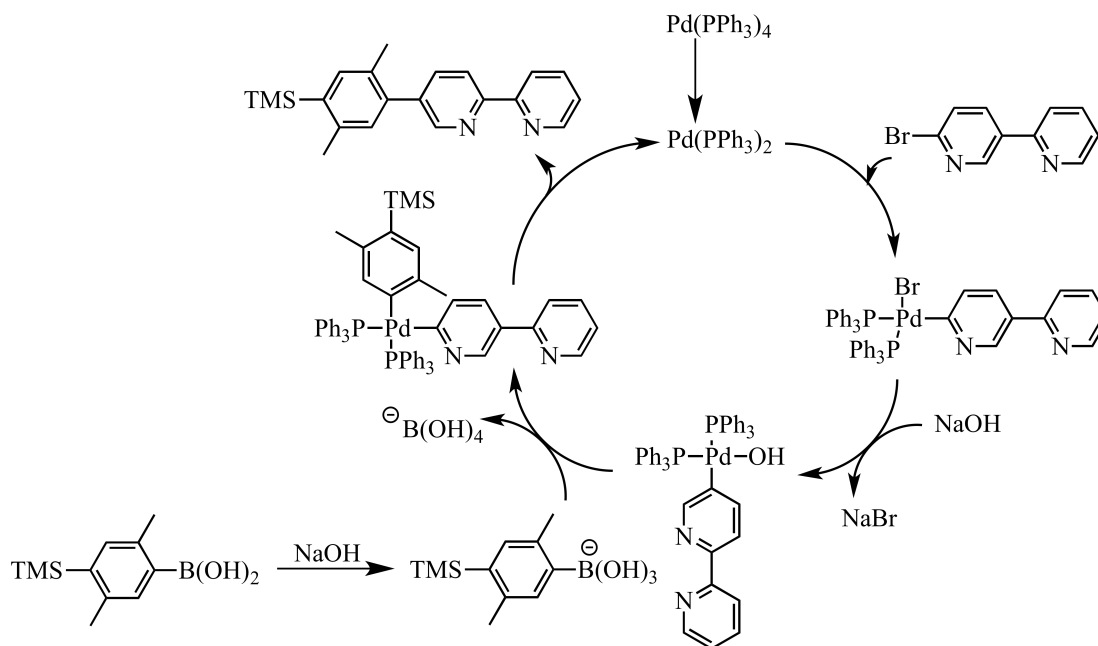
Scheme 4.15 Possible reaction mechanism for Miyaura-Suzuki reaction.

In my case, Na_2CO_3 was used as base. This forms *in situ* $NaHCO_3$ and NaOH. $NaHCO_3$ can react also in the way shown in scheme 4.15 for NaOH. Compound **B-4** was obtained as white crystals.

Compounds **B-6** (off-white crystals), **B-8** (colorless oil), and **B-10** (light yellow oil) were synthesized in a similar fashion.

For the iodination with ICl an electrophilic aromatic substitution takes place. First, the ICl divides into an iodonium ion and a chloride anion. The iodonium ion reacts with the bpy compound **B-4** to the desired I−xy−bpy (**B-5**). In scheme 4.16 the proposed mechanism for the iodination is shown with molecule **B-5** as example.
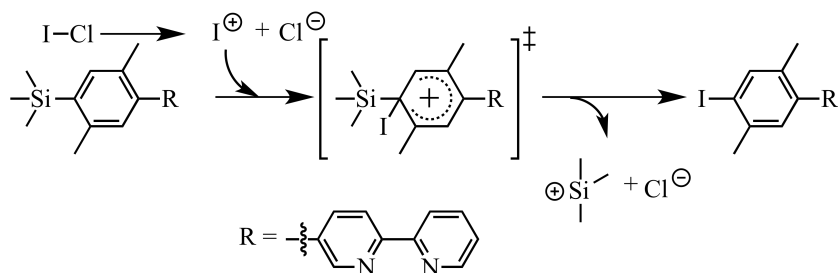
Scheme 4.16   Possible electrophilic aromatic substitution for compound **B-5**.

In this step a solvent mixture of methylene chloride and acetonitrile was used. By using just methylene chloride, the final Sonogashira-Hagihara coupling would not work even if the ^{1}H-NMR spectrum for I−xy−bpy (**B-5**) looked similar to the reaction with the solvent mixture.

All bpy compounds which were synthesized *via* Miyaura-Suzuki coupling and iodination are summarized in the table below including their yields for these reactions.

Table 4.2   Yields for bpy compounds.

Desired compound	Miyaura-Suzuki coupling	Iodination
B-5	88 %	92 %
B-7	59 %	60 %
B-9	84 %	84 %
B-11	60 %	80 %

Ruthenium precursor

bpy(CF$_3$)$_2$

4,4'-bis(trifluoromethyl)-2,2'-bipyridine was synthethized according to the procedure published by Kamachi et al.[49]. After purification *via* column chromatography the desired compound was isolated in 30 % yield.

A Negishi coupling takes places but in this case it is nickel catalyzed. The steps are similar to scheme 4.13. First, the oxidative addition takes place. The subsequent steps are the transmetalation and the reductive elimination.
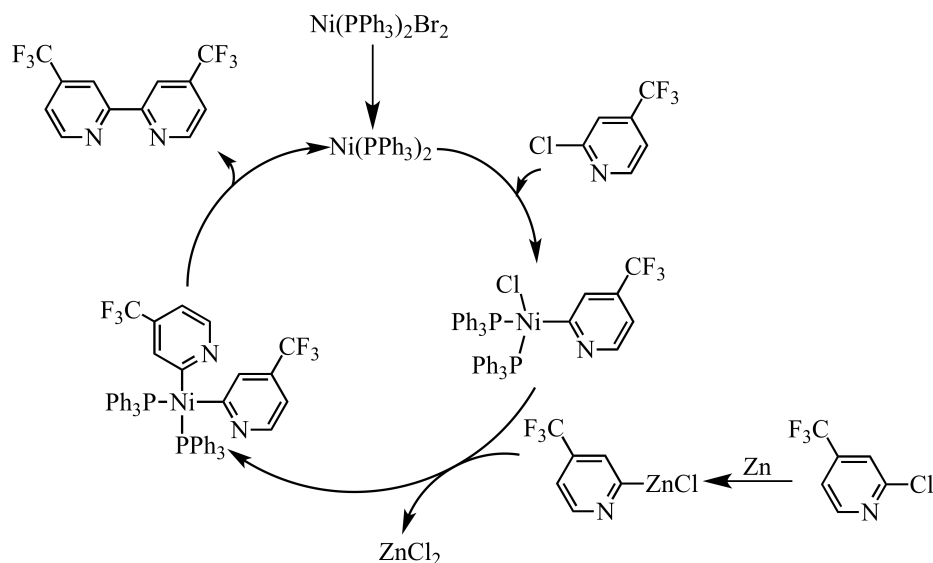
Scheme 4.17   Suggested nickel catalyzed Negishi mechanism.

Ru(bpy)$_2$Cl$_2$ and Ru(bpy(CF$_3$)$_2$)$_2$Cl$_2$

Bpy(CF$_3$)$_2$ was used to synthesize the ruthenium precursor for dyad **2**. This reaction was carried out as described by Yeomans et al. (method b)[130]. To reflux 1-methyl-2-pyrrolidinone, high temperatures are needed (melting point: 202-204 °C). Therefore, I decided to heat with the heat gun. This method seems not the best choice due to many byproducts. A group member found out that heating with a preheated sand bath is the best method. The yield is higher and no side products are obtained.

As precursor for the other complexes in this thesis *cis*-Ru(bpy)$_2$Cl$_2$ was used. This precursor has been prepared in many ways[131,132], e.g. *via* "ruthenium blue solution"[133]. In 1978, Sullivan et al. published a method starting from RuCl$_3$ which is nowadays often the method of choice[134]. The *cis*-Ru(bpy)$_2$Cl$_2$ precursor is often used in our group. Colleagues found out that eight hours is the best time for this reaction. If the synthesis was carried out longer, the byproduct Ru(bpy)$_3{}^{2+}$ becomes more prominent.

4.3 Synthesis of central molecules and dyads

4.3.1 Central molecules

In this thesis there are three central molecules:

1)   Boronmesityl substituted phenyl

2)   Tetramethoxybenzene

3)   Benzene
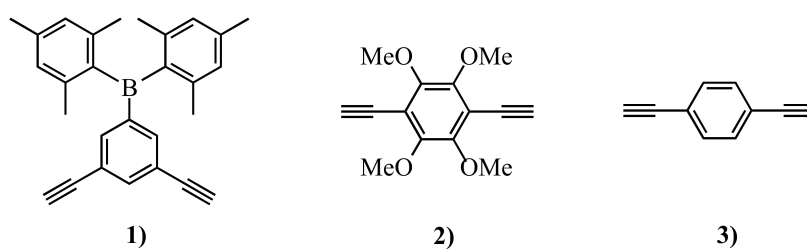
Figure 4.3   Central molecules in this thesis.

As can be seen in figure 4.3 all three molecules share a common feature: they all possess two alkyne groups. Those are needed for the final reaction steps to build the final ligand. Numerous reaction steps are necessary to make these central molecules.

Boronmesityl center

To get to the desired central molecule **12** (see scheme 4.18) three reaction steps are needed. First, a Sonogashira-Hagihara reaction is applied to attach the alkyne moiety, then a lithiation is followed by a reaction with dimesitylboron fluoride (FBmes$_2$), and finally deprotection of the alkyne is achieved with NaH.
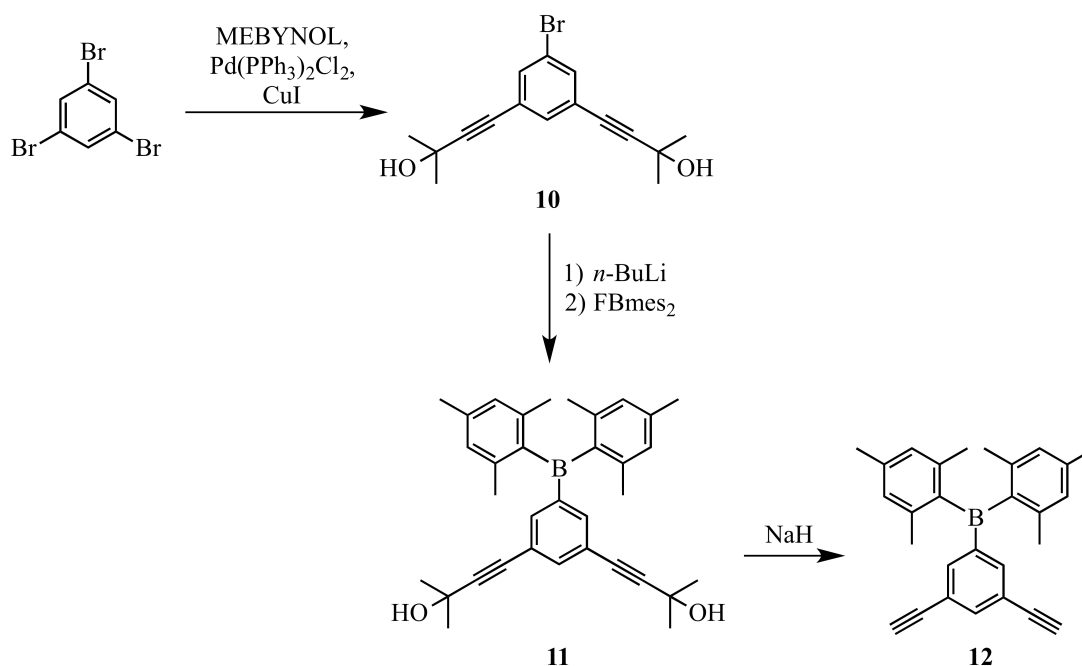
Scheme 4.18   Reaction pathway for the synthesis of the organoboron central molecule **12**.

First, 1,3,5-tribromobenzene was coupled to an alkyne in a C-C-coupling reaction. One of the most famous palladium-catalyzed C-C-coupling reactions is the Sonogashira-Hagihara coupling. In 1975, Sonogashira and Hagihara introduced a better way to perform cross-coupling reactions. They used less drastic conditions compared to Stephens-Castro coupling and avoided the separate synthesis and isolation of copper acetylides. With the use of bis(triphenylphosphine)paladium(II) dichloride (catalyst) and copper(I) iodide (cocatalyst) as well as triethylamine, terminal alkynes can react with arylhalides and lead to good yields under mild conditions. Therefore, it is now the most important method to prepare arylalkynes.

Even after all those years the exact mechanism for homogeneous reactions is still unknown. Physical measurements suggest plausible paths but it is very difficult to isolate organometallic intermediates for further studies. It is believed that the copper-catalyzed Sonogashira-Hagihara reaction is comprised by two independent catalytic cycles (see scheme 4.19).
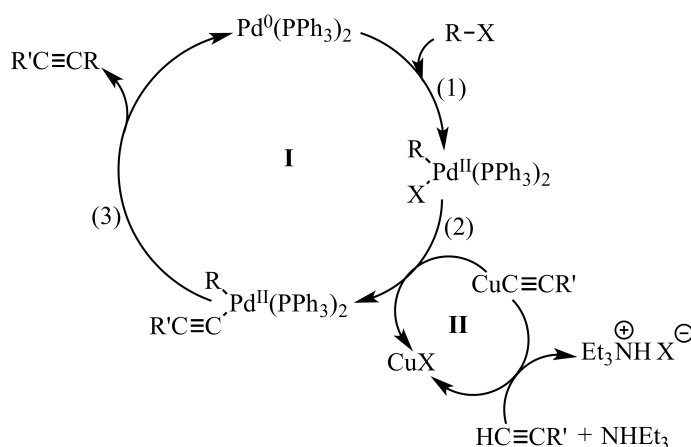
Scheme 4.19   Possible mechanism for Sonogashira-Hagihara coupling.

The upper cycle (I) shows the three initial steps. The aryl halide reacts with the palladium(0) species *via* oxidative addition (1). The thereby formed intermediate reacts with copper acetylide, which is built *via* deprotonation of the alkyne by the base (NEt_3) followed by copper(I) iodide reaction (cycle (II)). This step is called transmetalation (2) and the halide is cleaved off. Reductive elimination (3), the final step, sets the desired product free and the palladium(0) species is restored to its original state to enter the cycle again.

Scheme 4.20 is believed to explain how the palladium(0) species is generated.
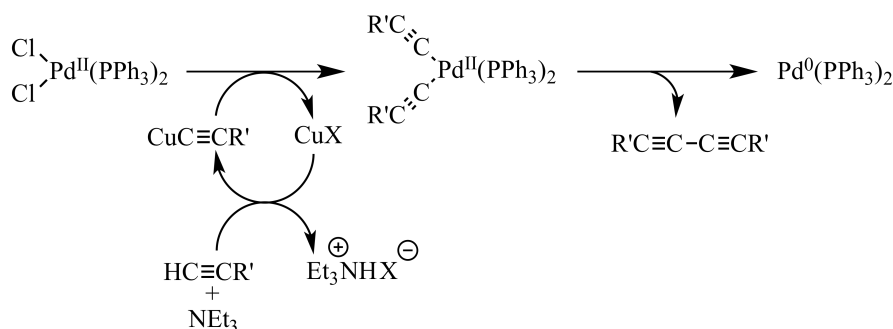
Scheme 4.20   Possible mechanism for formation of palladium(0) species.

The copper acetylide reacts *via* transmetalation to a dialkynylpalladium(II) complex followed by reductive elimination of the dialkyne and creation of a palladium(0) species.

The general reaction conditions consist of 4 mol% $Pd(PPh_3)_2Cl_2$, 2 mol% CuI and triethylamine (NEt_3) as solvent and base. In the first 15 minutes of heating a fluffy precipitate builds. If instead a black residue is formed, air was inside the flask or the triethylamine was not dry enough. As alkyl source MEBYNOL (2-methyl-3-butyn-2-ol) was the compound of choice. Compared to TMSA (trimethylsilyl alkyne) it is cheaper, and more stable. It can be stored for a longer time and at room temperature (compared to TMSA). An additional advantage is the easier separation of the mono-, di- and trisubstituted benzene molecules *via* column chromatography by using 1,3,5-tribromobenzene as staring material. This reaction step gave $Br-Ph-(mebynol)_2$ (**10**) as yellow crystals in 70 % yield.

The second step is a lithiation with a mechanism similar to scheme 4.4 followed by the reaction with dimesitylboron fluoride to get $mebynol-Bmes_2-mebynol$ (**11**) as a yellow solid in 58 % yield. It is known that reactions to attach boronmesityl do not often work in high yields[135]. Unfortunately, not only the desired product was obtained. An exchange of the bromine by a hydrogen also occurred. The separation of both products was not possible. This mixture might be caused by wet ($FBmes_2$). This compound is known to be highly hygroscopic.

The final step to form the central molecule $alkyne-Bmes_2-alkyne$ (**12**) (see figure 4.3) is the deprotection of the alkyne unit. For deprotection of MEBYNOL groups numerous ways are known. The alcohol moiety which protects the alkyne can be cleaved by a base such as sodium hydride (NaH)[136], potassium hydroxide (KOH)[137], sodium hydroxide (NaOH)[138], Bu_4OH[139] or even a base mixture like KOH/K_3PO_4[140]. In all cases the protection group is cleaved in the form of acetone. I decided to take NaH as base. The following scheme shows a possible mechanism for the deprotection.
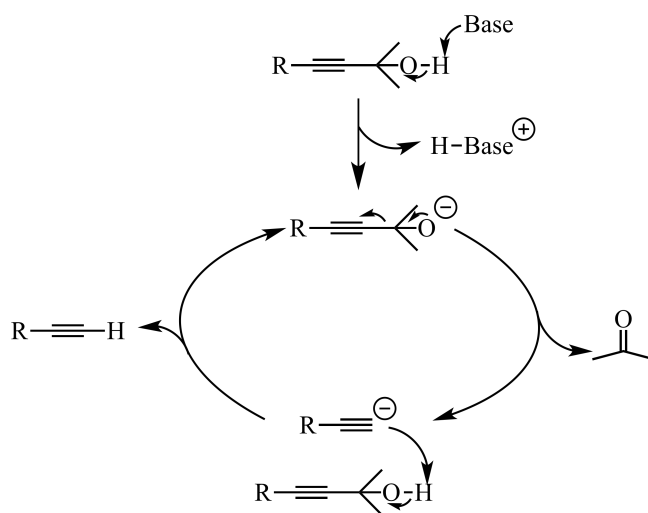
Scheme 4.21   Possible mechanism for MEBYNOL deprotection.

First, the base deprotonates the tertiary alcohol. With cleavage of acetone, an acetylide is formed. This intermediate can abstract a proton from another protected alkyne or from the protonated base. Either way, it will keep the reaction moving. The reaction between the acetylide and the alkyne molecule is reversible, therefore the acetone has to be removed. This can be done by an argon or nitrogen flow which carries out the acetone gas. The final reaction step provided the desired molecule **12** as light yellow crystals in 63 % yield.

Tetramethoxybenzene center

To get to the final central molecule (alkyne-tmb-alkyne (**20**)) as drawn in scheme 4.22 five to six reaction steps are needed.
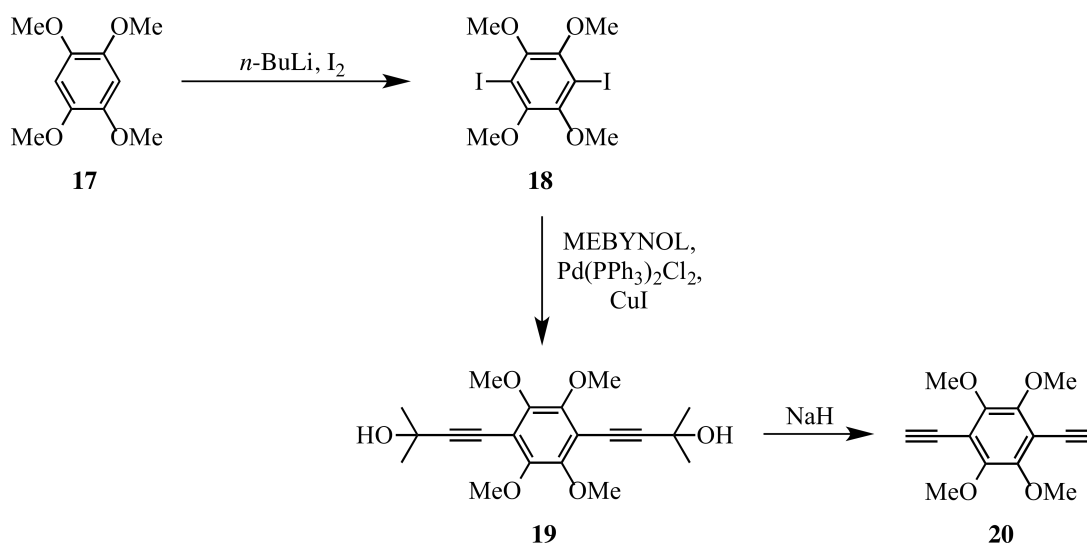
Scheme 4.22   Shortened synthesis overview to get the tetramethoxybenzene (tmb) center.

First, the tetramethoxybenzene (tmb) itself has to be synthesized. An overview for tmb synthesis is given in the scheme below.
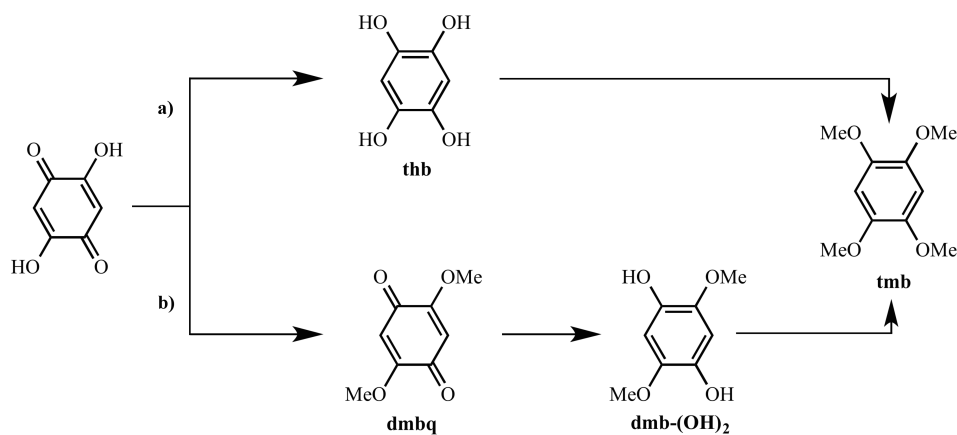
Scheme 4.23   Synthesis overview of the tetramethoxybenzene (tmb) center.

To synthesize the unsubstituted 1,2,4,5-tetramethoxybenzene two reaction pathways are possible.

Pathway a):   In a two-step synthesis starting from the commercially available 2,5-dihydroxy-1,4-benzoquinone and tin powder as well as hydrochloric acid as solvent and reagent[141], 1,2,4,5-tetra-hydroxybenzene (thb) was obtained in 83 % yield. Unfortunately, this compound decomposes quite rapidly and the complete removal of the hydrochloric acid is not easy. The second step is perfomed in dry DMF with potassium carbonate and iodomethane (CH_3I)[142]. The yield of 52 % is not optimal. By changing to dimethyl sulfate (($CH_3)_2SO_4$) and potassium hydroxide as base, the yield was even worse (38 %). Therefore I changed the synthetic strategy and followed pathway b.

Pathway b):   First the two hydroxy groups of 2,5-dihydroxy-1,4-benzoquinone were methylated. This step can be done in three ways. One way involves hydrochloric acid in methanol[143]. The second is a reaction with acetyl chloride in methanol[73]. The third, and the one I chose, is a reaction in methanol with boron trifluoride diethyl etherate ($BF_3 \cdot OEt_2$). This reaction was published by Vialut and co-workers in 2011[144]. The desired product (dimethoxybenzoquinone (dmbq) (**15**)) was obtained as beige needles in 88 % yield. In the initial step, as schown in scheme 4.24 a carbocation is generated[145] which is attacked in a nucleophilic way by the oxygen of the hydroxy group.
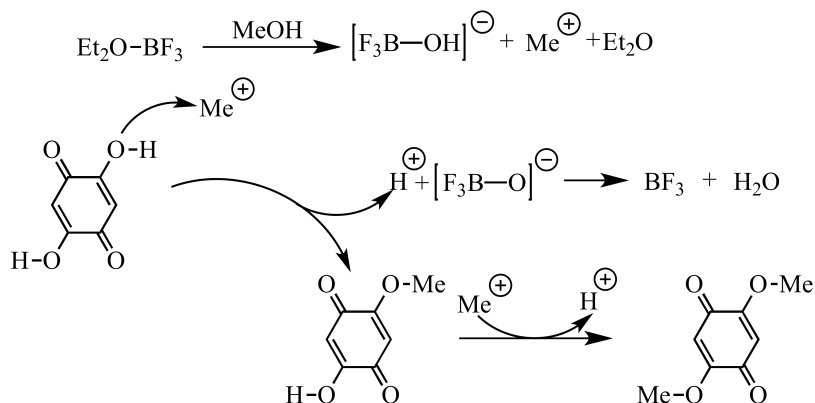
Scheme 4.24   Possible mechanism for double methylation of 2,5-dihydroxy-1,4-benzoquinone.

The second and third step were performed perviously in our group[73]. Reduction of the quinone of dmbq (**15**) with sodium borhydride ($NaBH_4$) in ethanol gave the dimethoxydihydroxybenzene ($dmb-(OH)_2$ (**16**)) with 83 % yield as light brown crystals. Scheme 4.25 shows a possible mechanism.
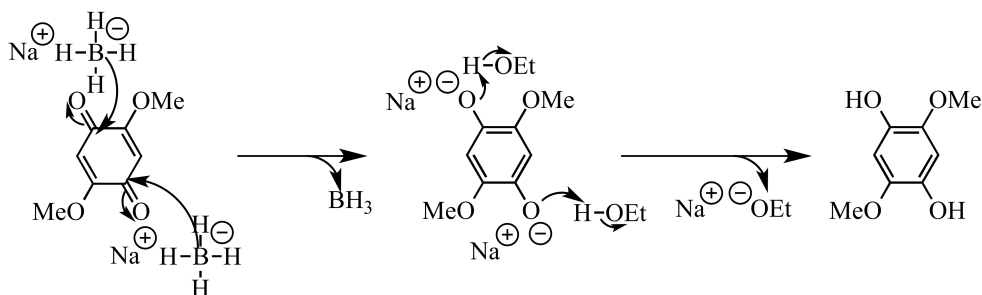
Scheme 4.25   Possible mechanism for double hydroxylation of 2,5-dimethoxy-1,4-benzoquinone.

In the next step, the crystals of $dmb-(OH)_2$ (**16**) were reacted with dimethyl sulfate, sodium bisulfite ($NaHSO_3$) and potassium hydroxide. The resulting off-white crystals of tmb (**17**) could be obtained in 89 % yield. The proposed mechanism for this step might follow scheme 4.26. There are two bases in this reaction. Potassium hydroxide is used to make the reaction side more reactive and sodium bisulfite is used to neutralize the monomethyl sulfuric acid. Sodium bisulfite acts as well as reduction agent.
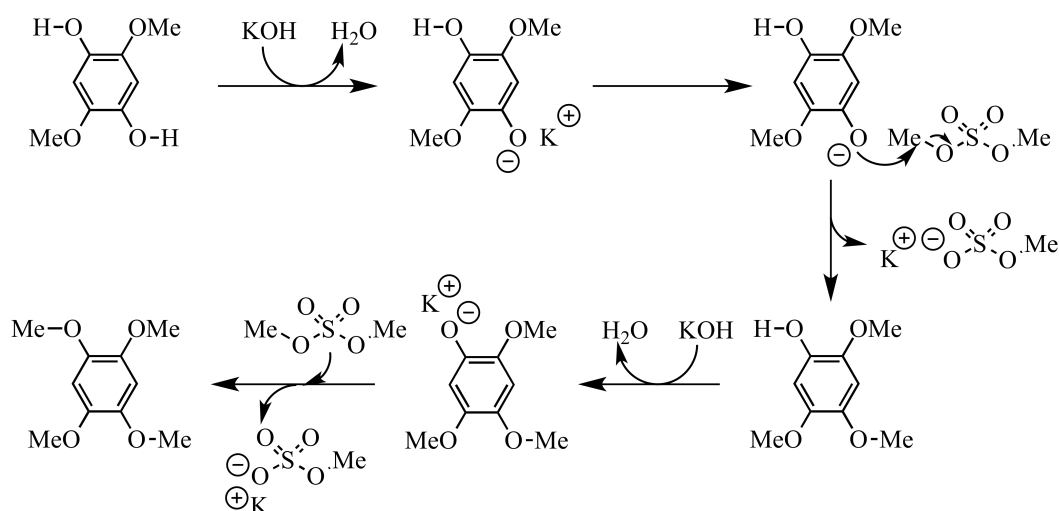
Scheme 4.26   Possible mechanism for double methylation of dmb−(OH)$_2$ (**15**).

To ensure a fast and complete Sonogashira-Hagihara coupling for the synthesis of molecule **19** the H-atoms in 3 and 6 position of tmb are replaced by iodine. In the literature, two synthesis pathways are known for 1,4-diiodo-2,3,5,6-tetramethoxybenzene (I−tmb−I (**18**)). One from 1974 where the desired molecule was a byproduct with only 9 % yield[146]. The other one is from 1992 where Staab and co-worker managed to produce it in 35 % yield[147]. A slight variation of the latter method gave the desired product in 68 % yield. The mechanism is similar to scheme 4.4.

Two additional steps had to be done to get to the final central molecule **20**. First, a Sonogashira-Hahgihara coupling followed by the deprotection of the alkyne moieties. The possible mechanism for both reactions are shown in scheme 4.19 and 4.21. Coupling works with 82 % yield and mebynol−tmb−mebynol (**19**) was obtained as off-white solid. Deprotection was carried out with only 0.5 equivalents of sodium hydride and gave alkyne−tmb−alkyne (**20**) as off-white crystals in 85 % yield. When more than 0.5 equivalents were used the reaction did not work, mebynol−tmb−mebynol (**19**) was destroyed .

Benzene center
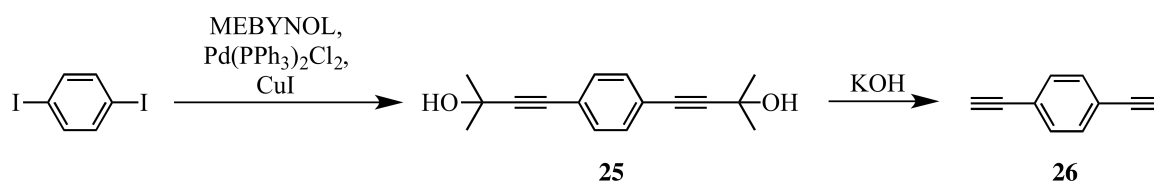
Scheme 4.27   Reaction overview for unsubstituted benzene center.

For the unsubstituted benzene central molecule **26** I chose 1,1-diiodophenyl as starting material due to the known reactivity order for Sonogashira-Hagihara reactions where aryl iodide is more reactive than aryl bromide or aryl chloride. The reaction took only 2 hours with quantitative yields , giving light yellow crystals after purification. For deprotection I chose the same procedure as Shu and co-workers with potassium hydroxide as base[148]. The desired product (**26**) was obtained in 54 % yield after purification as colorless crystals. Shu and co-workers obtained 98 % yield. For storage of compound **25**, a fridge was needed.

4.3.2 Ligands and dyads

Ligands In the beginning, I planned to obtain the ligand in a two step sequential synthesis. Either coupling with the amine part first followed by the bpy part or the other way around. Both ways did not lead to satisfying results. Therefore, I decided to do this reaction in one pot. For bpy$-$xy$-$alkyne$-$Bmes$_2$$-$alkyne$-Ph-$amine (**13**), the tmb ligands **21**, **23** and **24** as well as the unsubstituted benzene ligands **27**, **29** and **30** the synthetic strategy worked well by mixing all compounds (center molecule, bpy side, amine side) at once in a 1:1:1 equivalent ratio. In case of the biphenyl ligands **22** and **28**, this synthetic procedure did not work well. Ligand **28** could only be found in traces after column chromatography purification. For ligand bpy$-$alkyne$-$Bmes$_2$$-$alkyne$-Ph-$amine (**14**) the method had to be changed. First I$-$bpy (**B-3**) was put with the central molecule in the reaction flask. After one hour, the amine moiety (amine$-$Ph$-$I (**A-2**)) was added. This procedure was necessary due to preferred reaction between the amine compound and the central molecule. All yields are summarized in table 4.3.

Table 4.3 Yields for all ligands in this thesis.

Ligand	Yield	Yield^a
amine$-$Ph$-$alkyne$-$Bmes$_2$$-$alkyne$-xy-$bpy (**13**)	49 %	98 %
amine$-$Ph$-$alkyne$-$Bmes$_2$$-$alkyne$-$bpy (**14**)	31 %	62 %
amine$-$Ph$-$alkyne$-$tmb$-$alkyne$-$xy$-$bpy (**21**)	30 %	60 %
amine$-$Ph$_2$$-$alkyne$-tmb-$alkyne$-Ph_2$$-$bpy (**22**)	10 %	20 %
amine$-$fl$-$alkyne$-$tmb$-$alkyne$-$fl$-$bpy (**23**)	50 %	100 %
amine$-$fl$_2$$-$alkyne$-tmb-$alkyne$-fl_2$$-$bpy (**24**)	23 %	46 %
amine$-$Ph$-$alkyne$-$Ph$-$alkyne$-$xy$-$bpy (**27**)	50 %	100 %
amine$-$Ph$_2$$-$alkyne$-Ph-$alkyne$-Ph_2$$-$bpy (**28**)	*	
amine$-$fl$-$alkyne$-$Ph$-$alkyne$-$fl$-$bpy (**29**)	48 %	96 %
amine$-$fl$_2$$-$alkyne$-Ph-$alkyne$-fl_2$$-$bpy (**30**)	42 %	82 %

^{a}: Yields were referred to maximum yield of 50 %.

*: Only traces of the ligand were obtained.

Dyads Complexation of the ligands is the final step. Methanol and chloroform were added to the ruthenium precursor (Ru(bpy)$_2$Cl$_2$ or Ru(bpy(CF$_3$)$_2$)$_2$Cl$_2$), and the ligand. The mixture was heated over night. Column chromatography was needed to purify the complexes. By elution with acetone all unreacted ligand was eliminated. Changing the mixture to acetone/water (10:1) elutes the unreacted ruthenium precursor. With the final mixture (acetone/water/saturated aqueous potassium nitrate solution (100:10:1)) a separation of the desired dyad from the Ru(bpy)$_3$$^{2+}$ side product is possible. All complexation yields for the final dyads (see page 52) are summarized in table 4.4. The overall yield in the third column refers to all necessary reaction steps starting from commercially available compounds to the final molecules **1** to **9**.

Table 4.4 Yields for all dyads in this thesis.

Center	Dyad	Yield for last step	Overall yield
dimesitylboron benzene	**1**	53 %	2.3 %
	2	90 %	1.4 %
tetramethoxybenzene	**3**	38 %	1.7 %
	4	14 %	0.1 %
	5	22 %	0.7 %
	6	4 %	0.01 %
unsubstituted benzene	**7**	19 %	2.8 %
	8	14 %	1.1 %
	9	57 %	0.9 %

5 Summary

This thesis showcases donor-bridge-acceptor dyads for investigation of photoinduced charge transfer processes. Those processes take place in numerous natural processes like photosynthesis, oxygen binding, detoxification and respiration. The transfer can occur *via* a hopping or tunneling mechanism depending on the molecular structure. Two sets of molecules have been investigated. Bis(*p*-anisyl)amine is used as electron donor/hole acceptor. Tris(bipyridine)ruthenium(II) acts as the photosensitizer and electron acceptor/hole donor.

The first set of molecules, which is described in chapter 2, possesses a dimesitylboron substituent on the central benzene ring. Two dyads with different donor-acceptor distance were synthesized. To ensure the electron transfer, the shorter dyad (**2**) consists of a modified ruthenium(II) complex: in 4,4'- position of two bipyridine molecules CF_3-groups were attached to create an electron poor bipyridine ligand. As expected from the driving force calculations both dyads showed photoinduced electron transfer. The second part of this project focused on the photoinduced electron transfer upon fluoride addition. Triarylboron molecules are known as sensors for small anions. By having two mestiyl substituents attached to the organoboron compound it can bind selectively small anions like fluoride. We expected a change in the electron transfer rate due to an increased barrier height for the electron transfer after fluoride addition. Two scenarios can occur. One is the complete stop of electron transfer in the dyads. In the other scenario the electron transfer takes place but the rate constant changes. We observed that the electron transfer after irradiation still took place after fluoride addition. Unfortunately, in dyad **1** no significant rate difference was obtained whereas dyad **2** showed a slower recombination of the charge separated state. To study the charge transfer we also applied flash-quench experiments. Unfortunately, the used fluoride source reacted with most of the explored quenchers. Two quencher also reacted directly with the dyads. Therefore, further insights *via* flash-quench experiments were not possible.

The third chapter of this thesis was dedicated to the second set of molecules with a tetramethoxybenzene unit as center of the bridge. Our goal was to confirm our hypothesis that in tetramethoxybenzene dyads the charge transfer is faster than in the structurally identical dyads where an unsubstituted benzene replaces the tetramethoxybenzene unit. By having an electron-rich molecule in the bridging unit a tunneling mechanism might change into a hopping process. This results in a higher charge transfer rate. Four donor-bridge-acceptor dyads equipped with a tetramethoxybenzene unit in the bridge were synthesized. The donor-acceptor distance varies between 23 Å and 51 Å. Two dyads (**4** and **5**) differ not significantly in length but in the torsion angle between the phenyl rings of the spacer. This might have an influence on the charge transfer rate either. For comparison, three reference molecules with an unsubstituted benzene molecule in the bridge were synthesized. Estimation of the driving force for all dyads and their reference molecules showed that in principle photoinduced electron transfer should take place. Dyads **3** and **5** as well as their reference molecules (**7** and **8**) showed phototriggered electron transfer. By applying flash-

quench experiments we hoped to see charge transfer from the donor to the acceptor moiety in dyads **4**, **6**, and reference molecule **9**. These experiments confirmed that the charge transfer in the three molecules take as well place. To confirm our hypothesis temporal evolution of relevant transient absorption signals were used. Unfortunately, in all tetramethoxybenzene dyads (**3** to **6**) and their reference molecules (**7** - **9**), the formation and the recombination of the charge separated state is completed within the 10 ns laser pulse. To proof our hypothesis other facilities with a higher temporal resolution setup are necessary.

6 Experimental part

6.1 General information

UV/Vis measurements

All measurements were carried out on a Cary 5000 UV-Vis-NIR spectrometer at room temperature. Quartz cuvettes were purchased from Starna.

Cyclic voltammetry

All measurements were carried out on a Versastat3-200 potentiostat from Princeton Applied Research at room temperature. A glassy carbon disk was used as working electrode. A silver wire worked as counter-electrode. A second silver wire was employed as a quasi-reference electrode. Ferrocene was used for proper referencing of the potentials. 0.1 M $(Bu_4N)PF_6$ solution was used as an electrolyte. Four cycles with a scan rate of 0.5 V per second were performed. Acetonitrile (HPLC quality, from Fischer) or methylene chloride (spectroscopic grade, Alfa Aesar) were used as solvent. For each sample 1-2 ml of solution were used for measurements. Data analysis was carried out with Igor (Version 6.3.1).

Laser spectroscopy

To measure short lived species a LP920-KS spectrometer from Edinburgh Instruments was used which was equipped with a R928 photomultiplier and an iCCD camera from Andor. As excitation source a Quantel Brilliant b laser was used (excitation wavelength: 532 nm). The time resolution is approximately 10 ns. Experiments were carried out in the same cuvettes as used for UV/Vis. The measurements were carried out at room temperature and 2 ml aerated solution for each sample were used.

Steady state luminescence

A Fluorolog-322 instrument from Horiba Jobin-Yvon was used. The quartz cuvettes from Starna were filled with 2 ml aerated solution.

^{1}H-NMR

All spectra were measured on a 400 MHz Bruker Avance instrument. In ^{1}H spectra tetramethylsilane was used as reference. The solvent signals were used as internal standards.

Elemental analysis

A Vario EL III CHNS analyzer from Elementar was used for analyzing the substances.

Chemical crystallography

Crystal were measured with a CAD4 four circle diffractometer and a KappaCCD, both from Bruker-Nonius in Delft. All the solution and refinement work was done on PC's. As refinement package Crystals

was used. For the crystal structure figures showed in this thesis Mercury was used.

TLC

TLC were carried out on TLC Silica gel F$_{254}$ plates (20 x 20 cm) from Merck.

Column chromatography

For column chromatography SiliaFlash P60 (40-63 μm, 230-400 mesh) from Silicycle were used.

6.2 Chemicals

Purchased chemicals:

Chemical	CAS Number	Supplier
Bis(dibenzylideneacetone)palladium(0) ($>$ 98 %)	32005-36-0	Fluorochem
Bis(*p*-anisyl)amine (98 %)	101-70-2	Alfa Aesar
[Bis(trifluoroacetoxy)iodo]benzene (97 %)	2712-78-9	ABCR
Boron trifluoride diethyl etherate ($\geq$ 46 % BF_3)	109-63-7	Acros
1-Bromobenzene (99 %)	108-86-1	ABCR
5-Bromo-2-iodopyridine ($>$ 97 %)	223463-13-6	TCI
n-BuLi (2.5 M in hexane)	109-72-8	Acros
2-Chloro-4-(trifluoromethyl)pyridine (97 %)	81565-18-6	Fluorochem
1,4-Dibromo-2,5-dimethylbenzene (98+ %)	1074-24-4	Alfa Aesar
Dichlorotetrakis(dimethyl sulfoxide) ruthenium(II) (96 %)	89395-66-4	Sigma-Aldrich
2,5-Dihydroxy-1,4-benzoquinone (98 %)	615-94-1	Acros
1,4-Diiodobenzene (99 %)	624-38-4	Sigma-Aldrich
Dimesitylfluoroborane ($>$ 98 %)	436-59-9	TCI
Dimethyl sulfate (99 %)	77-78-1	Acros
Tri-*tert*-butylphosphonium tetrafluoroborate (97 %)	131274-22-1	Strem
Hydrazine monohydat (98 %, 64-65 % N_2H_4)	7803-57-8	Sigma-Aldrich
Palladium dichloride (99.9 %, 60 % Pd)	7647-10-1	ABCR
2-Pyridylzinc bromide (0.5M solution in THF, AcroSeal^{TM})	218777-23-2	Acros
2-Methyl-3-butyn-2-ol (98 %)	115-19-5	Alfa Aesar
1-Methyl-2-pyrrilidinone (99+ %)	872-50-4	Alfa Aesar
Ruthenium(III) chloride hydrate (0.5 H_2O)	14898-67-0	Sigma-Aldrich
Sodium hydride (60 % in oil)	7646-69-7	Sigma-Aldrich
Tetraethylammonium iodide (98 %)	68-05-3	Alfa Aesar
Tetramethylethylenediamine, extra dry (99 %)	110-18-9	Acros
1,3,5-Tribromobenzene (98 %)	626-39-1	Apollo
Tributyltin chloride (99 %)	1461-22-9	Acros
Triisopropyl borate (99 %)	5419-55-6	Flourochem
Trimethyl borate (99 %)	121-43-7	Acros
Trimethylsilyl chloride ($\geq$ 97 %)	75-77-4	Sigma-Aldrich
Triphenylphosphine	603-35-0	Merck

Dry methylene chloride, diethylether and tetrahydrofuran were purchased from a Pure Solv^{TM} micro solvent purification system from Innovative Technology. Triethylamine was purified and dried according to published methods. Other dry solvents were ordered from Sigma-Aldrich and used as received.

All temperatures mentioned are oil/ice bath temperatures.

Et_2O was distilled before column chromatography by Büchi Rotavapor$^{\circledR}$ to remove BHT as stabilizer.

6.3 General synthesis

All reactions were carried out under N_2-atmosphere.

Pd(PPh$_3$)$_2$Cl$_2$

$$
\begin{array}{c}
PPh_3 \\
| \\
Cl-Pd-Cl \\
| \\
PPh_3
\end{array}
$$

1.5 g (8.46 mmol) PdCl$_2$ and 1.94 g (26.02 mmol, 3.05 eq) KCl were suspended in 30 ml H$_2$O. The mixture was heated to 70 °C and turned dark red. After filtration under air, 4.45 g PPh$_3$ in 50 ml EtOH were added. A yellow precipitate formed and was filtered off. After washing with EtOH and Et$_2$O (three times each), the yellow residue was extracted with hot CHCl$_3$. Filtration and evaporation of the solvent yielded in an orange crystalline product which is air stable.

Yield: 4.98 g [84 %]

Pd(PPh$_3$)$_4$

$$
\begin{array}{c}
PPh_3 \\
| \\
Ph_3P-Pd-PPh_3 \\
| \\
PPh_3
\end{array}
$$
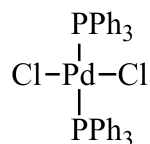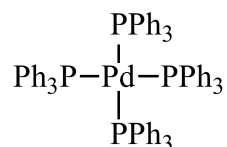
1.77 g (10.00 mmol) PdCl$_2$ and 13.1 g (50.00 mmol) PPh$_3$ were dissolved in 120 ml dry DMSO. This mixture was heated to 150 °C until it became clear. After removing the oil bath, 2.50 g (40.00 mmol) hydrazine solution were added. The reaction mixture was cooled with a water bath. A yellow precipitate formed. Filtration and washing twice with 5 ml dry EtOH, twice with 5 ml dry Et$_2$O under nitrogen, followed by drying in vacuum yielded yellow, air sensitive crystals which were used without further purification for Sonogashira-Hagihara coupling reactions.

GS I: *Buchwald-Hartwig amination*

The amine compound, halogen compound, NaO^{t}Bu, Pd(dba)$_2$, and (HP^{t}Bu)BF$_4$ were dissolved in dry toluene. After degassing, the mixture was heated to 125 °C and stirred over night. The solution was cooled to r.t., H$_2$O was added, extraction with CH$_2$Cl$_2$ was followed by separation of the organic layer. The organic phase was then dried over Na$_2$SO$_4$. After solvent removal, the residue was purified *via* column chromatography.

GS II: *Iodination of TMS protection group*

a) for amine compounds

The amine$-$X$-$TMS compound was dissolved in dry CH$_2$Cl$_2$ and cooled to -78 °C. ICl diluted in CH$_2$Cl$_2$ was added in the dark. After stirring for 10 min, the mixture was quenched with saturated

aqueous $Na_2S_2O_3$ solution and warmed to r.t. Separation of the organic phase, drying over Na_2SO_4 and evaporation of the solvent led to the crude product which had to be purified by column chromatography.

b) for bpy compounds

The $TMS-X-bpy$ compound was dissolved in dry CH_2Cl_2 and CH_3CN (1:4 solvent ratio). The solution was cooled to 0 °C. ICl diluted in CH_3CN was added dropwise but rapidly to the solution. The reaction was stirred for 5 min at 0 °C , then warmed to r.t. and stirred over night. After quenching with saturated aqueous $Na_2S_2O_3$ solution, phases were separated. The organic layer was dried over Na_2SO_4. Solvents were removed in vacuum. The crude product was purified by column chromatography.

GS III: *Sonogashira-Hagihara reaction*

Compound A, B (and eventually C) were dissolved in dry NEt_3. After deoxygenation of the solution, the catalyst mixture (4 mol% CuI and 2 mol% $Pd(PPh_3)_2Cl_2$) was added. After a second deoxygenation, the solution was heated to 96 °C and stirred until the reaction was completed. Then the solution was cooled to r.t., ethyl acetate (EA) was added. The mixture was washed with saturated aqueous NH_4Cl as well as with brine. The organic phase was collected, dried over Na_2SO_4 and solvents were evaporated. The crude product was purified *via* column chromatography.

GS IV: *Deprotection of MEBYNOL groups*

The MEBYNOL compound was dissolved in dry toluene. After addition of NaH, the solution was heated to 96 °C. When the reaction was finished, the precipitate was filtered off and solvent was removed. The raw product was purified by column chromatography.

GS V: *Complexation*

The ligand and ruthenium precursor were dissolved in dry $CHCl_3$ and dry MeOH (ratio: 1:3.3). The reaction mixture was heated to 75 °C and stirred over night. After the solvents were removed purification *via* column chromatography was performed.

6.4 Precursor molecules

6.4.1 Phenyl spacer

Br−xy−TMS (S-1)
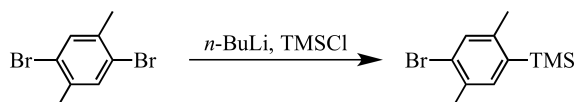
5.0 g (18.94 mmol) 1,4-dibromo-2,5-dimethylbenzene were dissolved in 40 ml dry THF. This solution was cooled to -78 °C and 8.34 ml (20.83 mmol, 1.1 eq, 2.5 M) *n*-BuLi were added dropwise. After stirring for 3 h at -78 °C, 2.64 ml (20.83 mmol, 1.1 eq) TMSCl solution were added dropwise. The reaction mixture was warmed to r.t. and stirred over night. Reaction was quenched with water, phases were separated. The organic phase was dried over Na_2SO_4 and solvent was evaporated. The off-white residue was purified *via* column chromatography.

Column: P (100 %)

$R_f = 0.83$

Yield: 4.77 g [98 %] of colourless oil (Lit.[104]: 97 %)

^{1}H NMR (400 MHz, $CDCl_3$): δδ = 7.38 (s, 1H), 7.32 (s, 1H), 2.43 (s, 3H), 2.40 (s, 3H), 0.36 (s, 9H) ppm

B(OH)$_2$−xy−TMS (S-2)
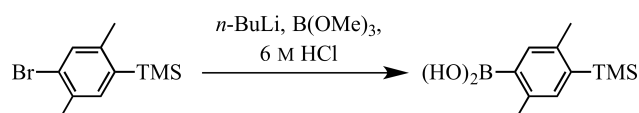
2.0 g (7.77 mmol) Br−xy−TMS (**S-1**) were dissolved in 25 ml dry THF. After cooling to -78 °C, 3.73 ml (9.33 mmol, 1.2 eq, 2.5 M) *n*-BuLi were added dropwise. The solution was stirred for 1 h at -78 °C. Then 1.04 ml (9.33 mmol, 1.2 eq) B(OMe)$_3$ were added dropwise. After removing the dry ice bath, the reaction mixture was stirred over night at r.t. 10 ml H_2O and 30 ml 6 M HCl were added. The mixture was extracted with CH_2Cl_2 followed by separation of the phases. The organic phase was dried over Na_2SO_4 and solvents were removed in vacuum.

Yield: 1.56 g [67 %] of white crystals (Lit.[105]: 70 %)

^{1}H NMR (400 MHz, $CDCl_3$): δ = 7.94 (s, 1H), 7.36 (s, 1H), 2.76 (s, 3H), 2.50 (s, 3H), 0.36 (s, 9H) ppm

Br−(Ph)$_2$−TMS (S-3)
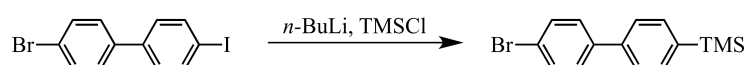
2.0 g (5.57 mmol) 4-bromo-4'-iodobiphenyl were suspended in 30 ml dry Et$_2$O and cooled to -78 °C. 2.34 ml (5.85 mmol, 1.05 eq, 2.5 M) *n*-BuLi were added dropwise. The solution was warmed to r.t. and stirred for 1 h. After cooling again to -78°C, 0.78 ml (6.13 mmol, 1.1 eq) TMSCl were added. Then the

solution was warmed to r.t and stirred over night. After addition of H_2O and saturated aqueous $Na_2S_2O_3$ solution the organic phases were collected and dried over Na_2SO_4 and evaporated. The pure product was obtained after column chromatography.

Column: P (100 %)

$R_f = 0.64$

Yield: 1.62 mg [95 %] of white crystals (Lit.[149]: 78 %)

^1H NMR (400 MHz, acetone-d_6): $\delta = 7.67 - 7.61$ (m, 8H), 0.30 (s, 9H) ppm

$B(OH)_2-Ph_2-TMS$ (S-4)
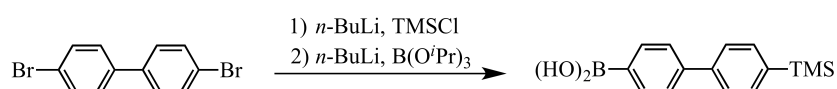
2.0 g (6.41 mmol) 4,4'-dibromobiphenyl were dissolved in 40 ml dry THF and cooled to -78 °C. 2.7 ml (6.73 mmol, 1.05 eq, 2.5 M) n-BuLi were added, followed by stirring for 40 min at -78°C. After cooling to -100 °C, 0.85 ml (6.73 mmol, 1.05 eq) TMSCl were slowly added. After 5 min reaction time this solution was warmed to r.t. and stirred for 40 min. The reaction mixture was cooled to -78 °C again and the second portion 3.07 ml (7.69 mmol, 1.2 eq, 2.5 M) of n-BuLi was added. Directly afterwards the reaction was cooled to -100 °C, and 4.44 ml (19.23 mmol, 3 eq) ($^iPrO)_3B$ were added dropwise. After 5 min at this temperature the mixture was warmed to r.t. and stirred over night. Pouring into 250 ml cold water, extraction with EA followed by drying over Na_2SO_4, and evaporation yielded a colorless oil. Purification *via* a short column (maximum length: 5 cm) was needed.

Column: P (100 %) → acetone (100 %)

Yield: 1.06 g [61 %] of white precipitate (Lit.[106]: 59 - 72 %)

^1H NMR (400 MHz, DMSO): $\delta = 8.08$ (s, 2H), 7.88 (d, J = 8.2 Hz, 2H), 7.71 – 7.57 (m, 6H), 0.27 (s, 9H) ppm

$Br-fluorene-Br$ (S-5)
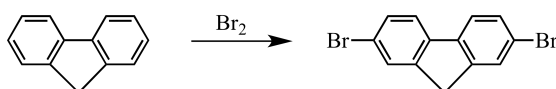
10.0 g (60 mmol) fluorene were dissolved in 70 ml CH_2Cl_2 and cooled to 0 °C. 6.16 ml (120 mmol, 2 eq) Br_2 dissolved in 20 ml CH_2Cl_2 were added in the dark. The ice bath was removed after 15 min and the mixture was stirred at r.t. over night. After addition of saturated aqueous $Na_2S_2O_3$ solution, the water phase was extracted with CH_2Cl_2, the organic layer was separated, dried over Na_2SO_4 and solvents were evaporated. The crude light yellow crystals were recrystallized from EtOH.

Yield: 16.30 g [84 %] of white fluffy crystals (Lit.[107]: 92 %)

^1H NMR (400 MHz, acetone-d_6): $\delta = 7.83$ (d, J = 8.2 Hz, 2H), 7.77 (s, 2H), 7.56 (dd, J = 8.2, 1.6 Hz, 2H), 3.98 (s, 2H) ppm

Br−fl−Br (S-6)
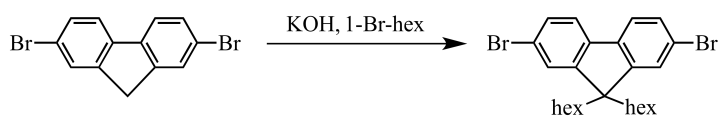
16.0 g (49.38 mmol) Br−fluorene−Br (**S-5**) were suspended in 80 ml DMSO. 13.85 g (246.90 mmol, 5 eq) freshly powdered KOH were added and the mixture was stirred for 15 min. 13.86 ml (98.76 mmol, 2 eq) 1-bromohexane were added. This solution was stirred at r.t. for 24 h, then poured into 600 ml ice water and extracted with CH_2Cl_2. The collected organic layer was dried over Na_2SO_4 and solvents were evaporated. The crude product was purified by column chromatography.

Column: P (100 %)

Yield: 24.0 g [99 %] of white crystals (Lit.[108]: 87 %)

^{1}H NMR (400 MHz, Acetone-d$_6$): δ = 7.77 (d, J = 8.1 Hz, 2H), 7.67 (d, J = 1.6 Hz, 2H), 7.53 (dd, J = 8.1, 1.5 Hz, 2H), 2.14 – 2.05 (m, 4H), 1.16 – 1.00 (m, 12H), 0.76 (t, J = 7.0 Hz, 6H), 0.58 (p, J = 7.6 Hz, 4H) ppm

Br−fl−TMS (S-7)
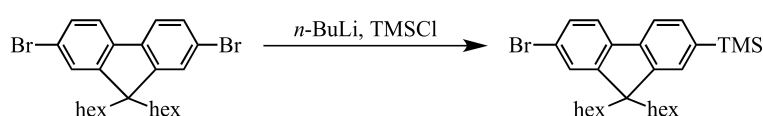
9.52 g (19.33 mmol) Br−fl−Br (**S-6**) were dissolved in 100 ml dry Et_2O and cooled to -78 °C. 8.12 ml (20.30 mmol, 1.05 eq, 2.5 M) *n*-BuLi were added slowly and the mixture was stirred at this temperature for 1 h. 2.7 ml (21.27 mmol, 1.10 eq) TMSCl were added dropwise. After

5 min the mixture was warmed to r.t. and stirred over night. After adding water, the solution was extracted with EA, dried over Na_2SO_4 followed by solvent removal. The crude product was purified by column chromatography.

Column: P (100 %)

R_f = 0.27 (P/EA (4:1))

Yield: 9.22 g [98 %] of colorless oil (Lit.[109]: 97 %)

^{1}H NMR (400 MHz, CDCl$_3$): δ = 7.82 – 7.73 (m, 2H), 7.70 – 7.62 (m, 2H), 7.52 (ddd, J = 9.8, 7.7, 2.0 Hz, 2H), 2.14 – 2.07 (m, 4H), 1.15 – 0.97 (m, 12H), 0.80 – 0.69 (m, 6H), 0.60 (q, J = 11.5, 10.6 Hz, 4H), 0.30 (s, 9H) ppm

B(OH)$_2$−fl−TMS (S-8)
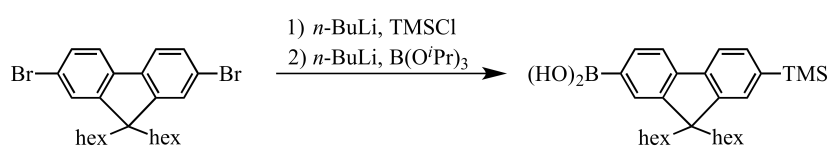
5.56 g (11.30 mmol) Br−fl−Br (**S-6**) were dissolved in 90 ml dry THF and cooled to -78 °C. 4.74 ml (11.86 mmol, 1.05 eq, 2.5 M) *n*-BuLi were added slowly and the mixture was stirred at this temperature

for 40 min. The solution was cooled to -100 °C, 1.5 ml (11.86 mmol, 1.05 eq) TMSCl were added dropwise. After 5 min, the mixture was warmed to r.t. within 40 min. The second portion of *n*-BuLi (5.44 ml, 13.6 mmol, 1.2 eq) was added after cooling again to -78 °C. This mixture was cooled directly to -100 °C and 7.82 ml (33.9 mmol, 3 eq) B(^{i}PrO)$_3$ were added. The reaction mixture was stirred for additional 5 min at this temperature. The dry ice bath was removed, the reaction was warmed to r.t and stirred over night. After pouring into 500 ml cold water, the solution was extracted with EA, dried over Na$_2$SO$_4$ followed by solvent removal. The crude product was purified by column chromatography.

Column: P (100 %) → P/EA (4:1)

R$_f$ = 0.27 (P/EA (4:1))

Yield: 4.92 g [97 %] of colorless oil which crystallizes after some time (Lit.[110]: 88 %)

^{1}H NMR (400 MHz, Acetone-d$_6$): δ = 7.98 (s, 1H), 7.89 (d, J = 8.5 Hz, 1H), 7.79 (t, J = 7.7 Hz, 2H), 7.65 (s, 1H), 7.53 (d, J = 7.5 Hz, 1H), 2.07-2.11 (m, 4H), 1.12 – 1.01 (m, 12H), 0.74 (t, J = 7.0 Hz, 6H), 0.65 – 0.56 (m, 4H), 0.31 (s, 9H) ppm

6.4.2 Amine compounds

amine−Ph (A-1)
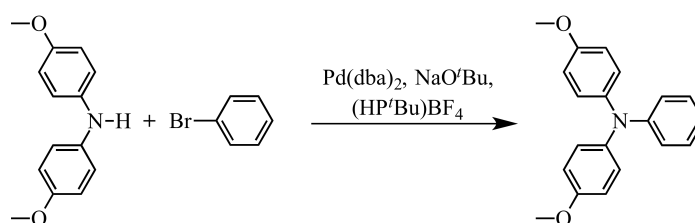
use **GS I**:

Bis(*p*-anisyl)amine	2.00 g (8.72 mmol)
1-bromobenzene	1.1 ml (10.47 mmol, 1.2 eq)
NaO^{t}Bu	16.76 g (174.50 mmol, 20 eq)
Pd(dba)$_2$	0.250 g (0.44 mmol, 5 mol%)
(HP^{t}Bu)BF$_4$	0.127 g (0.44 mmol, 5 mol%)
Solvent amount	150 ml

Bis(*p*-anisyl)amine, NaO^{t}Bu, Pd(dba)$_2$ and (HP^{t}Bu)BF$_4$ were dissolved in dry toluene. After deoxygenation, 1-bromobenzene was added.

Column: P (100 %) → P/CH$_2$Cl$_2$ (5:1) → (1:1)

R$_f$ = 0.61

Yield: 2.45 g [92 %] of light beige crystals (Lit.[150]: 77 %)

^{1}H NMR (400 MHz, acetone-d$_6$): δ = 7.17 (dd, J = 8.9, 7.1 Hz, 2H); 7.02 (d, J = 9.1 Hz, 4H); 6.89 (d, J = 9.1 Hz, 4H); 6.85 (d, J = 7.7 Hz, 2H); 6.82 (s, 1H); 3.78 (s, 6H) ppm

amine−Ph−I (A-2)
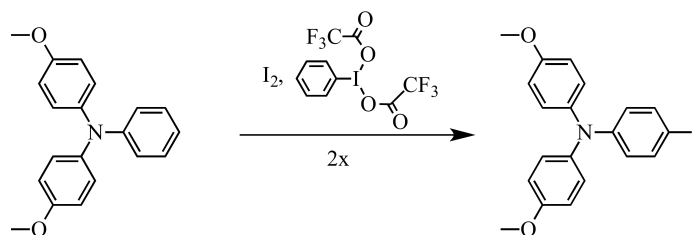
1.87 g (4.36 mmol) [bis(trifluoroacetoxy)iodo]benzene and 1.10 g (4.36 mmol) I_2 were dissolved in 15 ml dry CH_2Cl_2 and stirred for 1 h at r.t. 1.33 g (4.36 mmol) amine−Ph (**A-1**) was added in the dark. This solution was stirred at 60 °C for 1 h. Meanwhile a second solution of 0.94 g (2.18 mmol) [bis(trifluoroacetoxy)iodo]benzene and 0.55 g (2.18 mmol) I_2 in 10 ml dry CH_2Cl_2 was prepared and stirred for 1 h at r.t. The second solution was added to the first solution. The mixture was stirred for an additional hour at 60 °C. Then the solution was cooled to r.t. and saturated aqueous $Na_2S_2O_3$ solution was added. The organic phase was separated and dried over Na_2SO_4. Solvent was removed in vacuum. The green oily residue was purified by column chromatography.

Column: P (100 %) → P/CH_2Cl_2 (1:1)

R_f = 0.67 (P/CH_2Cl_2 (1:1))

Yield: 1.50 g [80 %] of off-white crystals (Lit.[119]: 85 %)

^{1}H NMR (400 MHz, acetone-d_6): δ = 7.46 (d, J = 9.0 Hz, 2H), 7.06 (d, J = 9.0 Hz, 4H), 6.91 (d, J = 9.0 Hz, 4H), 6.63 (d, J = 9.0 Hz, 2H), 3.79 (s, 6H) ppm

amine−Ph$_2$−TMS (A-3)
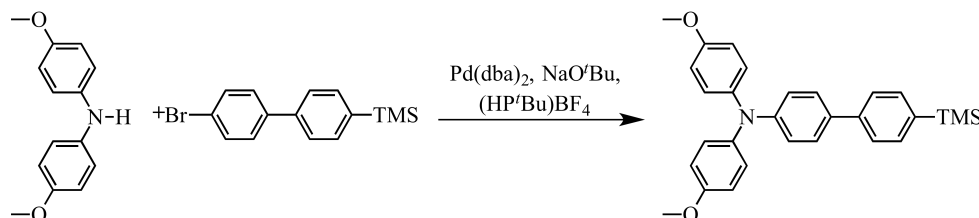
use **GS I**:

Bis(*p*-anisyl)amine	313.0 mg (1.36 mmol)
Br−Ph$_2$−TMS	500.0 mg (1.64 mmol, 1.2 eq)
NaO^{t}Bu	2.62 g (27.30 mmol, 20 eq)
Pd(dba)$_2$	39.2 mg (0.07 mmol, 5 mol%)
(HP^{t}Bu)BF$_4$	19.8 mg (0.07 mmol, 5 mol%)
Solvent amount	20 ml

Column: P (100 %) → P/CH_2Cl_2 (5:1) → (1:1)

R_f = 0.65 (P/CH_2Cl_2 (1:1))

Yield: 582.2 mg [94 %] of yellow oil

^{1}H NMR (400 MHz, acetone-d$_6$): δ = 7.59 (s, 4H), 7.51 (d, J = 8.7 Hz, 2H), 7.09 (d, J = 8.9 Hz, 4H), 6.96 – 6.89 (m, 6H), 3.80 (s, 6H), 0.28 (s, 9H) ppm

amine−Ph$_2$−I (A-4)
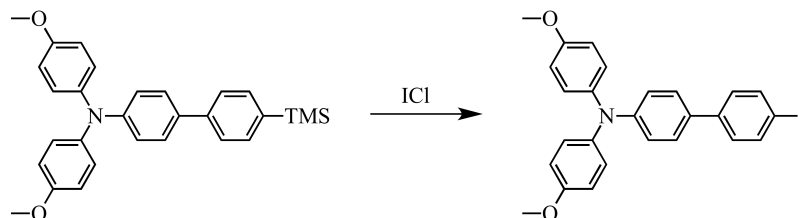
use **GS II a)**:

amine−Ph$_2$−TMS (**A-3**)	582 mg (1.29 mmol)
ICl	0.14 ml (2.56 mmol, 2 eq)
Solvent amount	20 ml

Column: P (100 %) → P/CH$_2$Cl$_2$ (5:1) → (1:1)

R$_f$ = 0.64 (P/CH$_2$Cl$_2$ (1:1))

Yield: 582.2 mg [94 %] of yellow oil

^{1}H NMR (400 MHz, acetone-d$_6$): δ = 7.69 (d, J = 8.6 Hz, 2H), 7.40 (d, J = 8.9 Hz, 2H), 7.32 (d, J = 8.6 Hz, 2H), 7.03 (d, J = 9.0 Hz, 4H), 6.94 – 6.83 (m, 6H), 3.74 (s, 9H) ppm

amine−fl−TMS (A-5)
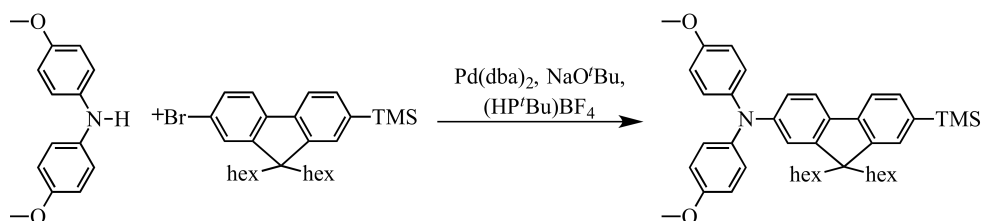
use **GS I**:

Bis(*p*-anisyl)amine	0.69 g (3.00 mmol)
Br−fl−TMS (**S-7**)	1.53 g (3.15 mmol, 1.05 eq)
NaO^{t}Bu	0.72 g (7.50 mmol, 2.5 eq)
Pd(dba)$_2$	0.09 g (0.15 mmol, 5 mol%)
(HP^{t}Bu)BF$_4$	0.04 g (0.15 mmol, 5 mol%)
Solvent amount	30 ml

Column: P/CH$_2$Cl$_2$ (3:1) → (1:1)

R$_f$ = 0.61 (P/CH$_2$Cl$_2$ (1:1))

Yield: 0.93 g [49 %] of light yellow oil

^{1}H NMR (400 MHz, acetone-d$_6$): δ = 7.67 – 7.54 (m, 3H), 7.47 (dd, J = 7.5, 1.0 Hz, 1H), 7.08 – 7.00

(m, 5H), 6.93 – 6.82 (m, 5H), 3.79 (s, 6H), 1.96 (td, J = 12.3, 11.4, 5.1 Hz, 2H), 1.91 – 1.80 (m, 2H), 1.10 (dd, J = 27.2, 6.9 Hz, 12H), 0.78 (d, J = 7.2 Hz, 6H), 0.74 – 0.59 (m, 4H), 0.29 (s, 9H) ppm

amine−fl−I (A-6)
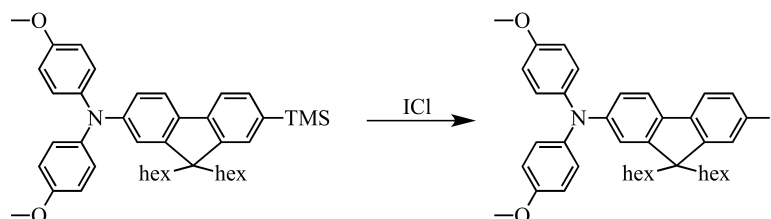
use **GS II a**):

amine−fl−TMS (**A-5**)	930 mg (1.47 mmol)
ICl	0.15 ml (2.93 mmol, 2 eq)
Solvent amount	20 ml

Column: P (100 %) → P/CH$_2$Cl$_2$ (1:1)

R$_f$ = 0.91 (P/CH$_2$Cl$_2$ (1:1))

Yield: 582.2 mg [94 %] of yellow oil

^{1}H NMR (400 MHz, acetone-d$_6$): δ = 7.75 (d, J = 1.4 Hz, 1H), 7.68 – 7.57 (m, 2H), 7.49 (d, J = 7.9 Hz, 1H), 7.08 – 6.97 (m, 5H), 6.93 – 6.81 (m, 5H), 3.79 (s, 6H), 1.98 – 1.83 (m, 4H), 1.11 (dd, J = 26.8, 6.6 Hz, 12H), 0.81 (t, J = 7.1 Hz, 6H), 0.72 – 0.57 (m, 4H) ppm

amine−fl−Br (A-7)
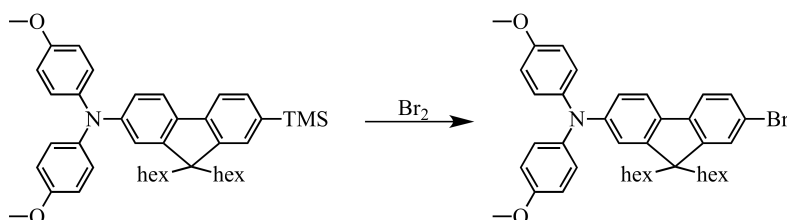
1.80 g (2.84 mmol) amine−fl−TMS (**A-5**) were dissolved in 20 ml CH$_2$Cl$_2$ and cooled to -78°C. 0.36 ml (7.10 mmol, 2.5 eq) Br$_2$ dissolved in 5 ml CH$_2$Cl$_2$ were added dropwise in the dark. The solution was stirred 5 min at this temperature. After removal of the dry ice bath, the solution was stirred over night. After addition of saturated aqueous Na$_2$S$_2$O$_3$ solution the phases were separated. The organic layer was dried over Na$_2$SO$_4$ and the solvent was removed. The remaining oil was purified by column chromatography.

Column: P (100 %) → P/CH$_2$Cl$_2$ (4:1)

R$_f$ = 0.31 (P/CH$_2$Cl$_2$ (4:1))

Yield: 1.71 g [94 %] of yellow oil

^{1}H NMR (400 MHz, acetone-d$_6$): δ = 7.64 – 7.53 (m, 3H), 7.45 (dd, J = 8.1, 1.9 Hz, 1H), 7.08 – 6.98 (m, 5H), 6.93 – 6.81 (m, 5H), 3.79 (s, 6H), 1.97 – 1.84 (m, 4H), 1.19 – 1.05 (m, 12H), 0.80 (t, J = 7.1 Hz, 7H), 0.71 – 0.60 (m, 4H) ppm

amine−fl$_2$−TMS (A-8)
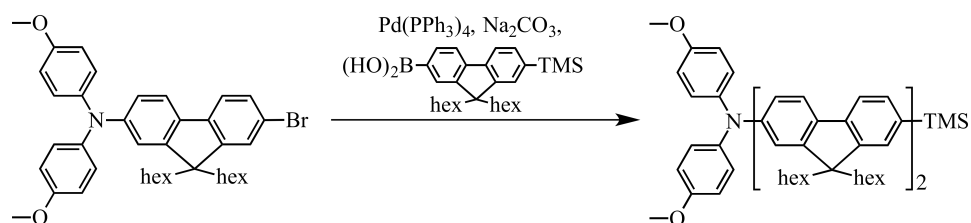
1.71 g (2.67 mmol) amine−fl−Br (**A-7**) and 1.80 g (4.00 mmol, 1.5 eq) B(OH)$_2$−fl−TMS (**S-8**) were dissolved in 60 ml dry toluene. After deoxygenation, 0.30 g (0.27 mmol, 10 mol%) Pd(PPh$_3$)$_4$ and 13 ml 2M aqueous Na$_2$CO$_3$ solution were added. The mixture was heated up to 96 °C and stirred over night. The reaction was cooled to r.t., CH$_2$Cl$_2$ was added and phases were separated. The organic phase was dried over Na$_2$SO$_4$ and solvents were evaporated. The brown oil was purified on a column.

Column: P/CH$_2$Cl$_2$ (10:1) → P/CH$_2$Cl$_2$ (3:1)

R$_f$ = 0.56 (P/CH$_2$Cl$_2$ (3:1))

Yield: 1.29 g [50 %] of yellow oil

^{1}H NMR (400 MHz, acetone-d$_6$): δ = 7.76 (ddt, J = 44.5, 28.6, 9.4 Hz, 9H), 7.54 (d, J = 7.3 Hz, 1H), 7.06 (d, J = 8.7 Hz, 5H), 6.94 − 6.80 (m, 5H), 3.80 (s, 6H), 2.22 − 2.10 (m, 6H), 1.97 − 1.76 (m, 6H), 1.17 − 1.00 (m, 24H), 0.82 − 0.64 (m, 20H), 0.32 (s, 9H) ppm

amine−fl$_2$−I (A-9)
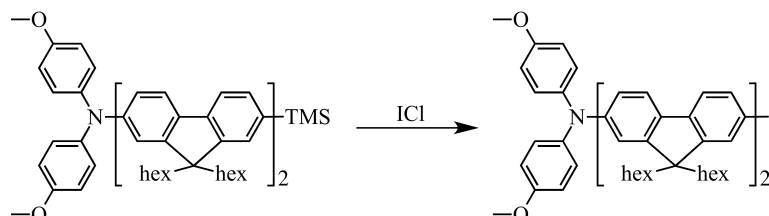
use **GS II a)**:

   amine−fl$_2$−TMS (**A-8**)   1.20 g (1.24 mmol)

   ICl   0.16 ml (3.11 mmol, 2 eq)

   Solvent amount   25 ml

Column: P/CH$_2$Cl$_2$ (10:1) → P/CH$_2$Cl$_2$ (4:1)

R$_f$ = 0.3 (P/CH$_2$Cl$_2$ (4:1))

Yield: 1.24 g [98 %] of yellow oil

^{1}H NMR (400 MHz, acetone-d$_6$): δ = 7.93 − 7.82 (m, 3H), 7.81 − 7.61 (m, 7H), 7.10 − 7.02 (m, 5H), 6.94 − 6.84 (m, 5H), 3.80 (s, 6H), 2.24 − 2.11 (m, 6H), 1.97 − 1.84 (m, 6H), 1.16 − 1.02 (m, 24H), 0.84 − 0.63 (m, 20H) ppm

6.4.3 Bipyridine compounds

Br−bpy (B-1)
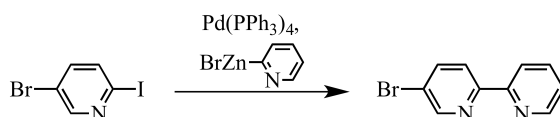
1.42 g (5.00 mmol) 5-bromo-2-iodopyridine were dissolved in 15 ml dry THF. After degassing, 0.116 g (0.10 mmol, 2 mol%) Pd(PPh$_3$)$_4$ catalyst was added. Then, 15.0 ml (7.50 mmol, 1.5 eq, 0.5M) 2-pyridylzinc bromide solution were added *via* syringe. The dark brown solution was stirred for 24 h at r.t., and then 150 ml of EDTA/Na$_2$CO$_3$ (1:1) were added until the precipitate was dissolved. The aqueous phase was extracted three times with Et$_2$O and the organic phase was dried over Na$_2$SO$_4$. The solvents were removed in vacuum. The beige residue was purified *via* column chromatography.

Column: P/Et$_2$O (2:1) → P/Et$_2$O (2:1) + 1% NEt$_3$

R$_f$ = 0.53 (P/Et$_2$O (2:1) + 1% NEt$_3$)

Yield: 1.12 g [96 %] of white crystals (Lit.[151]: 73 %)

^{1}H NMR (400 MHz, acetone-d$_6$): δ = 8.76 (d, J = 2.4 Hz, 1H), 8.71 − 8.65 (m, 1H), 8.44 (d, J = 9.1 Hz, 2H), 8.13 (dd, J = 8.5, 2.4 Hz, 1H), 7.94 (td, J = 7.8, 1.8 Hz, 1H), 7.47 − 7.42 (m, 1H) ppm

stannane−bpy (B-2)
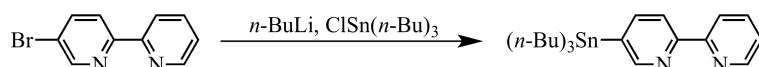
1.0 g (4.25 mmol) Br−bpy (**B-1**) was dissolved in 30 ml dry Et$_2$O. This solution was cooled to -78 °C. After dropwise addition of 1.87 ml (4.68 mmol, 2.5 M, 1.1 eq) *n*-BuLi, the mixture was stirred for 1 h at -78 °C. Then 1.27 ml (4.68 mmol, 1.1 eq) tributyltin chloride was added and the mixture was stirred for 1 h at the same temperature. After that the solution was warmed gradually to r.t. and stirred over night. The precipitate was filtered and solvent was removed. The oily residue was purified by column chromatography.

Column: P/EA (9:1)

R$_f$ = 0.46

Yield: 1.31 g [69 %] of yellow oil (Lit.[104]: 74 %)

^{1}H NMR (400 MHz, acetone-d$_6$): δ = 8.73 − 8.63 (m, 2H), 8.52 − 8.39 (m, 2H), 8.02 (dd, J = 7.7, 1.6 Hz, 1H), 7.90 (td, J = 7.8, 1.8 Hz, 1H), 7.43 − 7.35 (m, 1H), 1.67 − 1.56 (m, 6H), 1.43 − 1.32 (m, 6H), 1.25 − 1.16 (m, 6H), 0.90 (t, J = 7.3 Hz, 9H) ppm

I−bpy (B-3)
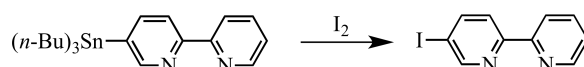
364.6 mg (0.819 mmol) of stannane−bpy (**B-2**) were dissolved in dry CH$_2$Cl$_2$ and 208 mg (0.819 mmol, 1 eq) I$_2$ were added in small portions. This solution was stirred at r.t. for 15 min. After addition of

saturated aqueous $Na_2S_2O_3$ the mixture was extracted with CH_2Cl_2 and dried over Na_2SO_4. Evaporation of the product yielded a brown solid. To purify the oil, column chromatography was performed.

Column: P (100%) → P/Et$_2$O (2:1)

R_f = 0.38 (P/Et$_2$O (2:1))

Yield: 306.9 mg [84 %] of off-white crystals

^{1}H NMR (400 MHz, acetone-d$_6$): δ = 8.91 (t, J = 1.5 Hz, 1H), 8.71 – 8.64 (m, 1H), 8.44 (dt, J = 8.0, 1.0 Hz, 1H), 8.34 – 8.28 (m, 3H), 7.93 (td, J = 7.8, 1.8 Hz, 1H), 7.44 (ddd, J = 7.5, 4.8, 1.2 Hz, 1H) ppm

TMS−xy−bpy (B-4)
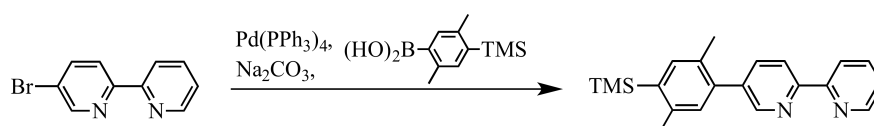
1.0 g (4.25 mmol) Br−bpy (**B-1**), 1.04 g (4.68 mmol, 1.1 eq) B(OH)$_2$-xy-TMS (**S-2**) and 1.35 g (12.76 mmol, 3 eq) Na_2CO_3 were dissolved in 20 ml THF/H$_2$O (1:1). After deoxygenation, 246.0 mg (0.213 mmol, 5 mol%) Pd(PPh$_3$)$_4$ were added. The mixture was heated to 96 °C and stirred for 2 d. The reaction was cooled to r.t., CH_2Cl_2 was added and phases were separated. The organic phase was dried over Na_2SO_4 and solvents were evaporated. The brown oil was purified on a column.

Column: P/Et$_2$O (2:1) → P/Et$_2$O (2:1) + 1% NEt$_3$

R_f = 0.39 (P/Et$_2$O (2:1)+1% NEt$_3$)

Yield: 1.21 g [88 %] of white crystals (Lit.[152]: 76 %)

^{1}H NMR (400 MHz, acetone-d$_6$): δ = 8.70 (d, J = 4.8 Hz, 1H), 8.65 (d, J = 2.3 Hz, 1H), 8.59 – 8.49 (m, 2H), 7.99 – 7.87 (m, 2H), 7.46 – 7.38 (m, 2H), 7.13 (s, 1H), 2.48 (s, 3H), 2.30 (s, 3H), 0.37 (s, 9H) ppm

I−xy−bpy (B-5)
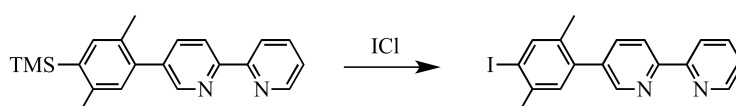
use **GS II b**):

TMS−xy−bpy (**B-4**)	1.37 g (4.14 mmol)
ICl	0.65 ml (12.43 mmol, 3 eq)
CH$_2$Cl$_2$	5 ml
CH$_3$CN	20 ml

Column: P (100%) → P/Et$_2$O (2:1) → P/Et$_2$O (2:1) + 1 % NEt$_3$

R_f = 0.30 (P/Et$_2$O (2:1) + 1 % NEt$_3$)

Yield: 1.46 g [92 %] of off-white crystals

^{1}H NMR (400 MHz, acetone-d$_6$): δ = 8.70 (d, J = 5.6 Hz, 1H), 8.65 (d, J = 2.3 Hz, 1H), 8.59 – 8.49 (m, 2H), 7.99 – 7.88 (m, 2H), 7.84 (s, 1H), 7.43 (dd, J = 8.1, 5.4 Hz, 1H), 7.27 (s, 1H), 2.44 (s, 3H), 2.28 (s, 3H) ppm

TMS−Ph$_2$−bpy (B-6)
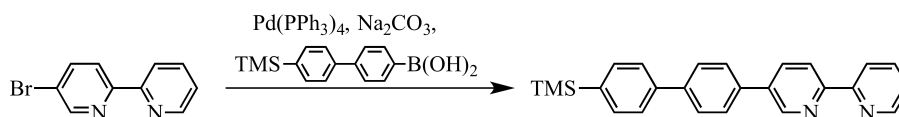
620.0 mg (2.64 mmol) Br−bpy (**B-1**) and 1.07 g (3.96 mmol, 1.5 eq) B(OH)$_2$−Ph$_2$−TMS (**S-4**) were dissolved in 40 ml toluene. Following deoxygenation, 305 mg (0.26 mmol, 10 mol%) Pd(PPh$_3$)$_4$ were added as well as 13 ml 2 M aqueous Na$_2$CO$_3$ solution. This mixture was heated to 100 °C and stirred over night. After cooling, the mixture was extracted with CH$_2$Cl$_2$. The organic layer was collected, dried over Na$_2$SO$_4$, and solvents were evaporated. The crude product was purified *via* a short column (5 cm).
Column: P/Et$_2$O (2:1) → P/Et$_2$O (2:1)+ 1 % NEt$_3$
R$_f$ = 0.13 (P/Et$_2$O (2:1) + 1 % NEt$_3$)
Yield: 1.46 g [59 %] of off-white crystals
^{1}H NMR (400 MHz, acetone-d$_6$): δ = 8.99 (d, J = 1.8 Hz, 1H), 8.73 (d, J = 4.3 Hz, 1H), 8.51 (dd, J = 18.5, 7.6 Hz, 2H), 8.10 (dd, J = 8.2, 2.2 Hz, 1H), 7.88 (t, J = 7.5 Hz, 1H), 7.75 (s, 4H), 7.65 (s, 4H), 7.36 (dd, J = 7.5, 4.5 Hz, 1H), 0.32 (s, 9H) ppm

I−Ph$_2$−bpy (B-7)

use **GS II b)**:

TMS−Ph$_2$−bpy (**B-6**)	0.35 mg (0.92 mmol)
ICl	0.15 ml (2.76 mmol, 3 eq)
CH$_2$Cl$_2$	5 ml
CH$_3$CN	20 ml

The crude product was washed with cold pentane and dried in vacuum.
Yield: 239 mg [60 %] of off-white solid
^{1}H NMR (400 MHz, CDCl$_3$): δ = 8.97 (d, J = 3.0 Hz, 1H), 8.71 (d, J = 4.8 Hz, 1H), 8.48 (dd, J = 19.2, 8.1 Hz, 2H), 8.07 (dd, J = 8.3, 2.4 Hz, 1H), 7.85 (td, J = 7.8, 1.8 Hz, 1H), 7.80 (d, J = 8.5 Hz, 2H), 7.77 − 7.63 (m, 4H), 7.39 (d, J = 8.5 Hz, 2H), 7.37 − 7.31 (m, 1H) ppm

TMS−fl−bpy (B-8)
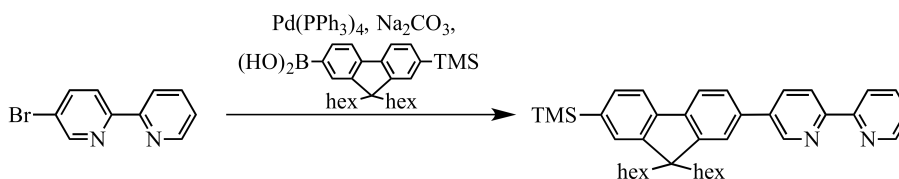
0.70 g (2.98 mmol) Br−bpy (**B-1**), 2.01 g (4.47 mmol, 1.5 eq) B(OH)$_2$−fl−TMS (**S-8**) were dissolved in 40 ml dry toluene. After deoxygenation, 0.34 g (0.298 mmol, 10 mol%) Pd(PPh$_3$)$_4$ were added.

Additional deoxygenation and addition of 15 ml 2 M aqueous Na_2CO_3 solution followed. This mixture was heated to 100 °C and stirred over night. After cooling, the reaction mixture was extracted with CH_2Cl_2. The organic layer was collected, dried over Na_2SO_4, and the solvent was evaporated. The crude product was purified *via* column chromatography.

Column: P (100 %) → P/Et_2O (10:1) → P/Et_2O (2:1)+ 1 % NEt_3

R_f = 0.21 (P/Et_2O (2:1) + 1 % NEt_3)

Yield: 1.40 g [84 %] of colorless oil

^{1}H NMR (400 MHz, acetone-d_6): δ = 9.07 (d, J = 3.2 Hz, 1H), 8.70 (dd, J = 5.2, 2.2 Hz, 1H), 8.61 – 8.50 (m, 2H), 8.28 (dd, J = 8.3, 2.4 Hz, 1H), 8.00 – 7.90 (m, 3H), 7.89 – 7.76 (m, 2H), 7.69 (s, 1H), 7.57 (d, J = 8.4 Hz, 1H), 7.47 – 7.39 (m, 1H), 2.17 (ddd, J = 10.9, 7.1, 5.8 Hz, 4H), 1.14 – 1.02 (m, 12H), 0.74 (t, J = 6.9 Hz, 6H), 0.72 – 0.59 (m, 4H), 0.33 (s, 9H) ppm

I−fl−bpy (B-9)
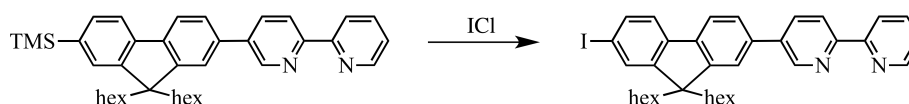
use **GS II b**):

TMS−fl−bpy (**B-8**)	1.40 g (2.5 mmol)
ICl	0.40 ml (7.49 mmol, 3 eq)
CH_2Cl_2	5 ml
CH_3CN	20 ml

Column: P (100 %) → P/Et_2O (2:1) → P/Et_2O (2:1) + 1 % NEt_3

R_f = 0. (P/Et_2O (2:1) + 1 % NEt_3)

Yield: 1.29 g [84 %] of light yellow oil

^{1}H NMR (400 MHz, acetone-d_6): δ = 9.07 (d, J = 2.3 Hz, 1H), 8.70 (ddd, J = 4.7, 1.7, 0.9 Hz, 1H), 8.56 (dd, J = 16.7, 8.1 Hz, 2H), 8.28 (dd, J = 8.3, 2.4 Hz, 1H), 8.01 – 7.87 (m, 4H), 7.86 – 7.67 (m, 3H), 7.47 – 7.38 (m, 1H), 2.28 – 2.09 (m, 4H), 1.08 (dt, J = 16.0, 8.6 Hz, 12H), 0.71 (dt, J = 32.7, 6.9 Hz, 10H) ppm

TMS−fl$_2$−bpy (B-10)
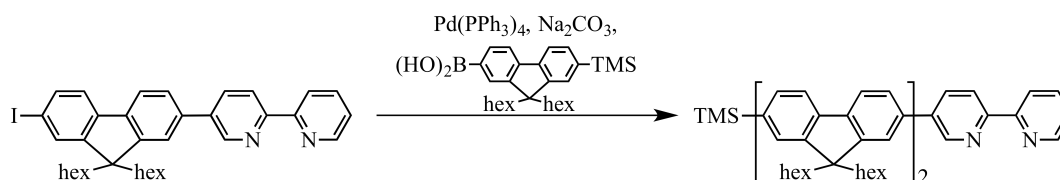
1.29 g (2.10 mmol) I−fl−bpy (**B-9**), 1.42 g (3.15 mmol, 1.5 eq) B(OH)$_2$−fl−TMS (**S-8**) were dissolved in 40 ml dry toluene. After degassing, 0.24 g (0.21 mmol, 10 mol%) Pd(PPh$_3$)$_4$ were added. Additional degassing and addition of 10 ml 2 M aqueous Na_2CO_3 solution followed. This mixture was heated to 100 °C and stirred over night. After cooling, the reaction mixture was extracted with CH_2Cl_2. The organic

layer was collected, dried over Na_2SO_4, and evaporated. The crude product was purified *via* column chromatography.

Column: P (100 %) → P/Et$_2$O (10:1) → P/Et$_2$O (2:1)+ 1 % NEt$_3$

R_f = 0.2 (P/Et$_2$O (2:1) + 1 % NEt$_3$)

Yield: 1.12 g [60 %] of light yellow oil

^{1}H NMR (400 MHz, acetone-d$_6$): δ = 9.09 (d, J = 2.2 Hz, 1H), 8.71 (d, J = 4.7 Hz, 1H), 8.57 (dd, J = 17.4, 8.1 Hz, 2H), 8.30 (dd, J = 8.3, 2.3 Hz, 1H), 8.04 − 7.74 (m, 12H), 7.68 (s, 1H), 7.56 (d, J = 7.4 Hz, 1H), 2.28 − 2.21 (m, 4H), 2.15 (dd, J = 9.0, 6.0 Hz, 4H), 1.10 (d, J = 13.5 Hz, 24H), 0.75 (q, J = 6.6 Hz, 20H), 0.33 (s, 9H) ppm

I−fl$_2$−bpy (B-11)
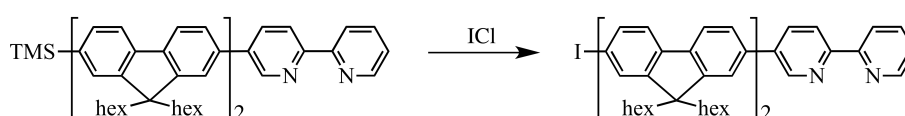
use **GS II b)**:

TMS−fl$_2$−bpy (**B-10**)	1.12 g (1.25 mmol)
ICl	0.2 ml (3.76 mmol, 3 eq)
CH$_2$Cl$_2$	5 ml
CH$_3$CN	20 ml

Column: P/Et$_2$O (10:1) → P/Et$_2$O (2:1)+ 1 % NEt$_3$

R_f = 0.33 (P/Et$_2$O (2:1) + 1 % NEt$_3$)

Yield: 0.982 g [80 %] of light yellow oil

^{1}H NMR (400 MHz, acetone-d$_6$): δ = 9.09 (d, J = 3.1 Hz, 1H), 8.71 (dd, J = 5.2, 1.3 Hz, 1H), 8.57 (dd, J = 16.9, 8.1 Hz, 2H), 8.30 (dd, J = 8.3, 2.4 Hz, 1H), 8.04 − 7.61 (m, 13H), 7.47 − 7.39 (m, 1H), 2.24 (ddt, J = 12.8, 9.4, 4.6 Hz, 4H), 2.18 − 2.09 (m, 4H), 1.10 (dt, J = 13.7, 8.0 Hz, 24H), 0.85 − 0.55 (m, 20H) ppm

6.4.4 Ruthenium precursors

bpy(CF$_3$)$_2$
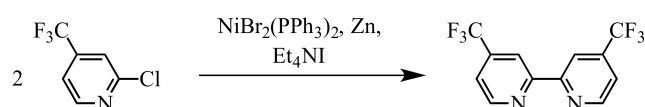
6.14 g (8.26 mmol, 0.3 eq) NiBr$_2$(PPh$_3$)$_2$, 2.70 g (41.4 mmol, 1.5 eq) zinc powder, and 7.08 g (27.54 mmol, 1 eq) Et$_4$NI were dissolved in 45 ml dry THF. This solution was deoxygenated. After addition of 5.0 g (27.54 mmol) 2-chloro-4-(trifluoromethyl)pyridine, the solution was deoxygenated again and heated to 70 °C. After 24 h, the solution was cooled, poured in 2 M aqueous NH$_3$/EDTA solution. After extraction with CH$_2$Cl$_2$, the precipitate was filtered. The organic layer was dried over Na_2SO_4 and evaporated to dryness. Purification *via* column chromatography was performed.

Column: P/CH_2Cl_2 (1:1) → CH_2Cl_2 (100%)

R_f = 0.76 (CH_2Cl_2 (100 %))

Yield: 2.40 g [30 %] of off-white crystals (Lit.[49]: 40 %)

^{1}H NMR (400 MHz, acetone-d_6): δ = 9.03 (d, J = 5.0 Hz, 2H), 8.77 – 8.72 (m, 2H), 7.86 (dd, J = 5.3, 1.3 Hz, 2H) ppm

Ru(bpy(CF$_3$)$_2$)$_2$Cl$_2$
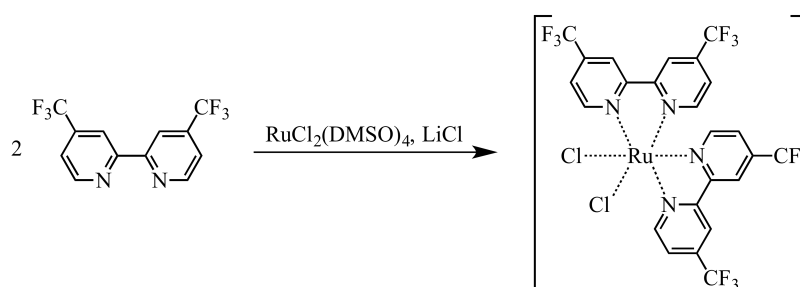
52 mg (0.178 mmol) bpy(CF$_3$)$_2$, 43.11 mg (0.09 mmol, 0.5 eq) $RuCl_2$(DMSO)$_4$ and 37.7 mg LiCl (0.9 mmol, 5 eq) were dissolved in 1 ml 1-methyl-2-pyrrolidinone. This mixture was heated to reflux for 15 min. The solvent was removed while the solution was still hot. The dry residue was purified by column chromatography.

column: CH_2Cl_2 (100 %) → CH_2Cl_2/acetone (2:1)

R_f = 0.87 (CH_2Cl_2/acetone (2:1))

Yield: 27.8 mg [32 %] of dark purple solid (Lit.[130]: 37 %)

^{1}H NMR (400 MHz, acetone-d_6): δ = 10.44 (d, J = 6.0 Hz, 2H), 9.24 – 9.19 (m, 2H), 9.09 – 9.04 (m, 2H), 8.20 (d, J = 6.1 Hz, 2H), 8.14 (dd, J = 6.0, 1.4 Hz, 2H), 7.43 (dd, J = 6.1, 1.8 Hz, 2H) ppm

Ru(bpy)$_2$Cl$_2$
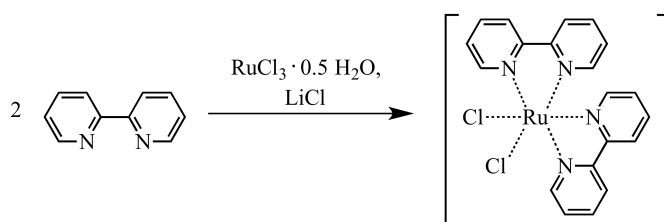
2.00 g (9.64 mmol) $RuCl_3$ · 0.5 H_2O, 3.03 g (19.41 mmol, 2.01 eq) bpy, and 2.86 g (67.50 mmol, 7 eq) LiCl were dissolved in DMF and heated to 163 °C for 8 h. After cooling, DMF was removed. The oily residue was treated with water and extracted with CH_2Cl_2. The organic layer was dried over Na_2SO_4 and evaporated. The dark purple residue was washed with Et_2O and water until the solution was clear.

Yield: 1.11 g [25 %] of dark solid (Lit.[134]: 65 - 70 %)

6.5 Boronmesityl dyads

Br−Ph−(mebynol)₂ (10)
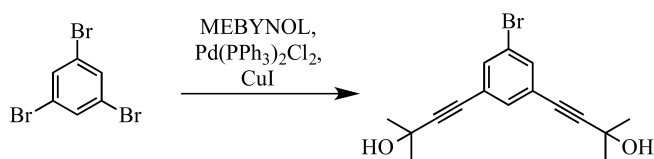
use **GS III**:

1,3,5-tribromobenzene	5.0 g (15.88 mmol)
MEBYNOL	3.41 ml (34.94 mmol, 2.2 eq)
Solvent amount	85 ml
time:	1 h

Column: P/EA (5:1) → (3:1)

R_f = 0.20 (P/EA (3:1))

Yield: 3.59 g [70 %] of yellow crystals (Lit.[153]: 60 %)

^{1}H NMR (400 MHz, CDCl₃): δ = 7.49 (d, J = 1.4 Hz, 2H), 7.40 (t, J = 1.4 Hz, 1H), 1.98 (s, 2H), 1.60 (s, 12H) ppm

mebynol−Bmes₂−mebynol (11)
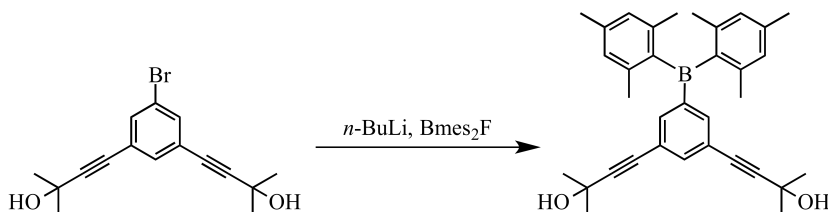
3.38 g (10.52 mmol) Br−Ph−(mebynol)₂ (**10**) were dissolved in 50 ml dry Et₂O. After cooling the solution to -78 °C, 13.9 ml (34.72 mmol, 3.3 eq, 2.5 M) *n*-BuLi were added. The solution was stirred for 2h (meanwhile the solution was warmed to r.t. then cooled again to -78 °C). 5.64 g (21.05 mmol, 2 eq) dimesitylfluoroborane dissolved in 50 ml dry Et₂O were added. The reaction was left at -78 °C for 10 min, then warmed to r.t. and stirred over night. After quenching with H₂O, phases were separated. The organic phase was dried over Na₂SO₄ and evaporated. The brown oil was purified by column chromatography.

Column: P (100 %) → P/EA (8:1)

R_f = 0.64

Yield: 2.99 g [58 %] of yellow crystals

^{1}H NMR (400 MHz, CDCl₃): δ = 7.59 (t, J = 1.7 Hz, 1H), 7.47 (d, J = 1.7 Hz, 2H), 6.82 (s, 4H), 2.31 (s, 6H), 1.96 (s, 12H), 1.58 (s, 12H) ppm

alkyne−Bmes₂−alkyne (12)
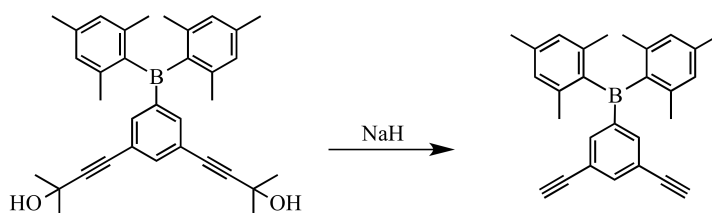
use **GS IV**:

mebynol−Bmes₂−mebynol (**11**)	2.99 g (6.1 mmol)
NaH	731.2 mg (18.3 mmol, 3 eq)
Solvent amount	50 ml

Column: P (100 %)

$R_f = 0.08$

Yield: 123 mg [49 %] of light yellow crystals

^{1}H NMR (400 MHz, CDCl₃): δ = 7.70 (t, J = 1.6 Hz, 1H), 7.59 (d, J = 1.7 Hz, 2H), 6.82 (s, 4H), 3.04 (s, 2H), 2.31 (s, 6H), 1.97 (s, 12H) ppm

amine−Ph−alkyne−Bmes₂−alkyne−xy−bpy (13)
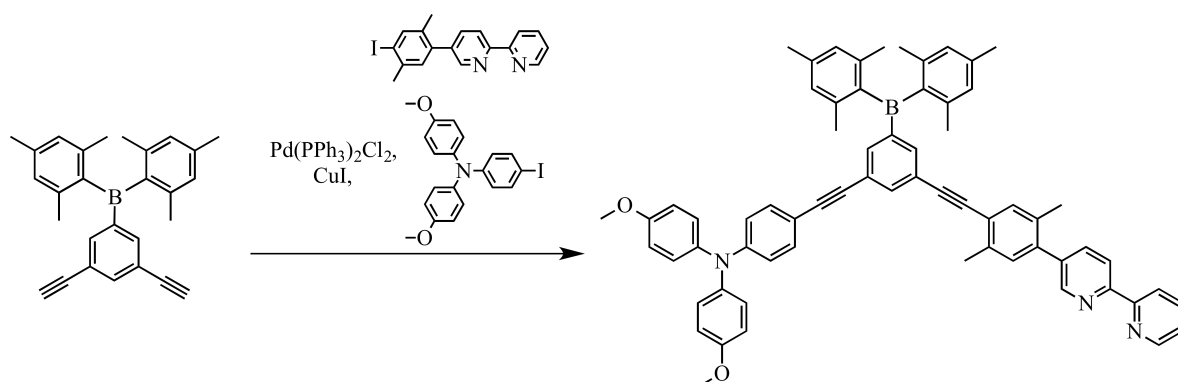
use **GS III**:

alkyne−Bmes₂−alkyne (**12**)	100 mg (0.267 mmol)
I−xy−bpy (**B-5**)	103.2 mg (0.267 mmol, 1 eq)
amine−Ph−I (**A-2**)	115.2 mg (0.267 mmol, 1 eq)
Solvent amount	20 ml
time: 1 h	

Column: CH₂Cl₂ (100 %) → P/EA/NEt₃ (100:10:1)

$R_f = 0.15$ (P/EA (5:1) + 1 % NEt₃)

Yield: 0.72 g [63 %] of light yellow solid

^{1}H NMR (400 MHz, acetone-d₆): δ = 8.70 (d, J = 4.1 Hz, 1H), 8.67 (d, J = 1.7 Hz, 1H), 8.55 (dd, J =

13.2, 8.1 Hz, 2H), 7.99 – 7.90 (m, 2H), 7.86 (s, 1H), 7.59 (s, 1H), 7.55 (s, 1H), 7.49 (s, 1H), 7.43 (dd, J = 8.0, 4.2 Hz, 1H), 7.33 (d, J = 8.9 Hz, 2H), 7.27 (s, 1H), 7.11 (d, J = 9.0 Hz, 4H), 6.94 (d, J = 9.0 Hz, 4H), 6.90 (s, 4H), 6.76 (d, J = 8.9 Hz, 2H), 3.80 (s, 5H), 2.51 (s, 4H), 2.30 (s, 8H) ppm

amine−Ph−alkyne−Bmes$_2$−alkyne−xy−bpyRubpy$_2$ (dyad 1)
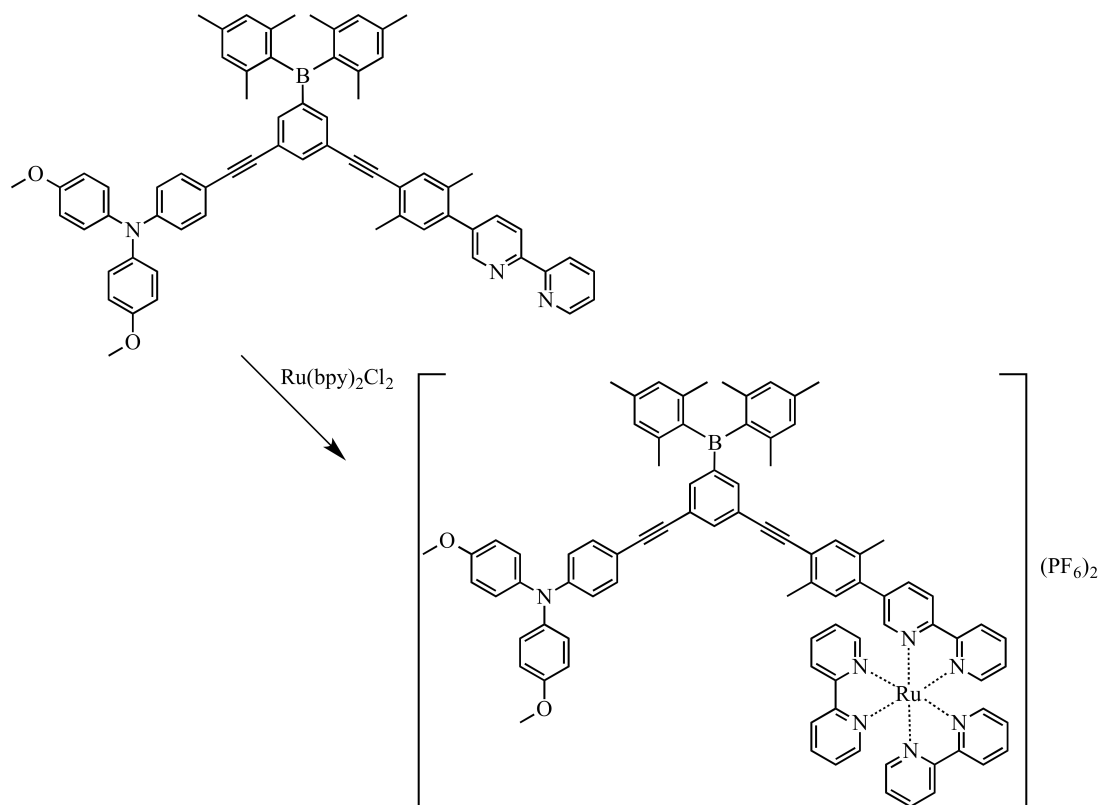
use **GS V**:

amine−ph−alkyne−Bmes$_2$−alkyne−xy−bpy (**13**)	155 mg (0.166 mmol)
Ru(bpy)$_2$Cl$_2$	80 mg (0.166 mmol, 1 eq)
CHCl$_3$	5 ml
MeOH	16 ml

Column: acetone (100 %) → acetone/H$_2$O (10:1) → acetone/H$_2$O/saturated aqueous KNO$_3$ (100:10:1) After column chromatography the solvents were removed. Addition of acetone precipitated KNO$_3$. Filtration with a P4 frit and removing solvent yielded the desired product. To purify the complex, it was dissolved in a minimal amount of acetone and dropped into a saturated aqueous KPF$_6$ solution. The resulting precipitate was washed with Et$_2$O and H$_2$O multiple times and dried in vacuum.

Yield: 129.6 mg [53 %] of orange solid

^{1}H NMR (400 MHz, acetone-d$_6$): δ = 8.96 (dd, J = 12.3, 8.0 Hz, 3H), 8.89 (t, J = 8.8 Hz, 4H), 8.28 – 8.19 (m, 7H), 8.14 – 8.05 (m, 5H), 7.93 (d, J = 1.6 Hz, 1H), 7.80 (t, J = 1.6 Hz, 1H), 7.65 – 7.51 (m, 8H), 7.35 (s, 1H), 7.31 (d, J = 8.9 Hz, 2H), 7.11 (d, J = 9.0 Hz, 4H), 6.95 (d, J = 9.0 Hz, 4H), 6.89 (s, 4H), 6.75 (d, J = 8.9 Hz, 2H), 3.80 (s, 6H), 2.40 (s, 3H), 2.30 (s, 6H), 2.03 (s, 12H), 1.98 (s, 3H) ppm

ESI-MS: m/z = 675.1 (calc. 675.0 for C$_{86}$H$_{74}$BN$_7$O$_2$Ru^{2+})

EA for $C_{86}H_{74}BN_7O_2RuP_2F_{12} \cdot 4\ H_2O \cdot CH_3CN$ calc.: C 60.31, H 4.89, N 6.39;   found: C 60.56, H 4.62, N 6.26

amine−Ph−alkyne−Bmes$_2$−alkyne−bpy (14)
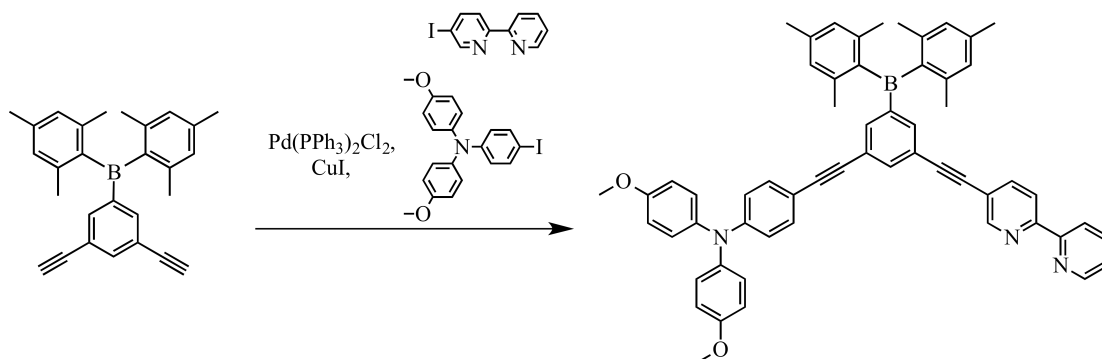
use **GS III**: a slight variation

alkyne−Bmes$_2$−alkyne (**12**)	100 mg (0.267 mmol)
amine−Ph−I (**A-2**)	115.2 mg (0,267 mmol, 1 eq)
I−bpy (**B-3**)	75.4 mg (0,267 mmol, 1 eq)
Solvent amount	10 ml

First, alkyne−Bmes$_2$−alkyne (**12**) and I−bpy (**B-3**) were dissolved in 5 ml solvent and stirred for 1 h at 96 °C. Then amine−Ph−I (**A-2**), dissolved in 5 ml solvent was added, and the mixture was stirred for 2 additional hours at 96 °C.

1. column: CH_2Cl_2 (100 %) → CH_2Cl_2/acetone (10:1)

2. column: P/EA (6:1) → (3:1)

R_f = 0.11 (P/EA (3:1))

Yield: 71.7 mg [31 %] of amorphous yellow solid

^{1}H NMR (400 MHz, acetone-d$_6$): δ = 8.82 (dd, J = 2.1, 0.8 Hz, 1H), 8.69 (ddd, J = 4.7, 1.7, 0.9 Hz, 1H), 8.55 – 8.45 (m, 2H), 8.06 (dd, J = 8.3, 2.2 Hz, 1H), 7.94 (td, J = 7.8, 1.8 Hz, 1H), 7.87 (s, 1H), 7.58 (d, J = 8.0 Hz, 2H), 7.43 (ddd, J = 7.5, 4.8, 1.2 Hz, 1H), 7.31 (s, 2H), 7.11 (d, J = 9.0 Hz, 4H), 6.94 (d, J = 9.0 Hz, 4H), 6.89 (s, 4H), 6.76 (d, J = 8.9 Hz, 2H), 3.80 (s, 6H), 2.30 (s, 6H), 2.04 (s, 12H) ppm

amine−Ph−alkyne−Bmes₂−alkyne−bpyRu((CF₃)₂bpy)₂ (dyad 2)
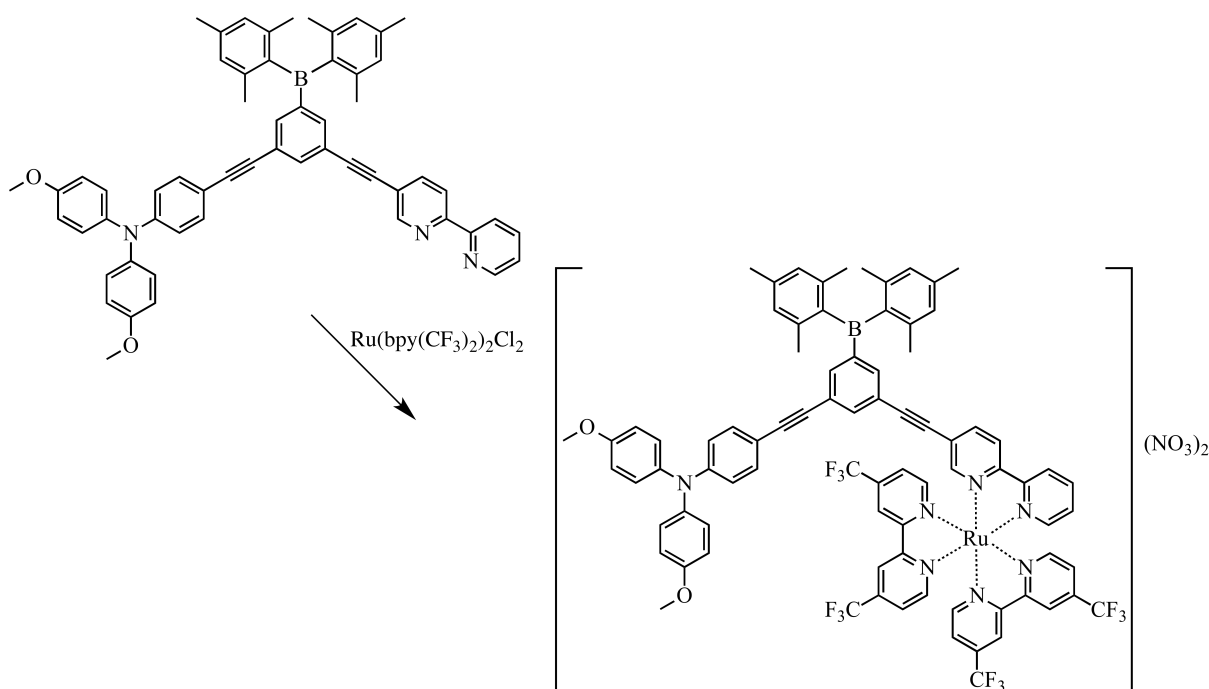
use **GS V**: with slight variation

amine−ph−alkyne−Bmes₂−alkyne−bpy (**14**)	45.2 mg (0.0053 mmol)
Ru(bpy(CF₃)₂)₂Cl₂	39.8 mg (0.0053 mmol, 1 eq)
AgNO₃	17.86 mg (0.105 mmol, 2 eq)
CHCl₃	1 ml
MeOH	4 ml

bpy−alkyne−Bmes₂−alkyne−Ph−amine (**14**), Ru(bpy(CF₃)₂)₂Cl₂, and AgNO₃ were dissolved in the solvent mixture, which was heated to 80 °C over night. Addition of brine and filtration removed the remaining silver.

Column: acetone (100 %) → acetone/H₂O (10:1) → acetone/H₂O/saturated aqueous KNO₃ (100:10:1)

After the column the solvents were removed. Addition of acetone precipitated KNO₃. Filtration with a P4 frit and removing solvent yielded the desired product.

Yield: 80.0 mg [90 %] of orange solid

^{1}H NMR (400 MHz, acetone-d₆): δ = 9.44 (dd, J = 15.6, 7.2 Hz, 4H), 8.97 (t, J = 8.6 Hz, 2H), 8.67 − 8.56 (m, 3H), 8.48 − 8.22 (m, 4H), 8.15 (d, J = 6.6 Hz, 1H), 7.94 (d, J = 5.9 Hz, 2H), 7.84 (t, J = 6.3 Hz, 2H), 7.67 (s, 1H), 7.60 − 7.54 (m, 2H), 7.38 − 7.25 (m, 2H), 7.11 (d, J = 9.0 Hz, 3H), 6.95 (d, J = 9.0 Hz, 3H), 6.88 (s, 3H), 6.74 (d, J = 8.9 Hz, 2H), 3.80 (s, 6H), 2.29 (s, 6H), 1.98 (s, 12H) ppm

EA for C₈₂H₆₂BF₁₂N₉O₈Ru · 10 H₂O   calc.: C 54.07, H 4.54, N 6.92;   found: C 53.93, H 4.86, N 6.54

6.6 Tetramethoxybenzene dyads

dmbq (15)
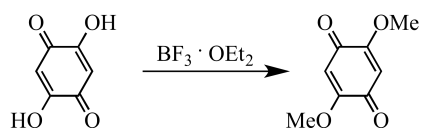
5.0 g (35.69 mmol) 1,4-dihydroxybenzoquinone were suspended in 75 ml dry MeOH. 12.5 ml (98.64 mmol, 2.76 eq) $BF_3 \cdot OEt_2$ were added to the suspension. The reaction mixture was heated to 100 °C for 2 h. After cooling to r.t., the precipitate was filtered off, washed with cold MeOH until the washing solution stayed clear and colourless. The solvent was evaporated.

Yield: 5.253 g [88 %] of beige needles (Lit. [144]: 71 %)

^{1}H NMR (400 MHz, CDCl$_3$): δ = 5.87 (s, 2H), 3.85 (s, 6H) ppm

dmb−(OH)$_2$ (16)
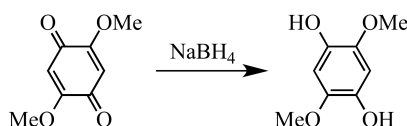
2.0 g (11.89 mmol) dmbq (**15**) were dissolved in 30 ml dry EtOH and cooled to 0 °C. 1.62 g (42.82 mmol, 3.6 eq) NaBH$_4$ were added to the solution portionwise over 20 minutes. After removing the ice bath, the solution thickened. The slurry mixture was stirred at r.t. for 4 h. After adding 50 ml 1 M HCl the clear brown solution was extracted with CH$_2$Cl$_2$ and Et$_2$O. The phases were separated, the organic phase was dried over Na$_2$SO$_4$, the solvents were evaporated.

Yield: 1.67 g [83 %] of light brown crystals (Lit. [73]: 89 %)

^{1}H NMR (400 MHz, CDCl$_3$): δ = 6.57 (s, 2H), 3.82 (s, 6H) ppm

tmb (17)
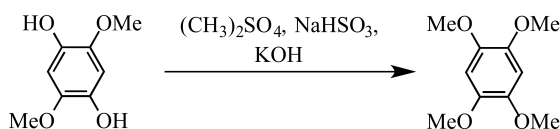
3.86 g (22.68 mmol) dmb−(OH)$_2$ (**16**) were dissolved in 50 ml EtOH and cooled to 0 °C. 9.68 ml (102.08 mmol, 4.5 eq) (CH$_3$)$_2$SO$_4$ were added *via* syringe dropwise. Then, 0.708 g (6.80 mmol, 30 mol%) NaHSO$_3$ and 8.91 g (158.79 mmol, 7 eq) KOH (dissolved in 20 ml H$_2$O) were added and the whole mixture was stirred for 30 min at 0 °C. Then the reaction was heated to 90 °C for 40 h. After addition of aqueous NH$_3$ solution and extraction with CH$_2$Cl$_2$, the phases were separated. The organic one was dried over Na$_2$SO$_4$ and solvent was removed in vacuum. The beige brown crystals were washed with very little cold MeOH.

Yield: 4.0 g [89 %] of white to off-white crystals (Lit. [73]: 82 %)

^{1}H NMR (400 MHz, CDCl$_3$): δ = 6.61 (s, 2H), 3.85 (s, 12H) ppm

I−tmb−I (18)
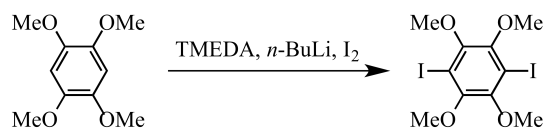
4.0 g (20.18 mmol) tmb (**17**) was dissolved in dry Et$_2$O. After addition of 7.22 ml (48.43 mmol, 2.4 eq) TMEDA the solution was cooled to 0 °C. Dropwise addition of 19.37 ml (48.43 mmol, 2.4 eq, 2.5 M) *n*-BuLi followed, then the mixture was warmed to r.t. and stirred for 1 h. Then, the mixture was cooled to 0 °C, and 12.29 g (48.43 mmol, 2.4 eq) I$_2$ were added. The resulting purple mixture was warmed to r.t. and stirred over night. After addition of saturated aqueous Na$_2$S$_2$O$_3$ solution and extraction with EA the organic layer was dried over Na$_2$SO$_4$ and evaporated. A short column (5 cm) was performed. The resulting solid was washed with cold MeOH.

Column: CH$_2$Cl$_2$ (100%)

Yield: 6.21 g [68%] of white crystals (Lit.[147]: 35 %)

^{1}H NMR (400 MHz, CDCl$_3$): δ = 3.85 (s, 12H) ppm

mebynol−tmb−mebynol (19)
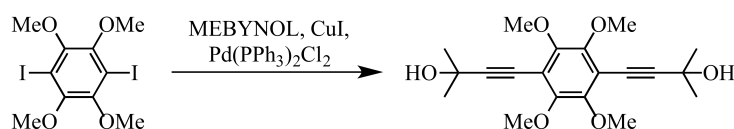
use **GS III**:

I−tmb−I (**18**)	1.0 g (2.22 mmol)
MEBYNOL	0.5 ml (4.89 mmol, 2.2 eq)
Solvent amount	25 ml

After evaporation of the solvents, the dry residue was dissolved in a minimal amount of EA and pentane was added until a white precipitate built. The precipitate was filtered off.

Yield: 659.7 mg [82 %] of off-white needles

^{1}H NMR (400 MHz, acetone-d$_6$): δ = 4.51 (s, 2H), 3.85 (s, 12H), 1.58 (s, 12H) ppm

alkyne−tmb−alkyne (20)
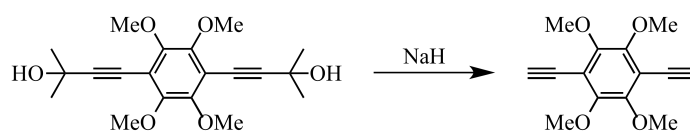
use **GS IV**:

mebynol−tmb−mebynol (**19**)	2.30 g (6.35 mmol)
NaH	126.9 mg (3.17 mmol, 0.5 eq)
Solvent amount	50 ml

Column: P/EA (4:1)

R_f = 0.66

Yield: 1.33 g [85 %] of off-white crystals

^{1}H NMR (400 MHz, CDCl$_3$): δ = 3.92 (s, 12H), 3.56 (s, 2H) ppm

amine−Ph−alkyne−tmb−alkyne−xy−bpy (21)
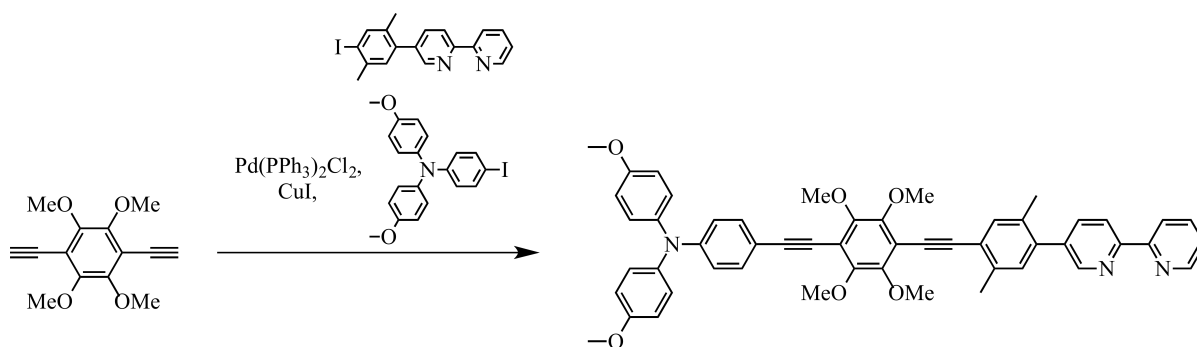
use **GS III**:

alkyne−tmb−alkyne (**20**)	100 mg (0.4 mmol)
I−xy−bpy (**B-5**)	156.8 mg (0.4 mmol, 1 eq)
amine−Ph−I (**A-2**)	175.2 mg (0.4 mmol, 1 eq)
Solvent amount	10 ml

Column: CH$_2$Cl$_2$ (100 %) → P/EA (3:1) + 1 % NEt$_3$

R_f = 0.13 (P/EA (3:1) + 1 % NEt$_3$)

Yield: 90 mg [27 %] of bright yellow solid

^{1}H NMR (400 MHz, acetone-d$_6$): δ = 8.69 (d, J = 3.7 Hz, 2H), 8.54 (dd, J = 12.9, 8.1 Hz, 2H), 7.95 − 7.87 (m, 2H), 7.51 (s, 1H), 7.44 − 7.34 (m, 3H), 7.27 (s, 1H), 7.11 (d, J = 9.0 Hz, 4H), 6.93 (d, J = 9.0 Hz, 4H), 6.81 (d, J = 8.8 Hz, 2H), 3.98 (d, J = 8.3 Hz, 12H), 3.79 (s, 6H), 2.59 (s, 3H), 2.32 (s, 3H) ppm

ESI-MS: m/z [M+H] = 608.72 (calc. 608.33 for C$_{52}$H$_{45}$N$_3$O$_6$+H)

amine−Ph−alkyne−tmb−alkyne−xy−bpyRubpy₂ (dyad 3)
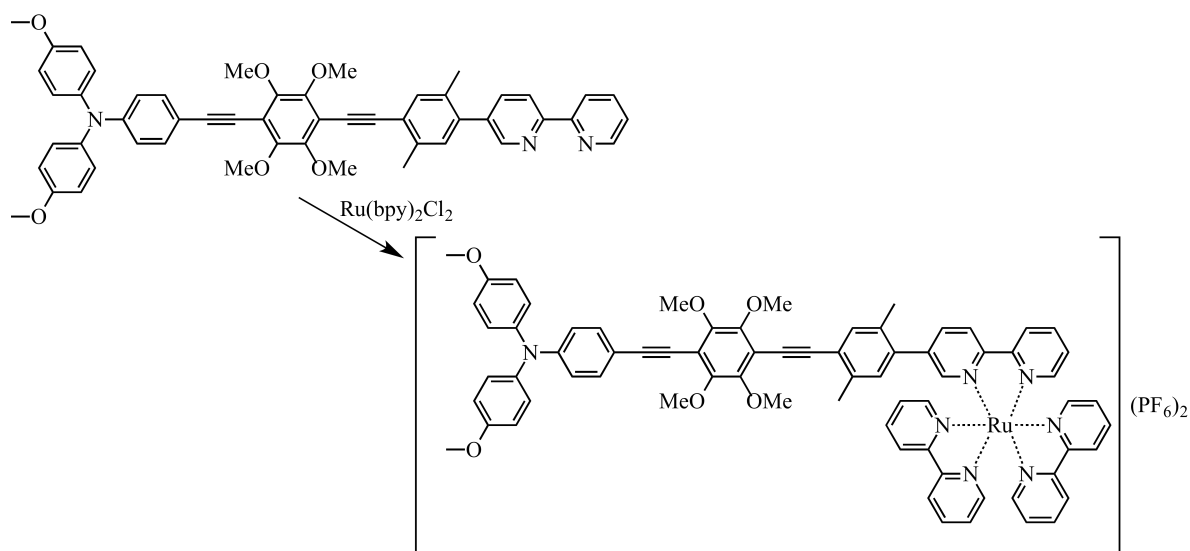
use **GS V**:

amine−ph−alkyne−tmb−alkyne−xy−bpy (**21**)	155 mg (0.166 mmol)
Ru(bpy)₂Cl₂	80 mg (0.166 mmol, 1 eq)
CHCl₃	5 ml
MeOH	16 ml

Column: acetone (100 %) → acetone/H₂O (10:1) → acetone/H₂O/saturated aqueous KNO₃ (100:10:1)

R_f = 0.26 (acetone/H₂O/KNO₃ (100:10:1))

After the column the solvents were removed, addition of acetone precipitated KNO₃. Following filtration with a P4 frit, the solvent was removed from the mixture. The dry complex was dissolved in a minimal amount of acetone and dropped into Et₂O where it precipitated. The precipitate was washed with Et₂O, H₂O and dried in vacuum. To purify the complex, it was dissolved in a minimal amount of acetone and dropped into a saturated aqueous KPF₆ solution. The resulting precipitate was washed with diethylether and water multiple times and dried in vacuum.

Yield: 129.6 mg [53 %] of orange solid

^{1}H NMR (400 MHz, acetone-d₆): δ = 8.92 – 8.80 (m, 6H), 8.26 – 8.16 (m, 7H), 8.13 – 8.06 (m, 4H), 7.97 (d, J = 1.8 Hz, 1H), 7.64 – 7.53 (m, 5H), 7.38 (d, J = 9.0 Hz, 3H), 7.18 – 7.09 (m, 5H), 6.95 (d, J = 9.0 Hz, 4H), 6.81 (d, J = 8.9 Hz, 2H), 3.95 (d, J = 2.0 Hz, 12H), 3.81 (s, 6H), 2.50 (s, 3H), 2.01 (s, 3H) ppm

ESI-MS: m/z = 610.92 (calc. 610.69 for $C_{72}H_{61}N_7O_6Ru^{2+}$)

HRMS: m/z = 610.6861 (calc. 610.6864 for $C_{72}H_{61}N_7O_6Ru^{2+}$)

EA for $C_{72}H_{61}F_{12}N_7O_6P_2Ru \cdot 2\ C_5H_{12}$ calc.: C 59.49, H 5.17, N 5.92;   found: C 59.24, H 5.47, N 5.95

amine−Ph$_2$−alkyne−tmb−alkyne−Ph$_2$−bpy (22)
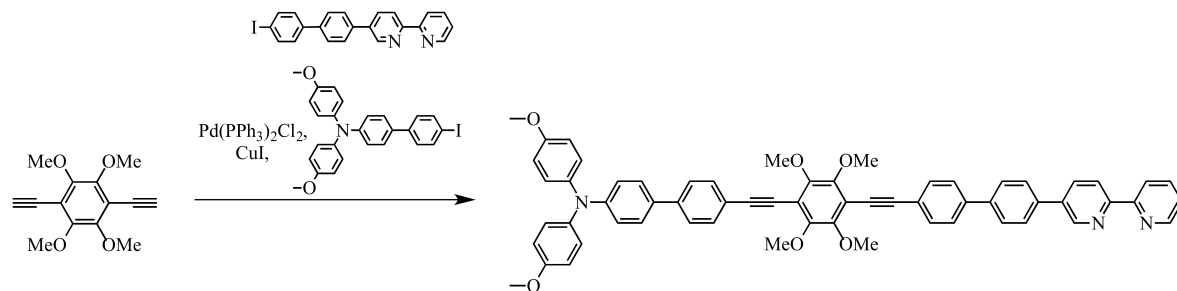
use **GS III**:

alkyne−tmb−alkyne (**20**)	100 mg (0.4 mmol)
I−Ph$_2$−bpy (**B-5**)	156.8 mg (0.4 mmol, 1 eq)
amine−Ph$_2$−I (**A-2**)	175.2 mg (0.4 mmol, 1 eq)
Solvent amount	10 ml

Column: CH$_2$Cl$_2$ (100 %) → P/EA (3:1) + 1 % NEt$_3$ → (1:1) + 2 % NEt$_3$

R$_f$ = 0.71 (P/EA (1:1) + 2 % NEt$_3$)

Yield: 37.5 mg [10 %] of light orange solid

^{1}H NMR (400 MHz, CD$_2$Cl$_2$): δ = 8.99 (d, J = 2.2 Hz, 1H), 8.69 (d, J = 5.2 Hz, 1H), 8.57 − 8.45 (m, 2H), 8.12 (dd, J = 8.4, 2.4 Hz, 1H), 7.89 − 7.80 (m, 5H), 7.75 − 7.67 (m, 4H), 7.60 (s, 4H), 7.47 (d, J = 8.8 Hz, 2H), 7.38 − 7.30 (m, 1H), 7.13 − 7.05 (m, 4H), 6.96 (d, J = 8.8 Hz, 2H), 6.90 − 6.83 (m, 4H), 4.01 (d, J = 3.5 Hz, 12H), 3.80 (s, 6H) ppm

amine−Ph$_2$−alkyne−tmb−alkyne−Ph$_2$−bpyRubpy$_2$ (dyad 4)
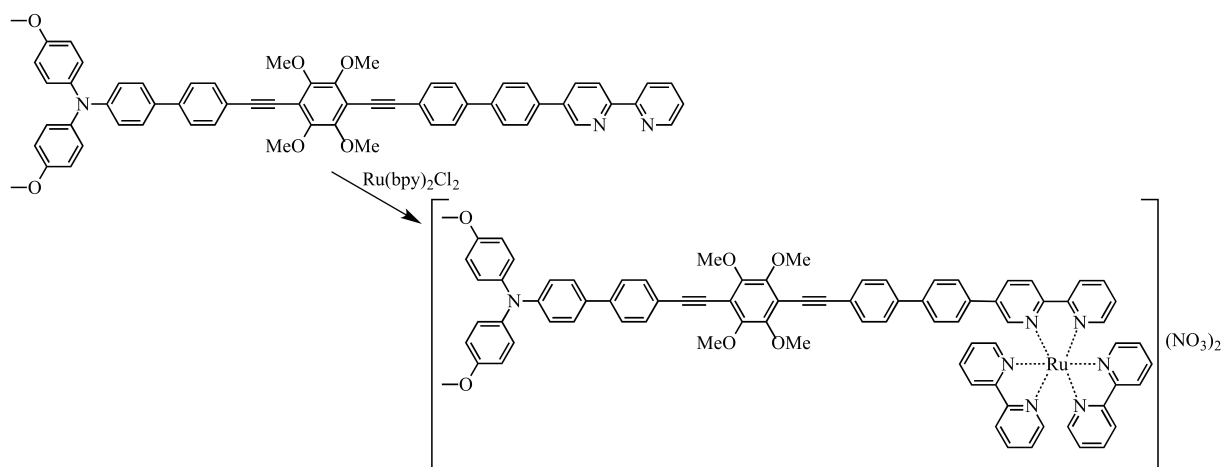
use **GS V**: with slight variation

amine−Ph$_2$−alkyne−tmb−alkyne−Ph$_2$−bpy (**22**)	37.5 mg (0.04 mmol)
Ru(bpy)$_2$Cl$_2$	19.5 mg (0.04 mmol, 1 eq)
AgNO$_3$	13.6 mg (0.105 mmol, 2 eq)
CHCl$_3$	3 ml
MeOH	10 ml

Column: acetone (100 %) → acetone/H$_2$O (10:1) → acetone/H$_2$O/saturated aqueous KNO$_3$ (100:10:1)

R$_f$ = 0.4 (acetone/H$_2$O/KNO$_3$ (100:10:1))

After the column the solvents were removed, addition of acetone precipitated KNO$_3$. Following filtration with a P4 frit, the solvent was removed from the mixture. The dry complex was dissolved in a minimal amount of methylene chloride and dropped into Et$_2$O where it precipitated. The precipitate was washed with Et$_2$O, H$_2$O and dried in vacuum.

Yield: 8.4 mg [14 %] of orange solid

^{1}H NMR (400 MHz, acetone-d$_6$): δ = 9.01 − 8.86 (m, 6H), 8.56 (dd, J = 8.6, 2.0 Hz, 1H), 8.28 − 8.17 (m, 9H), 8.09 (dd, J = 14.4, 5.6 Hz, 3H), 7.82 − 7.77 (m, 4H), 7.74 − 7.68 (m, 4H), 7.66 − 7.55 (m, 11H), 7.11 (d, J = 9.0 Hz, 4H), 6.94 (dd, J = 8.9, 5.8 Hz, 5H), 4.00 (d, J = 2.3 Hz, 12H), 3.81 (s, 6H) ppm

ESI-MS: m/z = 672.98 (calc. 672.77 for C$_{82}$H$_{65}$N$_7$O$_6$Ru^{2+})

HRMS: m/z = 672.7018 (calc. 672.7020 for C$_{82}$H$_{65}$N$_7$O$_6$Ru^{2+})

amine−fl−alkyne−tmb−alkyne−fl−bpy (23)
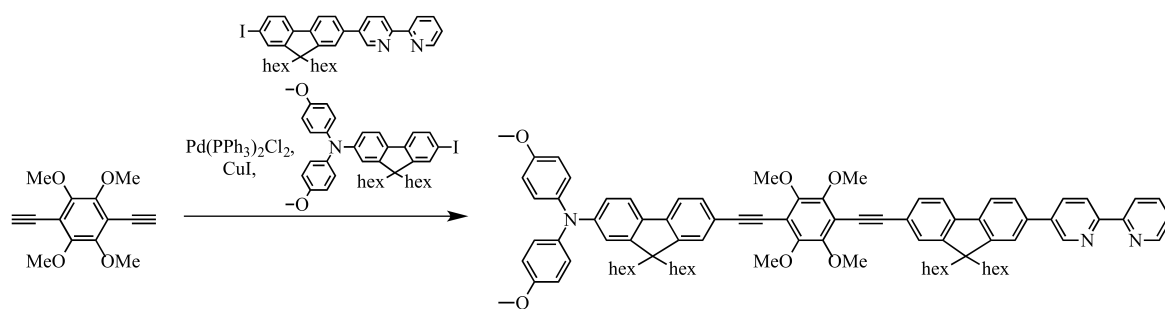
use **GS III**:

alkyne−tmb−alkyne (**20**)	50 mg (0.2 mmol)
I−fl−bpy (**B-9**)	125 mg (0.2 mmol, 1 eq)
amine−fl−I (**A-6**)	140 mg (0.2 mmol, 1 eq)
Solvent amount	15 ml

Column: CH_2Cl_2 (100 %) → P/Et$_2$O (2:1)

R$_f$ = 0.13 (P/Et$_2$O 2:1))

Yield: 130 mg [50 %] of bright yellow solid

^{1}H NMR (400 MHz, acetone-d$_6$): δ = 9.09 (d, J = 1.8 Hz, 1H), 8.73 – 8.68 (m, 1H), 8.57 (dd, J = 18.1, 8.1 Hz, 2H), 8.31 (dd, J = 8.3, 2.4 Hz, 1H), 8.06 – 7.91 (m, 4H), 7.85 (dd, J = 7.9, 1.7 Hz, 1H), 7.75 – 7.71 (m, 2H), 7.69 – 7.52 (m, 4H), 7.43 (dd, J = 8.5, 4.8 Hz, 1H), 7.11 – 7.00 (m, 5H), 6.95 – 6.83 (m, 5H), 4.02 (d, J = 3.6 Hz, 12H), 3.81 (s, 6H), 2.32 – 2.17 (m, 3H), 1.89 (m, 3H), 1.45 – 0.98 (m, 26H), 0.98 – 0.64 (m, 24H) ppm

ESI-MS: m/z [M+H] = 1293.23 (calc.1292.74 for $C_{88}H_{97}N_3O_6$+H)

amine−fl−alkyne−tmb−alkyne−fl−bpyRubpy₂ (dyad 5)
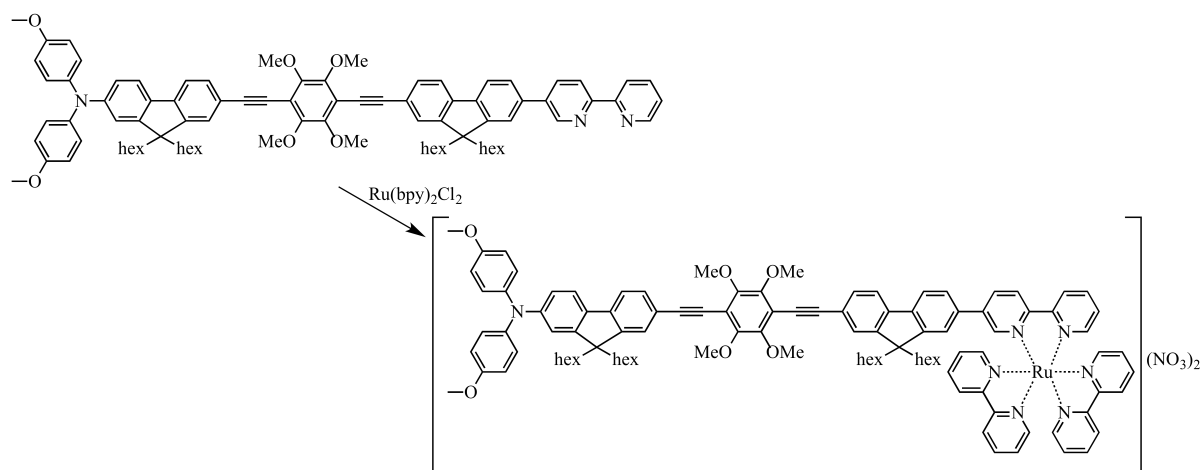
use **GS V**:

amine−fl−alkyne−tmb−alkyne−fl−bpy (**23**)	130 mg (0.1 mmol)
Ru(bpy)₂Cl₂	49 mg (0.1 mmol, 1 eq)
CHCl₃	3 ml
MeOH	10 ml

Column: acetone (100 %) → acetone/H₂O (10:1) → acetone/H₂O/saturated aqueous KNO₃ (100:10:1)

R_f = 0.4 (acetone/H₂O/KNO₃ (100:10:1))

After the column the solvents were removed. Addition of acetone precipitated KNO₃. Following filtration with a P4 frit, the solvent was removed from the mixture. The dry complex was dissolved in a minimal amount of acetone and dropped into Et₂O where it precipitated. The precipitate was washed with Et₂O, H₂O and dried in vacuum.

Yield: 41 mg [22 %] of orange solid

¹H NMR (400 MHz, acetone-d₆): δ = 8.99 – 8.86 (m, 6H), 8.62 (dd, J = 8.6, 2.0 Hz, 1H), 8.31 (td, J = 7.9, 1.4 Hz, 1H), 8.27 – 8.19 (m, 7H), 8.14 – 8.05 (m, 3H), 7.91 (d, J = 8.7 Hz, 2H), 7.73 (d, J = 7.8 Hz, 1H), 7.68 (dd, J = 6.9, 5.5 Hz, 3H), 7.65 – 7.49 (m, 9H), 7.11 – 7.00 (m, 5H), 6.95 – 6.83 (m, 5H), 4.01 (d, J = 2.2 Hz, 12H), 3.81 (s, 6H), 2.22 – 2.08 (m, 3H), 1.95 – 1.82 (m, 3H), 1.36 – 0.49 (m, 50H) ppm

ESI-MS: m/z = 853.23 (calc. 852.89 for $C_{108}H_{113}N_7O_6Ru^{2+}$)

HRMS: m/z = 852.8909 (calc. 852.8898 for $C_{108}H_{113}N_7O_6Ru^{2+}$)

EA for $C_{108}H_{113}N_9O_{12}Ru \cdot 2\ H_2O \cdot 2\ CH_3CN \cdot 2\ CH_2Cl_2$ calc.: C 64.64, H 6.04, N 7.27; found: C 64.43, H 6.24, N 7.45

amine−fl$_2$−alkyne−tmb−alkyne−fl$_2$−bpy (24)
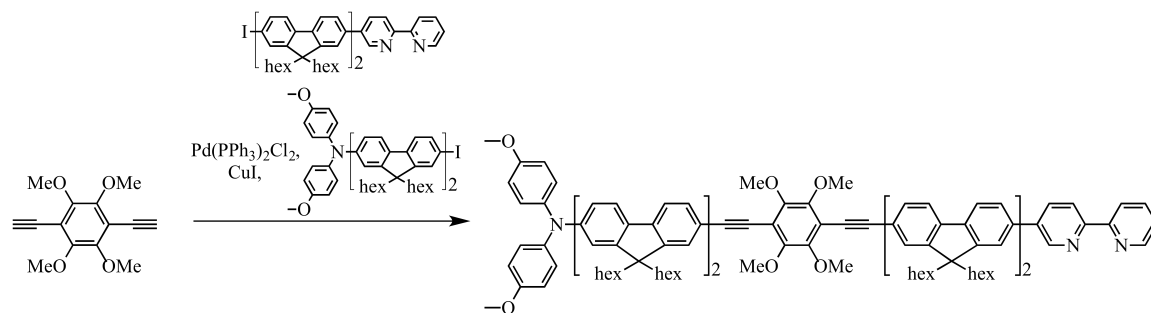
use **GS III**:

alkyne−tmb−alkyne (**20**)	100 mg (0.4 mmol)
I−fl$_2$−bpy (**B-11**)	390 mg (0.4 mmol, 1 eq)
amine−fl$_2$−I (**A-9**)	408 mg (0.4 mmol, 1 eq)
Solvent amount	20 ml

Column: CH$_2$Cl$_2$ (100 %) → P/Et$_2$O (2:1)

R$_f$ = 0.13 (P/Et$_2$O 2:1))

Yield: 186 mg [23 %] of bright yellow solid

^{1}H NMR (400 MHz, acetone-d$_6$): δ = 9.09 (d, J = 2.2 Hz, 1H), 8.71 (dd, J = 3.8, 1.5 Hz, 1H), 8.57 (dd, J = 17.6, 8.3 Hz, 2H), 8.31 (dd, J = 8.3, 2.3 Hz, 1H), 8.03 − 7.97 (m, 4H), 7.96 − 7.90 (m, 6H), 7.90 − 7.88 (m, 1H), 7.86 − 7.81 (m, 4H), 7.78 (dd, J = 8.0, 2.0 Hz, 2H), 7.74 − 7.70 (m, 3H), 7.68 − 7.62 (m, 3H), 7.46 − 7.41 (m, 1H), 7.07 (d, J = 9.0 Hz, 5H), 6.95 − 6.85 (m, 5H), 4.04 (d, J = 0.6 Hz, 12H), 3.81 (s, 6H), 2.28 − 2.16 (m, 12H), 1.98 − 1.86 (m, 4H), 1.12 (dd, J = 11.8, 4.3 Hz, 53H), 0.83 − 0.68 (m, 42H) ppm

amine−fl$_2$−alkyne−tmb−alkyne−fl$_2$−bpyRubpy$_2$ (dyad 6)
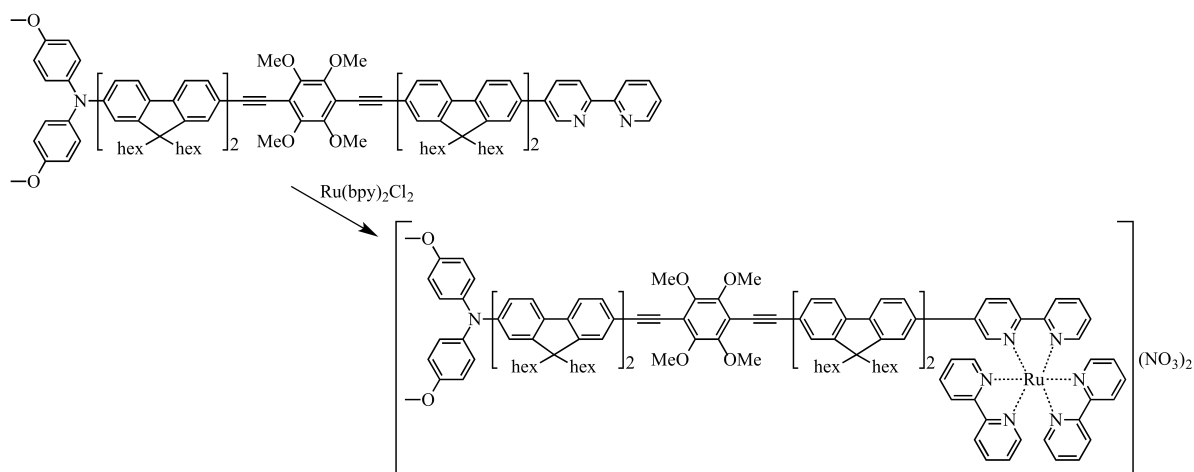
use **GS V**:

amine−fl$_2$−alkyne−tmb−alkyne−fl$_2$−bpy (**24**)	146.2 mg (0.07 mmol)
Ru(bpy)$_2$Cl$_2$	36.2 mg (0.07 mmol, 1 eq)
CHCl$_3$	3 ml
MeOH	10 ml

Column: acetone (100 %) → acetone/H$_2$O (10:1) → acetone/H$_2$O/saturated aqueous KNO$_3$ (100:10:1)

R$_f$ = 0.49 (acetone/H$_2$O/KNO$_3$ (100:10:1))

After the column the solvents were removed. Addition of acetone precipitated KNO$_3$. Following filtration with a P4 frit, the solvent was removed from the mixture. The dry complex was dissolved in a minimal amount of methylene chloride and dropped into Et$_2$O where it precipitated. The precipitate was washed with Et$_2$O, H$_2$O and dried in vacuum.

Yield: 7.5 mg [4 %] of orange solid

^{1}H NMR (400 MHz, acetone-d$_6$): δ = 9.00 – 8.86 (m, 6H), 8.65 – 8.60 (m, 1H), 8.36 – 8.18 (m, 9H), 8.17 – 8.06 (m, 3H), 7.92 (dd, J = 18.2, 7.9 Hz, 10H), 7.83 – 7.56 (m, 17H), 7.50 (d, J = 7.9 Hz, 1H), 7.07 (d, J = 9.0 Hz, 4H), 6.94 – 6.86 (m, 4H), 4.03 (d, J = 1.0 Hz, 12H), 3.81 (s, 6H), 2.26 – 2.16 (m, 12H), 1.92 – 1.87 (m, 4H), 1.20 – 1.01 (m, 53H), 0.84 – 0.67 (m, 42H) ppm

ESI-MS: m/z = 1185.62 (calc.1185.14 for C$_{158}$H$_{177}$N$_7$O$_6$Ru^{2+})

HRMS: m/z = 1185.6413 (calc.1185.1404 for C$_{158}$H$_{177}$N$_7$O$_6$Ru^{2+})

6.7 Benzene dyads

mebynol−Ph−mebynol (25)
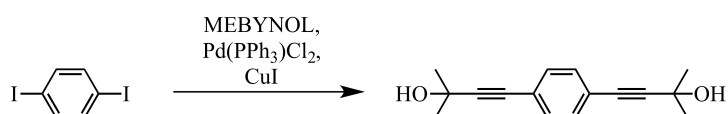
use **GS III**:

1,4-diiodobenzene	5.0 g (15.16 mmole)
MEBYNOL	3.25 ml (33.34 mmole, 2.2 eq)
Solvent amount	75ml
time:	2 h

Column: P/EA (5:1) → (1:1)

R_f = 0.67 (P/EA (1:1))

Yield: 3.67 g [quant.] of light yellow crystals (Lit.[148]: 95 %)

^{1}H NMR (400 MHz, acetone-d_6): δ = 7.36 (s, 4H), 1.53 (s, 12H) ppm

alkyne−Ph−alkyne (26)
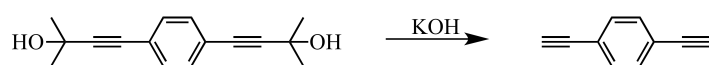
1.00 g (4.11 mmol) mebynol−Ph−mebynol (**25**) were dissolved in 20 ml toluene and 0.57 g (10.27 mmol, 2.5 eq) freshly powdered KOH were added. This solution was heated to 125°C for 3 h. The precipitate was filtered off and solvent was removed in vacuum. The crude product was purified by column and afterwards stored in the fridge.

Column: P (100 %)

R_f = 0.67

Yield: 0.40 g [78 %] of white crystals (Lit.[148]: 98 %)

^{1}H NMR (400 MHz, acetone-d_6): δ = 7.50 (s, 4H), 3.81 (s, 2H) ppm

amine−Ph−alkyne−Ph−alkyne−xy−bpy (27)
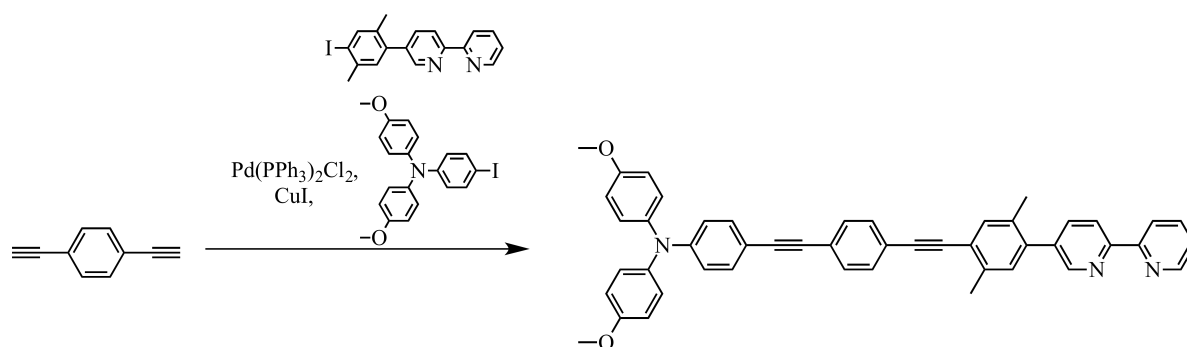
use **GS III**:

alkyne−Ph−alkyne (**26**)	100 mg (0.79 mmol)
I−xy−bpy (**B-5**)	306 mg (0.79 mmol, 1 eq)
amine−Ph−I (**A-2**)	342 mg (0.79 mmol, 1 eq)
Solvent amount	10 ml

Column: CH_2Cl_2 (100 %) → P/EA (3:1) + 1 % NEt_3

R_f = 0.13 (P/EA (3:1) + 1 % NEt_3)

Yield: 270 mg [50 %] of bright yellow solid

^{1}H NMR (400 MHz, acetone-d_6): δ = 8.74 – 8.66 (m, 2H), 8.61 – 8.50 (m, 2H), 7.95 (ddt, J = 7.8, 4.2, 1.9 Hz, 2H), 7.64 – 7.48 (m, 5H), 7.44 (ddd, J = 7.5, 4.8, 1.2 Hz, 1H), 7.39 – 7.27 (m, 3H), 7.16 – 7.09 (m, 4H), 6.99 – 6.92 (m, 4H), 6.79 (d, J = 8.9 Hz, 2H), 3.81 (s, 6H), 2.55 (s, 3H), 2.33 (s, 3H) ppm

ESI-MS: m/z [M+H]= 688.61 (calc. 688.29 for $C_{48}H_{37}N_3O_2$+H)

amine−Ph−alkyne−Ph−alkyne−xy−bpyRubpy$_2$ (dyad 7)
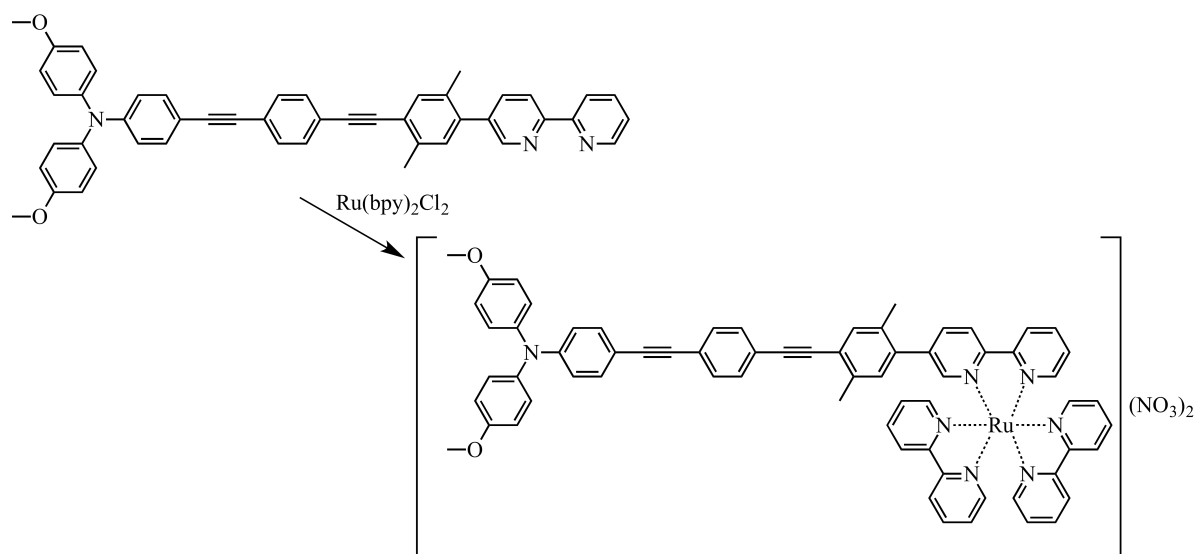
use **GS V**:

amine−Ph−alkyne−Ph−alkyne−xy−bpy (**27**)	213.4 mg (0.31 mmol)
Ru(bpy)$_2$Cl$_2$	150.3 mg (0.31 mmol, 1 eq)
CHCl$_3$	3 ml
MeOH	10 ml

Column: acetone (100 %) → acetone/H$_2$O (10:1) → acetone/H$_2$O/saturated aqueous KNO$_3$ (100:10:1)

R$_f$ = 0.4 (acetone/H$_2$O/KNO$_3$ (100:10:1))

After the column the solvents were removed. Addition of acetone precipitated KNO$_3$. Following filtration with a P4 frit, the solvent was removed from the mixture. The dry complex was dissolved in a minimal amount of CH$_3$CN and dropped into Et$_2$O where it precipitated. The precipitate was washed with Et$_2$O, H$_2$O and dried in vacuum.

Yield: 75 mg [19 %] of orange solid

^{1}H NMR (400 MHz, Acetone-d$_6$): δ = 9.01 − 8.87 (m, 6H), 8.28 − 8.06 (m, 11H), 7.95 (d, J = 1.8 Hz, 1H), 7.67 − 7.49 (m, 9H), 7.39 − 7.31 (m, 3H), 7.17 − 7.09 (m, 5H), 6.96 (d, J = 9.0 Hz, 4H), 6.79 (d, J = 8.9 Hz, 2H), 3.81 (s, 6H), 2.44 (s, 3H), 2.00 (s, 3H) ppm

ESI-MS: m/z = 550.86 (calc. 550.67 for C$_{68}$H$_{53}$N$_7$O$_2$Ru^{2+})

HRMS: m/z = 550.6643 (calc. 550.6652 for C$_{68}$H$_{53}$N$_7$O$_2$Ru^{2+})

EA for C$_{68}$H$_{53}$N$_9$O$_8$Ru · CH$_3$CN · 5 H$_2$O   calc.: C 61.98, H 4.9, N 10.33;   found: C 62.17, H 4.85, N 10.11

amine$-$Ph$_2$$-$alkyne$-Ph-$alkyne$-Ph_2$$-$bpy (28)
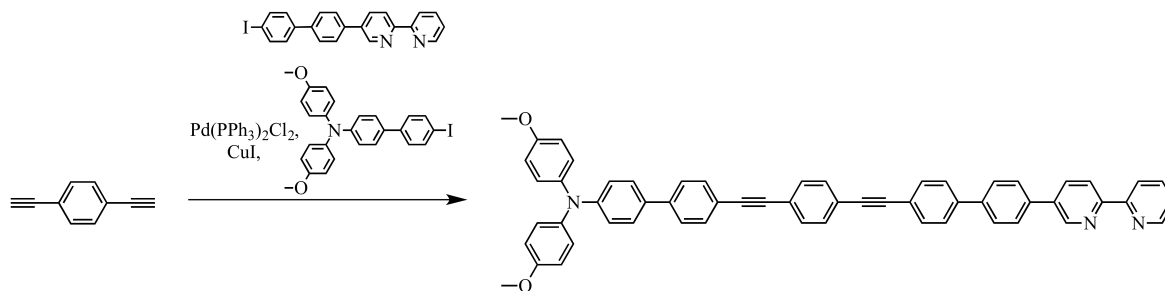
use **GS III**: slight variation

alkyne$-$Ph$-$alkyne (**26**)	28 mg (0.2 mmol)
I$-$Ph$_2$$-$bpy (**B-7**)	96 mg (0.2 mmol, 1 eq)
amine$-$Ph$_2$$-$I (**A-4**)	112 mg (0.2 mmol, 1 eq)
Solvent amount	7 ml

All compounds were dissolved in dry NEt$_3$. After deoxygenation the solution, the catalyst mixture (CuI and Pd(PPh$_3$)$_2$Cl$_2$) was added. After a second deoxygenation the solution was heated to 50 °C and stirred for 6 h.

Column: CH$_2$Cl$_2$ (100 %) $\rightarrow$ P/CH$_2$Cl$_2$ (1:1) + 1 % NEt$_3$

R_f = 0.13 (P/CH$_2$Cl$_2$ (1:1) + 1 % NEt$_3$)

Yield: 2.9 mg of yellow solid

^{1}H NMR (400 MHz, acetone-d$_6$) showed mixture of amine$-$Ph$_2$$-$alkyne$-Ph-$alkyne$-Ph_2$$-$bpy (**29**) and I$-Ph_2$$-$bpy (**B-7**) which could be confirmed in ESI-MS measurements.

amine−fl−alkyne−Ph−alkyne−fl−bpy (29)

use **GS III**:

alkyne−Ph−alkyne (**26**)	50 mg (0.4 mmol)
I−fl−bpy (**B-9**)	244 mg (0.4 mmol, 1 eq)
amine−fl−I (**A-6**)	272 mg (0.4 mmol, 1 eq)
Solvent amount	15 ml

Column: CH_2Cl_2 (100 %) $\rightarrow$ P/Et$_2$O (2:1)

R_f = 0.17 (P/Et$_2$O (2:1))

Yield: 222 mg [48 %] of bright yellow solid

^{1}H NMR (400 MHz, acetone-d$_6$): δ = 9.09 (d, J = 1.8 Hz, 1H), 8.71 (d, J = 7.1 Hz, 1H), 8.57 (dd, J = 17.8, 8.0 Hz, 2H), 8.31 (dd, J = 8.3, 2.4 Hz, 1H), 8.05 − 7.90 (m, 4H), 7.88 − 7.83 (m, 1H), 7.75 − 7.55 (m, 9H), 7.52 (dd, J = 7.8, 1.4 Hz, 1H), 7.43 (dd, J = 7.5, 4.8 Hz, 1H), 7.10 − 7.00 (m, 5H), 6.95 − 6.83 (m, 5H), 3.81 (s, 6H), 2.32 − 2.12 (m, 4H), 2.01 − 1.84 (m, 4H), 1.29 − 0.62 (m, 48H) ppm

ESI-MS: m/z [M+H] = 1173.19 (calc. 1172.70 for $C_{84}H_{89}N_3O_2$+H)

amine−fl−alkyne−Ph−alkyne−fl−bpyRubpy₂ (dyad 8)

use **GS V**:

amine−fl−alkyne−Ph−alkyne−fl−bpy (**29**)	222 mg (0.19 mmol)
Ru(bpy)₂Cl₂	92 mg (0.19 mmol, 1 eq)
CHCl₃	3 ml
MeOH	10 ml

Column: acetone (100 %) → acetone/H_2O (10:1) → acetone/H_2O/saturated aqueous KNO_3 (100:10:1)

R_f = 0.4 (acetone/H_2O/KNO_3 (100:10:1))

After the column the solvents were removed. Addition of acetone precipitated KNO_3. Following filtration with a P4 frit, the solvent was removed from the mixture. The dry complex was dissolved in a minimal amount of acetone and dropped into Et_2O where it precipitated. The precipitate was washed with Et_2O, H_2O and dried in vacuum.

Yield: 46.8 mg [14 %] of orange solid

^{1}H NMR (400 MHz, acetone-d_6): δ = 9.05 – 8.88 (m, 6H), 8.61 (dd, J = 8.6, 1.9 Hz, 1H), 8.34 – 8.17 (m, 8H), 8.16 – 8.03 (m, 3H), 7.89 (dd, J = 7.8, 3.4 Hz, 2H), 7.73 – 7.56 (m, 15H), 7.51 (dt, J = 7.9, 1.5 Hz, 2H), 7.10 – 7.00 (m, 5H), 6.95 – 6.83 (m, 5H), 3.80 (s, 6H), 2.14 (s, 4H), 1.99 – 1.85 (m, 4H), 1.34 – 0.47 (m, 52H) ppm

ESI-MS: m/z = 793.21 (calc. 792.87 for $C_{104}H_{105}N_7O_2Ru^{2+}$)

HRMS: m/z = 792.8687 (calc. 792.8687 for $C_{104}H_{105}N_7O_2Ru^{2+}$)

EA for $C_{104}H_{105}N_9O_8Ru \cdot 5\,H_2O$ calc.: C 69.39, H 6.44, N 7.00;   found: C 69.59, H 6.62, N 6.89

amine−fl$_2$−alkyne−Ph−alkyne−fl$_2$−bpy (30)

use **GS III**:

alkyne−Ph−alkyne (**26**)	25 mg (0.02 mmol)
I−fl$_2$−bpy (**B-11**)	195 mg (0.02 mmol, 1 eq)
amine−fl$_2$−I (**A-9**)	204 mg (0.02 mmol, 1 eq)
Solvent amount	15 ml

Column: CH$_2$Cl$_2$ (100 %) → P/EA (3:1) + 1 % NEt$_3$

R$_f$ = 0.13 (P/EA (3:1) + 1 % NEt$_3$)

Yield: 120 mg [33 %] of bright yellow solid

^{1}H NMR (400 MHz, acetone-d$_6$): δ = 9.09 (d, J = 2.1 Hz, 1H), 8.71 (d, J = 4.6 Hz, 1H), 8.57 (dd, J = 17.6, 8.0 Hz, 2H), 8.31 (dd, J = 8.3, 2.2 Hz, 1H), 8.03 − 7.87 (m, 11H), 7.86 − 7.75 (m, 6H), 7.74 − 7.64 (m, 8H), 7.60 (ddd, J = 7.8, 4.5, 1.4 Hz, 2H), 7.48 − 7.40 (m, 1H), 7.07 (d, J = 9.0 Hz, 5H), 6.95 − 6.85 (m, 5H), 3.81 (s, 6H), 2.31 − 2.15 (m, 12H), 1.98 − 1.79 (m, 4H), 1.20 (s, 6H), 1.09 (s, 52H), 0.83 − 0.65 (m, 43H) ppm

amine$-$fl$_2$$-$alkyne$-Ph-$alkyne$-fl_2$$-$bpyRubpy$_2$ (dyad 9)

use **GS V**: with slight variation

amine$-$fl$_2$$-$alkyne$-tmb-$alkyne$-fl_2$$-$bpy (**30**)	60.4 mg (0.03 mmol)
Ru(bpy)$_2$Cl$_2$	15.9 mg (0.03 mmol, 1 eq)
AgNO$_3$	12 mg (0.06 mmol, 2 eq)
CHCl$_3$	3 ml
MeOH	10 ml

Column: acetone (100 %) $\rightarrow$ acetone/H$_2$O (10:1) $\rightarrow$ acetone/H$_2$O/saturated aqueous KNO$_3$ (100:10:1)

R_f = 0.4 (acetone/H$_2$O/KNO$_3$ (100:10:1))

After the column the solvents were removed. Addition of acetone precipitated KNO$_3$. Following filtration with a P4 frit, the solvent was removed from the mixture. The dry complex was dissolved in a minimal amount of acetone and dropped into Et$_2$O where it precipitated. The precipitate was washed with Et$_2$O, H$_2$O and dried in vacuum.

Yield: 44.2 mg [57 %] of orange-red solid

^{1}H NMR (400 MHz, CD$_2$Cl$_2$) δ = 8.70 (dd, J = 23.0, 9.0 Hz, 2H), 8.63 – 8.56 (m, 4H), 8.38 (d, J = 10.5 Hz, 1H), 8.11 (t, J = 7.4 Hz, 5H), 7.94 – 7.44 (m, 37H), 7.41 (s, 1H), 7.33 (d, J = 8.9 Hz, 1H), 7.10 – 7.00 (m, 4H), 6.84 (d, J = 8.3 Hz, 4H), 3.80 (s, 6H), 2.15 – 1.82 (m, 17H), 1.14 – 1.03 (m, 46H), 0.76 (tq, J = 20.3, 6.9 Hz, 42H) ppm

HRMS: m/z = 1125.6211 (calc. 1125.1190 for C$_{154}$H$_{169}$N$_7$O$_2$Ru^{2+})

7 Appendices

7.1 Dyads Equipped with a Boronmesityl Bridging Unit

UV/Vis spactra

Additional UV/Vis spectra of the short (**2**) and the long dyad (**1**).

Figure 7.1 Dyad **1** $1 \cdot 10^{-5}$ M in DMF with TBAF.

Figure 7.2 Dyad **2** $1 \cdot 10^{-5}$ M in CH$_3$CN with TBAF.

Cyclic voltammograms

Additional cyclic voltammograms. The figure below shows the voltammograms in methylene chloride.

Figure 7.3 Ru(bpy)$_3$(PF$_6$)$_2$ (a), dyad **1** (b) and dyad **2** (c) in methylene chloride. Scan rate: 0.5 V/s, Fc$^{+/0}$ as internal standard.

The following figures show dyads **1** and **2** in acetonitrile before and after addition of 1 eq TBAF.

I

Figure 7.4 Dyad **1** in acetonitrile before and after 1 eq TBAF. Scan rate: 0.5 V/s, $Fc^{+/0}$ as internal standard.

Figure 7.5 Dyad **2** in acetonitrile before and after 1 eq TBAF. Scan rate: 0.5 V/s, $Fc^{+/0}$ as internal standard.

In table 7.1 all electrochemical potentials vs. $Fc^{+/0}$ for energy schemes are summarized.

Table 7.1 Electrochemical potentials vs. $Fc^{+/0}$ for the boron compounds, amine (**A-1**) and $Ru(bpy)_3^{2+}$ without TBAF.

Compound	E in CH_2Cl_2 [V]	E in CH_3CN [V]
$^*Ru^{II/I}$		0.40^a
$Ru^{II/I}$		-1.7
$Ru^{III/II}$ [154]	0.97	0.88
$MV^{II/I}$		-0.80
amine$^{I/0}$ (**A-1**)	0.27	0.27
$mes_2-B-Ph^{0/-}$		-2.57
$mes_2-B-(alkyne)_2^{0/-}$ (**11**)	i	-2.28

^{i} not determinable, ^{a} $E(Ru^{II/I}) + E_{00}$, where E_{00} is 2.12 V

The following figure shows the CV of compound **A-1**.

Figure 7.6   Triaryamine **A-1** in CH_2Cl_2 (dashed line) and CH_3CN (solid trace).

CVs of compound **12** in three different solvents.

Figure 7.7   Kinetic absorbtion decay of methylviologen.

Flash-quench expeiments

The next figure shows the kinetic absorption decay of MV^+. The formation of MV^+ is completed within the laser pulse. The recombination to MV^{2+} is a slow process compared to the formation.

Figure 7.8   Kinetic absorption decay of MV^+ in acetonitrile at 608 nm.

Synthesis

Synthesis of compound $Br-Ph-alkyne-Bmes_2-alkyne-Ph-Br$:

349.8 mg (0.94 mmol) alkyne$-$Bmes$_2$$-$alkyne (**12**) and 793.1 mg (2.80 mmol, 3 eq) 1-bromo-4-iodo-phenyl were dissolved in 15 ml dry NEt$_3$. After deoxygenation of the solution, the catalyst mixture (7.1 mg (0.4 mmol, 4 mol%) CuI and 13.1 mg (0.2 mmol, 2 mol%) Pd(PPh$_3$)$_2$Cl$_2$) was added. After a second deoxygenation, the solution was heated to 96 °C and stirred over night. Then the solution was cooled to r.t., Et$_2$O was added. The mixture was washed with saturated aqueous NH$_4$Cl as well as with brine. The organic phase was collected, dried over Na$_2$SO$_4$ and solvents were evaporated. The crude product was purified *via* column chromatography.
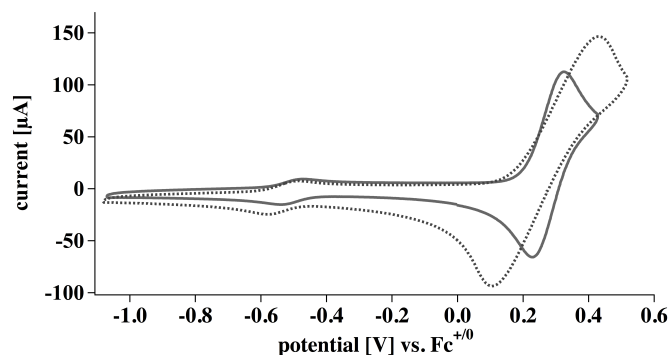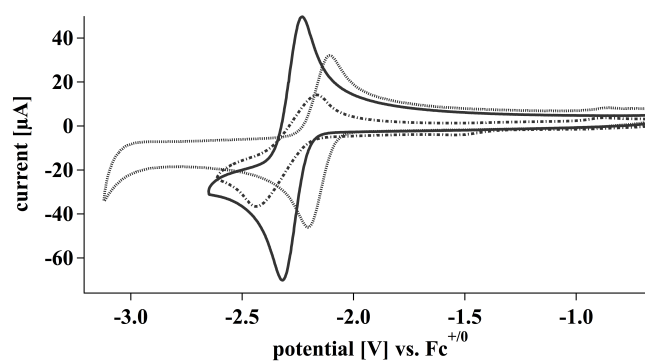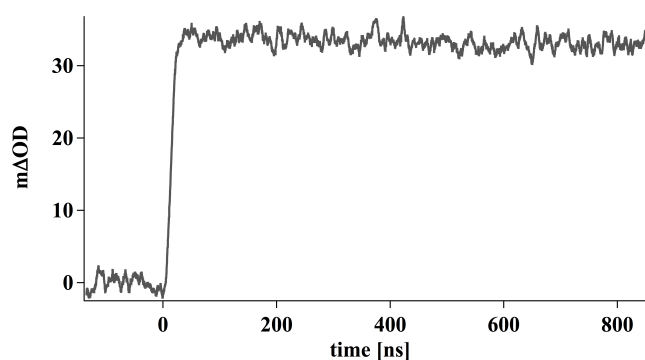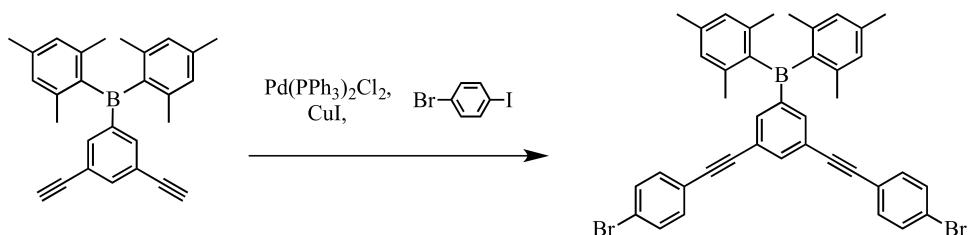
Column: P (100 %)

R$_f$ = 0.21

Yield: 517.1 mg [81 %] of yellow crystals

^{1}H NMR (400 MHz, CDCl$_3$): δ = 7.79 (t, J = 1.7 Hz, 1H), 7.62 (d, J = 1.7 Hz, 2H), 7.47 (d, J = 8.6 Hz, 4H), 7.35 (s, 4H), 6.84 (s, 4H), 2.32 (s, 6H), 2.00 (s, 12H) ppm

Synthesis of the reference molecule **R-1**:
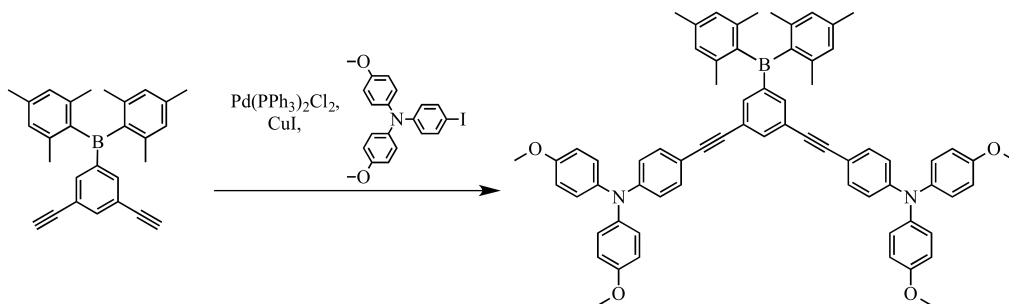
100 mg (0.27 mmol) alkyne$-$Bmes$_2$$-$alkyne (**12**) and 230 mg (0.54 mmol, 2 eq) amine$-$Ph$-$I (**A-2**) were dissolved in 10 ml dry NEt$_3$. After deoxygenation of the solution, the catalyst mixture (2 mg (0.01 mmol, 4 mol%) CuI and 4 mg (0.005 mmol, 2 mol%) Pd(PPh$_3$)$_2$Cl$_2$) was added. After a second deoxygenation, the solution was heated to 96 °C and stirred for 1h. Then the solution was cooled to r.t., CH$_2$Cl$_2$ was added. The mixture was washed with saturated aqueous NH$_4$Cl as well as with brine. The organic phase was collected, dried over Na$_2$SO$_4$ and solvents were evaporated. The crude product was purified *via* column chromatography.

Column: P (100 %) $\rightarrow$ P/CH$_2$Cl$_2$ (1:1)

R$_f$ = 0.86 (P/CH$_2$Cl$_2$ (1:1))

Yield: 159 mg [60 %] of yellow oily residue

^{1}H NMR (400 MHz, acetone-d$_6$): δ = 7.74 (t, J = 1.7 Hz, 1H), 7.48 (d, J = 1.7 Hz, 2H), 7.31 (d, J = 8.9

Hz, 4H), 7.11 (d, J = 9.0 Hz, 8H), 6.94 (d, J = 9.0 Hz, 8H), 6.88 (s, 4H), 6.75 (d, J = 8.9 Hz, 4H), 3.80 (s, 12H), 2.29 (s, 6H), 2.03 (s, 12H) ppm

7.2 Dyads Equipped with a Tetramethoxybenzene Bridging Unit

Table 7.2 Oxidation potentials for individual components of the desired dyads **3** - **6** in acetonitrile.

Compound	E_{ox} [V vs. Fc$^{+/0}$]	E_{red} [V vs. Fc$^{+/0}$]
Ru$^{III/II}$	0.9[72]	
amine$^{I/0}$	0.3[72]	
tmb$^{I/0}$	0.8[72]	
xy$^{I/0}$	1.68[72]	
fl$_1^{I/0}$	1.18^a[155]	-3.09[156]
fl$_2^{I/0}$	0.89^a[155]	-2.79[156]
Ph$^{I/0}$	2.10^b[157]	-3.68^b[158]
Ph$_2^{I/0}$	1.57^b[157]	

^{a} in methylene chloride[155], ^{b} Literature values reported in Volts versus SCE were converted to Volts vs. Fc$^{+/0}$ by subtracting 0.38 V[159]

7.3 Crystal structures

Dimesitylboron molecules

Table 7.3 Crystal data for alkyne$-$Bmes$_2$$-$alkyne (**12**).
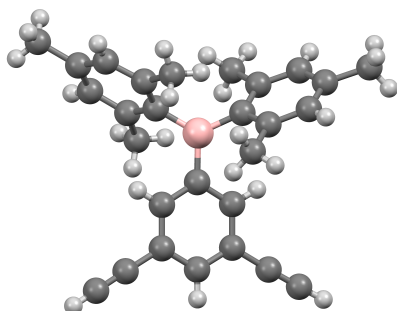
Formula	$C_{28}H_{27}B_1$
Formula weight	374.33 g $\cdot$ mol^{-1}
Z, calculated density	2, 1.107 mg $\cdot$ m^{-3}
F(000)	400
Description and size of crystal	colorless plate, 0.030 $\cdot$ 0.100 $\cdot$ 0.220 mm^3
Absorption coefficient	0.459 mm^{-1}
Min/max transmission	0.96 / 0.99
Temperature	123 K
Radiation(wavelength)	Cu K$_\alpha$ (λ = 1.54178 Å)
Crystal system, space group	triclinic, P -1
a	10.3753(6) Å
b	11.0992(7) Å
c	11.1683(7) Å
α	94.918(3)°
β	101.546(3)°
γ	114.790(3)°
V	1122.97(12) Å^3
Min/max Θ	4.116°/ 68.246°
Number of collected reflections	14563
Number of independent refections	4009 (merging r = 0.030)
Number of observed reflections	3349 (I > 2.0 σ (I))
Number of refined parameters	262
r	0.0463
rW	0.0645
Goodness of fit	1.1069

Figure 7.9 Crystal data for Br$-$Ph$-$alkyne$-$Bmes$_2$$-$alkyne$-Ph-$Br.
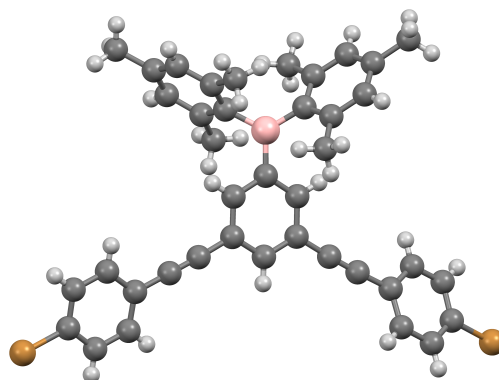
Formula	C$_{40}$H$_{33}$B$_1$Br$_2$
Formula weight	684.32 g $\cdot$ mol^{-1}
Z, calculated density	4, 1.403 mg $\cdot$ m^{-3}
F(000)	1392
Description and size of crystal	colorless plate, 0.030 $\cdot$ 0.130 $\cdot$ 0.250 mm^3
Absorption coefficient	3.365 mm^{-1}
Min/max transmission	0.65 / 0.90
Temperature	123 K
Radiation(wavelength)	Cu K$_\alpha$ (λ = 1.54178 Å)
Crystal system, space group	monoclinic, P 21/n
a	8.4039(4) Å
b	14.4778(6) Å
c	26.6553(12) Å
α	90°
β	92.5080(10)°
γ	90°
V	3240.0(3) Å^3
Min/max Θ	3.319°/ 68.317°
Number of collected reflections	29271
Number of independent refections	5855 (merging r = 0.026)
Number of observed reflections	5805 (I > 2.0 σ (I))
Number of refined parameters	388
r	0.0264
rW	0.0276
Goodness of fit	1.0262

Tetramethoxybenzene molecule

Table 7.4 Crystal data for amine−Ph−alkyne−tmb−alkyne−xy−bpy (**21**).
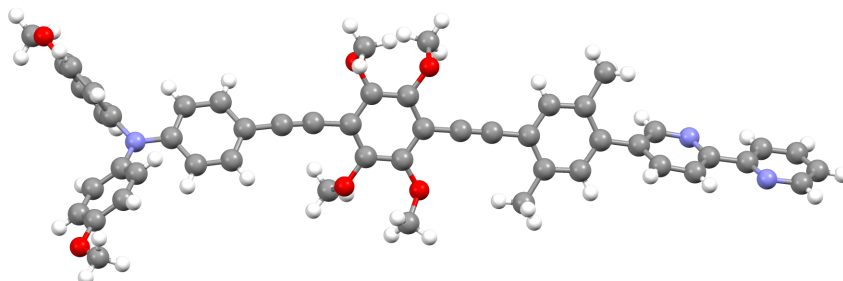
Formula	$C_{52}H_{45}N_3O_6$
Formula weight	$807.95 \text{ g} \cdot \text{mol}^{-1}$
Z, calculated density	$4, 1.272 \text{ mg} \cdot \text{m}^{-3}$
F(000)	1704
Description and size of crystal	yellow block, $0.070 \cdot 0.120 \cdot 0.220 \text{ mm}^3$
Absorption coefficient	0.668 mm^{-1}
Min/max transmission	0.92 / 0.95
Temperature	123 K
Radiation(wavelength)	Cu K_α ($\lambda = 1.54178$ Å)
Crystal system, space group	triclinic, P -1
a	11.8085(9) Å
b	15.4553(12) Å
c	25.507(2) Å
α	73.327(3)°
β	88.656(3)°
γ	71.560(3)°
V	4218.8(6) Å^3
Min/max Θ	1.813°/ 68.304°
Number of collected reflections	59075
Number of independent refections	15095 (merging r = 0.035)
Number of observed reflections	14218 (I > 2.0 σ (I))
Number of refined parameters	1099
r	0.0659
rW	0.0767
Goodness of fit	1.0740

7.4 ^{1}H and ^{13}C NMR spectra

^{1}H and ^{13}C NMR spectra for all characterized compounds can be found on the enclosed CD to this PhD thesis.

Molecules

7.5 Dyads

1

$(PF_6)_2$

2

$(NO_3)_2$

3

4

5

6

X

(NO$_3$)$_2$

7

hex   hex   hex   hex   (NO$_3$)$_2$

8

hex   hex   hex   hex   (NO$_3$)$_2$

9

XI
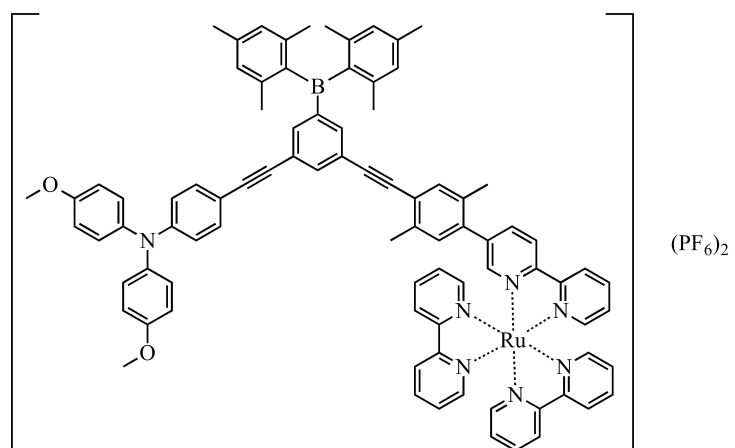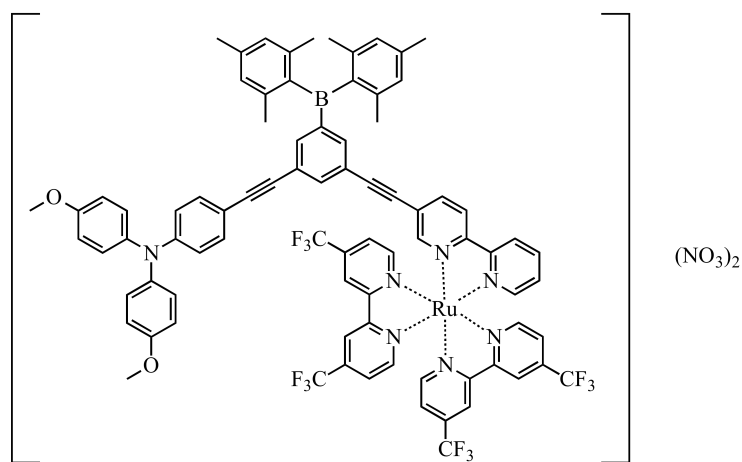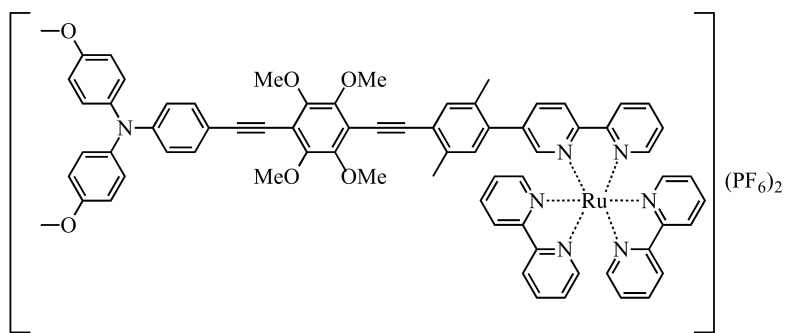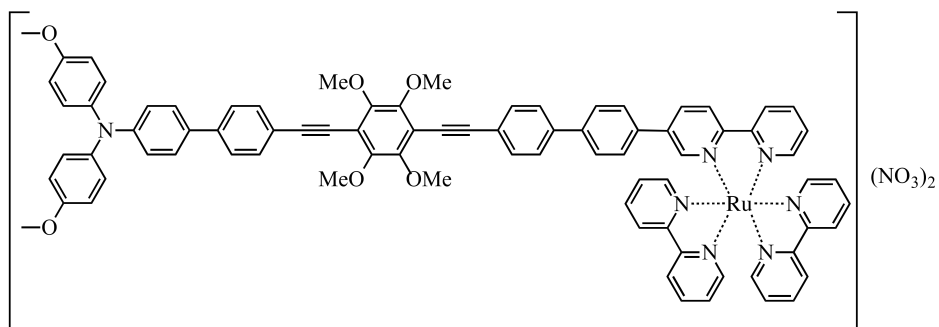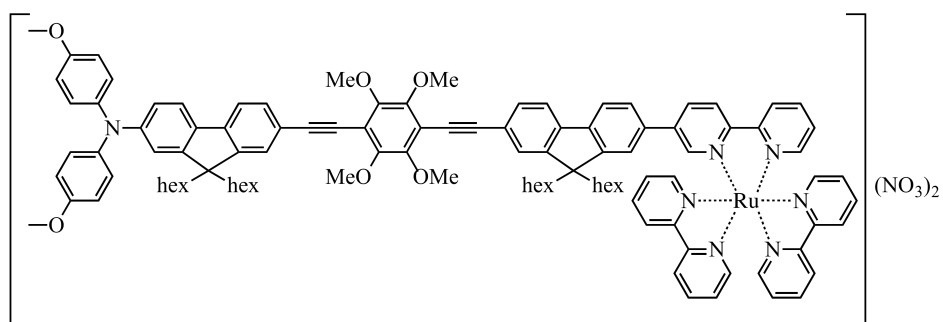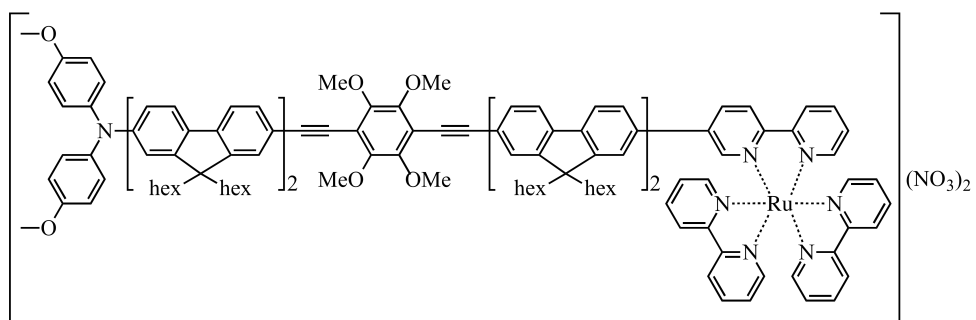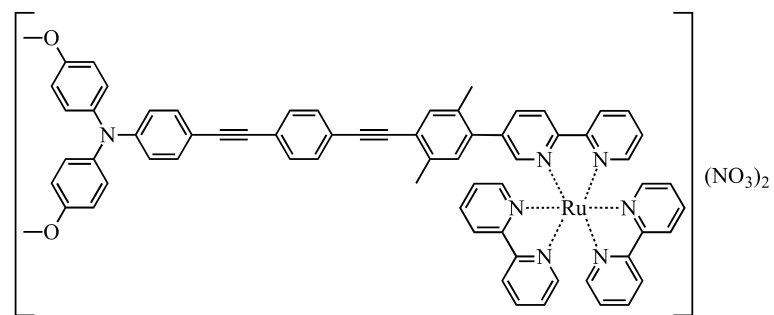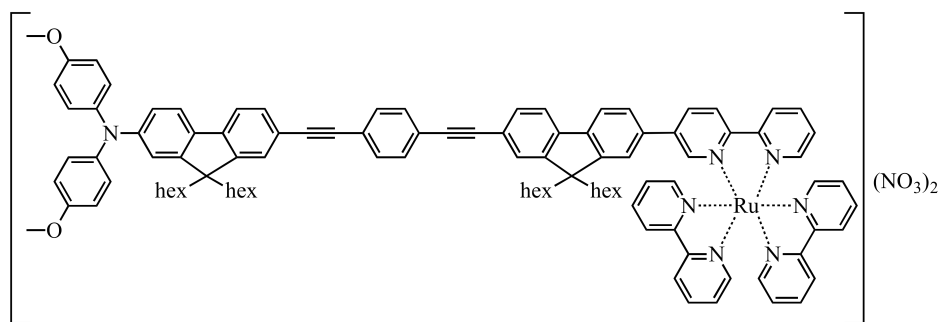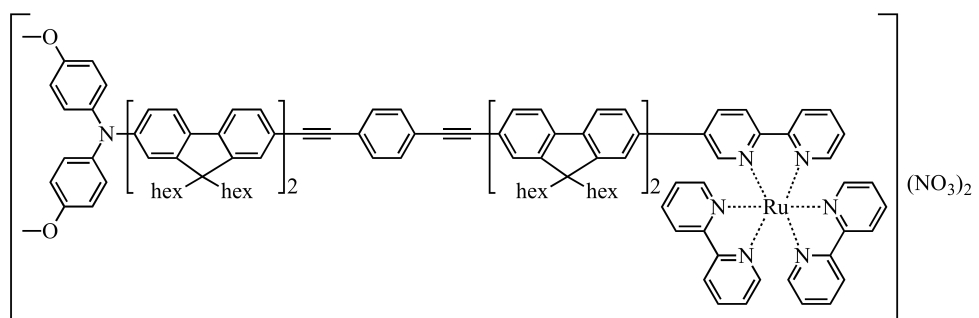
7.6 Central molecules and ligands
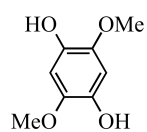
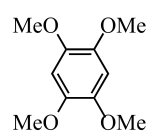**Boron compounds**
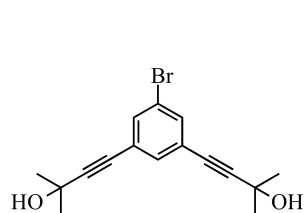
10
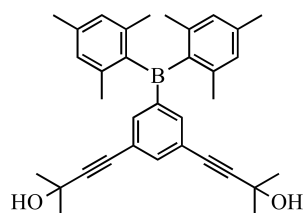
11
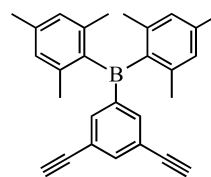
12
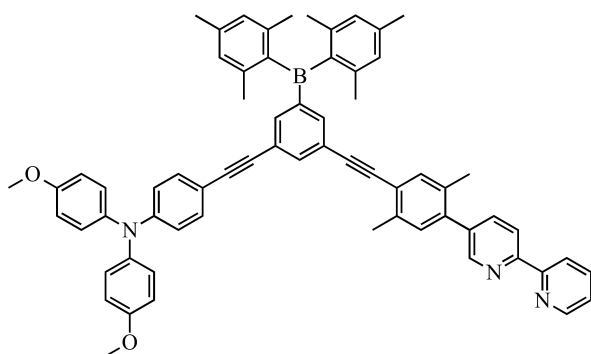
13
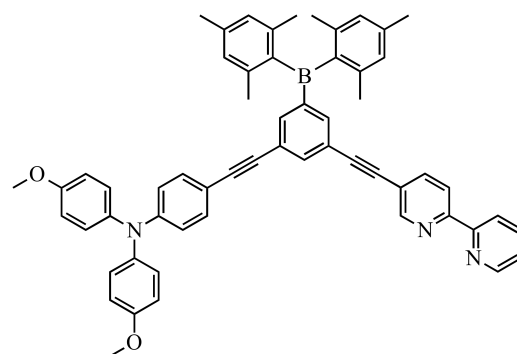
14
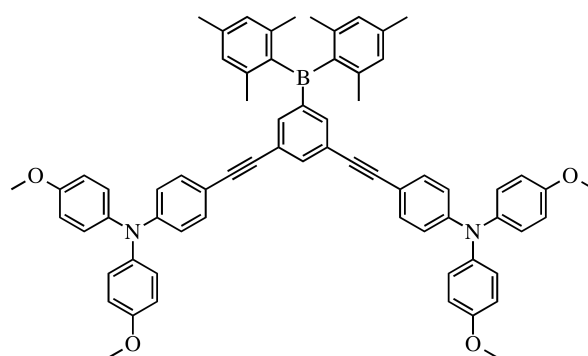
R-1

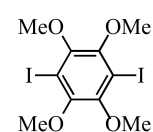Compound **10** is literature known.
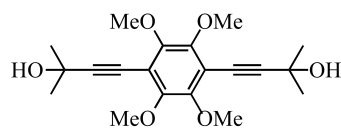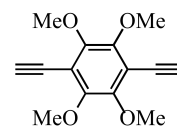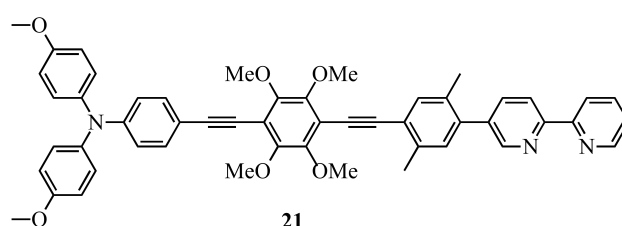
Tetramethoxybenzene compounds
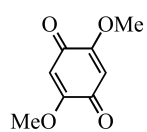
15

16

17

18

19

20

21
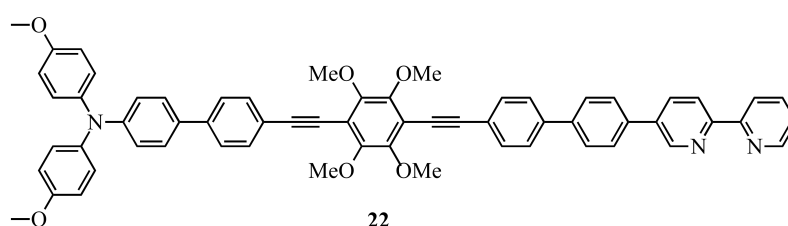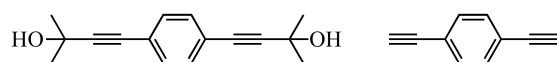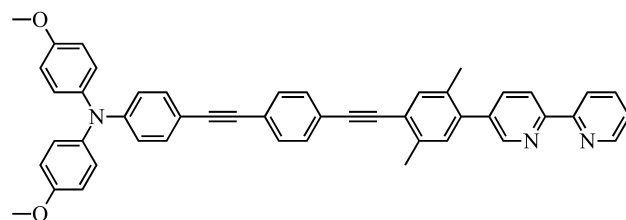

22
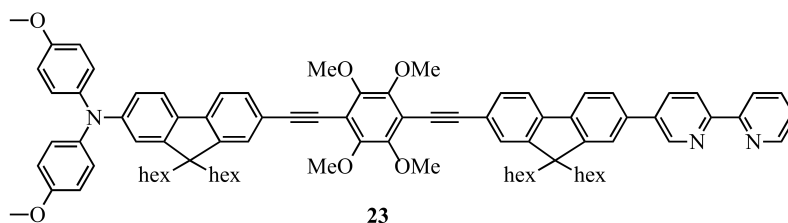
23
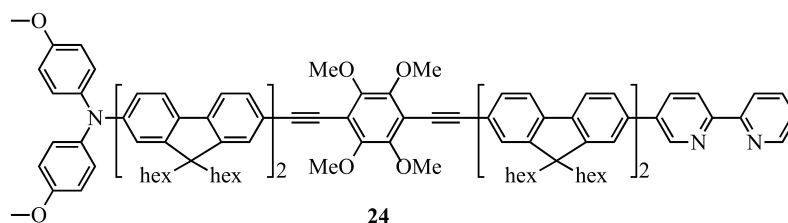
24

Compounds **15**, **16**, **17** and **18** are literature known.

Benzene compounds

25

26

27
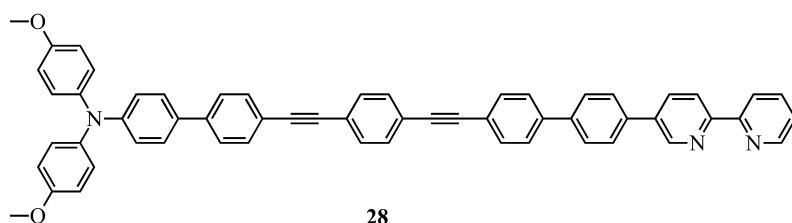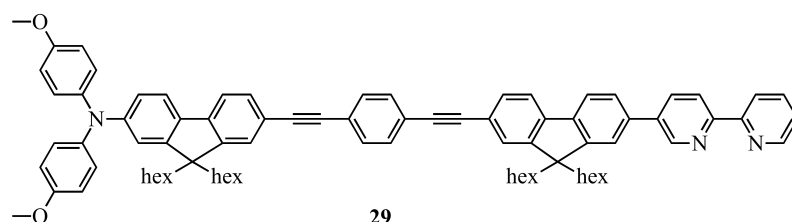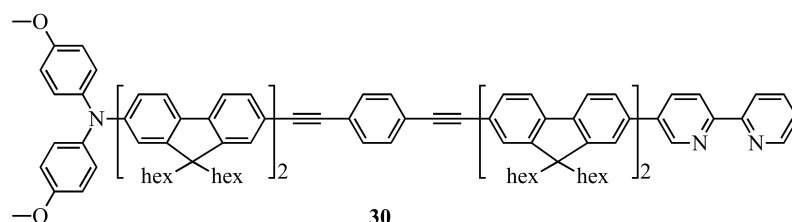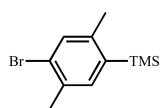

28

29

30

Compounds **25** and **26** are literature known.

7.7 Precursor molecules

Xylol spacer
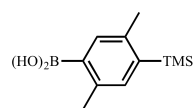
S-1　　　　　　　　　**S-2**

Biphenyl spacer
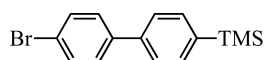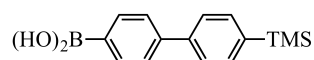
S-3　　　　　　　　　**S-4**

Fluorene spacer
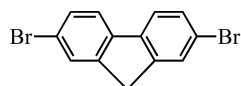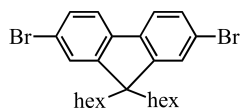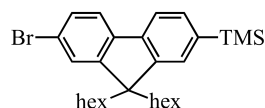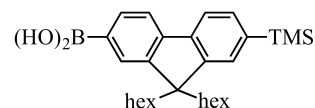
S-5　　　**S-6**　　　**S-7**　　　**S-8**

All molecules on this pages are literature known.

amine compounds
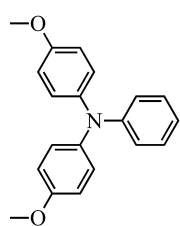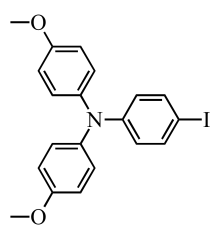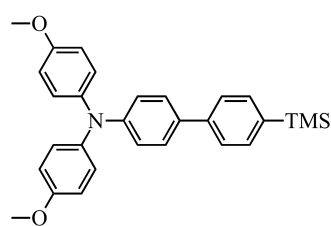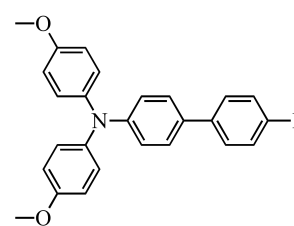
A-1   A-2   A-3   A-4
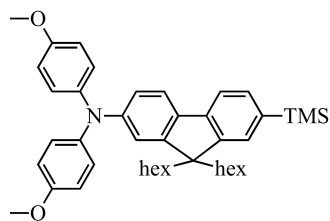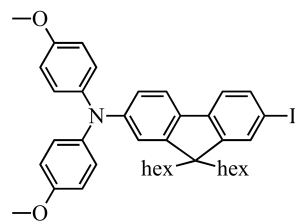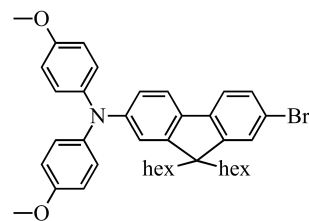
A-5   A-6   A-7
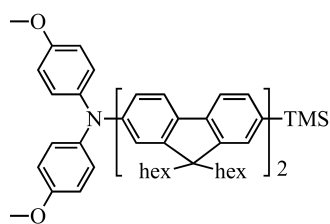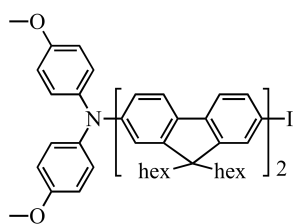
A-8   A-9

Compounds **A-1** and **A-2** are literature known.

bipyridine compounds
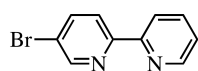
B-1
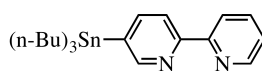
B-2
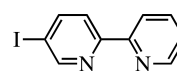
B-3
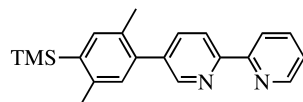
B-4
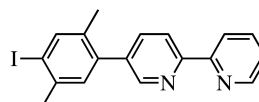
B-5
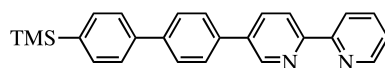
B-6
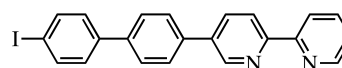
B-7
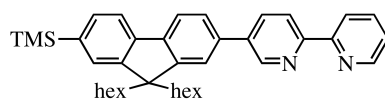
B-8
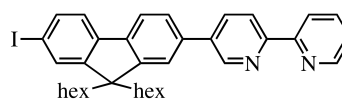
B-9
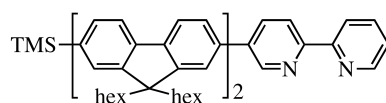
B-10
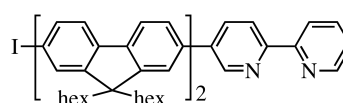
B-11

Compounds **B-1**, **B-2**, **B-3** and **A-4** are literature known.

Bibliography

[1] http://www.geohive.com/earth/his_proj_continent.aspx.

[2] Kärkäs, M. D.; Johnston, E. V.; Verho, O.; Åkermark, B. *Acc. Chem. Res.* **2014**, *47*, 100.

[3] Nocera, D. G. *Acc. Chem. Res.* **2012**, *45*, 767.

[4] Koolman, J.; Röhm, K.-H. *Taschenatlas der Biochemie, 3. Ed.*; Georg Thieme Verlag, 2003.

[5] Joyce, L. A.; Shabbir, S. H.; Anslyn, E. V. *Chem. Soc. Rev.* **2010**, *39*, 3621.

[6] Jablonski, A. *Z. Phys.* **1935**, *94*, 38.

[7] Marcus, R. A. *J. Chem. Phys.* **1956**, *24*, 966.

[8] Marcus, R. A. *J. Chem. Phys.* **1956**, *24*, 979.

[9] Paris, J. P.; Brandt, W. W. *J. Am. Chem. Soc.* **1959**, *81*, 5001.

[10] Crosby, G. A.; Perkins, W. G.; Klassen, D. M. *J. Chem. Phys.* **1965**, *43*, 1498.

[11] Juris, A.; Balzani, V.; Barigelletti, F.; Campagna, S.; Belser, P.; von Zelewsky, A. *Coord. Chem. Rev.* **1988**, *84*, 85.

[12] Scandola, F.; Balzani, V. *J. Chem. Educ.* **1983**, *60*, 814.

[13] Sutin, N.; Creutz, C. *J. Chem. Educ.* **1983**, *60*, 809.

[14] Issberner, J.; Vögtle, F.; Cola, L. D.; Balzani, V. *Chem. Eur. J.* **1997**, *3*, 706.

[15] Suzuki, K.; Kobayashi, A.; Kaneko, S.; Takehira, K.; Yoshihara, T.; Ishida, H.; Shiina, Y.; Oishi, S.; Tobita, S. *Phys. Chem. Chem. Phys.* **2009**, *11*, 9850.

[16] Ceroni, P.; Credi, A.; Venturi, M.; Balzani, V. *Photochem. Photobiol. Sci.* **2010**, *9*, 1561.

[17] Armaroli, N. *Chem. Soc. Rev.* **2001**, *30*, 113.

[18] Vincenzo Balzani, A. J., Paola Ceroni *Photochemistry and photophysics: concepts, research, application*; Wiley-VCH, 2014.

[19] Jańczyk, M.; Adamczyk-Woźniak, A.; Sporzyński, A.; Wróblewski, W. *Anal. Chim. Acta* **2012**, *733*, 71.

[20] Bresner, C.; Haynes, C. J. E.; Addy, D. A.; Broomsgrove, A. E. J.; Fitzpatrick, P.; Vidovic, D.; Thompson, A. L.; Fallis, I. A.; Aldridge, S. *New J. Chem.* **2010**, *34*, 1652.

[21] Cui, Y.; Li, F.; Lu, Z.-H.; Wang, S. *Dalton Trans.* **2007**, 2634.

[22] Varlan, M.; Blight, B. A.; Wang, S. *Chem. Commun.* **2012**, *48*, 12059.

[23] Entwistle, C. D.; Marder, T. B. *Chem. Mater.* **2004**, *16*, 4574.

[24] Entwistle, C. D.; Marder, T. B. *Angew. Chem. Inter. Ed.* **2002**, *41*, 2927.

[25] Yuan, Z.; Collings, J. C.; Taylor, N. J.; Marder, T. B.; Jardin, C.; Halet, J.-F. *J. Solid State Chem.* **2000**, *154*, 5.

[26] Elbing, M.; Bazan, G. *Angew. Chem., Int. Ed.* **2008**, *47*, 834.

[27] Liu, T.; Yu, Y.; Chen, S.; Li, Y.; Liu, H. *RSC Adv.* **2013**, *3*, 9973.

[28] Sun, Y.; Ross, N.; Zhao, S.-B.; Huszarik, K.; Jia, W.-L.; Wang, R.-Y.; Macartney, D.; Wang, S. *J. Am. Chem. Soc.* **2007**, *129*, 7510.

[29] Liu, Z.-Q.; Shi, M.; Li, F.-Y.; Fang, Q.; Chen, Z.-H.; Yi, T.; Huang, C.-H. *Org. Lett.* **2005**, *7*, 5481.

[30] Zhao, C.-H.; Wakamiya, A.; Inukai, Y.; Yamaguchi, S. *J. Am. Chem. Soc.* **2006**, *128*, 15934.

[31] Li, H.; Sundararaman, A.; Venkatasubbaiah, K.; Jäkle, F. *J. Am. Chem. Soc.* **2007**, *129*, 5792.

[32] Jäkle, F. *Chem.Rev.* **2010**, *110*, 3985.

[33] Jäkle, F. *Coord.Chem.Rev.* **2006**, *250*, 1107.

[34] Lorbach, A.; Hubner, A.; Wagner, M. *Dalton Trans.* **2012**, *41*, 6048.

[35] Hübner, A.; Qu, Z.-W.; Englert, U.; Bolte, M.; Lerner, H.-W.; Holthausen, M. C.; Wagner, M. *J. Am. Chem. Soc.* **2011**, *133*, 4596.

[36] Yamaguchi, S.; Shirasaka, T.; Akiyama, S.; Tamao, K. *J. Am. Chem. Soc.* **2002**, *124*, 8816.

[37] Bai, D.-R.; Liu, X.-Y.; Wang, S. *Chem. - Eur. J.* **2007**, *13*, 5713.

[38] Kaim, W.; Schulz, A. *Angew. Chem. Int. Ed. Engl.* **1984**, *23*, 615.

[39] Wade, C. R.; Gabbaï, F. P. *Inorg. Chem.* **2010**, *49*, 714.

[40] Lam, S.-T.; Zhu, N.; Yam, V. W.-W. *Inorg. Chem.* **2009**, *48*, 9664.

[41] Sun, Y.; Hudson, Z. M.; Rao, Y.; Wang, S. *Inorg. Chem.* **2011**, *50*, 3373.

[42] Szent-Györgyi, A. *Science* **1941**, *93*, 609.

[43] McConnell, H. M. *J . Chem. Phys* **1961**, *35*, 508.

[44] Kramers, H. A. *Physica* **1934**, *1*, 182.

[45] Anderson, P. W. *Phys. Rev.* **1950**, *79*, 350.

[46] Paddon-Row, M. N. *Acc. Chem. Res.* **1994**, *27*, 18.

[47] Wade, C. R.; Broomsgrove, A. E. J.; Aldridge, S.; Gabbaï, F. P. *Chem. Rev.* **2010**, *110*, 3958.

[48] Mengel, A. K. C.; He, B.; Wenger, O. S. *J. Org. Chem.* **2012**, *77*, 6545.

[49] Furue, M.; Maruyama, K.; Oguni, T.; Naiki, M.; Kamachi, M. *Inorg. Chem.* **1992**, *31*, 3792.

[50] Hankache, J.; Wenger, O. S. *Chem. - Eur. J.* **2012**, *18*, 6443.

[51] Chiu, C.-W.; Kim, Y.; Gabbaï, F. P. *J. Am. Chem. Soc.* **2009**, *131*, 60.

[52] Muller, P.; Brettel, K. *Photochem. Photobiol. Sci.* **2012**, *11*, 632.

[53] Wallin, S.; Davidsson, J.; Modin, J.; Hammarström, L. *J. Phys. Chem. A* **2005**, *109*, 4697.

[54] Sreenath, K.; Suneesh, C. V.; Gopidas, K. R.; Flowers, R. A. *J. Phys. Chem. A* **2009**, *113*, 6477.

[55] Mines, G. A.; Bjerrum, M. J.; Hill, M. G.; Casimiro, D. R.; Chang, I.-J.; Winkler, J. R.; Gray, H. B. *J. Am. Chem. Soc.* **1996**, *118*, 1961.

[56] do Socorro de P. Silva, M.; Diógenes, I. C.; de F. Lopes, L. G.; Ícaro de Sousa Moreira,; de Carvalho, I. M. *Polyhedron* **2009**, *28*, 661.

[57] Kim, Y.-H.; Rhim, S.; Park, J.; Kang, J. *J. Inclusion Phenom. Macrocyclic Chem.* **2012**, *74*, 317.

[58] Kannappan, R.; Bucher, C.; Saint-Aman, E.; Moutet, J.-C.; Milet, A.; Oltean, M.; Metay, E.; Pellet-Rostaing, S.; Lemaire, M.; Chaix, C. *New J. Chem.* **2010**, *34*, 1373.

[59] Kaur, P.; Kaur, S.; Singh, K. *Talanta* **2011**, *84*, 947.

[60] Guha, S.; Saha, S. *J. Am. Chem. Soc.* **2010**, *132*, 17674.

[61] Hu, Y. F.; Luo, J.; Lü, C. X. *Chin. Chem. Lett.* **2010**, *21*, 151.

[62] Sun, H.; DiMagno, S. G. *Angew. Chem. Int. Ed.* **2006**, *45*, 2720.

[63] Clark, J. H.; Smith, D. K. *Tetrahedron Lett.* **1985**, *26*, 2233.

[64] Cordes, M.; Giese, B. *Chem. Soc. Rev.* **2009**, *38*, 892–901.

[65] Genereux, J. C.; Barton, J. K. *Chem. Rev.* **2010**, *110*, 1642.

[66] Lloveras, V.; Vidal-Gancedo, J.; Figueira-Duarte, T. M.; Nierengarten, J.-F.; Novoa, J. J.; Mota, F.; Ventosa, N.; Rovira, C.; Veciana, J. *J. Am. Chem. Soc.* **2011**, *133*, 5818.

[67] Shafaat, H. S.; Leigh, B. S.; Tauber, M. J.; Kim, J. E. *J. Am. Chem. Soc.* **2010**, *132*, 9030.

[68] Clarke, J. R., T. M.; Durrant *Chem. Rev.* **2010**, *110*, 6736.

[69] Wienk, M. M.; Kroon, J. M.; Verhees, W. J. H.; Knol, J.; Hummelen, J. C.; Hal, P. A. v.; Janssen, R. A. J. *Angew. Chem., Int. Ed.* **2003**, *42*, 3371.

[70] Halls, J. J. M.; Pichler, K.; Friend, R. H.; Moratti, S. C.; Holmes, A. B. *Appl. Phys. Lett.* **1996**, *68*, 3120.

[71] Bakulin, A. A.; Dimitrov, S. D.; Rao, A.; Chow, P. C. Y.; Nielsen, C. B.; Schroeder, B. C.; Mc-Culloch, I.; Bakker, H. J.; Durrant, J. R.; Friend, R. H. *J. Phys. Chem. Lett.* **2013**, *4*, 209.

[72] Walther, M. E.; Wenger, O. S. *Inorg. Chem.* **2011**, *50*, 10901.

[73] Hanss, D.; Walther, M. E.; Wenger, O. S. *Chem. Commun.* **2010**, *46*, 7034.

[74] Madathil, M. M.; Khdour, O. M.; Jaruvangsanti, J.; Hecht, S. M. *J. Nat. Prod.* **2012**, *75*, 2209.

[75] Kim, B. G.; Chun, T. G.; Lee, H.-Y.; Snapper, M. L. *Bioorg. Med. Chem.* **2009**, *17*, 6707.

[76] Bruggemann, M.; Holst, C.; Hoppe, D. *Eur. J. Org. Chem.* **2001**, 647.

[77] Stahl, P.; Kissau, L.; Mazitschek, R.; Huwe, A.; Furet, P.; Giannis, A.; Waldmann, H. *J. Am. Chem. Soc.* **2001**, *123*, 11586.

[78] Poigny, S.; Huor, T.; Guyot, M.; Samadi, M. *J. Org. Chem.* **1999**, *64*, 9318.

[79] Poigny, S.; Guyot, M.; Samadi, M. *Tetrahedron* **1998**, *54*, 14791.

[80] Barr, D. P.; Aust, S. D. *Arch. Biochem. Biophys.* **1994**, *312*, 511.

[81] Dormont, L.; Delle-Vedove, R.; Bessière, J.-M.; Schatz, B. *Phytochemistry* **2014**, *100*, 51.

[82] Sato, H.; Guengerich, F. P. *J. Am. Chem. Soc.* **2000**, *122*, 8099.

[83] Koduri, R. S.; Whitwam, R. E.; Barr, D.; Aust, S. D.; Tien, M. *Arch. Biochem. Biophys.* **1996**, *326*, 261.

[84] Kersten, P. J.; Kalyanaraman, B.; Hammel, K. E.; Reinhammar, B.; Kirk, T. K. *Biochem J.* **1990**, *268*, 475.

[85] Yoshihara, T.; Yamaji, M.; Itoh, T.; Shizuka, H.; Shimokage, T.; Tero-Kubota, S. *Phys. Chem. Chem. Phys.* **2000**, *2*, 993.

[86] Amada, I.; Yamaji, M.; Sase, M.; Shizuka, H.; Shimokage, T.; Tero-Kubota, S. *Res. Chem. Intermed.* **1998**, *24*, 81.

[87] Nicolet, O.; Vauthey, E. *J. Phy.* **2002**, *106*, 5553.

[88] Schopf, G.; Rettig, W.; Bendig, J. *J. Photochem. Photobiol., A* **1994**, *84*, 33.

[89] Pirnat, K.; Gaberscek, M.; Dominko, R. *J. Power Sources* **2013**, *235*, 214.

[90] Glaser, R.; Blount, J. F.; Mislow, K. *J. Am. Chem. Soc.* **1980**, *102*, 2777.

[91] Li, H.; Lambert, C. *Chem. Eur. J.* **2006**, *12*, 1144.

[92] Quiroz-Guzman, M.; Brown, S. N. *Acta Cryst.* **2010**, *C66*, m171.

[93] Walther, M. E.; Grilj, J.; Hanss, D.; Vauthey, E.; Wenger, O. S. *Eur. J. Inorg. Chem.* **2010**, 4843.

[94] Potzel, O.; Taubmann, G. *Phys. Chem. Chem. Phys.* **2013**, *15*, 20288.

[95] Gerkin, R. E.; Lundstedt, A. P.; Reppart, W. J. *Acta Crystallogr., Sect. C: Cryst. Struct. Commun.* **1984**, *40*, 1892.

[96] Zweig, A.; Hodgson, W. G.; Jura, W. H. *J. Am. Chem. Soc.* **1964**, *86*, 4124.

[97] Stroyuk, O. L.; Rayevska, O. Y.; Kozytskiy, A. V.; Kuchmiy, S. Y. *J. Photochem. Photobiol., A* **2010**, *210*, 209.

[98] Spencer, J. F.; Price, G. M. *J. Chem. Soc., Trans.* **1910**, *97*, 385.

[99] Wittig, G.; Fuhrmann, G. *Ber. Dtsch. Chem. Ges. B* **1940**, *73B*, 1197.

[100] Gilman, H.; Langham, W.; Jacoby, A. L. *J. Am. Chem. Soc.* **1939**, *61*, 106.

[101] Sunthankar, S. V.; Gilman, H. *J. Org. Chem.* **1951**, *16*, 8.

[102] Wittig, G.; Schöllkopf, U. *Tetrahedron* **1958**, *3*, 91.

[103] Reich, H. J.; Green, D. P.; Phillips, N. H.; Borst, J. P.; Reich, I. L. *Phosphorus, Sulfur Silicon Relat. Elem.* **1992**, *67*, 83.

[104] Freys, J. C.; Wenger, O. S. *Eur. J. Inorg. Chem.* **2010**, 5509.

[105] Hwang, M. C.; Thangaraju, K.; So, K. H.; Shin, S.-C.; Kwon, S.-K.; Kim, Y.-H. *Synth. Met.* **2012**, *162*, 391.

[106] Wong, M. S.; Xia, P. F.; Zhang, X. L.; Lo, P. K.; Cheng, Y.-K.; Yeung, K.-T.; Guo, X.; Shuang, S. *J. Org. Chem.* **2005**, *70*, 2816.

[107] Hai, J.; Zhao, B.; Zhang, F.; Sheng, C.-X.; Yin, L.; Li, Y.; Zhu, E.; Bian, L.; Wu, H.; Tang, W. *Polymer* **2013**, *54*, 4930.

[108] Li, Q.; Zou, J.; Chen, J.; Liu, Z.; Qin, J.; Li, Z.; Cao, Y. *J. Phys. Chem. B* **2009**, *113*, 5816.

[109] Lin, T.-C.; Lee, Y.-H.; Hu, C.-L.; Li, Y.-K.; Huang, Y.-J. *Eur. J. Org. Chem.* **2012**, 1737.

[110] Belton, C. R.; Kanibolotsky, A. L.; Kirkpatrick, J.; Orofino, C.; Elmasly, S. E. T.; Stavrinou, P. N.; Skabara, P. J.; Bradley, D. D. C. *Adv. Funct. Mater.* **2013**, *23*, 2792.

[111] Bunnett, J. F. *Acc. Chem. Res.* **1978**, *11*, 413.

[112] Kosugi, M.; Kameyama, M.; Migita, T. *Chem. Lett.* **1983**, 927.

[113] Lindley, J. *Tetrahedron* **1984**, *40*, 1433.

[114] Biehl, E. *J. Org. Chem.* **1987**, *52*, 2619.

[115] Kunz, K.; Scholz, U.; Ganzer, D. *Synlett* **2003**, 2428.

[116] Paul, F.; Patt, J.; Hartwig, J. F. *J. Am. Chem. Soc.* **1994**, *116*, 5969.

[117] Guram, A. S.; Rennels, R. A.; Buchwald, S. L. *Angew. Chem., Int. Ed. Engl.* **1995**, *34*, 1348.

[118] Benhida, R.; Blanchard, P.; Fourrey, J.-L. *Tetrahedron Lett.* **1998**, *39*, 6849.

[119] Lambert, C.; Nöll, G.; Schmälzlin, E.; Meerholz, K.; Bräuchle, C. *Chem. – Eur. J.* **1998**, *4*, 2129.

[120] Phapale, V. B.; Guisán-Ceinos, M.; Buñuel, E.; Cárdenas, D. J. *Chem. - Eur. J.* **2009**, *15*, 12681.

[121] Knochel, P.; Almena Perea, J. J.; Jones, P. *Tetrahedron* **1998**, *54*, 8275.

[122] Pray, B. O.; Sommer, L. H.; Goldberg, G. M.; Kerr, G. T.; Giorgio, P. A. D.; Whitmore, F. C. *J. Am. Chem. Soc.* **1948**, *70*, 433.

[123] Eaborn, C.; Walton, D. R. M.; Young, D. J. *J. Chem. Soc. B* **1969**, 15.

[124] Stock, L. M.; Spector, A. R. *J. O* **1963**, *28*, 3272.

[125] Aalbersberg, W. G. L.; Barkovich, A. J.; Funk, R. L.; Hillard, R. L.; Vollhardt, K. P. C. *J. Am. Chem. Soc.* **1975**, *97*, 5600.

[126] Funk, R. L.; Vollhardt, K. P. C. *J. Chem. Soc., Chem. Commun.* **1976**, 833.

[127] Sauer, J.; Heldmann, D. K.; Pabst, G. R. *Eur. J. Org. Chem.* **1999**, *1999*, 313.

[128] Brotschi, C.; Mathis, G.; Leumann, C. J. *Chem. - Eur. J.* **2005**, *11*, 1911.

[129] Leroy-Lhez, S.; Parker, A.; Lapouyade, P.; Berlin, C.; Ducasse, L.; Oberlé, J.; Fages, F. *Photochem. Photobiol. Sci.* **2004**, *3*, 949.

[130] Anderson, P. A.; Anderson, R. F.; Furue, M.; Junk, P. C.; Keene, F. R.; Patterson, B. T.; Yeomans, B. D. *Inorg. Chem.* **2000**, *39*, 2721.

[131] Krause, R. A. *Inorganica Chimica Acta* **1978**, *31*, 241.

[132] Dwyer, F. P.; Goodwin, H. A.; Gyarfas, E. C. *Aust. J. Chem.* **1963**, *16*, 42.

[133] Rose, D.; Wilkinson, G. *J. Chem. Soc. A* **1970**, 1791.

[134] Sullivan, B. P.; Salmon, D. J.; Meyer, T. J. *Inorg. Chem.* **1978**, *17*, 3334.

[135] Jia, W.-L.; Bai, D.-R.; McCormick, T.; Liu, Q.-D.; Motala, M.; Wang, R.-Y.; Seward, C.; Tao, Y.; Wang, S. *Chem. - Eur. J.* **2004**, *10*, 994.

[136] S. J. Havens, P. M. H. *J. Org. Chem.* **1985**, *50*, 1763.

[137] D. E. Ames, C. T., D. Bull *Synthesis* **1981**, 364.

[138] Wuts, P. G. M.; Greene, T. W. *Green's Protective groups in Organic Synthesis, 4th Ed.*; Wiley-Interscience, 2007.

[139] Li, J.; Huang, P. *Beilstein J. Org. Chem.* **2011**, *7*, 426.

[140] Smeyanov, A.; Schmidt, A. *Synth. Commun.* **2013**, *43*, 2809.

[141] Filosa, R.; Peduto, A.; Aparoy, P.; Schaible, A. M.; Luderer, S.; Krauth, V.; Petronzi, C.; Massa, A.; de Rosa, M.; Reddanna, P.; Werz, O. *Eur. J. Med. Chem.* **2013**, *67*, 269.

[142] Wessig, P.; Möllnitz, K. *J. Org. Chem.* **2008**, *73*, 4452.

[143] Gan, X.; Jiang, W.; Wang, W.; Hu, L. *Org. Lett.* **2009**, *11*, 589.

[144] Viault, G.; Grée, D.; Das, S.; Yadav, J. S.; Grée, R. *Eur. J. Org. Chem.* **2011**, 1233.

[145] Armstrong, A.; Brackenridge, I.; Jackson, R. F. W.; Kirk, J. M. *Tetrahedron Lett.* **1988**, *29*, 2483.

[146] Kalamar, J.; Steiner, E.; Charollais, E.; Posternak, T. *Helv. Chim. Acta* **1974**, *57*, 2368, (Compound XVIIIa is I-TMB-I).

[147] Staab, H. A.; Weiser, J.; Futscher, M.; Voit, G.; Rückemann, A.; Anders, C. *Chem. Ber.* **1992**, *125*, 2285.

[148] Shu, W.; Guan, C.; Guo, W.; Wang, C.; Shen, Y. *J. Mater. Chem.* **2012**, *22*, 3075.

[149] Brown, A. E.; Eichler, B. E. *Tetrahedron Letters* **2011**, *52*, 1960.

[150] Jeux, V.; Demeter, D.; Leriche, P.; Roncali, J. *RSC Adv.* **2013**, *3*, 5811.

[151] Fang, Y.-Q.; Hanan, G. S. *Synlett* **2003**, *6*, 852.

[152] Hankache, J.; Wenger, O. S. *Chem. Commun.* **2011**, *47*, 10145.

[153] Liu, J.; Yan, C.; Li, S.; Wang, C.; Shen, Y. *Chin. J. Chem.* **2012**, *30*, 2861.

[154] Hankache, J.; Wenger, O. S. *Phys. Chem. Chem. Phys.* **2012**, *14*, 2685.

[155] Goldsmith, R. H.; Sinks, L. E.; Kelley, R. F.; Betzen, L. J.; Liu, W.; Weiss, E. A.; Ratner, M. A.; Wasielewski, M. R. *Proc. Natl. Acad. Sci. U. S. A.* **2005**, *102*, 3540.

[156] Zaikowski, L.; Kaur, P.; Gelfond, C.; Selvaggio, E.; Asaoka, S.; Wu, Q.; Chen, H.-C.; Takeda, N.; Cook, A. R.; Yang, A.; Rosanelli, J.; Miller, J. R. *J. Am. Chem. Soc.* **2012**, *134*, 10852.

[157] Merkel, P. B.; Luo, P.; Dinnocenzo, J. P.; Farid, S. *J. Org* **2009**, *74*, 5163.

[158] Mortensen, J.; Heinze, J. *Angew. Chem. Int. Ed. Engl.* **1984**, *23*, 84.

[159] Pavlishchuk, V. V.; Addison, A. W. *Inorg. Chim. Acta* **2000**, *298*, 97.

Danksagung

An dieser Stelle möchte ich mich nun bei allen bedanken, die zum Gelingen dieser Arbeit beigetragen haben.

Ein ganz besonderer Dank gilt Herrn Prof. Dr. Oliver Wenger für die Möglichkeit in seiner Gruppe promovieren zu dürfen, sowie für die interessanten Projekte, die ich bearbeiten durfte und die gewährte Freiheit während der Bearbeitung der Aufgabenstellung. Vielen Dank für die Unterstützung und das Feedback beim Erstellen dieser Dissertation. Ich danke auch für die Möglichkeit der Teilnahme an nationalen und internationalen Konferenzen. Frau Prof. Dr. Catherine Housecroft möchte ich für die freundliche Übernahme der Zweitgutachtertätigkeit danken. Prof. Dr. S. Willitsch danke ich für die Übernahme des Prüfungsvorsitzes.

Bei Heinz Nadig, Sylvie Mittelheisser und Daniel Häussinger bedanke ich mich für die Aufnahme zahlreicher NMR-, MS-Spektren sowie Elementaranalysen. Ein großer Dank gilt auch Brigitte Howald, Markus Hauri und Beatrice Erisman, die mir in administrativen Sachen sehr geholfen haben. Danken möchte ich auch dem gesammten Werkstatt-Team für die schnelle Bearbeitung diverser Probleme.

Bei allen Kollegen des 3. OG und im AKW (klingt doch immer wieder super) möchte ich mich für das tolle und freundschaftliche Arbeitsklima bedanken. Die sommerlichen Grillabende, Sekt-Pausen, Aperos sowie die Gruppenausflüge, welche stets die Gelegenheit boten sich ganz neu kennenzulernen (auch gruppenübergreifend), waren grandios. Vermissen werde ich besonders die (oft heiß ersehnten) Kaffeepausen, in denen unter anderem die Allgemeinbildung verbessert wurde:

Schlacht der Eidgenossen 18-irgendwas im Vorgarten (wer hätte gedacht, dass solch ein friedliches Volk sich so oft bekämpft hat) oder der wohl sehr berühmte schweizer Rapper mit dem stummen "E" sowie die zahlreichen Psychologen, deren Namen stets direkt wieder vergessen wurden. Auch die angeregten sowie stets lustigen Disskusionen über besondere Artikel in der *20 Minuten* und/oder *Blick am Abend* werden mir fehlen.

Ein besonderer Dank geht an meine Laborkollegen: Martin es war eine wunderbare Zeit als zwei Ossis im großen, weiten Westen, die am gleichen Tag Geburtstag haben, sich ein Labor in guten wie in stinkigen Zeiten geteilt haben. Auch das reine Mädelslabor mit Jing und Ann Christin in Basel hatte seine Vorzüge und stets bestand Gesprächsbereitschaft.

Ebenfalls ein besonderer Dank gilt Annabell, mit der ich das Vergnügen hatte zur selben Zeit in Göttingen die Promotion zu beginnen und die sich als sehr gute Cluster-Schwester herausgestellt hat. Sollte ich je wieder eine Kajaktour machen, ruf ich an. Des Weiteren denke ich, dass ich ihr zeigen konnte, nicht alle Blondinen sind vom gleichen Schlag :)

Vielen Dank auch an meine Bachelorstudenten Hauke und Svenja, die mir das Leben als Betreuerin sehr einfach gemacht haben und solch gute Resultate hervorgebringen konnten. Hauke danke ich außerdem für die Hilfe mit LaTex.

Ein herzlicher Dank gilt auch meinen Studienfreunden Ly, D.T., D.S., Moldi und Alex, mit denen der Kontakt auch nach dem Ende der gemeinsamen Studienzeit nicht abgebrochen ist. Besonders möchte ich

Ly für die Skype-Dates (wenn wir uns nicht *in persona* sehen konnten) danken, in denen wir die Verhaltensweisen der Studenten analysiert haben, die klassischen "Woooza" Situationen Revue passieren lassen und uns auch mal andere Dinge von der Seele reden konnten. Du warst mir stets eine große Stütze und ich hätte keine bessere Trauzeugin finden können. Mögen die Grillier-, Sektfestival-, Weihnachtsback-, Silvester- und Sportevents uns immer wieder zusammenführen. Danken möchte ich auch René, der mir die schweizer Sprache sowie Kultur näher gebracht hat, auch wenn wir immer noch nicht 100 %ig wissen, wo man frei parken kann: weiß oder blau? sowie stets da war wenn man in brauchte.

Der größte Dank geht an meine Eltern, die mir stets ein Vorbild waren. Sie haben mich durch ihre Liebe, ihre Unterstützung und das entgegengebrachte Vertrauen zu dem Menschen gemacht, der ich jetzt bin. Ich danke meiner Familie, die trotz der zahlreichen Niederschläge in der letzten Zeit, mir stets den Rücken freigehalten hat und für die schönen gemeinsamen Momente. Auch der Versuch zu verstehen, was ich eigentlich als Chemiker mache und euch die Grundregeln der Chemie

Gegensätze ziehen sich an	aber	*Gleiches gesinnt sich zu Gleichem.*
Weniger ist mehr	aber	*viel hilft viel.*

näher zu bringen, hat Spaß gemacht. Ein Dank gilt meiner Oma, die leider diesen Moment nicht mehr mit mir teilen kann. Ich hatte 28 tolle Jahre mit ihr und ohne sie wäre ich sicherlich nicht so begabt im Basteln, was mir auch im Labor sehr hilfreich war. Den wohl prägensten Eindruck hat mein Papa hinterlassen, denn er hat mir gezeigt, egal wie unfair das Leben auch zu dir ist, steh auf, denk positiv und kämpf weiter. Danke dafür.

Erziehung besteht aus zwei Dingen: Beispiel und Liebe.

F. Fröbel

Michael danke ich für seine uneingeschränkte Liebe, seine Art mich zum Lachen zu bringen, seine Geduld und sein Vertrauen. Ohne ihn hätten ich auch wesentlich weniger Obst zum Arbeiten :) Danke für die vielen schönen Jahre, die wir gemeinsam in Freiberg, Dresden, Göttingen, Efringen/Basel erlebt haben und die wir in Zukunft noch erleben werden.

Menschen zu finden, die mit uns fühlen und empfinden,
ist wohl das schönste Glück auf Erden.

C. Spitteler

Curriculum Vitae

Luisa G. Heinz

Personal Details

Maiden name: Reuter
Birthplace: Dresden, Saxony, Germany

Education and Professional Experience

September 2012 - October 2014	Ph.D. studies at the **University of Basel (CH)**
March 2011 - August 2012	Ph.D. studies at the **University of Göttingen (GER)**
	Supervisor: **Prof. Dr. Oliver S. Wenger**
October 2005 - December 2010	Diploma degree in Chemistry at the **University of Freiberg (GER)**
	Supervisor: **Prof. Dr. Edwin Weber**
	Thesis title: *New tetracarboxcylic tectones for porous solid state structures*
February 2009 - June 2009	Studienarbeit at the **University of Freiberg (GER)**
	Supervisor: **Prof. Dr. Edwin Weber**
	Thesis title: *Synthesis and characterization of 25,26,27,28-Tetra-methoxy-5,17-dinitrocalix[4]arene as potential channel builder*
	$\rightarrow$ specialized since 7th semester in organic chemistry
1997 - 2005	A-Level at the Johann-Andreas-Schubert School, **Dresden (GER)**
	major courses: Chemistry, Mathematics

List of Publications

Heinz, L. G.; Wenger, O. S., **Photoinduced electron transfer in a triarylamine-organoboron-Ru(2,2'-bipyridine)$_3$ $^{2+}$ compound**. *C. R. Chim.* **2016**, *doi:10.1016/j.crci.2015.08.007*.

Heinz, L. G.; Yushchenko, O.; Neuburger, M.; Vauthey, E.; Wenger, O. S., **Tetramethoxybenzene is a Good Building Block for Molecular Wires: Insights from Photoinduced Electron Transfer**. *J. Phys. Chem. A* **2015**, *119* (22), 5676–5684.

Gruber, T.; Eißmann, F.; Gruner, M.; **Heinz, L. G.**; Seichter, W. and Weber, E., **Simple dinitro substituted calix[4]arene forming a honeycomb-like architecture with hydrophobic channels**. *CrystEngComm* **2014**, *16*, 3730-3736.

Reuter, L. G.; Bonn, A. G.; Stückl, A. C.; He, B.; Pati, P. B.; Zade, S. S.; Wenger, O. S., **Charge Delocalization in a Homologous Series of α,α'-Bis(dianisylamino)-Substituted Thiophene Monocations**. *The Journal of Physical Chemistry A* **2012**, *116*, 7345-7352.

Schmidt, H. C.; **Reuter, L. G.**; Hamacek, J.; Wenger, O. S., **Multistage Complexation of Fluoride Ions by a Fluorescent Triphenylamine Bearing Three Dimesitylboryl Groups: Controlling Intramolecular Charge Transfer.** *The Journal of Organic Chemistry* **2011**, *76*, 9081-9085.

Poster Presentations

2013	SCS Fall Meeting, Lausanne, Switzerland
	Photoinduced Electron Transfer In Triarylamine-Boraryl-Ruthenium system
	Luisa G. Heinz, Markus Neuburger, Oliver S. Wenger
2012	PCC (PhD Community, University of Basel), Basel, Switzerland
	Photoinduced Electron Transfer in a Triarylamine-Boraryl-Ruthenium system
	Luisa G. Reuter, Hauke C. Schmidt, Oliver S. Wenger
2011	XXIV IUPAC Symposium on Photochemistry, Coimbra, Portugal
	Photoinduced Electron Transfer in a Triarylamine-Boraryl-Ruthenium system
	Luisa G. Reuter, Hauke C. Schmidt, Oliver S. Wenger